UNIVERSITÀ DEGLI STUDI FIRENZE

Dottorato di Ricerca in

Area del Farmaco e Trattamenti Innovativi

(Curriculum in Scienze Farmaceutiche)

CICLO XXXII

COORDINATRICE Prof. Elisabetta Teodori

Carbonic Anhydrase Inhibitors: Versatile Agents for the Treatment of Human Diseases

Settore Scientifico Disciplinare CHIM/08

Dottorando

Dott.ssa Berrino Emanuela

Tutore Scientifico

Prof. Claudiu T.Supuran

Tutore Teorico

Prof. Alessandro Mugelli

Coordinatrice

Prof. Elisabetta Teodori

Anni 2016/2019

Table of contents

<u>**Chapter 5: Experimental Section**</u>

Abstract

The Carbonic Anhydrases (CAs, EC 4.2.1.1) are ubiquitous metalloenzymes expressed in almost all living organisms. Being one of the main actors in pH regulation and in the maintenance of proper concentrations of CO_2, the dysruption of the activity of such enzymes, by means of adequate modulators, is a validated strategy for the treatment of human affecting pathologies and for the eradication of etiological agents (i.e. pathogenic bacteria, fungi and protozoa). In addition, CA-based biotechnological applications (i.e. CO_2 capture) may benefit from modulation of the enzymatic activity. CA Inhibitors (CAIs) have been extensively investigated over the time, and have been validated for the management of hypertensive glaucoma, systemic hypertension, epilepsy, obesity related diseases and recently neuropathic pain, inflammation and hypoxic tumors. Although CA activators (CAA) traditionally lacked interests, currently a repurposing of such compounds is underway with promising results as potential agents for the management of memory deficits related to neurodegenerative diseases.

In this Thesis work, an introductive overview on CAs as the main biological targets (**Chapter 1**) and three distinctive projets (**Chapters 2-4**) are reported ranging from synthetic chemistry to enzyme biology and spctrophotometry.

The first one (**Chapter 2**) concerns the synthesis and evaluation of new CAIs with Carbon Monoxide (CO) releasing properties for the management of RA. The reported compounds have been fully characterized, their CA inhibitory properties along with the CO releasing effect were assessed. In particular, a spectrophotometric assay was properly set with slight modifications of the protocols reported in the literature. This allowed to obtain a precise and quantitative evaluation of CO released over time from our compounds. The pain refief effect of the designed CAI-CORMs was also evaluated in a rat model of RA with very promising results.

The second project (**Chapter 3**) was aimed to synthetize a small series of CAI-AZT hybrids and to evaluate them as Telomerase Inhibitors, thus with possible antitumoral applications. The compounds synthetized have been profiled in vitro on seven CA isoforms (i.e. I, II, Va, VB, VII, IX and XII). The effects of our compounds on Telomerase Activity have been also determined showing a low-medium inhibition potency. Two promising derivatives have been identified with good IC_{50} and IC_{90} values. Co-crystallyzation of selected compounds in adduct with hCA II has been performed and their binding modes were determined.

The third project (**Chapter 4**) was entirely carried out during my six-months visiting student experience at the University of Poitiers in France, and it concerns the synthesis in Superacid medium of new mono and di-fluorinated diamines as CAIs. Insertion of one or more C-F bonds is a validated strategy in Medicinal Chemistry. Fluorine insertion can modulate pharmacokinetic and pharmacodynamic properties of the compounds, thus being an attractive tool in the design of bioactive compounds. Another unrelated project included in this Chapter, is the synthesis of enantiopure fluorinated tricyclic scaffolds obtained by means of a diastereoselective approach.

Abbreviation List

(h)CA, (human) carbonic anhydrase;

AAZ, acetazolamide;

BRZ, brinzolamide

CAI(s), carbonic anhydrase inhibitor(s);

CFA, Complete Freund's Adjuvant;

CMC, carboxymethylcellulose;

CO, Carbon monoxide;

Co_2CO_8, dicobalt octacarbonyl

CORMs, CO releasing molecules;

DCH, dicobalthexacarbonyl;

DCM, dichloromethane;

DCP. dichlorphenamide;

DeoxyMb, deoxy myoglobin;

DIPEA, N,N-Diisopropylethylamine;

DMF, dimethylformamide;

DPA, Diisopropylamine;

HF, hydrogen fluoride;

HO, Heme Oxygenases;

hTERT, human telomerase reverse transcriptase;

LDA, Lithium diisopropylamide;

Mb, Myoglobin;

MbCO, carbonylated myoglobin;

MZA, metazolamide;

nBuLi, n-Butyllithium;

NFSI, N-Fluorobenzenesulfonimide;

PET, positron emission tomography;

RA, Rheumatoid Arthritis;

ROS, reactive oxygen species;

SbF_5, Antimony pentafluoride;

SLT, sulthiame;

TEA, triethylamine;

TERC, telomerase RNA component;

TERT, telomerase reverse transcripatase;

THF, Tetrahydrofuran;

TPM, topiramate,

TsCl, Tosyl Chloride;

ZNS, zonisamide.

Chapter 1: The Carbonic Anhydrases

1.1 The Carbonic Anhydrases: an overview

As any other physiological parameter, the pH is kept at its optimum value through a dynamic equilibrium. Protons and bicarbonate ions concentrations are continuously modified as the consequence of intercourring metabolic pathways. pH homeostasis is required to be under tight control in all organisms and tissues/cells types [1] as minimal alterations of pH values determine important biological events often incompatible with survival [2]. In order to cope with pH modifications of physiological/pathological events, cells rely on different mechanisms such as those based on the buffering power of metabolically generated weak acids/bases [3-5]. The most important one is the HCO_3^- / CO_2 buffer system, since CO_2 is generated/used in many metabolic reactions [4,5].

$$CO_2 + H_2O \rightleftharpoons H_2CO_3 \rightleftharpoons HCO_3^- + H^+$$ **Equation 1.1**

The hydration of CO_2 with generation of bicarbonate and protons, does not allow this transformation to occur fast enough to satisfy the metabolic needs of most cells/tissues (**Equation 1.1**) [5]. The metalloenzymes Carbonic Anhydrases (CAs, EC 4.2.1.1) are listed among the most efficient catalysts, with catalytic turnovers for the equilibrium listed in **Equation 1.1** (k_{cat}/K_M) up to 10^8 M^{-1}/s^{-1} as for the CA II expressed in humans [4-6]. Regulation of such equilibrium is not limited to pH regulation itself, as in superior organisms such as the mammals it is actively involved in secretion of electrolytes, gluconeogenesis, urea biosynthesis and lipogenesis, bone and cardiovascular remodellings [5]. In algae, cyanobacteria and plants the expressed CAs are involved in regulation of photosynthesis by means of the Carbon-Concentrating mechanisms (CCMs) [7]. In pathogenic microorganism such as bacteria, fungi and protozoa, the reaction catalysed by CAs has a crucial role in regulating virulence and survival of microorganisms within the host environment [8-10].

It is clear the preminent role of such reaction and therefore the high value of agents able to modulate it with important applications spanning from the Medicinal Chemistry to the Biotechnological fields [5,11,12].

1.1.1 Classification of the Carbonic Anhydrases

Up to now eight distinct and genetically unrelated CA families are known to date and are reported with the Greek letters α–, β–, γ–, δ–, ζ–, η–, θ– and ι-CAs, with the latter being very recently discovered by a Japanese group [4,13,14]. The CAs possessing catalytic activity bear a metal ion within their cavity site [4,5]. The α-, β-, δ-, η– and θ– classes contain Zn (II), γ-class probably Fe (II), the ζ Cd (II) [4,13]. The latest discovered ι-CAs has been identified in marine phytoplankton and is believed to be a Mn (II) protein [14]. The metal ion (II) is coordinated in a tetrahedral geometry, coordinated by three aminoacidic residues and a water molecule/hydroxide ion in the coordination sphere [4].

The CA catalytic mechanism for the hydration reaction of CO_2 evolves in a ping-pong fashion, according to the scheme reported below using the α-CA isoform II as a model enzyme. [4,5,15] (**Scheme 1.1**).

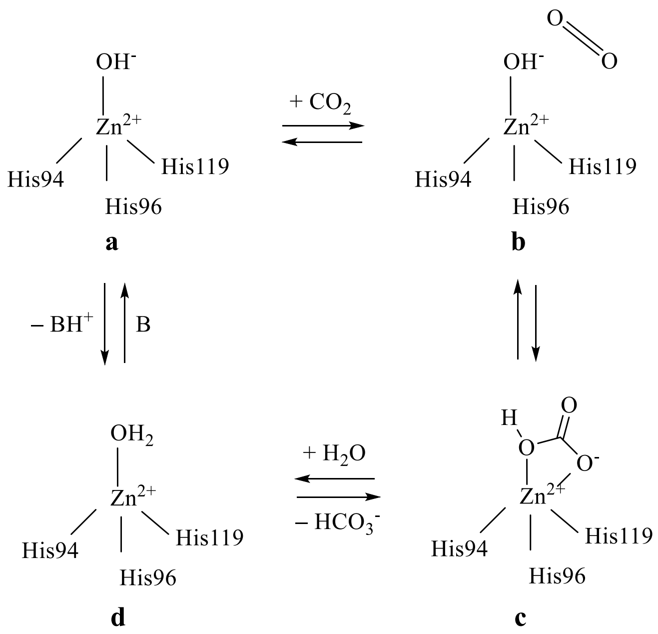

Scheme 1.1. Catalytic mechanism on human (h) isoform hCA II. [4,5] The same mechanism applies to the other hCAs, as well as to enzyme belonging to other CA genetic families than the α-class, to which hCAs belong, but the metal ion and the residues coordinating it may be different [4,5].

The CA catalytic cycle is well understood due to the wealth of kinetic and X-ray crystallographic studies of these enzymes [4,5,15]. It begins with the nucleophilic attack of the zinc-bound hydroxide species (**b**) towards the CO_2 substrate, properly bound within a hydrophobic pocket nearby. The formed bicarbonate adduct **c** is thereafter displaced by a water molecule to afford the inactive enzyme, with water as the fourth zinc ligand (adduct (**d**)). The regeneration of the zinc hydroxide species (**a**) requires a proton transfer reaction to occur. This transformation, which is also the rate-limiting step of the entire CA catalytic cycle, being assisted by a His residue placed in the middle of the enzyme active site cavity and acting as a proton shuttle residue. This residue possesses a flexible conformation within the active site, which allows the efficient formation of the nucleophilic species of the enzyme (**a**) (**Figure 1.1 a**) [4,5].

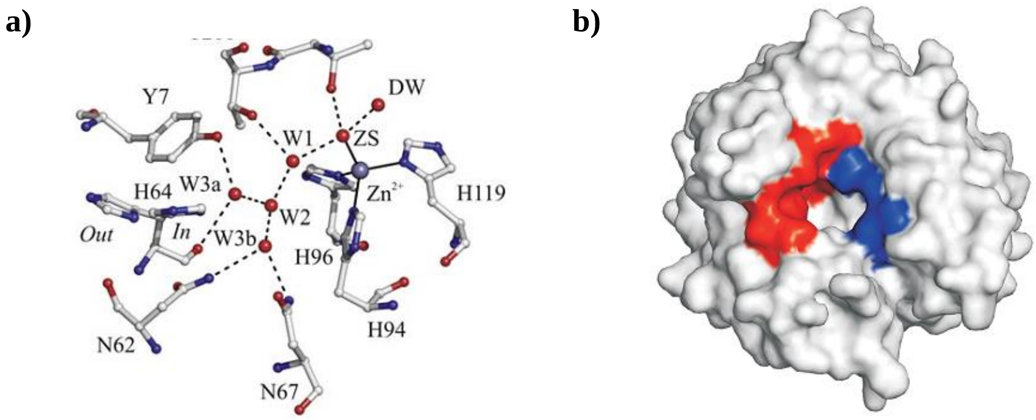

Figure 1.1. a) View of the hCA II active site (PDB accession code 1TE3); His64 is present both in its in and out conformation. Histidines coordinating the zinc ion and the deep water (DW) are also reported; **b)** Solvent accessible surface of hCA II. Residues delimiting the hydrophobic half of the active site cleft are shown in red (Ile91, Phe131, Val121, Val135, Leu141, Val143, Leu198, Pro202, Leu204 Val207 and Trp209), while residues delimiting the hydrophilic one are shown in blue (Asn62, His64, Asn67 and Gln92) [15,16].

CAs active sites are divided in a hydrophilic and hydrophobic sections (**Figure 1.1 b**) [15]. This peculiar structural feature creates preferential ways for the substrate (CO_2) to feed the enzyme and for the products (H^+, HCO_3^-) to be expelled, and thus contributes to the CA large efficiency [15,17].

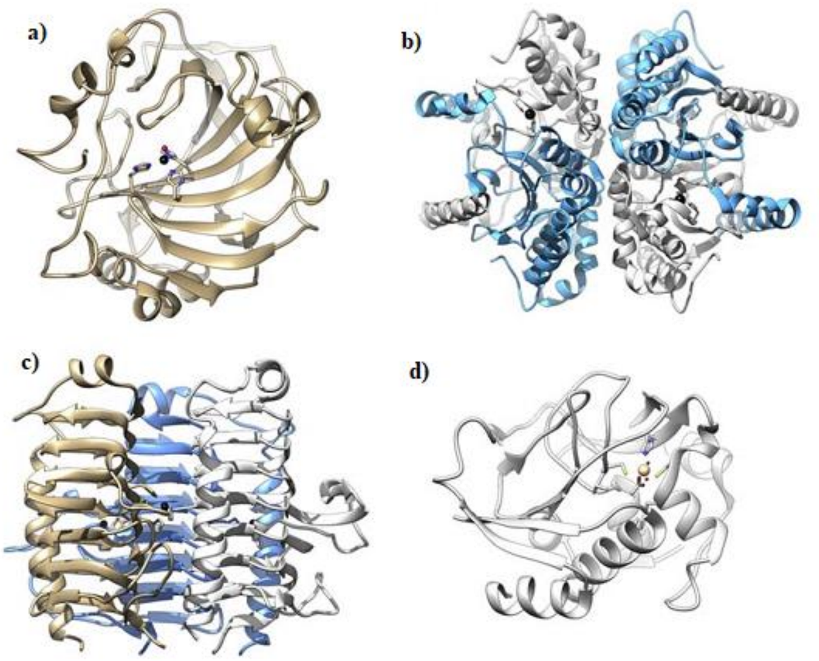

Figure 1.2. Oligomeric states of CAs. **a)** monomeric α-CA II (PDB 1F2W) [19]; **b)** tetrameric β-CA, VchCA (PDB 5CKX); **c)** homotrimeric γ-CA Cam (PDB1QRG), **d)** monomeric ζ–CA, R3 domain of Cd(II)-bound T. weissflogii enzyme (PDB U3K8).

Crystallographic studies demonstrated that most of the α-CAs are organized as monomers or homodimers (**Figure 1.2 a**) [15,18]. The β-class is composed by CAs in dimeric and tetrameric forms depending on the isoform considered (**Figure 1.2 b**) [20,21]. The prototype of γ-class CAs, the protein (Cam), has been characterized from the methanogenic archaeon Methanosarcina thermophila by Ferry's group [22,23] and showed a peculiar structure featuring a left-handed parallel β-helix fold. It has been also shown that this enzyme is active as a trimer (**Figure 1.2 c**). Monomeric state has been reported for the ζ class (**Figure 1.2 d**) [24], whereas for δ–, η–, θ – and ι– classes no crystallographic structures are reported so far.

1.1.2 α-CAs

The α-CAs are the best characterized enzymes as they are expressed in vertebrates, fungi, protozoa, plants, algae, diatoms, archaea and bacteria, being the most populous within CA families [5,18]. Although α-CAs from different species may differ for catalytic activity, cellular localization and oligomeric rearrangement, they all share the same active site architecture, with the Zinc ion coordinated by three histidine residues and a water molecule/hydroxide ion as nucleophilic species for the attack to the CO_2 substrate [4,5].

During my PhD my experimental work was mainly focused on the synthesis and evaluation of CA modulators as potential agents for the treatment of human affecting pathologies due to imbalances of the physiological homeostasis. For such a reason the CA class intended in this Chapter is limited to the α-class expressed in humans. Within the α-class 15 different isoforms have been identified so far. They all differ for cellular localization, tissue distribution and catalytic efficiency, although a rather high structural resemblance is retained [4,5]. Except for hCA VIII, X and XI, which are devoid of any catalytic activity [25], the other 12 isoforms are catalytically active and their biochemical and structural features are described in **Table 1.1**.

Isozyme	Subcellular localization	k_{cat}/K_M ($M^{-1}s^{-1}$)	Disease in which it is involved	Quaternary structure
hCAI	Cytosol	5.0×10^7	Retinal/celebral edema	Monomer
hCAII	Cytosol	1.5×10^8	Glaucoma Edema Epilepsy Altitude sickness	Monomer
hCAIII	Cytosol	2.5×10^5	Oxidative stress	Monomer
hCAIV	Membrane-associated	5.1×10^7	Glaucoma Retinitis pigmentosa Stroke	Monomer
hCAVA	Mitochondria	2.9×10^7	Obesity	Monomer
hCAVB	Mitochondria	9.8×10^7	Obesity	Monomer
hCAVI	Secreted	4.9×10^7	Cariogenesis	Dimer
hCAVII	Cytosol	8.3×10^7	Epilepsy	Monomer
hCAIX	Membrane-associated	5.4×10^7	Cancer	Dimer
hCAXII	Membrane-associated	3.5×10^7	Cancer Glaucoma	Dimer
hCAXIII	Cytosol	1.1×10^7	Sterility	Monomer
hCAXIV	Membrane-associated	3.9×10^7	Epilepsy Retinopathy	Monomer

Table 1.1 Biochemical and structural features of catalytically active hCA isoforms [26].

The catalytic efficiency of these isoforms widely ranges from a k_{cat}/K_M of 1.5×10^8 for the CA II to 2.5×10^5 as for the CA III [26-28]. These differences have been largely ascribed to the role played by the His 64 (or other residues in some limited cases) which acts as proton shuttle and to other residues assisting the proton extrusion from the cavity, which can vary from an isoform to another [16,17, 28-29].

CA I and CA II are cytosolic expressed isoforms and are largely expressed within all tissues. As showed in **Table 1.1**, CA I is much less catalytically efficient than CA II, but evidences suggested that CA I can act in place of CA II in some physiological processes such as cell respiration [30-32]. Since these isoforms are largely expressed and are involved in several metabolic processes, their modulation may have multiple therapeutic applications (i.e. antiglaucoma, diuretics, Alzheimer) [4,5,12]. CA III is also a cytosolic expressed isoform, with high abundance in skeletal muscles. A role in the management of oxidative stress in this compartment has been postulated for this isoform. Beside the regulation of CO_2 levels it has been speculated to provide protections from ROS [33-35].

CA IV is a GPI-anchored, membrane associated isoform with no *N*-glicosylation sites. The peculiar feature of CA IV is the presence of two disulfide bonds between Cys6-Cys18 and Cys 28-Cys211 [36-38]. These bonds confer to CA IV an unusual stability to denaturation by SDS and turned out to be essential for the enzyme activity as their reduction or alkylation resulted in inactivation up to 70 % [37]. CA IV is expressed in kidney, liver, alveolar and brain capillary endothelial cells, skeletal and cardiac muscles [38-42]. In particular, the presence of CAIV along with other membrane associated isoforms such as CA IX and XIV in the heart muscle highlighted their important role in regulating excitation-contraction coupling [41,42]. From the first study of CAs in a metabolon which showed the association of chloride bicarbonate anion exchange proteins (AEs) with CA II [43], several other studies demonstrated that CAIV is the extracellular component of a bicarbonate transport metabolon, formed along with an anion exchange protein and intracellular CA II [44]. A fisical and functional association between CA IV and Na^+/HCO_3^- cotransporter 1 (NBC-1) was discovered, confirming the role of this isoform in regulating heart processes [44,45]. In the T tubular membrane the buffering action is also supported by CA IX, mainly in the pathway of lactate transport [46]. A further validation of the strong connection between CAs and heart came from the observation of the role played by CA in mediating the hypertrophic response of cardiac myocytes to phenylephrine (PE) [47]. CA inhibition was found to mitigate the hypertrophic phenotype, thus suggesting that CA inhibition represents an effective therapeutic approach towards heart failure [47]. Moreover, the gene encoding CA IV was found to be induced at 2 to 24 h after stroke in ischemic brain and peripheral white blood cells, proving its role into the inflammatory responses after stroke [48]. Interestingly, CA IV was recently found to be a novel tumour suppressor in colorectal cancer (CRC) through the inhibition of the Wnt signalling pathway by targeting the WTAP–WT1–TBL1 axis. CAIV methylation can be thus used as an independent biomarker for the recurrence of CRC [49].

It is well reported in the literature that CA VA and CA VB are particularly involved in several metabolic processes, among which ureagenesis, gluconeogenesis and lipogenesis [50-52]. CA VA is the mitochondrial isoform mainly expressed in the liver, but it was detected also in skeletal muscle and kidney, whereas CA VB was found to be expressed in most tissues [53,54]. The role of mitochondrial CAs is to assist the mitochondrial pyruvate carboxylase enzyme (PC) to afford carbon units, in the form of bicarbonate ions. As HCO_3^- does not freely cross the inner mitochondrial membrane, mitochondrial CAs appear to be essential to convert CO_2 (permeable) to HCO_3^-, which are incorporated in the pyruvate to form oxaloacetate. The latter in turn is then converted into citrate through the reaction with acetyl coenzyme A (Ac-CoA) [5,55]. CA VA and B were also been found in neuronal cells of rodents [56]. Two possible roles have been hypothesized for these enzymes: *i*) regulation of intramitochondrial calcium levels and *ii*) regulation of neuronal bicarbonate homeostasis. The first process can be involved in prevention of neuronal degeneration whereas the second one could participate to neuronal transmission [57].

CA VI is the only secreted isoform isolated in saliva and milk. It has been postulated to be involved in cariogenesis process. However, the topic is still controversial [5,58-60].
CA VII is a cytosolic isoform endowed of high catalytic efficiency, as hCA II, but with limited tissue distribution [15,61]. It is mostly expressed in brain tissues, stomach, colon, liver and skeletal muscle. Besides the well defined role in epileptogenesis [62,63], a protecting role played by hCA VII in defending cells from oxidative stress has been suggested [64].

Among the many CA isoforms present in humans, CA IX and XII have a wide distribution in various tumors and are present in reduced amounts in normal tissues [5,65-70]. CA IX is a multi-domain membrane-associated enzyme, consisting of an *N*-terminal proteoglycan-like (PG) domain, a highly conserved catalytic domain (CD), a transmembrane (TM) and an intracytoplasmic section (IC) [67]. CA XII is also a multi-domain membrane-associated enzyme with an α-helical TM region and short IC tail but with no PG domain. Recent advances in the field validated CA IX, and marginally CA XII, as therapeutic targets for the treatment of metastatic tumors [65-70]. They are also expressed in normal tissues, with a very different distribution from each other. CA IX was identified in kidney, intestine, reproductive epithelium and eyes, whereas CA XII was mostly found in kidney, brain, lung, gut, reproductive tract and to be involved in the tumor growth according to slightly different mechanisms when compared to the IX [65,69, 71-74].

CA XIII is a cytosolic relatively recently discovered isoform among the CA family [75]. It was found to be widely expressed in gastrointestinal tract and reproductive organs but more inhibition and activation studies are needed in order to better define its physiological roles and any possible therapeutic application of its modulation [75].

CA XIV is a membrane associated isoform, and its role in regulation cardiac functionality has been already described within the CA IV discussion. It has also found to be involved in retinal and brain pH regulation. Its validation as therapeutic target still is far to be defined [41,76-78].

1.2 Carbonic Anhydrases as Drug Targets

1.2.1 CAIs Mechanisms

To date large series of compounds have been explored and/or used as CA inhibitors (CAIs), and many of them exert their enzymatic activity through different mechanisms [15]. The major chemical entities involved in inhibition of the CAs are divided in five main groups [15,79,80] (**Figure 1.3**).

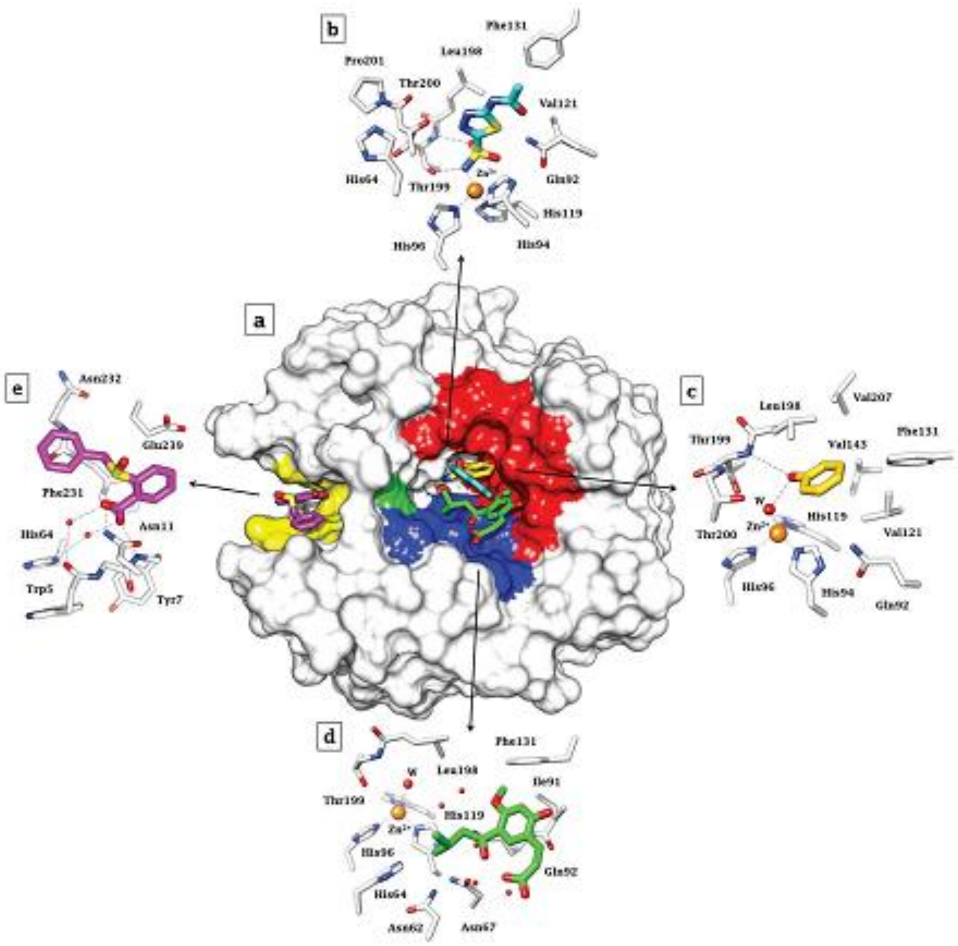

Figure 1.3. CA inhibition mechanisms. **(a)** hCA II active site with three superimposed inhibitors: acetazolamide **1**(blue); phenol **18** (yellow), hydrolyzed natural product coumarin green (**26**). The hydrophobic half of the active site is coloured in red, the hydrophilic one in blue. His64, the proton shuttle residue is in green (surface representation) (PDB files codes: 3HS4, 3F8E, 4QY3). The hydrophobic adjacent pocket where inhibitors bind outside the active site is shown in yellow with the inhibitor **28** represented in magenta. The detailed interactions for the binding of the four inhibitors, with their different inhibition mechanisms are shown in **(b)** for acetazolamide **1, (c)** for phenol **18**, **(d)** for the 2-hydroxy-cinammic acid derivative **26** band **(e)** for the benzoic acid derivative **28** [80].

To the first group belong the so called zinc binder inhibitors, which include the sulfonamides and their isosters, sulfamates and sulfamides [81], dithiocarbamates [82], monothiocarbamates [83] and xanthates [84], as well as carboxylic acids and hydroxamates

[85]. These compounds coordinate the zinc ion within the active site in the deprotonate form, thus replacing the water molecule/OH^-.

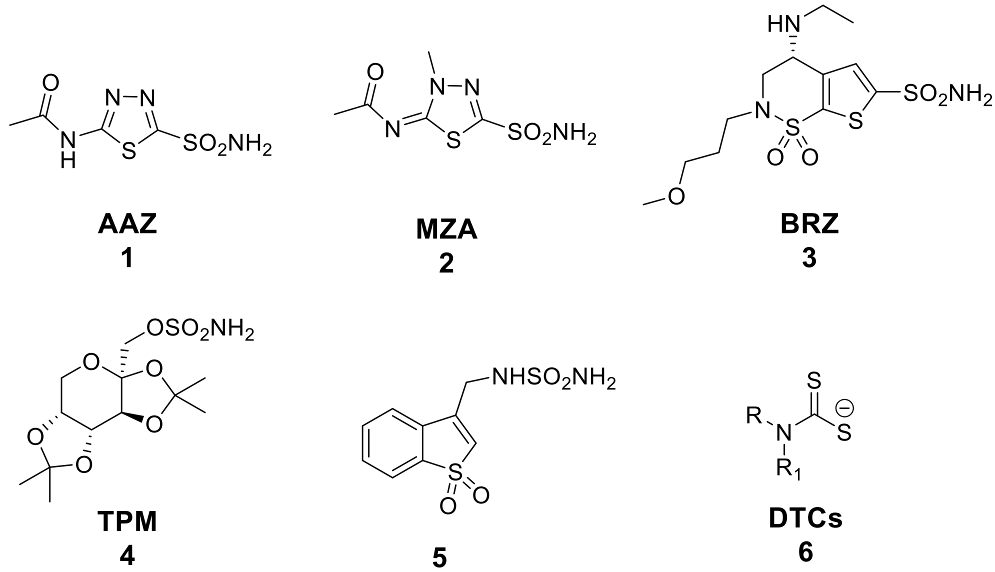

Figure 1.4. Some examples of Zinc Binder Inhibitors.

Among them, the primary sulfonamides ($R\text{-}SO_2NH_2$) containing compounds still represent the main class of CAIs explored, along with their bioisosteric analogs such as the sulfamates and sulfamides ($\text{-}NH\text{-}SO_2NH_2$) [86]. Acetazolamide **1**, Metazolamide **2**, Brinzolamide **3** and Topiramate **4** are only few examples of the sulfonamide based CAI clinically used [5,86-88]. These family of CA inhibitors is usually devoid of any selectivity towards a particular isoform over the others [5]. Thus alternative design approaches have been developed with the aim to address the lack of selectively profiles associated to the CAIs of this type. Among others, the "tail approach" is the most versatile [89,90]. Such an approach takes advantage from the ability of the tail moieties of the ligand to specifically interact with the aminoacid residues present at the rim of the enzyme cavity, which is the most variable among the various enzyme isoforms [89,90]. Moreover, the chemical variety associated to such tails can modulate the physical-chemical properties of the entire molecule, thus allowing the CA selectivity enzymatic profiles to be modulated by means of penetrability through membranes and other pharmacologic properties [15,89,90]. The tail approach led to the synthesis of a huge number of derivatives, some of them showing high selectivity towards CA IX and and XII. Pyridinium salts **7** and **8** [65,91], fluorescent sulfonamides **9** and **10** [65,92,93], compounds activated by hypoxia **11** [94], sugar containing CAIs (**12** among the others) [95], substituted-

1,2,3-triazinyl ones **13** [96] and ureido compounds **14-16** [97,98] are some successful such examples (**Figure 1.5**). Among the plethora of promising compounds investigated so far, the ureido derivative **17** SLC-0111 (also known as WBI-5111) entered Phase II clinical trials in association with gemcitabine for the treatment of hypoxic solid tumors in 2018 [99-101].

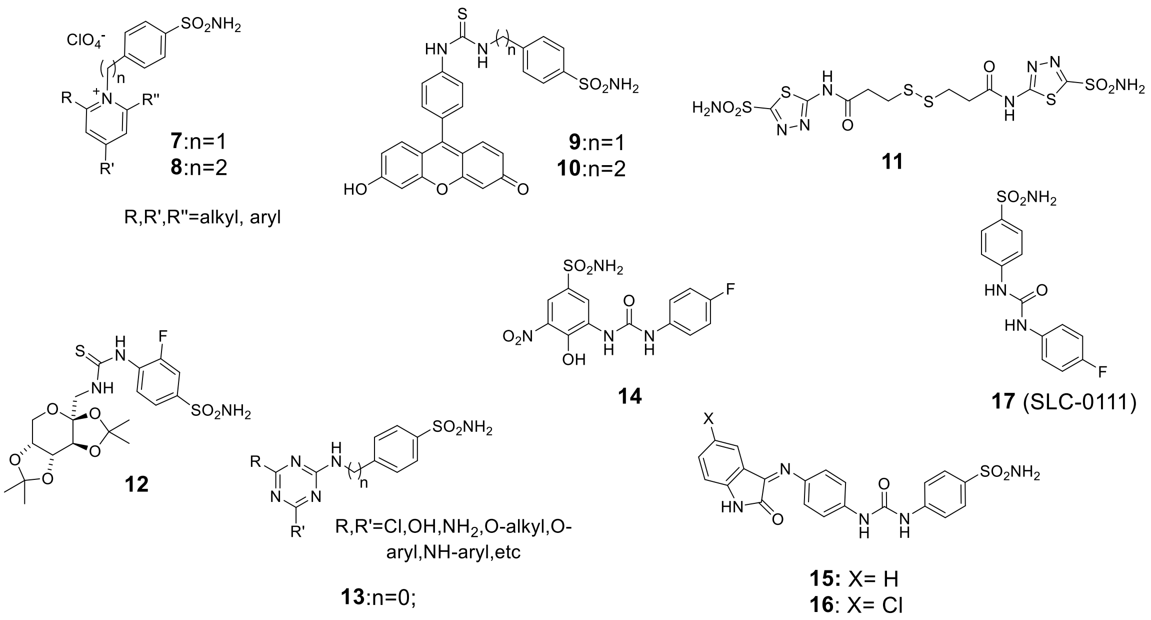

Figure 1.5. Structures of selective Zinc-binders CA IX inhibitors reported in the last years.

In the second group are present compounds that by anchoring the zinc coordinated water/OH^- hamper the continuation of the catalytic cycle. Phenols **18** [102], polyamines (**19** and **20** among the others) [103], thioxocoumarins **21** [104] and the sulfonic acids **23** obtained from CA catalyzed hydrolysis of benzo[*e*][1,2]oxathiine 2,2-dioxides, also known as sulfocoumarins **22** [105,106] do present such a binding mode (**Figure 1.6**).

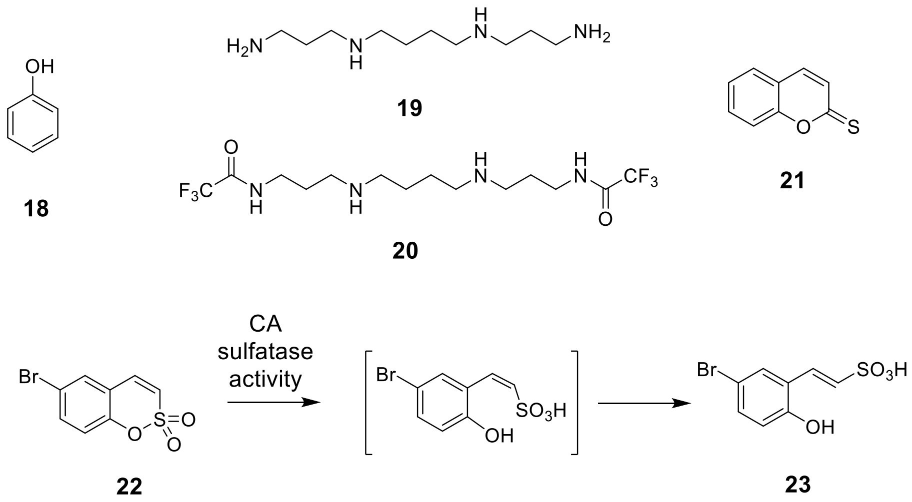

Figure 1.6. Examples of compounds which anchor the zinc-coordinated water molecule.

In particular, the polyamines are an unexpected class of CAIs. Before their mechanism of action as CAIs has been reveiled by means of X-ray crystallographic experiments of the spermine **19** in adduct with hCA II (**Figure 1.7**) , the aliphatic polyamines were thought to act exclusively as CAAs, such as the amino acids or biogenic amines [103]. A large screen of several natural and synthetic polyamines against all active hCA isoforms known to date, revealed for these compounds quite good inhibition potencies (K_I values from nanomolar to millimolar range) and interesting selectivity profiles. The latter, was found to be deeply affected by the substitution grade of the amines, the distance between the nitrogen atoms and the total length of the amine backbone [103]. However, after this first work published in 2010 [103], no others CAIs belonging to this class have been evaluated so far. A deeper exploration of these interesting and relatively unexplored inhibitors is fully justified.

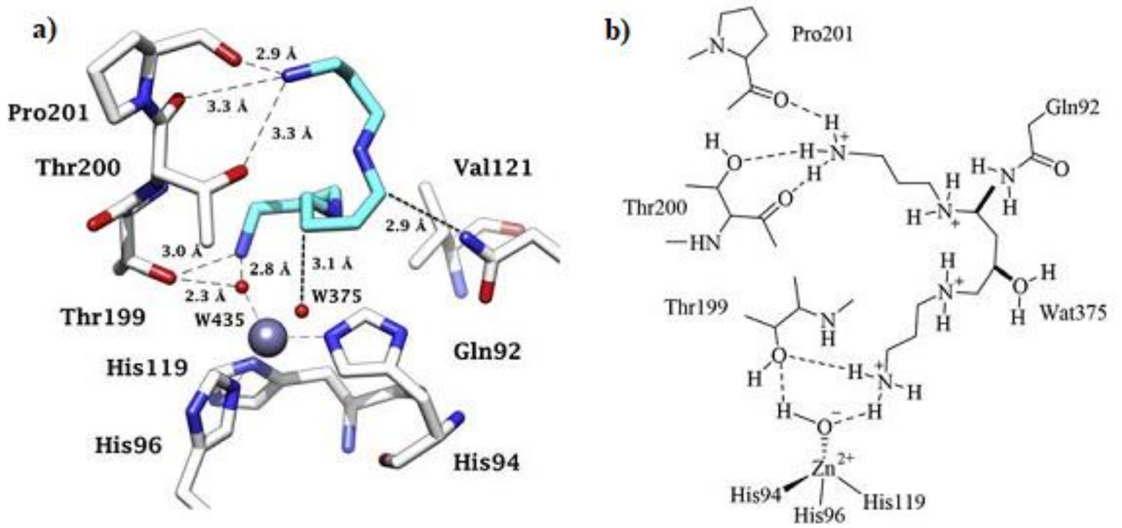

Figura 1.7. a) Spermine 1**9** (cyan) in adduct with hCA II (PDB 3KWA). Hydrogen bond distances are given in Å. **b)** Schematic illustration of the hCA II/ 1**9** interactions. Hydrogen bonds are shown as dashed lines. Two clashes are shown as thick lines [103]

The coumarins (general structure **24**) and some of their derivatives, such as thiocoumarin (general structure **25**), represent the third group of CAIs which have been proved to exert their inhibition through occlusion of the enzymatic cavity after hydrolysis of the lactone moiety [107-109]. This identifies the CAI-based cumarins as prodrugs, being active only when the α-CA esterase activity hydrolyses the lactone ring (generating compounds with general structures **26** and **27**) (**Figure 1.8**). Interestingly, this inhibitor class generally shows intrinsically selective inhibitory activity towards the tumor associated isoforms CA IX and CA XII over the ubiquitous isoforms CA I and II [107-110].

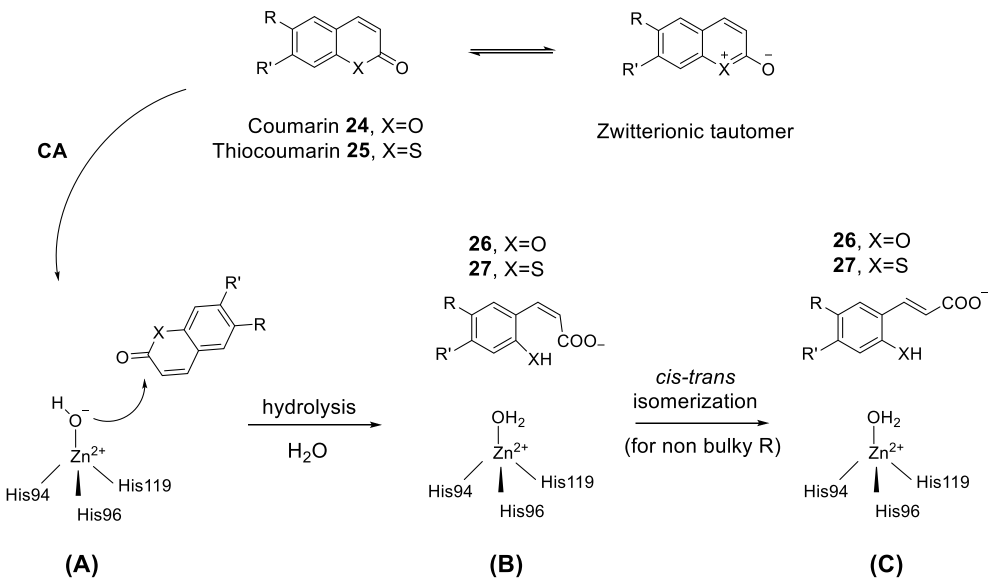

Figure 1.8. Proposed inhibition mechanism of CAs by coumarins/thiocoumarins **24**/**25**, leading to *cis*- or *trans*-2-hydroxy **26**/mercapto-cinnamic acids **27**. **(A)** Hydrolysis of the lactone ring. **(B)** Movement of the hydrolysis product (as *cis* stereoisomer) toward the entrance to the active site cavity. **(C)** *Cis–trans* isomerization of the hydrolysis product. [107,108].

The fourth class includes carboxylic acid derivatives of the 2-(benzylsulfinyl)benzoic acid type **28**, which bind outside of the active site (**Figure 1.9**) [111]. Originally these compounds were synthetized to extend the SAR knowledge of orto-substituted benzoic acid derivatives. However, the strong inhibition potency against CA II along with a very high selectivity justified further exploration of the binding mode of these compounds, by means of crystallographic studies. The results revealed that the compound **28** was bound in an enzyme pocket far from the catalytic cavity, surrounded by several residues such as His 64. The inhibition activity of these compounds was thus ascribed to the interaction of the carboxylic moiety with the proton shuttle, blocking it in the *out*, non active, conformation through a bridging of water molecules [111].

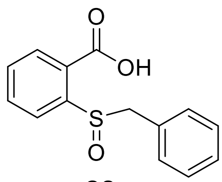

28

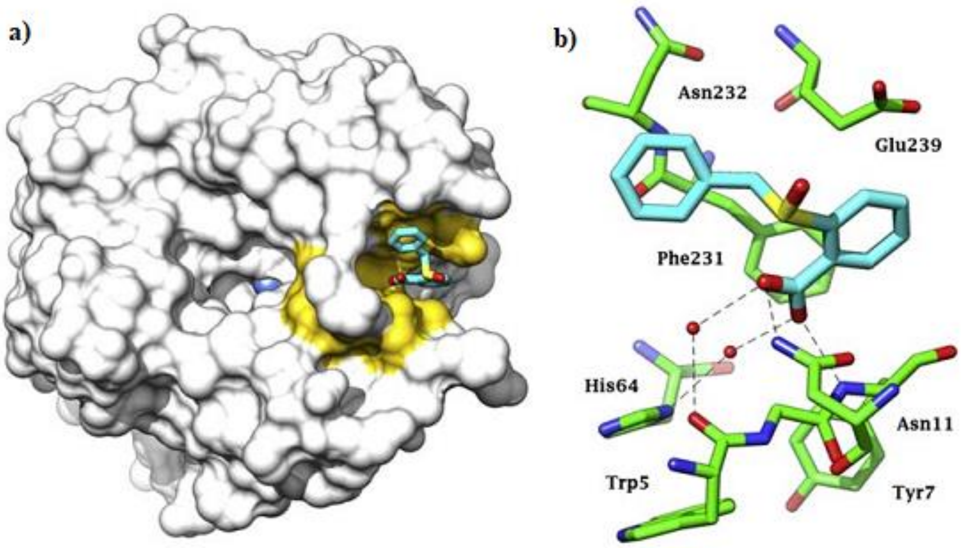

Figure 1.9. **a)** Solvent accessible surface of hCA II in its complex with **28**. Residues delimiting the cavity where the inhibitor is bound are highlighted ingold. The catalytic zinc ion is represented as a blue sphere at the bottom of the active site cavity. **b)** Cartoon view of the binding mode of **28** into hCA II accessory pocket. Hydrogen bonds are represented asblack dashed lines.

Finally, a fifth class of CAIs includes compounds that inhibit the enzyme by means of an unknown mechanism. This class include secondary/tertiary sulfonamides, ethers and other compounds, for which no X-ray crystal structures in adduct with the enzymes were obtained so far [112-114] (compounds **29-31**, among the others. **Figure 1.10**). Several series of this kind of compounds have been reported so far, with K_I values ranging from micro to nanomolar values. Among them, fluorinated tertiary benzensulfonamidic compounds are of particular interest because the crucial role played by the fluorine atom in determining they inhibition potency and selectivity. When compared to the chlorinated analogues, these fluorinated compounds showed indeed a very higher SI CA II/CAIX [113].

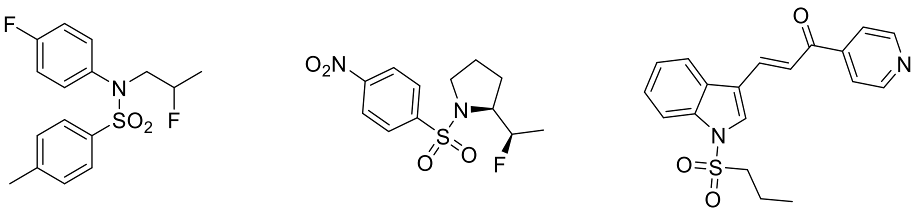

29 **30** **31**

Figure 1.10. CAIs that inhibit the enzyme by means of an unknown mechanism [112-114].

1.2.2 CAAs Mechanism

Early studies conducted in 1940 suggested that biogenic amines can also act as CA activators (CAAs) [115]. However, it was only in 1990s that CA activation mechanism was validated [116]. One of the main reasons behind the scepticism about the possibility to positively modulate CA activity came from the consideration that CA is a very efficient enzyme, which doesn’t need to be further activated [117]. This idea proved to be uncorrect. Kinetic and crystallographic studies confirmed the existence of an activation mechanism and that the main actors involved are the natural and synthetic amines [118-121]. Moreover, pharmaceutical applications for CAAs have also been defined, even if the field is relatively new [121-123]. The first crystallographic structure of a CA activator with CA II was obtained for CA II in complex with histamine **37**, and allowed us to understand the activation mechanism [116]. The catalytic cycle of CAAs are reported below (**Equation 1.2)** [118].

$$EZn^{2+} - OH_2 + A \rightleftharpoons \underbrace{[EZn^{2+} - OH_2 - A] \rightleftharpoons [EZn^{2+} - HO^- - AH^+]}_{\textbf{Enzyme-activator complexes}} \rightleftharpoons EZn^{2+} - HO^- + AH^+$$

Equation 1.2

As shown, the activators affect the rate-determining step of the catalytic cycle, helping the proton shuttle His 64 in the proton transfer process which generates the zinc-bound hydroxide species. The activator binding site is quite far from the zinc ion, in a region occupied by His 64. Interestingly, this has been proved to be also the same binding pocket of hydrolysed cumarins **26**, which act as CAIs occluding the entrance of the active site, as already said in **Section 1.2.1** (**Figure 1.11**) [80,108].

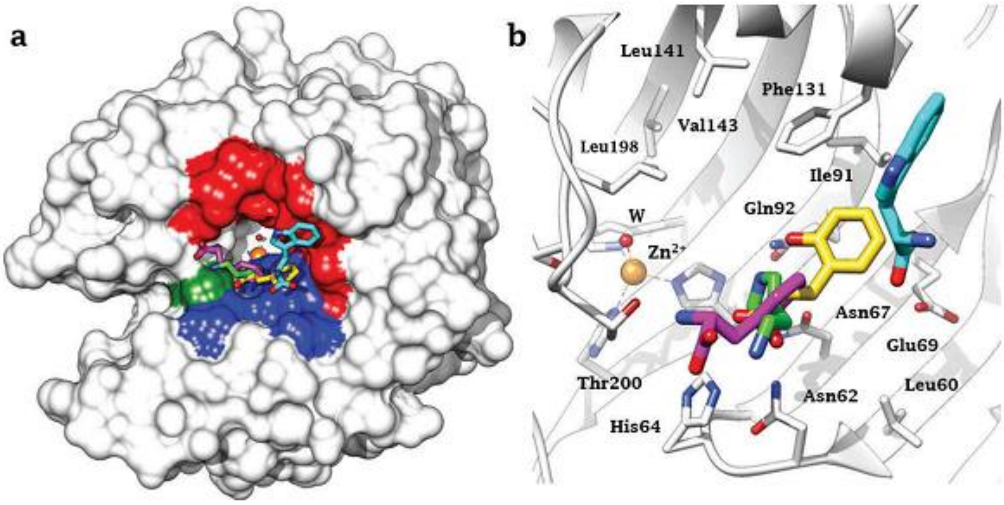

Figure 1.11. hCA II complexed with the CAAs and the hydrolyzed coumarin (2-hydroxycinamic acid **26**) [80].

Several other CAAs have been subsequently crystalized within the active site of several CA isoforms, such as D-His **32**, D-Trp **36** and L- and D-Phe **33** and **34**, thus further confirming the mechanism of action of such compounds (**Figure 1.12**) [118]. Many activation data against several isoforms have been also collected analysing these compounds and analogues thereof by means of Stopped-Flow technique, allowing the first definition of SARs for this class [118]. However, these results also highlighted the non-selectivity showed by most of the analyzed compounds. Moreover, it could be better to find CAAs with no structural relation with autacoid molecules to avoid side effects and a complex pharmacology [118].

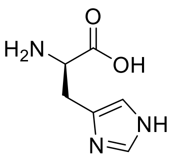

D-His
32

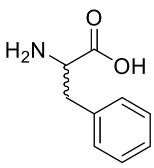

L-Phe, 33
D-Phe, 34

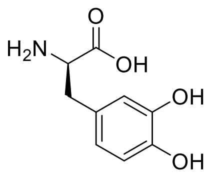

D-DOPA
35

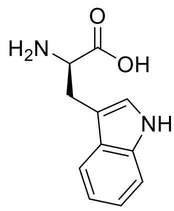

D-Trp
36

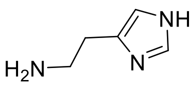

Histamine
37

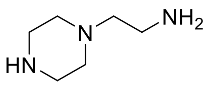

38

Figure 1.12. Some CAAs reported so far.

1.2.3 CA modulators: Pharmacological Applications

In light of the wide distribution of CA isoforms in several living species and considering the large number of isoforms (12 catalitically active), modulation of CA activity may have pharmacological applications. Some of them are known since long time, whereas others have been emerged only recently [5,124-134].

First generation of CAIs, including acetazolamide **1**, metazolamide **2**, sulthiame **39** and dichlorphenamide **40** have been used as antiglaucoma, antiepileptic and diuretics (**Figures 1.4** and **1.13**) [5,88,124-127]. FDA-Approved indications for **AAZ** include glaucoma, idiopathic intracranial hypertension, congestive heart failure, altitude sickness, periodic paralysis and epilepsy [5,88,124-127]. Topical agents such as brinzolamide **3** have been subsequently introduced in clinics [5,125,126]. The use of CAIs as antiobesity drugs is also a validated approach [128], with a delayed-release formulation containing topiramate **4** and phentermine available on the market and a bupropion-zonisamide slow-release compound undergoing FDA phase III clinical development [130-132].

New applications of CAIs in therapy are in the management of neuropatic pain and arthritis, where the involvement of CAs II, VII, IX and XII in the rising and mainainance of the pathologies has been highlighted [133-135]. Moreover, the role of CA IV and other CA isoforms in regulating excitation-contraction coupling in heart and the evidences that inhibition of CAs can revert cardiomioctyte hypertrophy highlithed a primising use of CAIs for the treatment of heart related diseases [41,47].

Validation of CA IX and XII as antitumor targets opened the way for a new promising therapeutic approach to treat cancer [136,137]. Among the selective CA IX inhibitors designed so far, noteworthy SLC-0111 **17** (also known as WBI-5111 since its acquisition from Welichem Biotech Inc.), entered Phase II clinical trials in association with gemcitabine for the treatment of hypoxic solid tumors in 2018 (**Figure 1.5**) [99-101].

Another recent and intriguing applications of CAIs as antiinfectives is currently taking place. CAs from pathogens have been found to be crucial for pH homeostasis, biosynthetic reactions, for virulence and quorum sensing regulation [138]. The effect of their inhibition on cellular viability has been characterized for some microorganisms, whereas for others the exact role played by CAs is still under investigations [138] (compounds **42**, **43**, **44**, among the others. **Figure 1.13**).

CA activations is also a recently growing research field. As these compounds have been found to enhance cognitions in mouse models, pharmacological applications for such derivatives have been delineated in the field of neurodegenerative diseases and aging [118,122,123].

The indiscriminate CA modulation leads to undesired side effects. For this reason, to ensure an effective and safe pharmacological outcome from the CA modulators, a proper selectivity profile is required [5,15]. Enormous progresses have been made in this direction during the last years, with several approaches introduced (i.e. tail approach) and new chemotypes discovered acting with various mechanisms [15,89,90]. However, addressing a proper selectivity to the pharmacological target still represents a challenge. The hybridization strategy, consisting in merging multiple pharmacophoring entities hitting different biological targets, is also a recently pursued approach in the design of new effective CA modulators, which has been exploited for CA inhibition up to now. This multi-target design approach has been used for the synthesis of antiglaucoma, antiinflamatory and antitumor agents, with promising results obtained (compounds **45** and **46** among the others. **Figure 1.13**) [135,139,140].

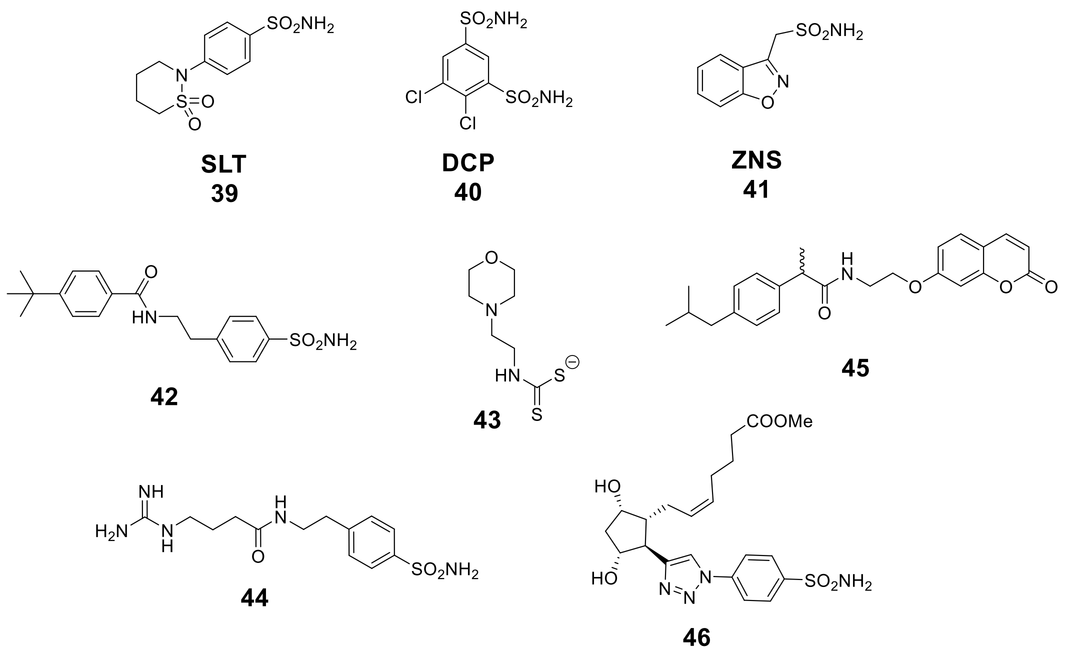

Figure 1.13. Example of CAIs in clinical use or with promising pharmacological applications.

1.3 Measuring the CA Inhibition/Activation

1.3.1 Stopped Flow CO_2 Hydrase Assay

To evaluate the activity of a CA modulator, the most used and well-established assay is currently the stopped flow kinetic method [141]. This spectrophotometric method allows to define the K_I values (or K_A for activators) as measure of the effectiveness of a modulator in varying the hydration reaction rate. In this assay, a solution of the enzyme is mixed with a saturated solution of the substrate CO_2, and the rate of reaction progress is measured using an appropriate pH indicator. The lowest is the ligand concentration used to modulate the enzyme activity, the more potent the compound results.

During my PhD I applied this method to determine the inhibition potency of compounds synthetized on the course of various projects. These works led to the indentifications of some interesting lead componds, with several therapeutic applications [142-150].

1.4 References

1. Busa WB, Nuccitelli R. Metabolic regulation via intracellular pH. Am J Physiol. 1984, 246,409-38.
2. Aoi W, Marunaka Y. Importance of pH Homeostasis in Metabolic Health and Diseases: Crucial Role of Membrane Proton Transport. Biomed Res Int. 2014, 2014-8.
3. Saleh AM, Rombola G, Batlle DC. Intracellular H+ buffering power and its dependency on intracellular pH. Kidney Int. 1991, 39, 282-8.
4. Supuran CT. Structure and function of carbonic anhydrases. Biochem J. 2016, 473, 2023–32.
5. Supuran CT. Carbonic anhydrases: novel therapeutic applications for inhibitors and activators. Nature Reviews Drug Discovery. 2008, 7, 168–81.
6. Supuran CT, De Simone G. In: Supuran CT, De Simone G, editors. Carbonic anhydrases as biocatalysts. Walthman, MA: Elsevier; 2015. p. 3.
7. Kaplan A, Reinhold L. CO2 concentrating mechanisms in photosynthetic microorganisms. Annu Rev Plant Physiol Plant Mol Biol. 1999, 50, 539–70.
8. Krungkrai SR, Suraveratum N, Rochanakij S, Krungkrai J. Characterisation of carbonic anhydrase in Plasmodium falciparum. Int J Parasitol. 2001, 31, 661–8.
9. Sein KK, Aikawa M. The pivotal role of carbonic anhydrase in malaria infection. Med Hypotheses. 1998, 50, 19–23.
10. Joseph P, Ouahrani-Bettache S, Montero JL, Nishimori I, Minakuchi T, Vullo D, et al. A new betacarbonic anhydrase from Brucella suis, its cloning, characterization, and inhibition with sulfonamides and sulfamates, leading to impaired pathogen growth. Bioorg Med Chem. 2011, 19, 1172–78.
11. Kanbar B, Ozdemir E. Thermal stability of carbonic anhydrase immobilized within polyurethane foam. Biotechnol Prog. 2010, 26,1474–80.
12. Supuran CT. Carbonic anhydrase inhibitors and their potential in a range of therapeutic areas. Expert Opin Ther Pat. 2018, 28,709–12.
13. Smith KS, Jakubzick C, Whittam TS, Ferry JG. Carbonic anhydrase is an ancient enzyme widespread in prokaryotes. Proc Natl Acad Sci USA. 1999, 96, 15184-9.
14. Jensen EL, Clement R, Kosta A, et al. A new widespread subclass of carbonic anhydrase in marine phytoplankton. Isme J. 2019, 13, 2094–06.

15. Alterio V, Di Fiore A, D'Ambrosio K, et al. Multiple binding modes of inhibitors to carbonic anhydrases: how to design specific drugs targeting 15 different isoforms? Chem Rev. 2012, 112, 4421–68.
16. Fisher Z, Hernandez Prada JA, Tu C, Duda D, Yoshioka C, An H, et al. Structural and kinetic characterization of active-site histidine as a proton shuttle in catalysis by human carbonic anhydrase II. Biochemistry. 2005, 44, 1097-05
17. Domsic JF, McKenna R. Sequestration of carbon dioxide by the hydrophobic pocket of the carbonic anhydrases. Biochim Biophys Acta. 2010, 1804, 326-31.
18. Lomelino CL, Andring JT, McKenna R. Crystallography and its impact on carbonic anhydrase research. Int J Med Chem. 2018, 2018, 9419521
19. Minakuchi T, Nishimori I, Vullo D, Scozzafava A, Supuran CT. Molecular cloning, characterization and inhibition studies of the Rv1284 □-carbonic anhydrase from Mycobacterium tuberculosis with sulfonamides and a sulfamate. J Med Chem. 2009, 52, 2226-32
20. Lehneck R, Neumann P, Vullo D, Elleuche S, Supuran CT, Ficner R, et al. Crystal structure of two tetrameric carbonic anhydrases from the filamentous ascomycete Sordariamacrospora. FEBS J. 2014, 281, 1759-72.
21. Ferraroni M, Del Prete S, Vullo D, Capasso C, Supuran CT. Crystal structure and kinetic studies of a tetrameric type II □-carbonic anhydrase from the pathogenic bacterium Vibrio cholerae. Acta Crystallogr D Biol Crystallogr. 2015, 71, 2449-56
22. Iverson TM, Alber BE, Kisker C, Ferry JG, Rees DC. A closer look at the active site of gamma-class carbonic anhydrases: high-resolution crystallographic studies of the carbonic anhydrase from Methanosarcina thermophila. Biochemistry. 2000, 39, 9222-31.
23. Alber BE, Ferry JG. A carbonic anhydrase from the archaeon Methanosarcina thermophile. Proc Natl Acad Sci USA. 1994, 91, 6909-13.
24. Alterio V, Langella E, Viparelli F, Vullo D, Ascione G, Dathan NA, et al. Structural and inhibition insights into carbonic anhydrase CdCA1 from the marine diatom Thalassiosira weissflogii. Biochimie. 2012, 94, 1232-41.
25. Aspatwar A, Tolvanen ME, Ortutay C, Parkkila S. Carbonic anhydrase related proteins: molecular biology and evolution. Subcell Biochem. 2014, 75, 135-56

26. Hilvo M, Baranauskiene L, Salzano AM, Scaloni A, Matulis D, Innocenti A, et al. Biochemical characterization of CA IX, one of the most active carbonic anhydrase isozymes. J Biol Chem 2008, 283, 27799-809.
27. Silverman DN, Lindskog S. The catalytic mechanism of carbonic anhydrase: implications of a rate-limiting protolysis of water. Acc Chem Res. 1988, 21, 30-6.
28. Paranawithana SR, Tu C, Jewell DA, Laipis PJ, Silverman DN. Catalytic enhancement of carbonic anhydrase III by introduction of histidine 64 as proton shuttle. In: Botre' F, Gros G, Storey BT, editors. Carbonic anhydrases from biochemistry and genetics to physiology and clinical medicine. Weinheim: Verlag Chemie. 1991, p. 14-21.
29. Tu CK, Silverman DN, Forsman C, Jonsson BH, Lindskog S. Role of histidine 64 in the catalytic mechanism of human carbonic anhydrase II studied with a site-specific mutant. Biochemistry. 1989, 28, 7913-8.
30. Chang X, Zheng Y, Yang Q. Carbonic anhydrase I (CA1) is involved in the process of bone formation and is susceptible to ankylosing spondylitis. Arthritis Res Ther. 2012, 14,176.
31. Chang X, Han J, Zhao Y, Yan X, Sun S, Cui Y. Increased expression of carbonic anhydrase I in the synovium of patients with ankylosing spondylitis. BMC Musculoskelet Disord. 2010, 11, 279.
32. Supuran CT, Scozzafava A. Carbonic anhydrases as targets for medicinal chemistry. Bioorg Med Chem. 2007, 15, 4336–50.
33. Kim G, Levine R. Molecular determinants of S-glutathionylation of carbonic anhydrase 3. Antioxid Redox Signal. 2005, 7, 849–54.
34. Kim G, Lee T, Wetzel P, Geers C, Robinson M, Myers TG, et al. Carbonic anhydrase III is not required in the mouse for normal growth, development, and life span. Mol Cell Biol. 2004, 24, 9942–7.
35. Dai H, Hong C, Liang S, Yan M, Lai G, Cheng A, et al. Carbonic anhydrase III promotes transformation and invasion capability in hepatoma cells through FAK signaling pathway. Mol Carcinog. 2008, 47, 956–63.
36. Zhu XL, Sly WS. Carbonic anhydrase IV from human lung. Purification, characterization, and comparison with membrane carbonic anhydrase from human kidney. J Biol Chem. 1990, 265, 8795–801

37. Waheed A, Okuyama T, Heyduk T, Sly WS. Carbonic anhydrase IV: purification of a secretory form of the recombinant human enzyme and identification of the positions and importance of its disulfide bonds. Arch Biochem Biophys. 1996, 333, 432–8.
38. Waheed, A.; Sly, W.S. Membrane associated carbonic anhydrase IV (CA IV): a personal and historical perspective. Subcell Biochem. 2014, 75,157-79.
39. Brown D, Zhu XL, Sly WS. Localization of membrane-associated carbonic anhydrase type IV in kidney epithelial cells. Proc Natl Acad Sci USA. 1990, 87, 7457–61.
40. Waheed A, Zhu XL, Sly WS, Wetzel P, Gros G. Rat skeletal muscle membrane associated carbonic anhydrase is 39-kDa, glycosylated, GPI-anchored CA IV. Arch Biochem Biophys. 1992, 294, 550–6.
41. Scheibe RJ, Gros G, Parkkila S, Waheed A, Grubb JH, Shah GN, et al. Expression of membrane-bound carbonic anhydrases IV, IX, and XIV in the mouse heart. J Histochem Cytochem. 2006, 54, 1379–91.
42. Sender S, Decker B, Fenske CD, Sly WS, Carter ND, Gros G. Localization of carbonic anhydrase IV in rat and human heart muscle. J Histochem Cytochem. 1998, 46, 855–61
43. Sterling, D., Reithmeier, R.A., and Casey, J.R. A Transport Metabolon: Functional Interaction of Carbonic Anhydrase II and Chloride/Bicarbonate Exchangers. J Biol Chem. 2001, 276, 47886 – 47894.
44. Sterling D, Alvarez BV, Casey JR. The extracellular component of a transport metabolon. Extracellular loop 4 of the human AE1 Cl-/HCO3- exchanger binds carbonic anhydrase IV. J Biol Chem. 2002, 277, 25239–46.
45. Alvarez BV, Loiselle FB, Supuran CT, Schwartz GJ, Casey JR. Direct extracellular interaction between carbonic anhydrase IV and the human NBC1 sodium/bicarbonate co-transporter. Biochemistry. 2003, 42,12321–9.
46. Hallerdei J, Scheibe RJ, Parkkila S, Waheed A, Sly WS, Gros G, et al. T tubules and surface membranes provide equally effective pathways of carbonic anhydrase-facilitated lactic acid transport in skeletal muscle. PLoS One. 2010, 5,15137.
47. Alvarez BV, Johnson DE, Sowah D, et al. Carbonic anhydrase inhibition prevents and reverts cardiomyocyte hypertrophy. J Physiol. 2007, 579(Pt 1), 127–145
48. Tang Y, Xu H, Du X, et al. Gene expression in blood changes rapidly in neutrophils and monocytes after ischemic stroke in humans: a microarray study. J Cerebr Blood F. Met. 2006, 26, 1089–1102.

49. Zhang J, Tsoi H, Li X et al. Carbonic anhydrase IV inhibits colon cancer development by inhibiting the Wnt signalling pathway through targeting the WTAP–WT1–TBL1 axis. Gut. 2016, 65, 1482-93.
50. Dodgson SJ, Cherian K. Mitochondrial carbonic anhydrase is involved in rat renal glucose synthesis. Am J Physiol. 1989, 257, 791-6.
51. Lynch CJ, Fox H, Hazen SA, Stanley BA, Dodgson S, Lanoue KF. Role of hepatic carbonic anhydrase in de novo lipogenesis. Biochem. J 1995, 310,197-202.
52. Shah GN, Rubbelke TS, Hendin, J, Nguyen H, Waheed A, Shoemaker JD, Sly WS. Targeted mutagenesis of mitochondrial carbonic anhydrases VA and VB implicates both enzymes in ammonia detoxification and glucose metabolism. PNAS. 2013, 110, 7423–7428.
53. Shah GN, Hewett-Emmett D, Grubb JH, Migas MC, Fleming RE, Waheed A, et al. Mitochondrial carbonic anhydrase CA VB: differences in tissue distribution and pattern of evolution from those of CA VA suggest distinct physiological roles. Proc Natl Acad Sci USA 2010, 97, 1677–82.
54. Fujikawa-Adachi K, Nishimori I, Taguchi T, Onishi S. Human mitochondrial carbonic anhydrase VB—cDNA cloning, mRNA expression, subcellular localization, and mapping to chromosome X. J Biol Chem. 1999, 274, 21228–33.
55. Supuran CT. Carbonic anhydrase inhibitors in the treatment and prophylaxis of obesity. Expert Opin Ther Pat. 2003, 13, 1545-50.
56. Ghandour MS, Parkkila AK, Parkkila S, Waheed A, Sly WS. Mitochondrial carbonic anhydrase in the nervous system: expression in neuronal and glial cells. J Neurochem. 2000, 75, 2212–20.
57. Asiedu M, Ossipov MH, Kaila K, Price TJ. Acetazolamide and midazolam act synergistically to inhibit neuropathic pain. Pain. 2010, 148, 302–8.
58. Fernley RT, Wright RD, Coghlan JP. A novel carbonic anhydrase from the ovine parotid gland. FEBS Lett. 1979, 105, 299–302.
59. Thatcher BJ, Doherty AE, Orvisky E, Martin BM, Henkin RI. Gustin from human parotid saliva is carbonic anhydrase VI. Biochem Biophys Res Commun. 1998, 250, 635–41.
60. Kitade K, Nishita T, Yamato M, Sakamoto K, Hagino A, Katoh K, et al. Expression and localization of carbonic anhydrase in bovine mammary gland and secretion in milk. Comp Biochem Physiol A Mol Integr Physiol. 2003, 134, 349–54.

61. Montgomery JC, Venta PJ, Eddy RL, Fukushima YS, Shows TB, Tashian RE. Characterization of the human gene for a newly discovered carbonic anhydrase, CA VII, and its localization to chromosome 16. Genomics. 1991, 11, 835–48.
62. Halmi P, Parkkila S, Honkaniemi J. Expression of carbonic anhydrases II, IV, VII, VIII and XII in rat brain after kainic acid induced status epilepticus. Neurochem Int. 2006, 48, 24–30.
63. Ruusuvuori E, Li H, Huttu K, Palva JM, Smirnov S, Rivera C, et al. Carbonic anhydrase isoform VII acts as a molecular switch in the development of synchronous gamma-frequency firing of hippocampal CA1 pyramidal cells. J Neurosci. 2004, 24, 2699–707.
64. Del Giudice R, Monti DM, Truppo E, Arciello A, Supuran CT, De Simone G, et al. Human carbonic anhydrase VII protects cells from oxidative damage. Biol Chem. 2013, 394, 1343–8.
65. Svastová E, Hulíková A, Rafajová MA, et al. Hypoxia activates the capacity of tumor-associated carbonic anhydrase IX to acidify extracellular pH. FEBS Lett. 2004, 577, 439–45.
66. Chiche J, Ilc K, Laferriere J, Trottier E, Dayan F, Mazure NM, et al. Hypoxia-inducible carbonic anhydrase IX and XII promote tumor cell growth by counteracting acidosis through the regulation of the intracellular pH. Cancer Res. 2009, 69, 358-68.
67. Alterio V, Hilvo M, Di Fiore A et al Crystal structure of the catalytic domain of the tumor-associated human carbonic anhydrase IX, PNAS 2009, 106, 16233-238.
68. Lee SH, McIntyre D, Honess D, et al. Carbonic anhydrase IX is a pH-stat that sets an acidic tumour extracellular pH in vivo. British Journal of Cancer. 2018, 119, 622–30.
69. Neri D, Supuran CT. Interfering with pH regulation in tumours as a therapeutic strategy. Nat Rev Drug Discov. 2011, 10, 767-77.
70. Berrino E, Supuran CT. Novel approaches for designing drugs that interfere with pH regulation. Expert Opin Drug Discov. 2019, 14, 231–248.
71. Karhumaa P, Parkkila S, Türeci O., et al. Identification of carbonic anhydrase XII as the membrane isozyme expressed in the normal human endometrial epithelium. Mol Hum Reprod. 2000, 6, 68-74.
72. Parkkila S, Parkkila AK, Saarnio J, et al. Expression of the membrane-associated carbonic anhydrase isozyme XII in the human kidney and renal tumors. J Histochem Cytochem. 2000, 48, 1601-8.

73. Pastoreková S, Parkkila S, Parkkila A-K, Opavsk˝ R, Zelnik V, Saarnio J, Pastorek J. Carbonic anhydrase IX, MN/CA IX: analysis of stomach complementary DNA sequence and expression in human and rat alimentary tracts. Gastroenterology. 1997, 112, 398–408.
74. Tureci O, Sahin U, Vollmar E, Siemer S, Gottert E, Seitz G, et al. Human carbonic anhydrase XII: cDNA cloning, expression, and chromosomal localization of a carbonic anhydrase gene that is overexpressed in some renal cell cancers. Proc Natl Acad Sci USA. 1998, 95, 7608–13.
75. Lehtonen J, Shen B, Vihinen M, Casini A, Scozzafava A, Supuran CT, et al. Characterization of CA XIII, a novel member of the carbonic anhydrase isozyme family. J Biol Chem. 2004, 279, 2719–27.
76. Fujikawa-Adachi K, Nishimori I, Taguchi T, Onishi S. Human carbonic anhydrase XIV (CA14): cDNA cloning, mRNA expression, and mapping to chromosome 1. Genomics. 1999, 61, 74–81.
77. Kaunisto K, Parkkila S, Rajaniemi H, Waheed A, Grubb J, Sly WS. Carbonic anhydrase XIV: luminal expression suggests key role in renal acidification. Kidney Int 2002, 61, 2111–8.
78. Parkkila S, Parkkila AK, Rajaniemi H, Shah GN, Grubb JH, Waheed A, et al. Expression of membraneassociated carbonic anhydrase XIV on neurons and axons in mouse and human brain. Proc Natl Acad Sci U S A 2001, 98, 1918–23.
79. Supuran CT. How many carbonic anhydrase inhibition mechanisms exist? J Enzyme Inhib Med Chem. 2016, 31, 345-60.
80. Nocentini A, Supuran CT. Advances in the structural annotation of human carbonic anhydrases and impact on future drug discovery. 2019, 14, 1175-1197
81. D'Ambrosio K, Smaine FZ, Carta F, et al. Development of potent carbonic anhydrase inhibitors incorporating both sulfonamide and sulfamide groups. J Med Chem. 2012, 55, 6776–83.
82. Carta F, Aggarwal M, Maresca A, et al. Dithiocarbamates: a new class of carbonic anhydrase inhibitors. Crystallographic and kinetic investigations. Chem Commun (Camb). 2012, 48, 1868-70.
83. Vullo D, Durante M, Di Leva FS, et al. Monothiocarbamates Strongly Inhibit Carbonic Anhydrases in Vitro and Possess Intraocular Pressure Lowering Activity in an Animal Model of Glaucoma. J Med Chem. 2016, 59, 5857-67.

84. Abellán-Flos M, Tanç M, Supuran CT, et al. Multimeric xanthates as carbonic anhydrase inhibitors. J Enzyme Inhib Med Chem. 2016, 31, 946-52.
85. Di Fiore A, Maresca A, Supuran CT, De Simone G. Hydroxamate represents a versatile zinc binding group for the development of new carbonic anhydrase inhibitors. Chem Commun (Camb). 2012, 48, 8838-40.
86. Carta, F.; Supuran, C.T; Scozzafava, A. Sulfonamides and their isosters as carbonic anhydrase inhibitors. Future Med. Chem. 2014, 6, 1149-1165.
87. Carta F, Supuran CT. Diuretics with carbonic anhydrase inhibitory action: a patent and literature review (2005-2013). Expert Opin Ther Pat. 2013, 23, 681–691.
88. Supuran CT. Acetazolamide for the treatment of idiopathic intracranial hypertension. Expert Rev Neurother.2015, 15, 851–856.
89. Casini A, Scozzafava A, Mincione F, Menabuoni L, Ilies MA, Supuran CT. Carbonic anhydrase inhibitors: water-soluble 4-sulfamoylphenylthioureas as topical intraocular pressurelowering agents with long-lasting effects. J Med Chem. 2000, 43, 4884–4892.
90. Scozzafava A, Menabuoni L, Mincione F, Supuran CT. Carbonic anhydrase inhibitors. A general approach for the preparation of water-soluble sulfonamides incorporating polyaminopolycarboxylate tails and of their metal complexes possessing long-lasting, topical intraocular pressure-lowering properties. J Med Chem. 2002, 45, 1466–1476.
91. Perut F, Carta F, Bonuccelli G, et al. Carbonic anhydrase IX inhibition is an effective strategy for osteosarcoma treatment., Expert Opin Ther Targets. 2015, 19, 1593-05.
92. Dubois L, Lieuwes NG, Maresca A, et al. Imaging of CA IX with fluorescent labelled sulfonamides distinguishes hypoxic and (re)-oxygenated cells in a xenograft tumour model. Radiother Oncol. 2009, 92, 423-8.
93. Cecchi A, Hulikova A, Pastorek J, et al. Carbonic anhydrase inhibitors. Design of fluorescent sulfonamides as probes of tumor-associated carbonic anhydrase IX that inhibit isozyme IX-mediated acidification of hypoxic tumors. J. Med. Chem. 2005, 48, 4834–41.
94. De Simone G, Vitale RM, Di Fiore A, et al. Carbonic anhydrase inhibitors: Hypoxia-activatable sulfonamides incorporating disulfide bonds that target the tumor-associated isoform IX. J Med Chem. 2006, 49, 5544-51.
95. Casini A, Antel J, Abbate F, et al. Carbonic anhydrase inhibitors: SAR and X-ray crystallographic study for the interaction of sugar sulfamates/sulfamides with isozymes I, II and IV. Bioorg Med Chem Lett. 2003, 13, 841-5.

96. Carta F, Garaj V, Maresca A, et al. Sulfonamides incorporating 1,3,5-triazine moieties selectively and potently inhibit carbonic anhydrase transmembrane isoforms IX, XII and XIV over cytosolic isoforms I and II: solution and X-ray crystallographic studies. Bioorg Med Chem. 2011, 19, 3105–3119.
97. Nocentini A, Trallori E, Singh S, Lomelino CL, Bartolucci G, Di Cesare Mannelli L, et al. 4-Hydroxy-3-nitro-5-ureido-benzenesulfonamides selectively target the tumor-associated carbonic anhydrase isoforms IX and XII showing hypoxia-enhanced antiproliferative profiles. J Med Chem 2018, 61, 10860-74.
98. Eldehna WM, Abo-Ashour MF, Nocentini A, El-Haggar RS, Bua S, Bonardi A, et al. Enhancement of the tail hydrophobic interactions within the carbonic anhydrase IX active site via structural extension: design and synthesis of novel N-substituted isatins-SLC-0111 hybrids as carbonic anhydrase inhibitors and antitumor agents. Eur J Med Chem. 2019, 162, 147-60.
99. Pacchiano F, Carta F, McDonald PC, et al. Ureido-substituted benzenesulfonamides potently inhibit carbonic anhydrase IX and show antimetastatic activity in a model of breast cancer metastasis. J Med Chem. 2011, 54, 1896–02.
100. Safety Study of SLC-0111 in Subjects With Advanced Solid Tumours. Available online: https://clinicaltrials.gov/ct2/show/NCT02215850.
101. A Study of SLC-0111 and Gemcitabine for Metastatic Pancreatic Ductal Cancer in Subjects Positive for CAIX (SLC-0111-17-01). Available online: https://clinicaltrials.gov/ct2/show/NCT03450018.
102. Karioti A, Carta F, Supuran CT. Phenols and Polyphenols as Carbonic Anhydrase Inhibitors. Molecules. 2016, 21, 1649.
103. Carta F, Temperini C, Innocenti A, et al. Polyamines inhibit carbonic anhydrases by anchoring to the zinc-coordinated water molecule J Med Chem. 2010, 53, 5511-22.
104. Ferraroni M, Carta F, Scozzafava A et al. Thioxocoumarins Show an Alternative Carbonic Anhydrase Inhibition Mechanism Compared to Coumarins. J Med Chem. 2016, 59, 462-73.
105. Tars K, Vullo D, Kazaks A, J et al. Sulfocoumarins (1,2-benzoxathiine-2,2-dioxides): a class of potent and isoform-selective inhibitors of tumor-associated carbonic anhydrases. J Med Chem. 2013, 56, 293-300.

106. Nocentini A, Carta F, Tanc M, et al. Deciphering the Mechanism of Human Carbonic Anhydrases Inhibition with Sulfocoumarins: Computational and Experimental Studies. Chemistry. 2018, 24, 7840-7844.

107. Maresca A, Temperini C, Vu H, et al. Non-zinc mediated inhibition of carbonic anhydrases: coumarins are a new class of suicide inhibitors. J Am Chem Soc. 2009, 131, 3057–62.

108. Maresca A, Temperini C, Pochet L, Masereel B, Scozzafava A, Supuran CT. Deciphering the mechanism of carbonic anhydrase inhibition with coumarins and thiocoumarins. J Med Chem 2010, 53, 335-44.

109. Singh S, Lomelino CL, Mboge MY, et al. Cancer Drug Development of Carbonic Anhydrase Inhibitors beyond the Active Site. Molecules. 2018, 23, 1045.

110. De Luca L, Mancuso F, Ferro S, et al. Inhibitory effects and structural insights for a novel series of coumarin-based compounds that selectively target human CA IX and CA XII carbonic anhydrases. Eur J Med Chem. 2018, 143, 276-82.

111. D'Ambrosio K, Carradori S, Monti SM, Out of the active site binding pocket for carbonic anhydrase inhibitors. Chem Commun (Camb). 2015, 51, 302-5.

112. Le Darz, A.; Martin-Mingot, A.; Bouazza, F., et al. Fluorinated pyrrolidines and piperidines incorporating tertiary benzenesulfonamide moieties are selective carbonic nhydrase II inhibitors, J. Enzyme Inhib. Med. Chem. 2014, 30, 737-745.

113. Supuran CT, Thibaudeau S. et al. New superacid synthesized (fluorinated) tertiary benzenesulfonamides acting as selective hCA IX inhibitors: toward a new mode of carbonic anhydrase inhibition by sulphonamides. Chem. Commun. 2013, 49, 6015-17.

114. Peerzada MN, Khan P, Ahmad K, Hassan MI, Azam A. Synthesis, characterization and biological evaluation of tertiary sulfonamide derivatives of pyridyl-indole based heteroaryl chalcone as potential carbonic anhydrase IX inhibitors and anticancer agents. Eur J Med Chem. 2018, 155, 13-23.

115. Main RE, Locke A. Activation of carbonic anhydrase by histamine. J Biol Chem 1941;140:LXXXI

116. Briganti F, Mangani S, Orioli P, Scozzafava A, Vernaglione G, Supuran CT. Carbonic anhydrase activators: x-ray crystallographic and spectroscopic investigations for the interaction of isozymes I and II with histamine. Biochemistry. 1997, 36, 10384-92.

117. Clark AM, Perrin DD. A re-investigation of the question of activators of carbonic anhydrase. Biochem J. 1951, 48, 495-503.

118. Supuran CT. Carbonic anhydrase activators. Future Med Chem. 2018, 10, 561–573.
119. Temperini C, Scozzafava A, Supuran CT. Carbonic anhydrase activation and the drug design. Curr Pharm Des. 2008, 14, 708–715.
120. Clare BW, Supuran CT. Carbonic anhydrase activators: structure activity correlations for a series of isozyme II activators. J Pharm Sci. 1994, 83, 768–773.
121. Bhatt A, Mondal UK, Supuran CT, et al. Crystal structure of carbonic anhydrase II in complex with an activating ligand: implications in neuronal function. Mol Neurobiol. 2018, 55, 7431–7437.
122. Canto de Souza L, Provensi G, Vullo D, et al. Carbonic anhydrase activation enhances object recognition memory in mice through phosphorylation of the extracellular signal-regulated kinase in the cortex and the hippocampus. Neuropharmacology. 2017, 118, 148–156.
123. Provensi G, Carta F, Nocentini A, et al. A New Kid on the Block? Carbonic Anhydrases as Possible New Targets in Alzheimer's Disease. Int J Mol Sci. 2019, 20, 4724.
124. Carta F, Supuran CT. Diuretics with carbonic anhydrase inhibitory action: a patent and literature review (2005-2013). Expert Opin Ther Pat. 2013, 23, 681–691.
125. Carta F, Supuran CT, Scozzafava A. Novel therapies for glaucoma: a patent review 2007–2011. Expert Opin Ther Pat.2012, 22, 79–88.
126. Masini E, Carta F, Scozzafava A, et al. Antiglaucoma carbonic anhydrase inhibitors: a patent review. Expert Opin Ther Pat. 2013, 23, 705–716.
127. Aggarwal M, Kondeti B, McKenna R. Anticonvulsant/antiepileptic carbonic anhydrase inhibitors: a patent review. Expert Opin Ther Pat. 2013, 23, 717–724.
128. Scozzafava A, Supuran CT, Carta F. Antiobesity carbonic anhydrase inhibitors: a literature and patent review. Expert Opin Ther Pat. 2013, 23, 725–735.
129. Supuran CT. Applications of carbonic anhydrases inhibitors in renal and central nervous system diseases. Expert Opin Ther Pat. 2018, 28, 713–721.
130. Aronne LJ et al. Evaluation of phentermine and topiramate versus phentermine/topiramate extended-release in obese adults. Obesity (Silver Spring, Md.). 2013, 21, 2163–71.
131. FDA. New Drug Application 22580- VI-0521 QNEXA (phentermine/topiramate). 2012, 1–200

132. Gadde KM, Yonish GM, Foust MS, Wagner HR. Combination therapy of zonisamide and bupropion for weight reduction in obese women: a preliminary, randomized, open-label study. J Clin Psychiatry. 2007, 68, 1226–9.

133. Supuran CT. Carbonic anhydrase inhibition and the management of neuropathic pain. Expert Rev Neurother.2016, 16, 961–968.

134. Margheri F, Ceruso M, Carta F, et al. Overexpression of the transmembrane carbonic anhydrase isoforms IX and XII in the inflamed synovium. J Enzyme Inhib Med Chem.2016;31, 60–63.

135. Bua S, Di Cesare Mannelli L, Vullo D, et al. Design and synthesis of novel nonsteroidal anti-inflammatory drugs and carbonic anhydrase inhibitors hybrids (NSAIDs-CAIs) for the treatment of rheumatoid arthritis. J Med Chem. 2017, 60, 1159–1170.

136. Monti SM, Supuran CT, De Simone G. Anticancer carbonic anhydrase inhibitors: a patent review (2008e2013). Expert Opin Ther Pat. 2013, 23, 737-49.

137. Nocentini A, Supuran CT. Carbonic anhydrase inhibitors as antitumor/antimetastatic agents: a patent review (2008-2018). Expert Opin Ther Pat. 2018, 28, 729-40.

138. Capasso C, Supuran CT. Bacterial, fungal and protozoan carbonic anhydrases as drug targets. Expert Opin Ther Targets. 2015, 19, 1689-704.

139. Sikazwe DMN. The multi-target drug design era is here, consider it. Drug Design.2012, 1, 1000–1001.

140. Long DD, Frieman B, Hegde SS, et al. A multivalent approach towards linked dual-pharmacology prostaglandin F receptor agonist/carbonic anhydrase-II inhibitors for the treatment of glaucoma. Bioorg Med Chem Lett.2013, 23, 939–943.

141. Khalifah RG. The carbon dioxide hydration activity of carbonic anhydrase I. Stop-flow kinetic studies on the native human isoenzymes B and C. J Biol Chem. 1971, 246, 2561-2573.

142. Berrino E, Milazzo L, Micheli L, et al. Synthesis and Evaluation of Carbonic Anhydrase Inhibitors with Carbon Monoxide Releasing Properties for the Management of Rheumatoid Arthritis. J Med Chem. 2019, 62, 7233-7249.

143. Huentupil Y, Peña L, Novoa N, Berrino E, et al. New sulfonamides containing organometallic-acylhydrazones: synthesis, characterisation and biological evaluation as inhibitors of human carbonic anhydrases. J Enzyme Inhib Med Chem. 2019, 34, 451-458.

144. Eysteinsson T, Gudmundsdottir H, Hardarson AO, Berrino E et al. Carbonic Anhydrase Inhibitors of Different Structures Dilate Pre-Contracted Porcine Retinal Arteries. Int J Mol Sci. 2019, 20, 467.
145. Eldehna WM, Abo-Ashour MF, Berrino E, et al. SLC-0111 enaminone analogs, 3/4-(3-aryl-3-oxopropenyl) aminobenzenesulfonamides, as novel selective subnanomolar inhibitors of the tumor-associated carbonic anhydrase isoform IX. Bioorg Chem. 2019, 83, 549-558.
146. Küçükbay H, Buğday N, Küçükbay FZ, Berrino E et al. Synthesis and carbonic anhydrase inhibitory properties of novel 4-(2-aminoethyl)benzenesulfonamide-dipeptide conjugates. Bioorg Chem. 2019, 83, 414-423.
147. Georgey HH, Manhi FM, Mahmoud WR et al. 1,2,4-Trisubstituted imidazolinones with dual carbonic anhydrase and p38 mitogen-activated protein kinase inhibitory activity. Bioorg Chem. 2019, 82, 109-116.
148. Berrino E, Bozdag M, Del Prete S, et al Inhibition of α-, β-, γ-, and δ-carbonic anhydrases from bacteria and diatoms with N'-aryl-N-hydroxy-ureas. J Enzyme Inhib Med Chem. 2018, 33, 1194-1198.
149. Bua S, Berrino E, Del Prete S, et al. Synthesis of novel benzenesulfamide derivatives with inhibitory activity against human cytosolic carbonic anhydrase I and II and Vibrio cholerae α- and β-class enzymes. J Enzyme Inhib Med Chem. 2018, 33, 1125-1136.
150. Salerno S, Barresi E, Amendola G, Berrino E et al. 4-Substituted Benzenesulfonamides Incorporating Bi/Tricyclic Moieties Act as Potent and Isoform-Selective Carbonic Anhydrase II/IX Inhibitors. J Med Chem. 2018, 61, 5765-5770.
151. Berrino E, Bua S, Mori M, et al. Novel Sulfamide-Containing Compounds as Selective Carbonic Anhydrase I Inhibitors. Molecules. 2017, 22, 1049.

Chapter 2: Synthesis and Evaluation of Carbonic Anhydrase Inhibitors with Carbon Monoxide Releasing Properties

2.1 Introduction

2.1.1 Carbon Monoxide (CO)

Carbon monoxide (CO) is a colourless and odourless gas produced by incomplete combustion of carbon containing material. CO toxicity is mainly based on its superior affinity for the Fe (II) heme containing proteins, such as the haemoglobin, when compared to molecular oxygen [1]. Exposure to CO gas produces effects ranging from headache and dizziness to coma and death [1]. The small amounts of CO needed to determine unconsciousness and death (i.e. 12.800 ppm) as well as the immediate possibility to detect it in the atmosphere are the main reasons which determined the classification of this gas among the most dangerous poisons to date [2].

Evidences reported by Tenhunen and Schmi dt in 1968 of the endogenous production of CO in human body during the degradation of Heme proteins paved the way to possible physiological roles played by this molecule [3]. Following studies supported such an observations and further fostered a repurposing of CO from toxic and lethal agent to natural mediator with physiologically relevant roles [4,5].

Carbon Monoxide (CO), along with Nitric Oxide (NO) and Hydrogen Sulfide (H_2S), belongs to the class of the gaso-transmitters [6,7]. Such a signalling molecules are actively involved in regulating many key cellular functions and processes, which among others include cytoprotection, apoptosis, proliferation, inflammation, and gene transcription [8-10]. The pharmacology of these mediators is a research field which continuously attracts enormous interests within the scientific community in light of unprecedently reported applications for biomedical purposes [6].

The endogenous production of CO occurs during the oxidative metabolism of Heme to Biliverdin by means of the enzymes Heme Oxygenase (HO; gene name HMOX1) 1 (inducible) and 2 (constitutive) as shown in **Figure 2.1** [3,11].

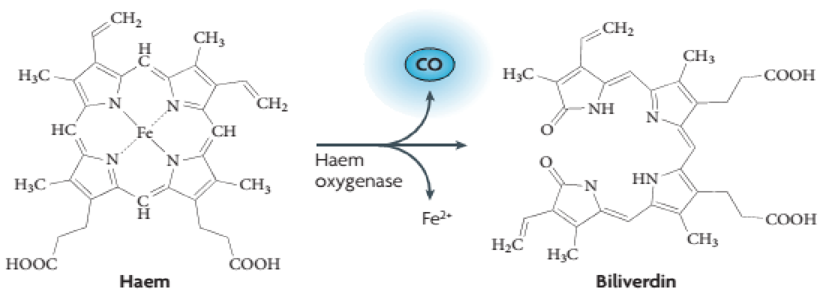

Figure 2.1. Endogenous production of CO during Heme degradation [5].

The crucial physiological role of CO has been confirmed in organisms lacking HO1 by using embryos as models which do not survive after fertilization or developed evident organ anomalies and enhanced sensitivity to stress stimuli. HMOX1 was found among the most actively transcripted genes, as it is deeply involved in adaptive cellular responses associated to altered redox states [12]. Such an evidence suggested cytoprotective and homeostatic effects exerted by CO, along with other Heme products such as iron, ferritin or bile pigments [13].

Once generated by HOs at low concentrations, CO exerts its physiological effects mostly by interacting with heme containing proteins (i.e. soluble Guanylyl Cyclase (sGC), NADPH oxidase and mitochondrial Cytochrome-C Oxidase) [13-15]. Non-heme containing proteins such as p38 or STAT3 have been suggested to be targeted by this gas too [16,17]. sGC activity is strongly enhanced by CO and a NO-like smooth cell muscular relaxation is induced [18].

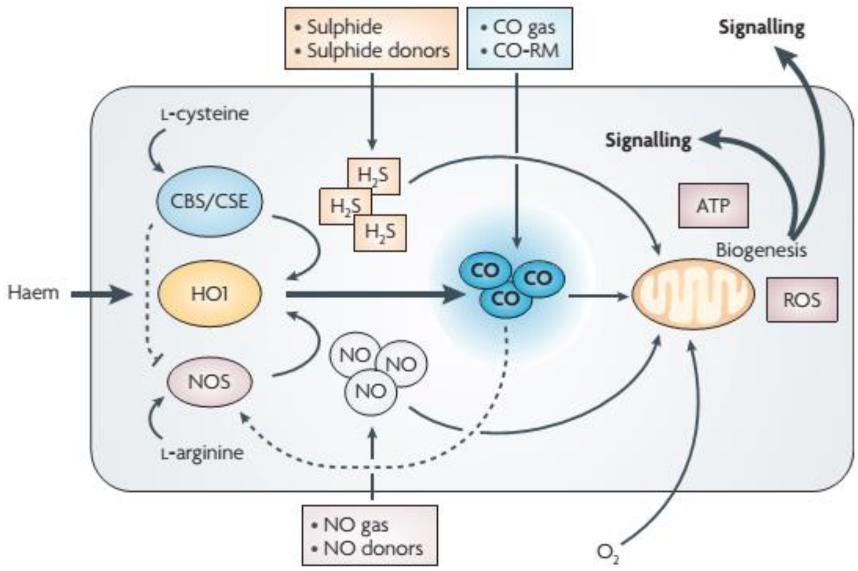

Figure 2.2. Gaso-transmitter pathways and their interrelations [5].

The close biological relationship between NO and CO gases is very intriguing, as cells were found to compensate reduced levels of NO by increasing the production of CO when pathological events occur **(Figure 2.2)**. The mechanisms underlying such an effect were ascribed to the ability of CO to increase NO production by activation of the NO Synthase (NOS), which gas in turn activates HO1 with further production of CO [18,20]. Although these gases have almost superimposable roles, the higher chemical stability of CO when compared to NO, makes it able to reach remote tissutal sites. Is therefore evident the advantage to use CO as a therapeutic agent also considering that the binding of CO to the biological targets (i.e. heme containing proteins) is far more selective when compared to NO and H_2S [4,5].

2.1.2 CO Releasing Molecules (CORMs): a Powerful Alterative to Gaseous CO

The administration of exogenous CO at low concentrations is demonstrated to exert therapeutic effects in models of cardiovascular diseases, infections, organ transplantation and inflammatory disorders [4,5]. Currently, inhaled CO is used in several clinical trials with promising results in patients subjected to organ transplantations and lung injuries [4,5]. The main drawbacks associated to the use of CO gas are related to its safe administration and lack of selectivity for any tissue, which implies the use of proper devices and trained personnel in order to avoid risks of an excessive loading of CO and consequent lethal intoxications [4,5]. In this context, is the use of CO releasing molecules (CORMs) instead, which turned out to be a valid alternative to inhaled gaseous CO. As a matter of fact, CORMs can be administered orally or by injection thus allowing easier handling and storage of CO. In addition, the proper design of CORM moieties determines the release of CO in a controlled manner with beneficial therapeutic effects [21] (**Figure 2.3**).

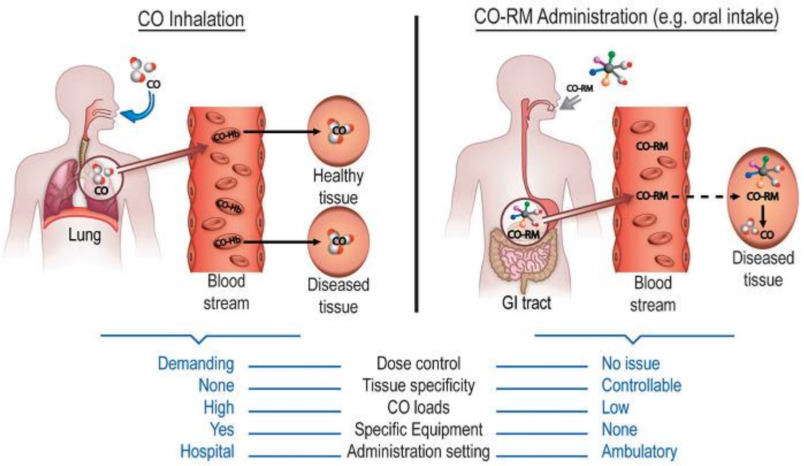

Figure 2.3. Alternative pathways for the therapeutic delivery of CO to diseased tissues with their main advantages and disadvantages.

In 2002 the first CORM species was reported in the literature as the lipid-soluble metal carbonyl complex tricarbonyldichlororuthenium(II) dimer ($[Ru(CO)_3Cl_2]_2$) also known as **CORM-2** (compound **47** in **Figure 2.4**) [21]. This compound was found able to induce vasodilation and hypotension in appropriate study models by means of CO gas releasing [21].

These results paved the way for a new and promising research field, by proving for the first time the feasibility to use CO delivering platforms for biomedical applications [21,22].

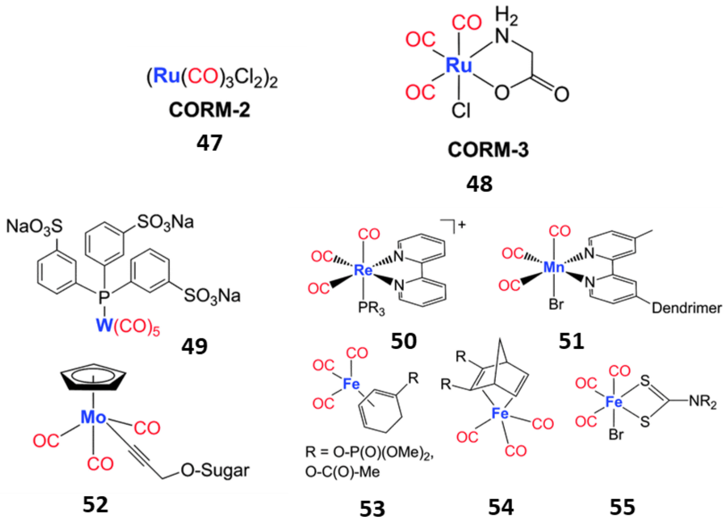

Figure2.4. Examples of CORMs of the metallo-organic type described in the literature.

Several other CORMs have been described in the literature to date (**Figure 2.4**). Most of them are of the metallo-organic type, constituted by a transition metal core centre (i.e. coordination sphere) surrounded by a variable number of CO residues [22]. To the metal core are ascribed the CO release mechanism, the kinetics as well as the spectroscopic features, with the latter being useful for imaging purposes [22]. The introduction of an organic portion linked to the metal core, called "drug sphere", has been demonstrated, in some cases, to deeply affect the biological properties of the entire molecule, influencing also the CO release rate (**Figure 2.5**).

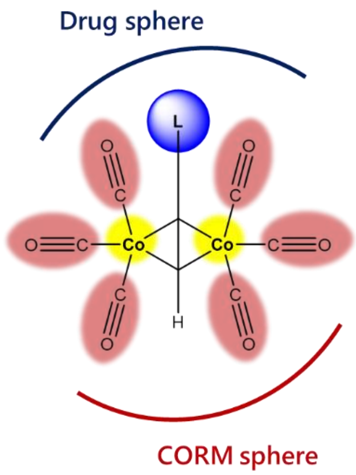

Figure2.5. Schematic representation of a CORM, bearing a CORM sphere and a Drug sphere; L= co-ligand.

Among the transition metal carbonyl complexes, the alkyne dicobalt hexacabonyl (DCH) based compounds are of particular interest in Organic Chemistry as protecting groups of terminal alkynes with marginal consideration for therapeutic as well as for imaging purposes.

The synthesis of DCH complexes was firstly reported by Greenfield et al. in 1956 when treating alkyne moieties with dicobalt octacarbonyl $Co_2(CO)_8$ [23,26]. Structural NMR analyses accounted for a change of the organic molecular geometry from linear to the *Z*-alkene configuration (**Figure 2.6**).

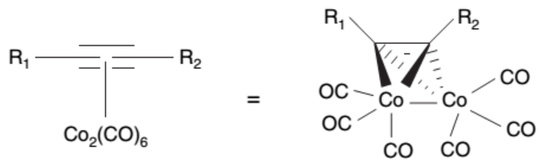

Figure2.6. Representation and structural model for (alkyne)$Co_2(CO)_6$ complexes.

Conventional application of these complexes in synthetic chemistry appears as important intermediates in the Pauson-Khand and in the Nicholas reactions [25]. Removal of the $Co_2(CO)_6$ complex to restore the free alkyne functionality is usually performed using $(Me)_3NO$ in MeOH at r.t.

The biological application of DCH derivatives begun around 1987-1997, when different groups evaluated their potential antiproliferative activity against cell lines [27-29]. In particular, the compound derived from acetylsalicylic acid (Co-ASS **59**, **Figure 2.7**) revealed to be among the most potent [29].

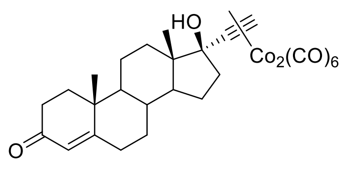

56

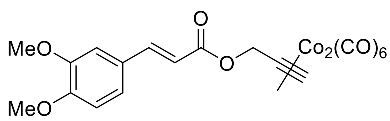

57

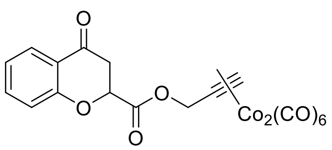

58

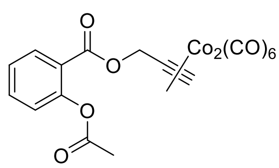

59

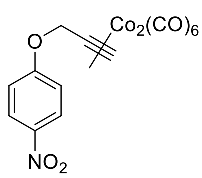

60

Figure 2.7. Structures of representative alkyne dicobalt hexacabonyl complexes reported so far [5,29].

Interestingly modifications on the organic scaffold led to decrease of the potency or complete suppression of the biological properties. These results shed light on the crucial role played by the "drug sphere" in determining a biological activity. Overall the CORM species reported until now lack of any intended target selectivity, and this represents the main hurdle scientists have to face.

The straightforward synthetic procedures, versatile chemical design and possibility to create large molecular diversities varying the nature of the co-ligand, modulation of the CO release as well as specific spectroscopic features, make CORMs powerful CO-based theragnostic agents for the management of human diseases.

To the best of our knowledge CORMs are currently used for tumors and cardiovascular related diseases [26,28]. In consideration of the role of CO in regulating signalling pathways closely related to inflammation events we sought to investigate the role of CORMs in the management of such a disease [31,32]. Up to now several derivatives have been evaluated in both acute and chronic models of inflammation [31,32]. Of particular note is the water-soluble tricarbonylchloro(glycinato)ruthenium (II) complex (**CORM-3**, compound **48** in **Figure 2.4**), which has been reported to effectively down-regulate the immune and inflammatory responses in a model of Rheumatoid Arthritis (RA) [33].

2.1.3 CA Involvement in Rheumatoid Arthritis (RA)

Within the RA context it has recently been reported that the metalloenzymes CAs are deeply involved in the pathogenesis and progress of the disease [34-37]. RA is a chronic and systemic inflammatory disease caused by a faulty autoimmune response, which primary affects the lining of the joints, thus causing erosion of the cartilage, bone damage, and joints deformity at the later stages. The dimension and the impact of RA in the society are well reported [38,39]. RA symptoms deeply impact life quality of the affected patients, who are progressively unable to carry out activities in every domain of their lives [38,39]. State-of-the-art RA pharmacological treatments include two main classes: (i) drugs acting to slow or stop the course of the disease and to inhibit the joints tissutal damages and (ii) those acting to ease the symptoms [38-40]. The first class of drugs includes the disease-modifying antirheumatic drugs (DMARDs), biologics, JAK-inhibitors, and anti-inflammatory drugs. The latter are represented by the nonsteroidal anti-inflammatory drugs (NSAIDs) [40]. Usually a therapeutic RA protocol accounts for the combination of both drug classes along with the recommendation to conduct proper physical activities, with the intent to achive a better control of the symptoms [39,40]. Despite recent progresses in RA treatment, there is still no effective cure.

Various contributions demonstrated the abnormal expression of CA I, IV, IX and XII isoforms in the serum and the synovium specimens of patients affected by RA [34-37]. CAs play a crucial role in modulating cellular pH values, by reversibly catalysing the conversion of CO_2 to bicarbonate and protons [37,41] and their overexpression was demonstrated to negatively affect cellular immunity processes and to enhance RA associated symptoms [42-44]. Proof-of-concept studies demonstrated that the inhibition of the involved CA isoforms significantly relieved the RA ache symptoms on *in vivo* models of the disease [45,46]

We report for the first time the synthesis and biological evaluation of a series of small molecule hybrids consisting of a CORM tail section, based on the dicobalthexacarbonyl (DCH) complex, linked to a Carbonic Anhydrases Inhibitor (CAI) warhead [47]. Our interest on these relatively poor investigated CORMs, mainly relies on the kinetic data which do classify them as slow CO releasers [26,48,49]. In addition, the emission of CO units from DCHs takes place only when oxidation of the metal core occurs, thus not spontaneously [50]. Overall these features allow DCH based compounds to release CO in a more controlled manner when compared to other CORMs, and this makes them particularly suitable for pharmacological purposes. The possibility to trigger CO release by making use of the chemical species produced from cellular oxidative stress processes which are typical of some diseases (e.g. in inflammation), led us to consider such compounds as potential tools for the management of RA and its associated symptoms. The new CAI-CORMs molecular hybrids here reported are intended to merge in a single molecular entity two therapeutically active portions, with the aim to obtain a synergistic antihyperalgesic effect. Moreover, the insertion of the CAI head can confer selectivity of such hybrids for the inflamed tissues in which some of the involved isoforms are overexpressed [37].

2.2 CAI-CORM Dual Hybrids for the Management of RA: Proof-of-Concept

2.2.1 Design and synthesis

In this work we designed new CAI-CORM hybrids incorporating units which are tied by means of various spacers. Specifically, the CAI “head” was primarily intended: *i*) to overcome the lack of selectivity of unsubstituted CORMs for specific biological entities by means of targeting the hCA isoforms involved in inflammation diseases; *ii*) to lead to an enhancement of the antihyperalgesic effects due to the hCAs inhibition. As a whole, the CAI-CORM hybrids should have an enhancement of the antinociceptive effect when compared to the single entities (CORM and CAI) administered separately. In this study we decided to include both classical (e.g. the primary sulfonamides **61-68**) and non-classical CAIs, e.g., coumarin (**69**, **70**, **73**), sulfocoumarins (**71** and **72**) and thioxocoumarin (**74**) scaffolds [51,52]. Although few examples of DHC derivatives from internal acetylenes are described in the literature [53], in this proof-of-concept study we focused our attention on terminal acetylenes only. Different spacers between the CAI head and the CORM tail have been introduced within our molecules with the aim to explore any effects of the bioisosteric substitution on CA selectivity and CO release kinetics.

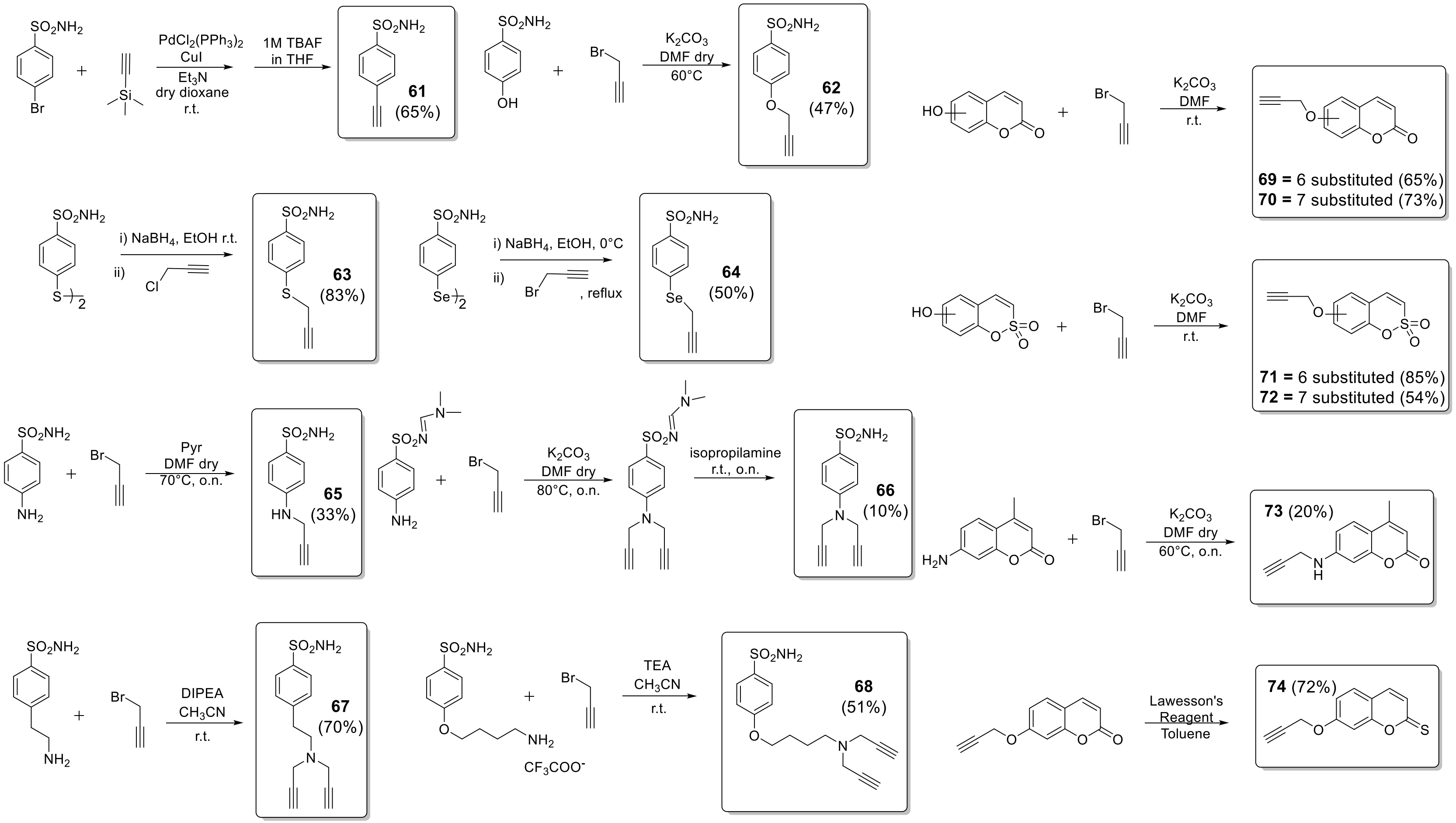

Scheme 2.1: Synthetic procedures for the preparation of CAIs **61-74.**

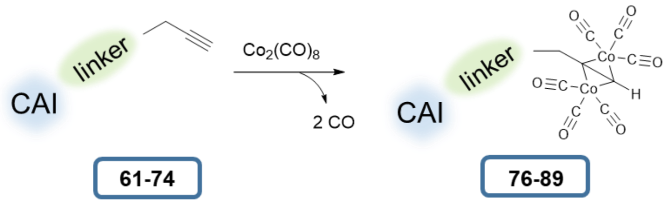

Scheme 2.2: Schematic representation of the dicobalt-hexacarbonyl insertion to afford compounds **76-89**.

As reported in **Scheme 2.1-2.2**, compound **61** has the ethynyl group directly attached to the benzenesulfonamide moiety in *para* position, whereas in compounds **72-76** the propargyl moiety is separated from it by different heteroatoms (O, S, Se and N). In compound 7**7**, an ethylene spacer between the ring and the propargyl moiety was inserted by using 4-(2-aminoethyl)benzenesulfonamide as starting material. A further elongation of the scaffold was obtained with compound **78**, which contains two heteroatoms (*O* and *N*) separated by a butyl spacer and a double propargylated terminal function. Among the non-classical CAIs **69-74**, we included 6- and 7- propargylated coumarins and sulfocoumarins, the 7-substituted aminocoumarin and 7 substituted thioxocoumarin (**Scheme 2.1-2.2**).

The acetylenic precursors **62, 65-74** were all synthesized by using propargyl bromide as alkylating agent and potassium carbonate (K_2CO_3) or *N*,*N*-Diisopropylethylamine (DIPEA) as a base,[39] whereas the compound **61** was obtained by means of Sonogashira coupling reaction. Finally, reaction of propargyl halides with the *in situ* obtained aryl sulphides and selenols afforded the corresponding thio and seleno ethers **63** and **64** (**Scheme 2.1**). Then the terminal acetylenic precursors **61-74** were all treated with dicobalt octacarbonyl in slight excess (1.05 eq. for **61-65** and **69-74** or 2.1 eq. for **66-68**) to afford the final compounds **76-89** at r.t. and in high yields after silica gel column chromatography purification (**Scheme 2.2**) [54].

2.2.2 *In vitro* Biological Evaluation: CA Inhibition

Acetylenic precursors **61-74** and their corresponding CAI-CORM dual hybrids **76-89** were investigated as inhibitors of the hCAs I, II, IV, IX and XII by means of the stopped flow CO_2 hydrase assay [55]. The inhibition data, compared to those of the standard sulfonamide inhibitor acetazolamide (**AAZ**), are reported in **Table 2.1**.

	KI (nM)*										
	hCA I	**hCA II**	**hCA IV**	**hCA IX**	**hCA XII**		**hCA I**	**hCA II**	**hCA IV**	**hCA IX**	**hCA XII**
61	1080.0(45)	71.6(45)	1356.8	54.0(45)	44.5(45)	**76**	6.0	0.39	494.8	249.0	969.6
62	2340.0(39)	28.7(39)	1734.8	8.2(39)	2.3(39)	**77**	1345(39)	40.9(39)	>10000	5.4(39)	0.90(39)
63	30.2(48)	29.5(48)	838.9(48)	7.6(48)	0.86	**78**	>10000	5.9	>10000	2.7	3.7
64	7.3(49)	9.3(49)	33.4	2.7(49)	2.8	**79**	268.9	7.0	82.1	34.9	704.7
65	851.7	96.5	>10000	415.9	783.8	**80**	900.9	215.4	929.1	>10000	>10000
66	6400(39)	1785(39)	1621.7	9.0(39)	4.9(39)	**81**	876(39)	165(39)	8915.8	6.2(39)	7.5(39)
67	4014.0	5.8	370.8	55.7	9.1	**82**	>10000	74.6	>10000	259.2	40.4
68	816.7	0.44	1716.5	3.8	0.8	**83**	>10000	507.2	>10000	2073.2	53.1
69	>10000	>10000	69.2	4747.6	56.4	**84**	>10000	>10000	111.3	3.9	5.0
70	>10000(56)	>10000(56)	76.4	1350.0(56)	730.0(56)	**85**	>10000(56)	>10000(56)	228.6	>10000(56)	>10000(56)
71	>10000	>10000	59.7	474.3	44.5	**86**	>10000	>10000	55.1	394.8	669.7
72	>10000	>10000	62.2	6187.6	30.3	**87**	>10000	>10000	72.5	4.6	38.0
73	>10000	>10000	48.3	170.8	34.7	**88**	>10000	2849.6	39.5	2.9	7.7
74	>10000(56)	>10000(56)	47.2	>10000(56)	>10000(56)	**89**	>10000(56)	>10000(56)	21.9	>10000(56)	>10000(56)
AAZ	250	12	74	25.8	5.7	**AAZ**	250	12	74	25.8	5.7

Table 2.1. Inhibition data of hCA I, hCA II, hCA IV, hCA IX and hCA XII with compounds **61-74** and **76-89** and the standard sulfonamide inhibitor acetazolamide (**AAZ**) by a Stopped flow CO_2 hydrase assay [55]. * Mean from 3 different assays, by a stopped flow technique (errors were in the range of ± 5-10 % of the reported values).

The structure-activity relationships (SARs) for the sulfonamide containing compounds **61-68** and **76-83** and the coumarin, sulfocoumarin and thiooxocoumarin derivatives **69-74** and **84-89** are reported below:

i) The shortest derivative 4-ethynylbenzenesulfonamide **61** was a good inhibitor of hCA II, IX and XII isoforms (K_Is of 71.6, 54.0 and 44.5 nM), whereas the hCAs I and IV were poorly inhibited (K_Is of 1080.0 nM and 1356.8 nM respectively). The introduction of an oxygen atom at the phenyl ring to afford the propargyloxy moiety, as in compound **62**, determined a clear increase of the inhibition potency against the cytosolic hCA II and the tumor associated isoforms hCA IX and XII, of up to 2.5, 6.5 and 20 fold respectively. The same compound **62** was slightly less potent when compared to **61** against hCA I and IV (see Table 1). The bioisosteric substitution of the oxygen in **62** with a sulfur (**63**) or selenium (**64**) atom instead retained the inhibition activity against hCA II, IX and XII and led to a clear enhancement of the inhibition potency against the hCAs I and IV. In particular the propargylthioether derivative **63** resulted to be 77.5, 2.1, 1.1 and 2.7 fold more potent when compared to **62** against the hCAs I, IV, IX and XII. The selenium derivative **64** was up to 320.5, 3.1, 51.9 and 1.1 fold more potent when compared to **62** against the hCAs I, II, IV and IX isoforms. As a whole, the bioisosteric replacement of the oxygen in **62** with a sulfur or selenium determined an increase of the inhibition potencies. However, only the thioether **63** retained the selectivity profile of the parent compound **62**, whereas the selenium analogue **64** showed a rather “flat” inhibition profile over the enzymatic isoforms considered in this study. The introduction in **62** of a nitrogen atom instead of oxygen, to afford compound **65**, negatively affected the inhibition potency towards all hCA isoforms. In particular, **65** resulted ineffective against hCA IV (K_I > 10000 nM), whereas the remaining isoforms showed high K_I values spanning between 96.5 and 851.7 nM (see **Table 2.1**). Conversely, the bis-propargylated derivative **66** revealed to be a highly potent and selective inhibitor of the tumor associated isoforms IX and XII over CA I, II and IV. As reported in **Table 2.1** the experimentally obtained K_I values were of 9.0 and 4.9 nM for hCA IX and XII, respectively. The calculated selectivity indexes (SI) (i.e. defined as the K_I values ratio of compound **66** for the tumor associated isoforms IX and XII over the abundantly and cytosolic expressed hCA II) were rather high, i.e., 198 and 364 respectively. The insertion in **66** of a spacer between the benzene sulfonamide moiety and the bis-propargylated end (i.e. compounds **67** and **68**) restored the inhibition activity against hCA II (K_Is of 5.8 and 0.44 nM for **67a** and **68** respectively). Interestingly, the ethyl spacer in compound **67** determined an increase of the inhibition potency against hCA IV when compared to the parent compound **66**

(K_Is of 370.8 and 1621.7 nM respectively). Conversely, compound **67** resulted to be 6.2 and 1.9 fold less potent in inhibiting the tumor associated IX and XII isoforms. As for the longer spacer containing compound **68**, a lower inhibition potency against hCA IV was observed (K_Is of 1716.5, 370.8, and 1621.7 for **68**, **67** and **66** respectively), whereas all the remaining isoform were effectively inhibited. The sub-nanomolar inhibition values of **68** for hCA isoforms II and XII (i.e. 0.44 and 0.8 nM respectively) are of particular note. Such results are clearly ascribed to additional interactions the linker adopts with the amino acid residues defining the enzymatic cavities.

ii) The insertion of the CORM moiety, as in compounds **76-83**, seemed to differently affect the inhibition potencies against the isoforms herein considered. The *in vitro* kinetic data on hCA I revealed an enhanced inhibition activity for compounds **76**, **77** and **81** when compared to the parent propargylated intermediates **61**, **62** and **66**. In particular the CAI-CORM hybrid **76** was 180 fold more potent when compared to its precursor **61**, followed by **81** and **77** (i.e 7.3 and 1.7 fold respectively more potent than **66** and **62**). Conversely, compounds **78-80**, **82** and **83** did not well tolerate such a modification, which determined reduction of the potency for **79** and **80** and complete loss of activity shown by compounds **78, 82** and **83** (see **Table 2.1** for details). As for hCA II, enhancement of the inhibition potencies was observed for compounds **76**, **78**, **79**, and **81** (see **Table 2.1**), whereas higher K_I values for **82** and **83** when compared to their precursors can be detected (74.6 nM *vs* 5.8 nM for **82** and 507.2 *vs* 0.44 for **83**). The introduction of the CO-releasing moiety in compounds **62** and **65** to afford the hybrids **77** and **80** resulted in a slight increase of the K_I values up to 1.4 and 2.3 fold respectively. Among the hybrids tested on the hCA IV, only compounds **76** and **80** resulted to be more active when compared to their precursors (see **Table 2.1**) and the selenium ether **79** retained a high nanomolar inhibition activity (K_I 82.1 nM). All the remaining compounds of the series resulted ineffective in inhibiting the hCA IV. The introduction of the CORM moiety in **61** to afford the hybrid **76** determined a significant loss of the inhibition potency against the tumor associated hCA IX (K_Is of 54.0 and 249.0 nM respectively). Both the propargyl ether **77** and its sulfur bioisostere **78** showed slightly increase of the inhibition when compared to their precursors **62** and **63** (i.e. 1.5 and 2.7 fold). The same trend was not observed for the selenium containing ethers **64** and **79**. As reported in **Table 2.1** the CORM containing moiety **79** was 12.9 fold less potent that its precursor. Quite interestingly, the DCH functionality as in the mono-*N*-propargyl derivative **80** resulted detrimental for its inhibition activity (K_I > 10000), whereas in the bis-substituted **66** a slight increase of the inhibition potency against the hCA IX was obtained (K_Is of 9.0 and 6.2 nM for compounds **66** and **81** respectively). Finally, the insertion of the CORM moiety within the elongated derivatives **67** and **68** did result in high nanomolar CAIs **82** and **83** (see Table 1). The kinetic profile for the second tumor associated hCA isoform (i.e. hCA XII) was simpler when compared to the other enzymes herein explored. As shown in **Table 2.1** the introduction of the CORM moiety within the series herein reported, determined a decrease on the inhibition potencies. The only exception was represented by the propargyl ether **77** which was 2.6 fold more potent when compared to its parent compound **62** (K_Is of 2.3 and 0.9 nM respectively).

iii) In agreement with the data reported in the literature for the coumarins, sulfocoumarins and thiooxocoumarins CAI classes [see **Chapter 1, section 1.2.1**] the compounds **69-74** proved to be ineffective in inhibiting the cytosolic isoforms hCA I and II (K_Is > 10000). Isoform hCA IV was effectively inhibited by all compounds tested and showed K_I values ranging from 47.2 to 76.4 nM. Unfortunately, all compounds tested showed a rather flat kinetic profile which does not allow to define a proper SAR (see **Table 2.1**). As for the tumor associated hCA IX, the best inhibitor was the 7-substituted aminocoumarin **73** followed by 6-substituted sulfocoumarin **71**, with K_I values of 170.8 and 474.3 nM respectively. All remaining compounds resulted low micromolar hCA IX inhibitors (i.e. the 6- and 7-substituted coumarins **69**, **70** and the sulfocoumarin **72**) or ineffective (i.e. the thiooxocoumarin **74**). Better results were obtained for the hCA XII. As reported in **Table 2.1** the 6-substituted coumarin **69** was a medium potency inhibitor of the hCA XII isoform (K_I of 56.4 nM), whereas its regioisomer at 7 position (compound **70**) resulted to be 12.9 fold less potent (K_I of 730.0 nM). Conversely, a tighter inhibition profile was observed for the 6- and 7-substituted sulfocoumarin regioisomers **71** and **72** with the latter being 1.5 more potent (K_Is of 44.5 and 30.3 nM). Finally, the methyl coumarin **73** resulted a low-medium nanomolar inhibitor of the hCA XII (K_I of 34.7 nM) and the thiooxocoumarin **74** was ineffective (K_I > 10000).

iv) The insertion of the DCH moiety on compounds **69-74** to afford the hybrids **84-89** showed no influence on the inhibition potencies against the hCA I (K_Is > 10000). As for the hCA II, only the 7-substituted-4-methyl coumarin **88** was a low micromolar inhibitor (K_I of 2849.6 nM) whereas all the other compounds resulted ineffective (K_Is > 10000). The 6- and 7-substituted coumarins **84** and **85** showed lower inhibition potencies against the hCA IV when compared to their parents **69** and **70**. In addition the presence of the DCH moiety enhanced the selectivity of the 6-substituted compound towards hCA IV of almost 2 fold (see Table 1). Interestingly the 6-substituted sulfocoumarin bearing the CORM tail **86** resulted slightly more potent than its precursor **71** in inhibiting the hCA IV (K_Is of 55.1 and 59.7 nM respectively). On the contrary, the regioisomer at position 7 (i.e. compound **87**) showed an opposite inhibition profile (see **Table 2.1**). Again the introduction of the CORM moiety determined a reduction of the K_I values of both the 4-methyl coumarin and the thiooxocoumarin scaffolds substituted at 7-position (see **73** to **88** and **74** to **89** in **Table 2.1**). Significant inhibition improvements against hCA IX was observed for compounds **84**, **87** and **88** which resulted to be 1217.3, 1345.1 and 58.9 fold more potent when compared to the parent compounds **69**, **72** and **73**. In addition, the K_I values obtained were among the lowest in the series (i.e. 3.9, 4.6 and 2.9 nM respectively). It is worth noting that the inhibition profile for such compounds on hCA IX strictly depends on their regioselectivity. **Table 2.1** clearly showed that the 6-substituted derivative **84** was a low nanomolar inhibitor (K_I 3.9 nM) whereas its 7-substituted counterpart **85** resulted ineffective (K_I > 10000 nM). The opposite trend was observed for the sulfocoumarins **86** and **87** with the former being 85.2 less potent against the hCA IX isoform. Finally the thiooxocoumarin **89** resulted ineffective in inhibiting the tumor associated isoform as its non-substituted counterpart **74** (K_Is > 10000 nM). The last hCA considered (i.e. hCA XII) showed a kinetic trend almost superimposable to the hCA IX except for **86** which resulted far less potent when compared to its precursor **71** (K_Is of 669.7 and 44.5 nM respectively).

2.2.3 CO Release Assay

A spectrophotometric-based assay to evaluate the CO-releasing rate from the CORM moieties was first reported by Motterlini et al. in 2002 [21]. This method allows to quantify the CO gas release by following the absorption variations in the visible region of the deoxy-Myoglobin (II) (deoxy-Mb) UV-Vis spectrum, which is characterized by a large band centred at 553 nm (**Figure 2.8 a**). CO has a great affinity for the Mb heme iron (II) and when it is released by a CORM in solution with deoxy-Mb, it immediately binds to the heme iron in 1:1 ratio, inducing the formation of the Mb ferrous CO complex (Mb-CO), whose spectrum in the visible region is characterized by two bands at 541 and 576 nm (**Figure 2.8 a**) [56].

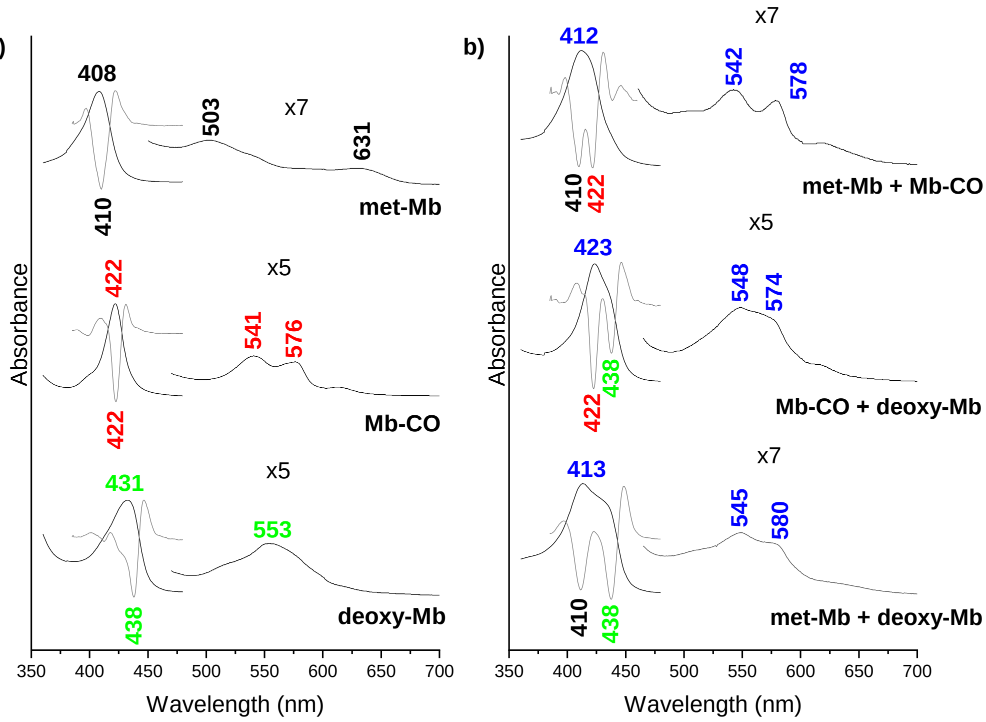

Figure 2.8 a) Absorption and second derivative spectra of (from top to bottom) met-Mb (III), Mb-CO (II) and deoxy-Mb (II). The 450-700 nm region has been expanded 7-fold for met-Mb and 5-fold for Mb-CO and deoxy-Mb. **b)** Absorption and second derivative spectra of three different mixtures (from top to bottom) met-Mb + Mb-CO, Mb-CO + deoxy-Mb, and met-Mb + deoxy-Mb. The 450-700 nm region has been expanded 7-fold for met-Mb + Mb-CO and met-Mb + deoxy-Mb, and 5-fold for Mb-CO + deoxy-Mb.

Since the Mb redox potential is in favours of the formation of the oxidized met-Mb (III) form, unable to bind CO, the continuous presence of a reducing agent (i.e. sodium dithionite) during the assay is necessary to prevent the deoxy-Mb (II) from oxidation.

In the present work we used the spectrophotometric-based assay according to Motterlini's. We acquired the whole UV-Vis spectrum and focused on the Soret region to better distinguish the bands corresponding to different Mb species formed during the assay (**Figure 2.9**). In fact as the reducing agent is gradually consumed deoxy-Mb is promptly oxidized to met-Mb thus resulting in a mixture of met-Mb and Mb-CO, whose spectrum in the visible region, showing two bands at 542 and 578 nm (**Figure 2.8 b**) is very similar to that of pure Mb-CO (541 and 576 nm, **Figure 2.8 a**). Differently the second derivative spectrum in the Soret region, being this band very sensitive to the Mb oxidation state, allows to clearly distinguish each form in the mixture: Met-Mb at 410 nm, Mb-CO at 422 nm, and deoxy-Mb at 438 nm (**Figure 2.8 b**).

Moreover, the reducing agent sodium dithionite shows an intense absorption band around 315 nm (data not shown), whose intensity can be used to estimate its presence in solution.

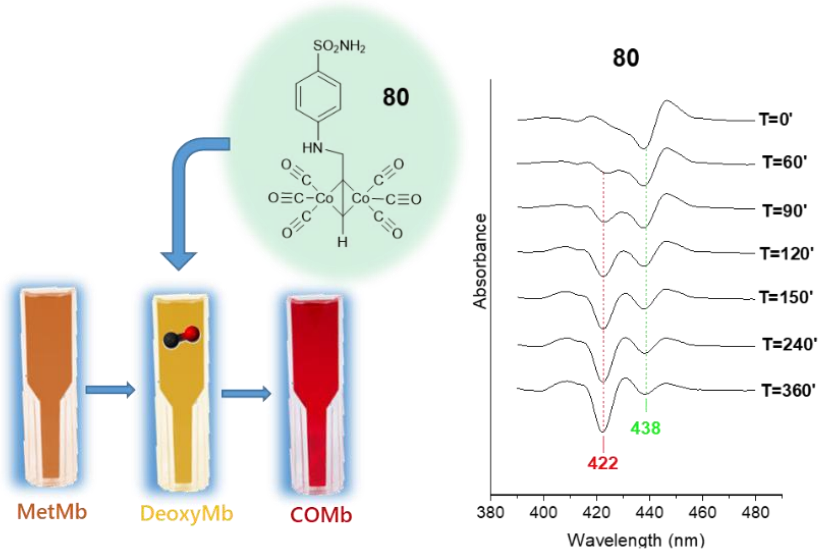

Figure 2.9 Schematic representation of the spectrophotometric assay on the CAI-CORM hybrid **80**, chosen as an example, performed for 360 minutes. The increase of the 422 nm Mb-CO band and the concomitant decrease of the 438 nm deoxy-Mb band were monitored.

At the end of the assay the solution was flushed with CO to carbonylate the residual Mb and ensure that the final Mb concentration was identical to that measured at the beginning of the experiment. Surprisingly for each sample we found out that the Mb concentration was diminished of about 25% (**Figure 2.10 A**). Therefore, two blank solutions containing met-Mb + the tested CORM and met-Mb + sodium dithionite (i.e. deoxy-Mb) were prepared and the respective UV-Vis spectra acquired for the 360 minutes assay time. **Figure 2.10 B and C** show that the absorbance of the met-Mb + CORM mixture remains unchanged after 360 minutes, while there is an intensity decrease of about 45% in the deoxy-Mb sample (corrected for the dilution factor due to the necessary re-addition of sodium dithionite from time to time), implying that the prolonged exposure of Mb to sodium dithionite causes a partial degradation of the protein.

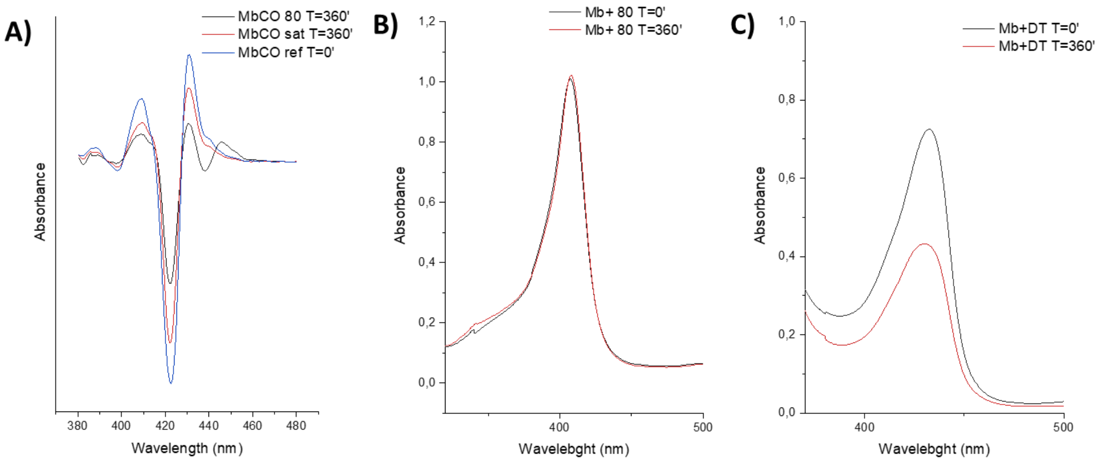

Figure 2.10. A) Second derivative spectra in the Soret region of Mb-CO obtained: by flushing half of the deoxy-Mb solution with CO at the beginning of the experiment (blue line); after 360 minutes from the addition of compound **80** to the other half of the deoxy-Mb solution (black line); by flushing with CO the previous sample at the end of the assay (red line); UV-Vis spectra of the two blank solutions met-Mb + CORM **80** (**B**) and met-Mb + sodium dithionite (**C**) at time 0 (black lines) and after 360 minutes from the addition (red lines).

The relative amount of Mb-CO (χCO) formed in presence of deoxy-Mb at each time point (t) was calculated by measuring the absorbance at Mb-CO and deoxy-Mb absorption maxima (422 and 431 nm, respectively) and applying a previously reported equation [57]:

$$\chi_{CO}(t) = \frac{A(422)\times A^{r}_{deoxy}(431) - A(431)\times A^{r}_{deoxy}(422)}{A(422)\times\left[A^{r}_{deoxy}(431) - A^{r}_{CO}(431)\right] + A(431)\times[A^{r}_{CO}(422) - A^{r}_{deoxy}(422)]}$$

Equation 2.1

At each time point (t), the Mb-CO (and therefore the released CO) concentration is given by:

$$[Mb - CO]_t = \chi_{CO}(t) \times [Mb]_0$$

Equation 2.2

where $[Mb]_0$ is the total Mb concentration, measured at the beginning of the assay. Due to the Mb degradation induced by sodium dithionite, a correction to the previous equation is necessary:

$$[Mb - CO]_t = \chi_{CO}(t) \times ([Mb]_0 - [Mb]_{d(t)})$$

Equation 2.3

Where $[Mb]_{d(t)}$ is the degraded Mb concentration at time *t* and is calculated with the following equation, assuming as constant the Mb degradation rate:

$$[Mb]_{d(t)} = \frac{[Mb]_0 - [Mb]_{360}}{360'} \times t \qquad \textbf{Equation 2.4}$$

Where $[Mb]_{360}$ is the Mb concentration obtained by flushing the solution with CO at the end of the assay (360 minutes).

The obtained results are also supported by the curve fitting analysis of the UV-Vis spectra of the Mb + CORM solution at each time point (**Figure 2.11**), as shown in **Figure 2.12** (red and blue lines).

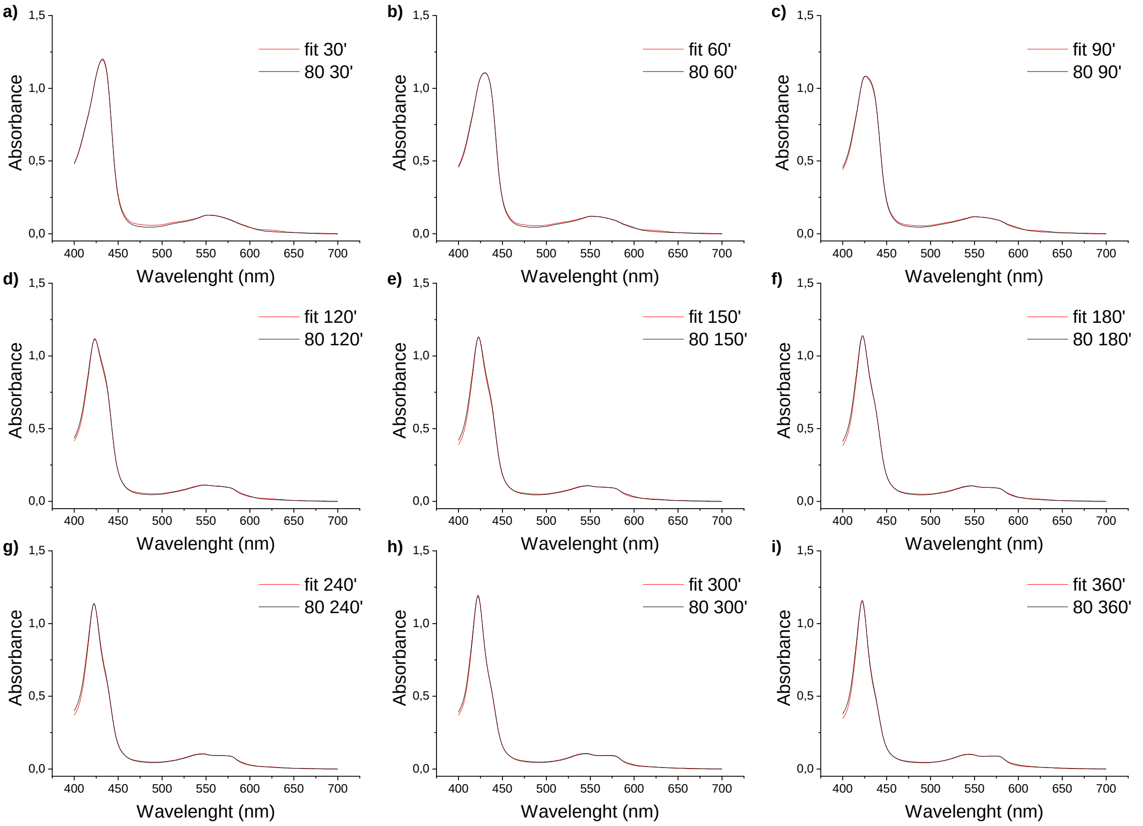

Figure 2.11: UV-Vis spectra at each time point of the compound **80** spectrophotometric assay (black lines), together with the curvefitting analysis (red lines) obtained by mixing the pure deoxy-Mb and Mb-CO reference UV-Vis spectra.

Conversely, the non-corrected equation after 90 minutes from the beginning of the assay leads to an overestimation of the released CO (**Figure 2.12**, black line), that increases over time with the amount of degraded Mb.

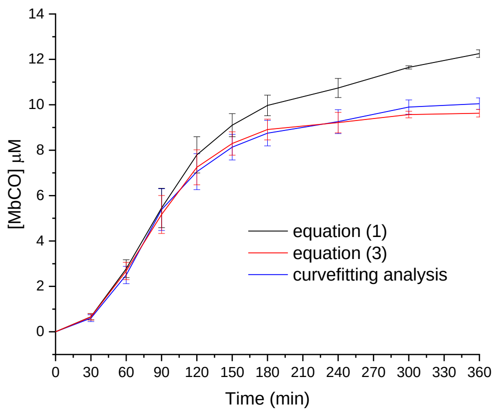

Figure 2.12. [Mb-CO] values obtained by: the non-corrected **Equation 2.1** (black), the corrected **Equation 2.3** (red) and the curve fitting analysis (blue).

The assay was performed on a selection of 4 compounds (**80**, **85**, **86** and **88**), encompassing various chemical structures and compared to a previously reported cobalt based CORM compound **90** [50]**,** used as a reference (**Figure 2.13**).

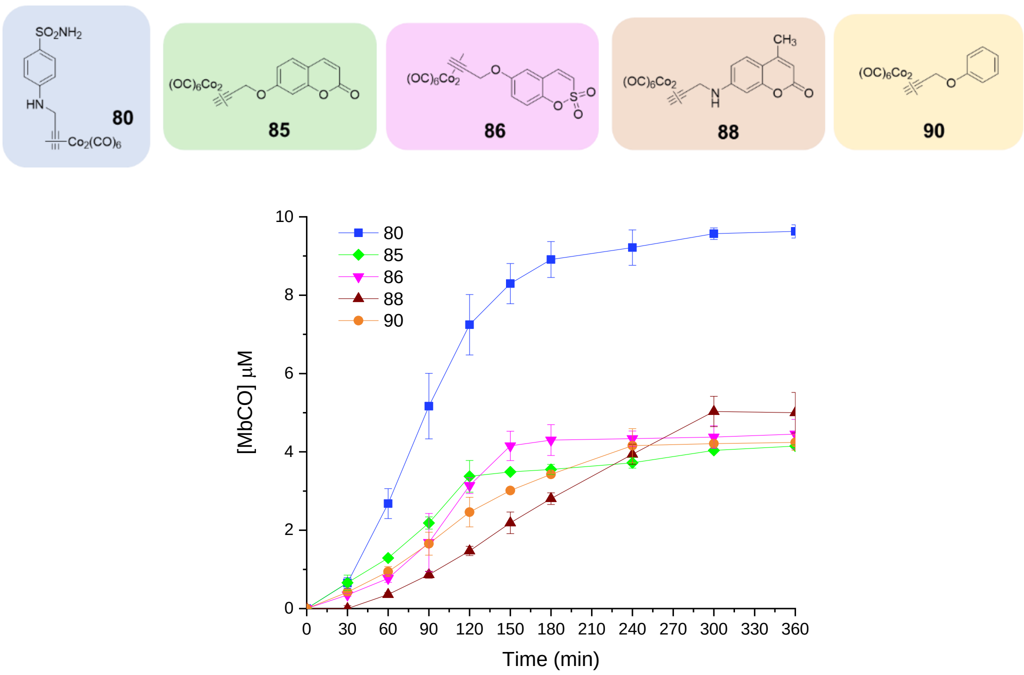

Figure 2.13. Chemical structures of the CAI-CORMs **80**, **85**, **86**, **88** and **90** and their CO release profiles as obtained from the spectrophotometric assay (mean of 3 results).

Starting from a 20 μM CAI-CORM concentration in a 20 μM deoxy-Mb solution, the CO release profiles of the analysed compounds were reported as the MbCO concentration formed over time (**Figure 2.13**). Among all the tested hybrids, **80** clearly revealed to be the fastest CORM also in comparison to the reference compound **90**. As shown in **Figure 2.13,** compound **80** released 2.7 µM of MbCO just after 60 min of incubation. Such a value was approximately twice the amount generated from compound **85** at the same time point (**Figure 2.13**) and even higher when compared to the reference compound **90**. The CO release from **80** constantly continued up to 150 min (8.3 µM of MbCO) and then it began to slow down reaching a plateau after 300 min (9.6 µM of CO liberated). The CO release profiles showed by the coumarin and sulfocoumarin containing hybrids **85** and **86** were quite similar. The first reached a plateau at 120 minutes (3.5 µM of MbCO), whereas the latter at 150 min of incubation (4.2 µM of MbCO). Overall the CO releasing trend for both **85** and **86** was reasonably close to the reference **90**. Interestingly the 4-methyl-7-aminocoumarin **88** ensured a constant CO release up to 300 min (5 µM of released CO) when it reached a plateau. As reported before, the CORM moiety herein considered is classified among the slow CO releasers and thus our hybrids may be properly handled by means of their $T_{1/X}$ (**Figure 2.14**).

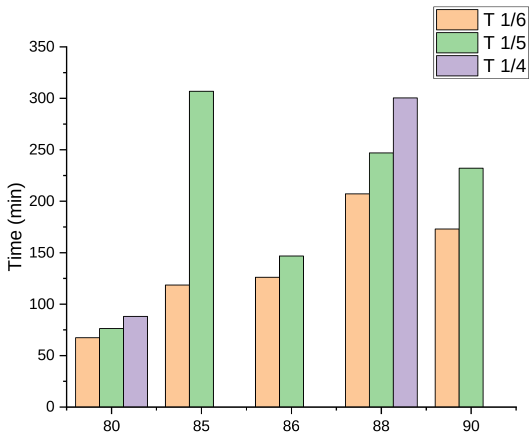

	$T_{1/6}$	$T_{1/5}$	$T_{1/4}$
80	67,4	76,3	88,1
85	118,6	306,8	-
86	126,1	146,76	-
88	207,2	247	300,4
90	173	232,1	-

Figure 2.14. $T_{1/6}$, $T_{1/5}$ and $T_{1/4}$ values (defined as the time necessary for a CORM solution to produce a Mb-CO concentration equal, respectively, to 1/6, 1/5 and 1/4 of its own concentration) of the analysed compounds based on the spectrophotometric assay.

The $T_{1/6}$ values of all the compounds range from 67.4 to 207.2 min. The ratios between the $T_{1/6}$ values of the coumarin containing compounds (**85**, **86** and **88**) over the sulfonamide one **80** are of 1.8, 1.9, 3.1, respectively. Also, the reference **90** showed a $T_{1/6}$ values 2.6 fold higher when compared to **80**. Remarkable differences in CO release kinetics were more evident when the $T_{1/5}$ values were considered. In this case the value ratios are 4.0, 1.9, 3.2 and 3.0, respectively (**Figure 5**). Such large differences are clearly due to the effects of the CAI scaffolds on the CORM moiety. This makes the CAI-CORM compounds herein reported particularly interesting as potentially useful for biomedical purposes.

2.2.4 *In vivo* evaluation of Pain relief effects

2.2.4.1 Paw pressure Test

The acute pain reliever effect of the CAI-CORMs hybrids molecules **80, 85, 86** and **88** (10 – 100 mg kg^{-1}), performed by Prof. Gheraldini's group at University of Florence, was evaluated by means of the paw pressure test in a rat model of RA induced by CFA i.a. The obtained data are reported in **Figure 6**.

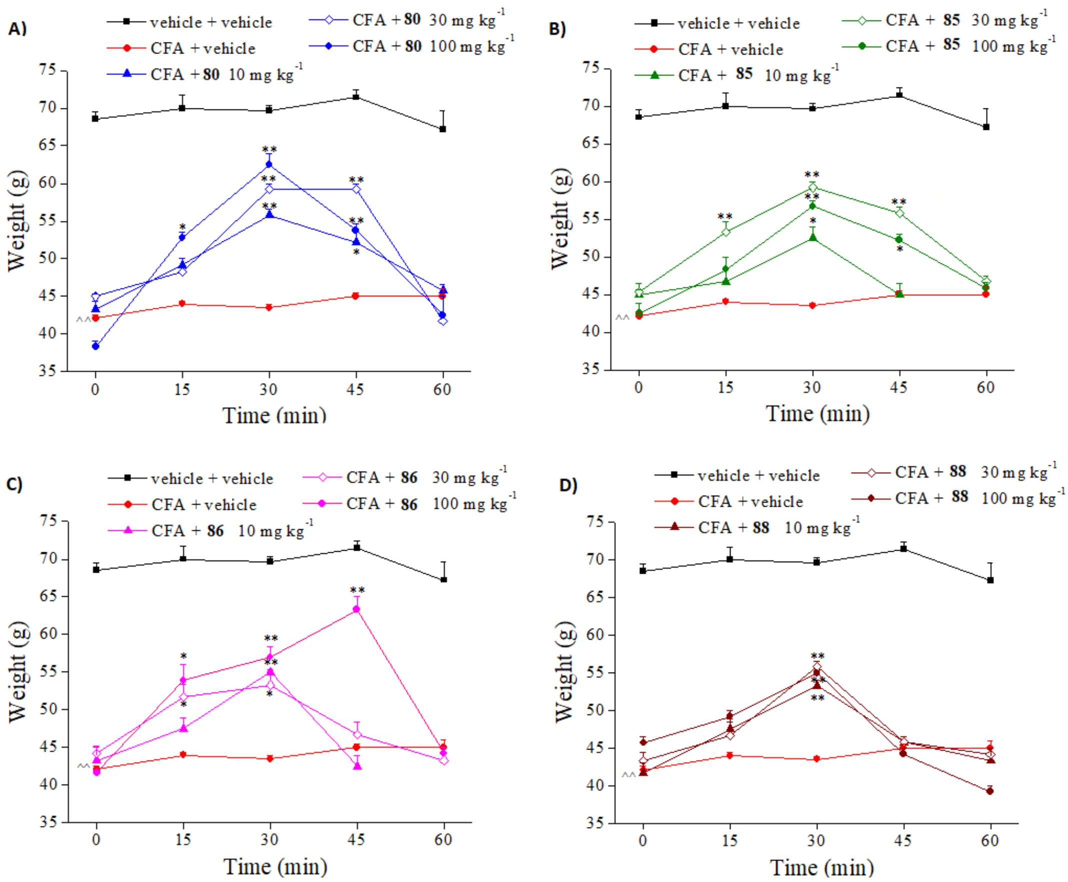

Figure 2.15. Acute pain relieving effect of **80 (A)**, **85 (B)**, **86 (C)** and **88 (D)** (10 – 100 mg kg^{-1}) in a CFA i.a. injection-induced RA model in rats. The Paw pressure test was used to assess the hypersensitivity toward a noxious mechanical stimulus.

The sulfonamide containing CORM hybrid **80** was able to increase the pain threshold in a dose dependent manner being effective already at 10 mg kg^{-1} and peaking 30 min after administration. The effect of **80** lasted up to 60 min. Interestingly, the administration of **80** at 30 mg kg^{-1} resulted in enhancement of the antinociceptive effect which peaked at 30 min and stayed still for additional 15 min followed by a progressive activity depletion within 15 min. The use of **80** at higher doses (100 mg kg^{-1}) restored the symmetry of the activity curve, the compound peaked at 30 min after administration with higher affects which lasted up to 60 min. As for the 7-substituted coumarin **85** a modest response was reported at 10 mg kg^{-1} (see **Figure 2.15 B**). Interestingly, the administration of the same compound at higher doses determined the maximum antinociceptive response only when 30 mg kg^{-1} were used, since 100 mg kg^{-1} dosage resulted in a slight reduction. As for the sulfocoumarin **86** a rather unclear trend was observed. At 10 mg kg^{-1} the compound exerted an anti-hypersensitivity effect similar to that evoked by the molecules **85** (see **Figures 2.15 C** and **B**) with the latter being slightly less potent. The increase of the concentration (i.e. 30 mg kg^{-1}) resulted in a slight decrease of the maximum effect (registered at 30 min) but a significant response appeared already after 15 min and a residual antinociceptive response was present after 45 min of administration. Unexpectedly the highest dose of **85** (100 mg kg^{-1}) determined an overall enhancement of the biological response as well as shifting of the maxim peak to 45 min with values comparable to **80** at the same concentration (see **Figures 2.15 A** and **C**). Unfortunately, the strong response of **85** vanished in just 15 min after the maximum response was registered. The compound **88** did not reveal a dose-dependent anti-hypersensitivity profile (**Figure 2.15 D**). All three concentrations used determined a maximum response at 30 min after administration and the effect lasted up to 45 min.

We focused on the sulfonamide containing moiety **80** since its CAI warhead does not necessitate any enzymatically induced change to exert the activity [51], and thus no additional effects on the CO releasing kinetics would be expected upon binding with the hCA enzymes. **Figure 2.16** reports the acute pain relieving activity of **80** at its maximum activity dosage (i.e. 100 mg kg^{-1}) compared to the CAI **65**, compound **90** and the NSAID ibuprofen usually employed to relieve articular aches [58].

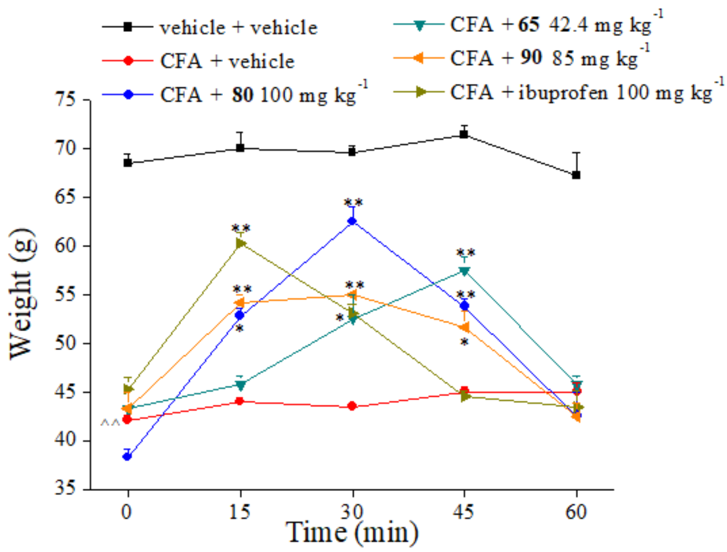

Figure 2.16. Acute pain relieving effect of **65**, **80**, **90** and **Ibuprofen** in a CFA i.a. injection-induced RA model in rats tested at a dosage equimolar to 100 mg kg^{-1} of the composite compound **80** (42.4, 85 and 100 mg kg^{-1} respectively). The measurements were accomplished on day 14 after CFA injection. Compounds were suspended in 1% carboxymethylcellulose (CMC) and orally administered. The values reported are the mean of 10 rats performed in 2 different experimental sets. ^^P<0.01 vs vehicle + vehicle treated animals; *P<0.05 and **P<0.01 vs CFA + vehicle group.

None of the tested compounds changed the pain threshold of the contralateral paw, thus suggesting that such molecules do not influence the normal pain sensitivity (data not shown). The high nanomolar CAI **65** showed an anti-hyperalgesic activity which constantly raised up to 45 min after administration and then rapidly declined within 15 min. Ibuprofen mirrored **65** activity giving a slighter intense peak at 15 min which gradually diminished up to 45 min. Interestingly the anti-hyperalgesic effects of **90** covered the lack of activity of both **65** and **80** although with less intensity. In this context the CAI-CORM hybrid **80** clearly showed the advantage of our strategy intended to merge in a single molecular entity two therapeutically active portions. **Figure 2.16** shows that **80** is superior in its anti-hyperalgesic effects when compared to the single components **65** and **90**. In addition the symmetry of the curve was consistent with a biological response being exerted by both the CAI and the CORM sections merged within the hybrid.

2.2.4.2 Incapacitance Test

The efficacy of hybrids **80**, **85**, **86** and **88** was also evaluated against the spontaneous pain, which was measured as the hind limb weight bearing alterations originated by monolateral damage (Incapacitance test, **Figure 2.17**).

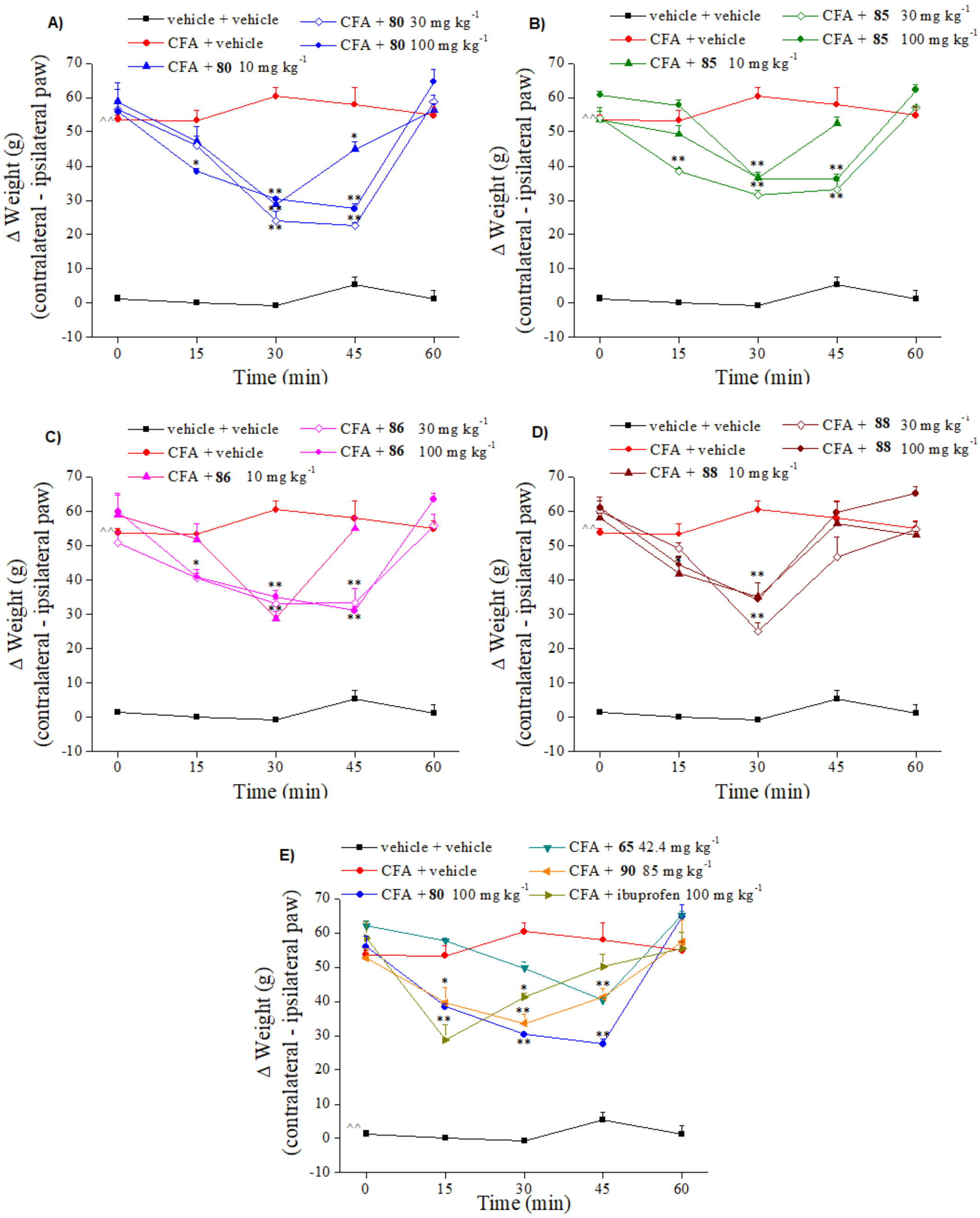

Figure 2.17. Acute pain relieving effect of **80 (A)**, **85 (B)**, **86 (C)** and **88 (D)** (10 – 100 mg kg^{-1}) in a CFA i.a. injection-induced RA model in rats. The incapacitance test was performed in order to assess the hind limb weight bearing alterations, which were measured as postural imbalance related to pain stimuli. The data values are the mathematical difference between the

weight applied on the contralateral and ipsilateral paw (Δ weight). The single molecules CAI (**65**) and CORM (compound **90**), were tested at a dosage equimolar to 100 mg kg^{-1} of the composite compound **80** (42.2 mg kg^{-1} and 85 mg kg^{-1}, respectively. Ibuprofen 100 mg kg^{-1} was used as reference drug **(E)**. The measurements were accomplished on day 14 after CFA injection. Compounds were suspended in 1% carboxymethyl cellulose (CMC) and orally administered. The values reported are the mean of 10 rats performed in 2 different experimental sets. ^^P<0.01 vs vehicle + vehicle treated animals; *P<0.05 and **P<0.01 vs CFA + vehicle group

The difference values between the weight burdened on the contralateral and ipsilateral paw (Δ weight) was increased in CFA-treated animals when compared to the values of the control group (53.6 ± 1.4 g *vs* 1.3 ± 1.0 g, respectively). Compound **80** was active since the lowest concentration (10 mg kg^{-1}) halved the Δ weight 30 min after administration. The higher dosages showed a long-lasting effect, starting from 15 min up to 45 min after treatment (**Figure 2.17 A**). Similar results were obtained with the administration of the hybrid **86** (**Figure 2.17 C**) whereas compounds **85** and **88** did not shown a dose-dependent efficacy. In both cases the dosage of 30 mg kg^{-1} performed the best pain relieving effect 30 min after injection (**Figures 2.17 C** and **D**, respectively). In agreement with the paw pressure test also the incapacitance experiments clearly showed that the single administration of the CAI **65**, **ibuprofen** and **90** determine anti-hyperalgesic effect with lower intensity when compared to the hybrid **80 (Figure 2.17 E**). In addition the curve of **80** showed a rather symmetrical profile and thus supporting our merging based approach.

2.2.4.3 Irwin test

To exclude a possible toxicity induced by the acute compound's administration, behavioural, autonomic and neurological parameters were evaluated giving an arbitrary score by the Irwin test. All hybrids were administered at the highest dose used during the evaluation of the painkiller effect (100 mg kg^{-1}). All observational categories were not significantly affected by the acute administration of compounds **80**, **85**, **86** and **88** as reported in **Table 2.2**.

CORMs	**80**	**85**	**86**	**88**	**Limits**
Dose	100 mg kg^{-1}	100 mg kg^{-1}	100 mg kg^{-1}	100 mg kg^{-1}	
Behaviour					
Spontaneous activity	4	4	4	4	4 - 0
Passivity	0	0	0	0	0 - 4
Cleaning	0	0	0	0	4 - 0
Curiosity	4	4	4	4	4 - 0
Reactivity	4	4	4	4	4 - 0
Vocalization	0	0	0	0	0 - 4
S.N.C. excitement					
Straub tail	0	0	0	0	0 - 4
Tremors	0	0	0	0	0 - 4
Convulsions	0	0	0	0	4 - 0
Movement					
Ataxia	0	0	0	0	0 - 4
Stereotipies	0	0	0	0	0 - 4
Straightening reflex	4	4	4	4	4 - 0
Muscolar tone					
Physical strenght	4	4	4	4	4 – 0
Reflexes					
Palpebral reflex	4	4	4	4	4 - 0
Autonomic signes					
Piloerection	0	0	0	0	0 - 4
Exophthalmos	0	0	0	0	0 - 4
Cyanosis	0	0	0	0	0 - 4
Flush	0	0	0	0	0 - 4
Pallor	0	0	0	0	0 - 4
Palpebral opening	4	4	4	4	4 - 0
Salivation	0	0	0	0	0 - 4
Lacrimation	0	0	0	0	0 - 4
Hypo-hyperthermia	0	0	0	0	-4/+4
Writhing	0	0	0	0	0 - 4
Toxicity					
Immediate death	0	0	0	0	0 - 4
Delayed death (48 h)	0	0	0	0	0 - 4

Table 2.2. Irwin test.

2.3 CAI-CORM dual hybrids: extension of the library

On the basis of the promising results obtained we pursued a deeper investigation aimed to explore the influence on the CO release rate when the length of the tether connecting the CAI portion to the CORM moiety was varied. Moreover, we aimed to quantify the CO release when the dicobalt hexacarbonyl complexes were placed on internal alkynes and compared with the analogous terminal ones.

2.3.1 Design and synthesis

We extended the compound library, by synthetizing 15 new compounds including 4,6 and 7 substituted coumarins, *p*-amino and *p*-hydroxy-benzensulfonamide derivatives. The alkyne precursors **91-105** were all synthesized by reacting hydroxyl/amino coumarins or *p*-amino/*p*-hydroxy-benzensulfonamides with the proper alkyl halide, using potassium carbonate (K_2CO_3) or pyridine as a base [54] (**Scheme 2.3**).Then the precursors **91-105** were all treated as previously discussed with dicobalt octacarbonyl in slight calculated excess (1.05 eq. for **91-103** and **105** or 2.1 eq. for **104**) to afford the final compounds **106-120** at r.t. and in high yields after a flash chromatography purification step (**Scheme 2.4**) [54].

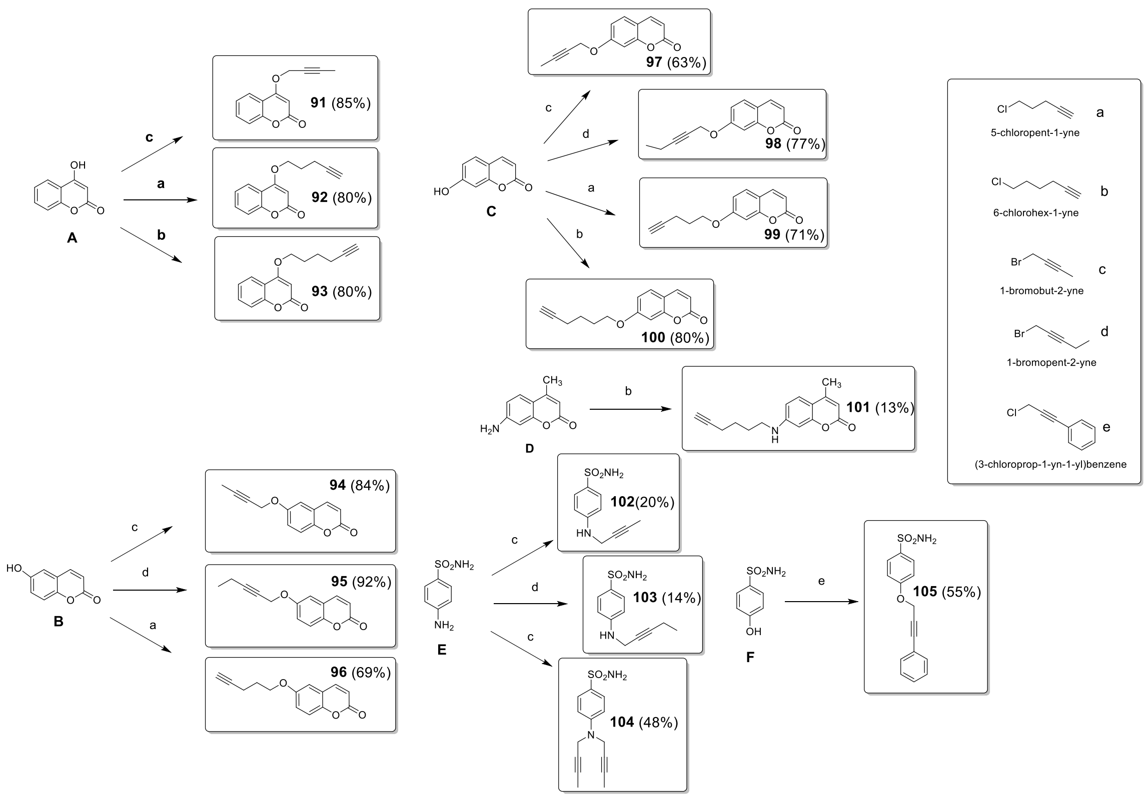

Scheme 2.3: Synthetic procedures for the preparation of CAIs **91-105**.

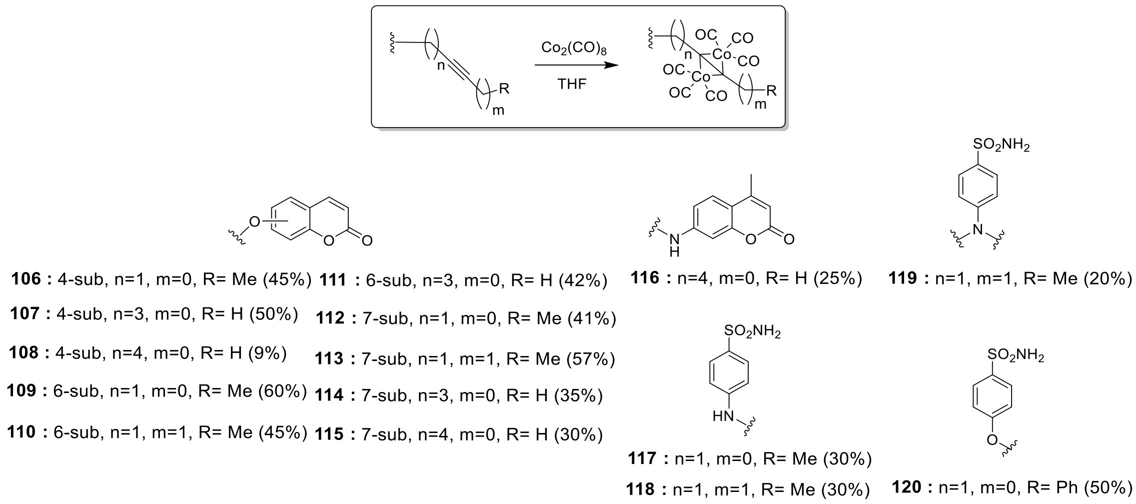

Scheme 2.4: Synthetic procedures for the preparation of CAI-CORMs **106-120**.

2.3.2 *In vitro* Biological Evaluation: hCA inhibition

CAI-CORM dual hybrids **106-120** were investigated as inhibitors of the hCAs I, II, IX and XII by means of the stopped flow CO_2 hydrase assay [55]. The inhibition data, compared to those of the standard sulfonamide inhibitor acetazolamide (**AAZ**), are reported in **Table 2.3**.

	K_I (nM)*			
	hCA I	**hCA II**	**hCA IX**	**hCA XII**
106	>10000	>10000	8.2	6.8
107	>10000	>10000	8.9	8.5
108	>10000	>10000	9.5	7.5
109	>10000	>10000	8.5	5.6
110	>10000	>10000	8.9	8.1
111	>10000	>10000	14.8	6.2
112	>10000	>10000	27.8	7.3
113	>10000	>10000	8.4	8.0
114	>10000	>10000	24.5	3.7
115	>10000	>10000	31.0	2.7
116	>10000	>10000	9.5	5.8
117	957.6	2349.0	27.8	4.6
118	3010.0	4245.0	26.5	2.1
119	6191.0	9.5	25.8	27.8
120	5638.0	35.8	141.9	2.7
AAZ	250	12	25.8	5.7

Table 2.3. Inhibition data of hCA I, hCA II, hCA IX and hCA XII with compounds **106-120** and the standard sulfonamide inhibitor acetazolamide (**AAZ**) by a Stopped flow CO_2 hydrase assay [55].* Mean from 3 different assays, by a stopped flow technique (errors were in the range of ± 5-10 % of the reported values).

i) In agreement with the data reported in literature, coumarins **106-116** showed high selectivity against the hCA IX and XII over the cytosolic isoforms I and II with K_I values comprised in the low nanomolar range (2.7 nM-31.0 nM). In particular, 4- and 6- substituted coumarins **106-111** revealed to be almost 3 fold more potent against hCA IX when compared to the 7-substituted derivatives **112-115**, against the same isoform. On the other hand, hCA XII revealed to be strongly inhibited by all the reported derivatives (K_I values between 2.7 nM-8.5 nM), with no detectable influence of structure changings on the K_I values.

ii) As for sulfonamide-based compounds **117-120**, a strong inhibition activity against hCA IX and XII can be observed too. In particular, *p*-hydroxy benzensulfonamide compound **120**, bearing the 3-phenylprop-2-yn-1-yl)oxy dicobalt hexacarbonyl tail, showed a medium-low K_I value against hCA IX (141.9 nM), being 5 fold less potent then the *p*-amino benzensulfonamides **117-119**. Quite interestingly low inhibition activity for the hCA I was showed by all derivatives, which can be explained considering the steric hindrance of the CORM moiety. Noteworthy, the di-alkylated compound **119** and the *p*-hydroxy benzensulfonamide derivative **120** strongly inhibit hCA II (K_I values of 9.5 and 35.8 nM respectively). Conversely, monosubstituted *p*-amino benzensulfonamides **117** and **118** showed K_I values against the same isoforms in the high nanomolar range (2349.0 nM and 4245.0 nM, respectively), thus revealing to be the most promising inhibitors among the series, with calculated selectivity index (SI) between the hCAII and IX of 83.9 and 163.3, respectively.

2.3.3 CO release assay

The release of CO was assessed by means of the Carbonylated Myoglobin (MbCO) formation assay over the time. Three compounds were chosen among the series, which allowed us to make a proper comparison between the CO release rate showed by the first series of compounds and the newly reported ones.

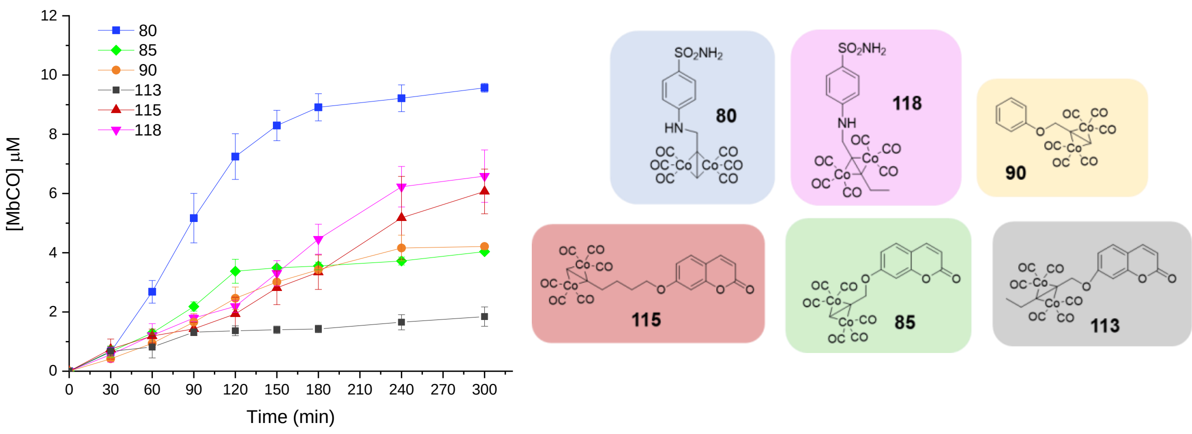

Figure 2.18. CO release profiles of CAI-CORMs **113, 115** and **118**, as obtained from the spectrophotometric assay (mean of 3 results), compared to CO release from CAI-CORMs **80**, **85** and CORM **90**.

Among the sulfonamide CAI bearing compounds, a CO release comparison between the terminal CORM **80** with its internal counterpart **118** was operated. In analogy for the coumarin series **85** was compared to **113**. Noteworthy the distance between the CAI head and the CORM moiety are kept constant in all cases.

Compound **80** formed 9.5 μM of MbCO after 5 hours of incubation whereas its CORM internal counterpart **118** generated just 6.6 μM of MbCO at the same time point. As reported form the kinetic curves in **Figure 2.18** the CO release of **80** resulted faster when compared to **118** and thus suggesting than the placement of the CORM species within an internal alkyne system tunes down the release rate of CO. Such a speculation was further confirmed when the CO release curves associated to the coumarin compound **85** with the **113** were compared. Again, the internal alkyne DHC **113** showed a strong reduction of the CO release rate in respect to **85** and thus in agreement with the same kinetic trend previously reported for the sulfonamide CAI-CORM derivatives.

The effects on the CO release when the length of the spacer was altered were evaluated by using **85** and **115**. The difference among the two species is the insertion of 3 sp^3 hybridized carbon atoms. The curves in **Figure 2.18** showed that 6 μM of MbCO were formed by compound **115** after 5 h incubation whereas the shorter derivative **85** provided 4 μM of carbonylated myoglobin at the same time point. Noteworthy the curve profile of the coumarin **115** was close to the ones of the sulfonamide CAI type (i.e. compare **115** with **118** and the previously discussed in **2.2.3**).

2.4 Conclusions

In summary, two new series of small molecule dual hybrids (CAI-CORMs) possessing a CAI warhead linked to a CORM tail were reported. In the first one we included all terminal acetylenic derivatives to be derivatized with $Co_2(CO)_8$. All the reported compounds **61-74** and **76-89** have been evaluated *in vitro* for their hCA inhibitory properties which allowed to identify the best performing ones on the isozymes mainly involved in major human affecting diseases. A selection of the CAI-CORM containing derivatives (i.e. **80**, **85**, **86** and **88**) were assayed *in vitro* for their CO releasing properties by using a slightly modified Motterlini's procedure, focusing on the Soret region of the Mb absorption spectra and applying the second derivative. This approach allowed to better distinguish the bands corresponding to the different Mb species formed during the assay. In addition we evaluated the *in vivo* pain relief effect of our compounds in a CFA i.a. injection-induced RA model in rats. Among the tested compounds, the sulfonamide hybrid **80** revealed to have an interesting profile, which was superior in terms of intensity as well as time distribution when compared to the single entities administered separately (i.e. **65** and **80**) and to the reference NSAID **ibuprofen**.

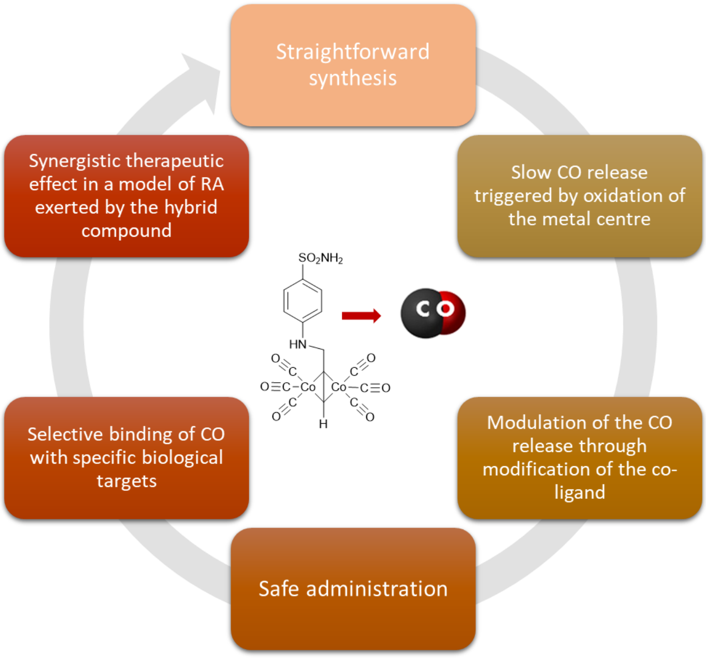

Figure 2.19. Schematic representation of the advantages related to the use of CAI-CORM hybrids for the management of RA.

In light of our promising results we decided to extend the library of CAI-CORM dual hybrids, in order to delineate more accurate SARs. We included in the second series compounds bearing an internal alkyne group and spacers of different lengths between the CAI and the CORM portions. The results obtained from the CO release assay performed on the titled compounds **113, 115** and **118** supported our hypothesis about the important role played by the co-ligand in influencing the CO release from the CORMs.

To the best of our knowledge the present study is the first to give solid support to the use of CAI-CORM hybrids for the management of human affecting disease such as RA related symptoms. In addition we demonstrated an efficient strategy (i.e. the hybridization approach) which allows: *i*) to control the release of CO gas from a CORM containing molecule. The electronic effects of the CORM containing scaffolds (i.e. the CAI warhead) influenced the CO release rate; *ii*) to diminish the lack of selectivity towards targets of biological interests. Such a drawback is a feature of CORMs and by making use of CORM-CAI hybrids we promoted a site targeted delivery towards cells overexpressing specific hCAs; *iii*) to make pharmaceutically useful and accessible a gaso-transmitter, such as the CO, which has been traditionally left behind the preferred H_2S or NO.

2.5 References

1. Haldane JB. Carbon monoxide as a tissue poison. Biochem J. 1927, 21, 1068–75.
2. Koyuncu S, Bol O, Ertan T. The detection of occult CO poisoning through noninvasive measurement of carboxyhemoglobin: A cross-sectional study. Am J Emerg Med. 2019, 1, 1583-83.
3. Tenhunen R, Marver HS and Schmid R. The enzymatic conversion of haem to bilirubin by microsomal haem oxygenase. Proc. Natl Acad. Sci. USA 1968, 61, 748–755.
4. Foresti R, Bani-Hani MG and Motterlini R. Use of carbon monoxide as a therapeutic agent:promises and challenges. Intensive Care Med. 2008, 34, 649–58.
5. Motterlini R, Otterbein, L.E. The therapeutic potential of carbon monoxide. Nat Rev Drug Discov. 2010, 9, 728-743.
6. Papapetropoulos A, Foresti R and Ferdinandy P. Pharmacology of the 'gasotransmitters' NO, CO and H2S: translational opportunities. Br J Pharmacol. 2015, 172, 1395-1396.
7. Yang G, Sener A, Ji Y, Pei Y, Pluth MD. Gasotransmitters in Biology and Medicine: Molecular Mechanisms and Drug Targets. Oxid. Med. Cell. Longev. 2016, 4627308.
8. Boehning D, Snyder SH. Circadian rhythms. Carbon monoxide and clocks. Science. 2002, 298, 2339–2340.
9. Kobayashi A, Ishikawa K, Matsumoto H, Kimura S, Kamiyama Y, Maruyama Y. Synergetic antioxidant and vasodilatory action of carbon monoxide in angiotensin II-induced cardiac hypertrophy. Hypertension 2007, 50, 1040–1048.
10. Bilban M, Haschemi A, Wegiel B, Chin BY, Wagner O, Otterbein LE. Haem oxygenase and carbon monoxide initiate homeostatic signaling. J Mol Med. 2008, 86, 267–279.
11. Maines M D. The haem oxygenase system: a regulator of second messenger gases. Annu Rev Pharmacol. Toxicol. 1997, 37, 517–554.
12. Poss KD, Tonegawa S. Reduced stress defense in haem oxygenase 1-deficient cells. PNAS USA. 1997, 94, 10925–30.
13. Stocker R. Antioxidant activities of bile pigments. Antioxid Redox Signal. 2004, 6, 841–49.
14. Boczkowski J, Poderoso JJ, Motterlini R. CO–metal interaction: vital signaling from a lethal gas. Trends Biochem Sci. 2006, 31, 614–621.

15. Kapetanaki SM. et al.Interaction of carbon monoxide with the apoptosis-inducing cytochrome c-cardiolipin complex. Biochemistry. 2009, 48, 1613–19.
16. Otterbein LE.et al.Carbon monoxide has antiinflammatory effects involving the mitogen-activated protein kinase pathway. Nature Med. 2000, 6, 422–428.
17. Zhang X, Shan P, Alam J, Fu XY, Lee PJ. Carbon monoxide differentially modulates STAT1 and STAT3 and inhibits apoptosis via a PI3K/Akt and p38 kinase-dependent STAT3 pathway during anoxiareoxygenation injury. J Biol Chem. 2004, 280, 8714–21.
18. Sarady JK.et al. Carbon monoxide protection against endotoxic shock involves reciprocal effects on iNOS in the lung and liver. FASEB J. 2004, 18, 854–56.
19. Zuckerbraun B.S. et al. Carbon monoxide protects against liver failure through nitric oxide-induced haem oxygenase 1. J Exp Med. 2003, 198, 1707–16.
20. Wegiel B. et al. Nitric oxide-dependent bone marrow progenitor mobilization by carbon monoxide enhances endothelial repair after vascular injury. Circulation. 2010, 121, 537–48.
21. Motterlini R, Clark JE, Foresti R, Sarathchandra P, et al. Carbon monoxide-releasing molecules: characterization of biochemical and vascular activities. Circ Res. 2002, 90, E17–E24.
22. Romão CC, Blättler WA, Seixas JD, Bernardes GJL. Developing drug molecules for therapy with carbon monoxide. Chem Soc Rev. 2012, 41, 3571-3583.
23. Greenfield H, Sternberg HW, Friedel RA, et al. Acetylenic dicobalt hexacarbonyls. Organometallic compounds derived from alkynes and dicobalt octacarbonyl. J Am Chem Soc. 1956, 78, 120 -4.
24. Green JR. Chemistry of propargyldicobalt cations: recent developments in the Nicholas and related reactions. Curr Org Chem. 2001, 5, 809 -26.
25. Omae I. Three characteristic reactions of organocobalt compounds in organic synthesis. Appl Organomet Chem 2007, 21, 318 -44.
26. Ott I, Kircher B, Dembinski R. Alkyne hexacarbonyl dicobalt complexes in medicinal chemistry and drug development Expert Opin Ther Patents. 2008, 18, 327-337.
27. Hyama T, Nishide K, Saimoto H, et al. Chem Abstr 1987, 107, 229145b.
28. Jung M, Kerr DE, Senter PD. Bioorganometallic chemistry: synthesis and antitumor activity of cobalt carbonyl complexes. Arch Pharm. 1997, 330, 173 -6.

29. Ott I, Schmidt K, Kircher B, et al. Antitumor-active cobalt-alkyne complexes derived from acetylsalicylic acid: studies on the mode of drug action. J Med Chem 2005, 48, 622 -9.
30. Jung M, Kerr DE, Senter PD. Bioorganometallic chemistry: synthesis and antitumor activity of cobalt carbonyl complexes. Arch Pharm 1997, 330, 173 -6.
31. Bathoorn E, Slebos DJ, Postma DS, Koeter GH, van Oosterhout AJ et al.Anti-inflammatory effects of inhaled carbon monoxide in patients with COPD: a pilot study. Eur Respir J. 2007, 30, 1131−37.
32. Otterbein LE, Bach FH, Alam J, Soares M, Lu HT, Wysk M, et al. Carbon monoxide has anti-inflammatory effects involving the mitogen-activated protein kinase pathway. Nat Med. 2000, 6, 422−428.
33. Ferrándiz ML, Maicas N, Garcia-Arnandis I, Terencio, MC, Motterlini Ret al. Treatment with a CO-releasing molecule (CORM-3) reduces joint inflammation and erosion in murine collagen-induced arthritis. Ann Rheum Dis. 2008, 67, 1211−1217.
34. Chang X, Han J, Zhao Y, Yan X, Sun S, Cui Y. Increased expression of carbonic anhydrase I in the synovium of patients with ankylosing spondylitis. BMC Musculoskeletal Disord. 2010, 11, 279− 290.
35. Zheng Y, Wang L, Zhang W, Xu H, Chang X. Transgenic mice over-expressing carbonic anhydrase I showed aggravated joint inflammation and tissue destruction. BMC Musculoskeletal Disord. 2012, 13, 256−265.
36. Liu C, Wei Y, Wang J, Pi L, Huang J, Wang, P. Carbonic anhydrases III and IV autoantibodies in rheumatoid arthritis, systemic lupus erythematosus, diabetes, hypertensive renal disease, and heart failure. Clin Dev Immunol. 2012, 2012, 1-6.
37. Margheri F, Ceruso M, Carta F, Laurenzana A, et al. Overexpression of the transmembrane carbonic anhydrase isoforms IX and XII in the inflamed synovium. J. Enzyme Inhib Med Chem. 2016, 31, 60−63.
38. Myasoedova E, Crowson CS, Kremers HM, Therneau TM, Gabriel SE. Is the incidence of rheumatoid arthritis rising? results from Olmsted County, Minnesota, 1955−2007. Arthritis Rheum. 2010, 62, 1576−1582.
39. Agarwal SK. Core management principles in rheumatoid arthritis to help guide managed care professionals. J Manag Care Pharm. 2011, 17, S03−S08.
40. Crofford LJ. Use of NSAIDs in treating patients with arthritis. Arthritis Res Ther. 2013, 15(Suppl 3),S2

41. Supuran CT. Carbonic anhydrases: novel therapeutic applications for inhibitors and activators. Nat Rev Drug Discov. 2008, 7, 168–81.
42. Farr M, Garvey K, Bold AM, Kendall MJ, Bacon PA. Significance of the hydrogen ion concentration in synovial fluid in rheumatoid arthritis. Clin Exp Rheumatol. 1985, 3, 99−104.
43. Steen KH, Steen AE, Reeh PW. A dominant role of acid pH in inflammatory excitation and sensitization of nociceptors in rat skin, in vitro. J. Neurosci. 1995, 15, 3982−3989.
44. Lardner A. The effects of extracellular pH on immune function. J Leukoc Biol. 2001, 69, 522−530.
45. Bua S, Di Cesare Mannelli L, Vullo D, Ghelardini C, Bartolucci G, Scozzafava A, Supuran, CT, Carta F. Design and synthesis of novel Nonsteroidal Anti-Inflammatory Drugs and Carbonic Anhydrase Inhibitors hybrids (NSAIDs-CAIs) for the treatment of rheumatoid arthritis. J Med Chem. 2017, 60, 1159−70.
46. Akgul O, Di Cesare Mannelli L, Vullo D, Angeli A, Ghelardini C, Bartolucci G, et al. Discovery of Novel Nonsteroidal Anti-Inflammatory Drugs and Carbonic Anhydrase Inhibitors Hybrids (NSAIDs−CAIs) for the Management of Rheumatoid Arthritis. J Med Chem. 2018, 61, 4961−4977.
47. Berrino E, Milazzo L, Micheli L, et al. Synthesis and Evaluation of Carbonic Anhydrase Inhibitors with Carbon Monoxide Releasing Properties for the Management of Rheumatoid Arthritis. J Med Chem. 2019, 62, 7233-7249.
48. Gong Y, Zhang T, Li M, Xi N, Zheng Y, Zhao Q, Chen Y, Liu B. Toxicity, bio-distribution and metabolism of CO-releasing molecules based on cobalt. Free Radic Biol Med. 2016, 97, 362–374.
49. Wilson JL, Fayad Kobeissi S, Oudir S, Haas B, Michel B, Dubois Randé JL, Ollivier A, et al. Design and Synthesis of New Hybrid Molecules That Activate the Transcription Factor Nrf2 and Simultaneously Release Carbon Monoxide. Chem Eur J. 2014, 20, 14698 – 14704.
50. Schimler SD, Hall DJ, Debbert SL. Anticancer (hexacarbonyldicobalt)propargyl aryl ethers: Synthesis, antiproliferative activity, apoptosis induction, and effect on cellular oxidative stress. J. Inorg Biochem. 2013, 119, 28–37.
51. Alterio V, Di Fiore A, D'Ambrosio K, Supuran CT, De Simone G. Multiple binding modes of inhibitors to carbonic anhydrases: how to design specific drugs targeting 15 different isoforms? Chem Rev. 2012, 112, 4421−4468.

52. Lomelino CL, Supuran CT, McKenna R. Non-Classical Inhibition of Carbonic Anhydrase. Int J Mol Sci. 2016, 17, 1150.

53. Sergeant CD, Ott I, Sniady A, Meneni S, Gust R, Rheingold AL, Dembinski R. Metallo-nucleosides: synthesis and biological evaluation of hexacarbonyl dicobalt 5-alkynyl-2 ′-deoxyuridines.Org Biomol Chem. 2008, 6, 73-80.

54. Carta F, Di Cesare Mannelli L, Pinard M, Ghelardini C, Scozzafava A, McKenna R, Supuran CT. A class of sulfonamide carbonic anhydrase inhibitors with neuropathic pain modulating effects. Bioorg Med Chem. 2015, 23, 1828-40.

55. Khalifah RG. The carbon dioxide hydration activity of carbonic anhydrase. I. Stop-flow kinetic studies on the native human isoenzymes B and C. J Biol Chem. 1971, 246, 2561-73.

56. Atkin AJ, Lynam JM, Moulton BE, Sawle P, Motterlini R, Boyle NM, Pryce MT, Fairlamb IJS. Modification of the deoxy-myoglobin/carbonmonoxymyoglobin UV–vis assay for reliable determination of CO-release rates from organometallic carbonyl compounds. Dalton Trans. 2011, 40, 5755–5761.

57. Smulevich G, Droghetti E, Focardi C, Coletta M, Ciaccio C, Nocentini MA. rapid spectroscopic method to detect the fraudulent treatment of tuna fish with carbon monoxide. Food Chemistry. 2007, 101, 1071–77.

58. Di Cesare Mannelli L, Bani D, Bencini A, Brandi ML, Calosi L, Cantore M, Carossino AM, Ghelardini C, Valtancoli B, Failli P. Therapeutic effects of the superoxide dismutase mimetic compound MnIIMe2DO2A on experimental articular pain in rats. Mediators Inflammation 2013, 2013, 1−11.

Chapter 3: CAI-AZT compounds as Telomerase Inhibitors

3.1 Introduction

3.1.1 Telomeres and Telomerases

All somatic cells do possess limited replicative potential as the replication apparatus is not able to copy chromosomes up to their entire length [1]. Such an effect is properly referred as the Hyflick limit [2]. A progressive shortage of the chromosome ends (i.e. the telomeres) is observed after every single replicative cell cycle [3] up to the critical limit, which triggers cells senescence programs, such as apoptosis, with cell death [4]. Telomeres are repetitive, non-coding, hexameric nucleotide repeats which in humans are composed by the TTAGGG sequence with a 3'-single-stranded overhang [5,6]. Their role, along with the telomere-associated shelterin complex, is to protect chromosomes from degradation and fusion and ultimately to maintain genome stability [5-9]. The shelterin complex is composed by the association of six proteins which specifically bind to the telomeric DNA, thus protecting it from being recognized as damaged site [8-10]. Overall such a physical replicative limitation of the DNA is thought to be an evolutionary protective mechanism aimed to avoid replication of abnormal chromosomes [11]. Telomeres shortening can be properly reverted by the enzyme Telomerase, which synthetizes new telomeric DNA from RNA template (Reverse Transcriptase, RT) [12]. Telomerase is a complex ribonucleoprotein holoenzyme having as catalytic component the reverse transcriptase telomerase protein (hTERT). The other main protein is the the telomerase RNA template (hTERC) which contains a RNA sequence complementary to the telomeres and serves as base for replication **(Figure 3.1)** [12-16]. Besides the canonical function of telomeres elongation, telomerases were also found to act as transcriptional regulator of Wnt/β-catenin signalling pathway, thus playing a crucial role in determining cell growth, differentiation and apoptosis in a non-telomeric manner [17-19].

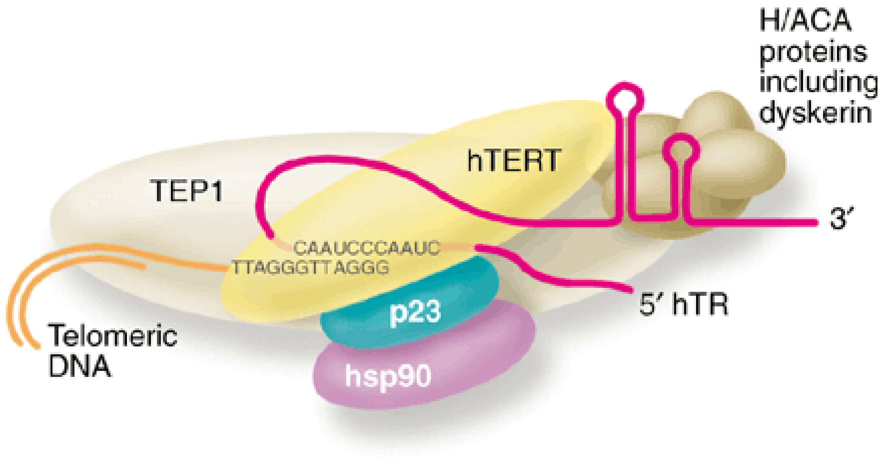

Figure 3.1. Telomerase complex and interaction with telomeric DNA.

This enzyme is normally expressed in adult germline cells and stem cells, whereas its activity is usually not detectable in somatic cells (**Figure 3.2**) [20,21]. Noteworthy it is speculated that a precise and strictly regulated action of telomerases can be also retrieved in normal cells, as telomerase dysfunction and premature telomeres loss have been associated with many diseases [21,23]. ROS and other stress factors, such as inflammatory cytokines, were found to directly reduce telomerase activity and contribute to early telomeres shortening in immune system cells [24,25]. Traslocation of telomerase from nuclei to mitochondria upon stress stimuli was also observed, thus implying a possible telomere-independent physiological function [26]. Short telomeres are also important symptoms of several diseases or can occur as the consequence of them [27,28]. Telomere length and aging have been found to be related [29]. In this context, positive modulation of telomerase activity may have therapeutic applications [30-32].

In 1994, a link between telomerase activity and cancer was reported for the first time [33]. Later, the relationship between telomerase expression and cell immortality was demonstrated by means of telomerase transfection in normal human cells, with a consequent five fold extension of cells lifespan [4]. To date telomerase is considered as tumor marker, being found active in 85% of malignant tumors (**Figure 3.2**).

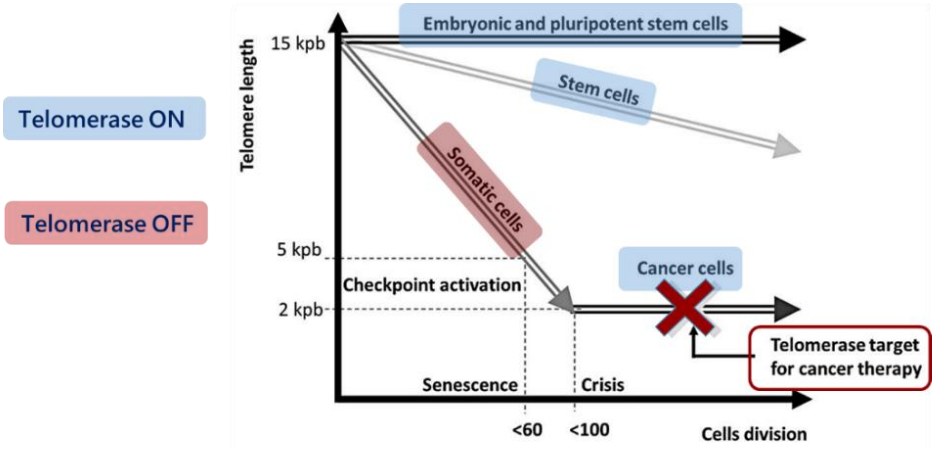

Figure 3.2. Telomere length *versus* cell divisions. Cancer cells, which re-activate or upregulate teomerase fully maintain telomeres but generally at reduced length when compared to germinal and stem cells.

The catalytic subunit hTERT was found to be over-expressed in several kind of tumors [34-36] and its regulatory role in metastatic events was also observed [37]. Enhancement of activity of telomerase in cancer cells occurs as consequence of mutations or epigenetic inputs on the hTERT promoter [11,40]. Limitless replicative potential is one of the hallmarks of cancer and is mainly due to the reactivation of the telomerase [39]. This observation makes this enzyme a potential target for developing potent and selective drugs [38,39].

3.1.2 Modulation of Telomerase Activity

3.1.2.1 Telomerase Activators

Transient somatic activation of telomerase to restore telomere length may be a powerful strategy for the treatment of chronic or degenerative diseases, as reported in several studies conducted in the last years [31,32,40-43]. Among the various approaches used to achieve telomere activation, are the use of low molecular weight natural compounds (Compounds **121-123** among the others in **Figure 3.2**) [44-47]. An example of this kind is the cycloastragenol **121** (**TA-65**) which was introduced in the market for the management of accelerated immunosenescence in HIV-affected patients.

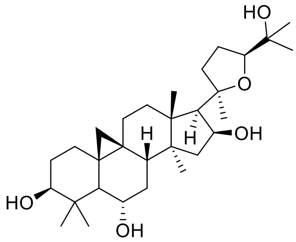

Cycloastragenol
121

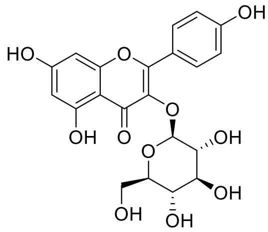

Astragaline
122

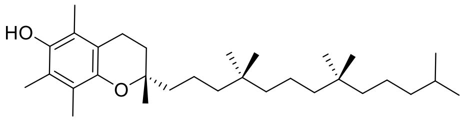

α-tocopherol
123

Figure 3.3. Natural compounds which activate telomerase.

TA-65 acts as telomerase activators in immune cells, neonatal keratinocytes and fibroblasts via the ERK-pathway and subsequent enhancement of the telomerase expression, thus leading to telomerase elongation without increasing cancer incidence [44-46].

Although such a therapeutic strategy looks quite promising, the activation of telomerase has important limitations. Since detectable telomerase activity is required to induce any therapeutic effects, this implies that the targeted cells are those devoid of it when pathological events take place. The pharmacological intervention is therefore aimed to restore a constitutive level of telomerase activity, and the stem cells and lymphocytes are the ideal candidates [48,49]. Moreover, the extended cell life time determines accumulation of genetic and epigenetic mutations, with an increased propensity to develop cancer transformations for the targeted cells [48,49].

3.1.2.2 Telomerase Inhibitors

Telomerase is a selective target as it is largely expressed in tumors and virtually absent in normal somatic cells [33,39,50]. The interference with high proliferative cells activities, such as stem and germinal cells, possessing an active form of telomerase was also found to be limited. Since they possess longer telomeres when compared to cancer cells, it is possible to affect tumor cell proliferation before the shortening of heathy cell telomeres become critical

[48-50]. Moreover, inhibition of telomerase led not only to reduction of tumor growth, but also to the elimination of tumor cells by means of apoptosis induction [51]

Telomerase inhibitors reported so far act by means of a direct inhibition of hTERT or hTERC subunits or preventing telomere binding to telomerase (compounds **124-128**, among the others. **Figure 3.4**) [49,52-57]. Imetelstat **124**, a thio-phosphoramidate oligonucleotide telomerase inhibitor complementary to the template part of telomerase RNA, is currently in clinical trial in hematologic myeloid malignancies promoted by Geron corp. Ongoing clinical studies of Imetelstat consist of IMerge™, a Phase 2/3 trial in lower risk myelodysplastic syndromes (MDS) and IMbark™, a Phase 2 trial in Intermediate-2 or High-risk myelofibrosis [57].

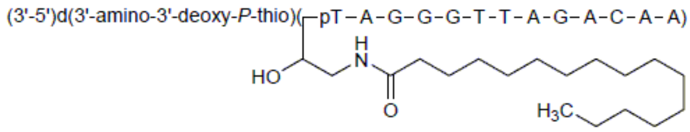

Imetelstat
124

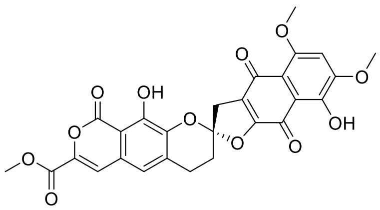

β-Rubromycin
125

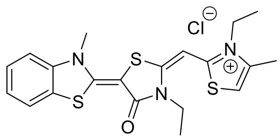

FJ5002
126

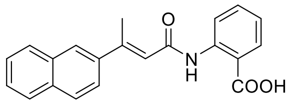

BIBR 1532
127

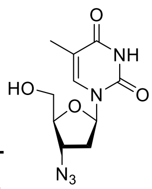

AZT
128

Figure 3.4. Some examples of Telomerase inhibitors reported in literature.

Making use of the DNA polymerase activity of the telomerases, nucleoside and nucleotide analogues have been extensively investigated as telomerase inhibitors. In particular the catalytic domain of telomerase is a functional RT, and chain-terminator RT inhibitors have been evaluated as antitumor agents (**Figure 3.5**) [58]. The first study of this type was conducted by Blackburn in 1994 in the ciliated protozoan *Tetrahymena thermophile* and revealed that the azidothymidine (**AZT,** compound **128**) was able to decrease the *de novo* telomere addition, thus resulting in telomeres shortening [59]. Further studies showed that in spite of the low affinity of **AZT** for mammalian DNA polymerases, its triphosphate derivative (**AZT-TP**) was incorporated into the eukaryotic genome [60]. This incorporation process was demonstrated mediated by the telomerases as it didn't occur in primary fibroblast cell which lack of such an enzyme [61]. Furthermore, by using immunofluorescence labeled antibodies against **AZT**, it was demonstrated that it was preferentially integrated into the telomeric region of tumor cell DNA in a model of Chinese hamster ovary cells CHO [62].

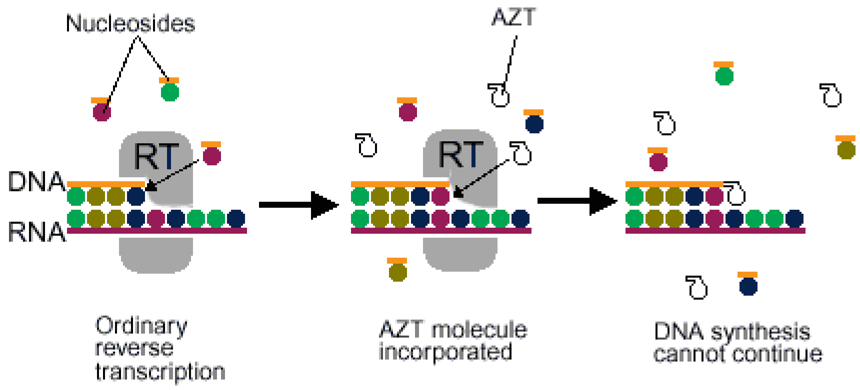

Figure 3.5. Incorporation process for AZT.

Recently, the same group reported **AZT** acting as telomerase inhibitors also affected hTERT non-conventional functions [19, 63]. This study proved that **AZT** dosage exerted different mechanism of action. **AZT** decreased cell migration and modified the organization of actin subunits in the cytoskeleton. As a consequence of the inhibition of hTERT extratelomeric effect on Wnt/β-catenin pathway less aggressive tumor phenotypes were observed [63].

Several studies demonstrated the efficiency of **AZT** in affecting tumor growth [64-66]. Treatment of patients affected by T cell leukemia/lymphoma with **AZT** turned out to have positive effects [64]. Moreover, association of **AZT** with other antitumor agents such as cisplatin, paclitaxel or 5-fluorouracil in treating leukemic cell lines and blood lymphocytes have been evaluated in several clinical trials, highlighting a synergistic interaction between the drugs [67-69]. A recent study by Yan Liu et al. revealed that **AZT** can be also useful in human pluripotent stem cell (hPSC) –based cell therapy [70]. This therapeutic approach, aimed to address numerous neurological disorders, is hampered by the potential tumorigenic properties associated with hPSC transplantation. **AZT** treatment was found to prevent overgrowth of hPSC-derived natural precursors and enhances the differentiation of cortical neurons in both cell cultures and hPSC-transplanted mouse brain [70].

Some drawbacks in using **AZT** as antitumor agent are its potential tumorigenic properties, under certain conditions and the slowness of the mechanism of action, which can expose the patient to dangerous side effects before the action of **AZT** is fully functional [71]. In this context, it must be said that there are general problems associated with the use of telomerase inhibitors for cancer therapy [72,73]. First, cancer cell senescence induced by telomerase inhibitors only occurs when telomeres have reached the critical length, thus implying that such agents require appropriate time to be effective. Moreover, even if limited, a negative effect on high proliferative cells functionality can eventually occur [19,21,50]. Induction of senescence by telomeric dysfunction may also result in activation of oncogenes and/or silencing of tumor suppressor genes, which promote malignant transformation to occur [74,75]. For these reasons, the simultaneous action on more tumor targets can be more effective in providing complete tumor eradication with a better safety profile.

3.1.3 CA IX/XII and Tumors

Among the many CA isoforms present in humans, CA IX and XII have a wide distribution in various tumors and are scarcely expressed in normal tissues [76,77]. As mentioned in **Chapter 1**, **Section 1.1.2**, recent advances in the field validated CA IX, and marginally CA XII, as therapeutic target for the treatment of metastatic tumors [78]. CA IX is mostly expressed in tissues where hypoxic conditions occur, such as the majority of solid tumors. Constitutive expression of CA IX is typical of the stomach and gut lining. All these findings led to the definition of CA IX as a tumor-associated enzyme [76-78]. The role of CA IX in pH regulation within tumor hypoxic cells is schematically reported below [79,80] (**Figure 3.6**).

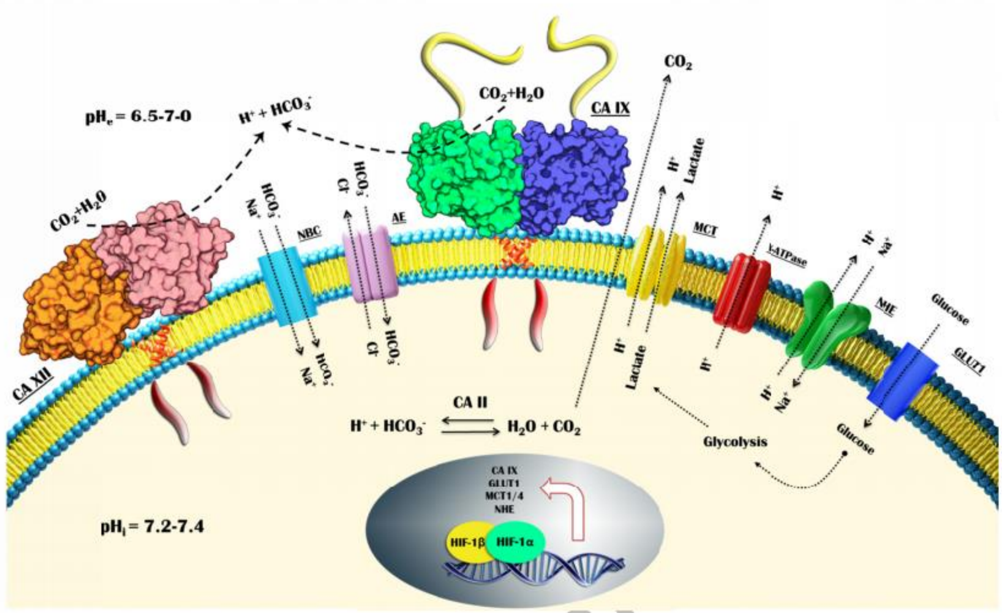

Figure 3.6. Role of CA IX (and CA XII) in supporting tumor growth and proliferation by maintaining the altered tumor pH gradient (along with the other transporters mentioned here) [80].

This isozyme participates in a complex pH regulation machinery depicted schematically in Fig. 3, based on the metabolic switch typical of tumor cells known as "Warburg effect" [81,82]. Altered proton dynamics is a hallmark of cancer cells, in which the extracellular pH drops to values of 6.5-6.8, whereas the intracellular pH becomes slightly alkaline (7.2-7.3) [82,83]. This phenomenon was found to be a consequence of the increased glycolytic rate occurring in the early stages of carcinogenesis, which remains stable during tumor progression even in the presence of normoxia [82,84]. This type of glucose metabolism leads to the production of a large amount of H^+ and lactic acid. To avoid a dangerous accumulation of acid species, the overexpression of proteins involved in pH regulation, such as MTC4, CA IX and CA XII are also up-regulated mainly as response to HIF factors [85,96]. All these proteins, together with V-ATPase and the bicarbonate transporters cooperate to the extrusion of acids from the tumor cells, which leads extracellular pH drop [85,86]. This acidification of the extracellular compartment is beneficial for the tumor growth as many evidences supported the idea that the glycolytic shift confers a survival advantage to cancer cells over the normal ones [85]. From the drug design view point, the crucial role played by tumor proton dynamics on cancerogenesis shed light on new possible targets against cancer progression [79,81]. Considering the expression of CA IX in different types of tumors along with its role in creating and maintaining a pH gradient in cancer cells, the development of small molecules CAIs as specific CA IX inhibitors represents a successful field for the agents interfering with pH regulation, with several potent inhibitors reported so far [79-81].

A great interest has been also turned to the CA IX "interactome", constituted by various protein that cooperate with CA IX within the cell [87,88]. One of the latest findings was provided by Dedhar's group on the mutual relationship between CA IX and matrix metalloproteinase 14 (MMP14) [88]. These authors demonstrated that CA IX provides the H+ ions needed by MMP14 for the proteolytic cleavage of collagen, thus confirming the role of CA IX in the migration and invasion mechanism of tumors [88].

3.2 "CA-Telomerase" dual hybrid inhibitors

3.2.1 Design and synthesis

Since CA IX/XII and Telomerase are validated targets for hypoxic tumor treatment, we aimed to obtain "CA-Telomerase" dual hybrid inhibitors (**Figure 3.7**). Such an approach is expected to achieve superior therapeutic performances associated to the limitations of co-administration of the therapeutic agents alone. The hybridization was performed exploiting the "click chemistry" approach, which allows to join small moieties efficiently and granting access to wide molecular diversities. In particular, we performed a Copper-Catalyzed Azide–Alkyne Cycloaddition (CuAAC) which involves the coupling between an azide moiety and a terminal alkyne leading to the rapid and regioselective formation of the 1,4-product triazole under mild reaction conditions [89,90]. The formation of 1,2,3-triazole scaffold represents an additional value since Bozorov et al. reported that such a moiety is the most used in Medicinal Chemistry in the last decade [91]. The reasons for such an interest are mainly related to the stabilility under metabolic processes as well as good tolerance to pH fluctuations. In addition, the abundancy of electrons within the ring allows to establish H-bonds and π-π stacking interactions with the biological targets and thus ensuring a better stabilization of the adduct formed [91].

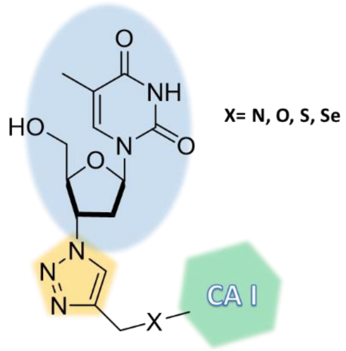

Figure 3.7. Schematic representation of the synthetized hybrids consisting of a CA Inhibitor portion linked to AZT through triazole moiety

Some AZT-ligand hybrids herein considered have been previously reported in the literature by means of the same synthetic approach. In particular, the fluorescent probes coumarin–nucleoside conjugates have been described although no biological applications were reported [92]. Another study considered the synthesis and cytotoxic evaluation of some ester-triazole-linked triterpenoid–AZT conjugates [93]. Cytotoxic analysis of these hybrids and their triterpenoid precursors revealed moderate to good cytotoxic activities against two human tumor cell lines (KB, Hep-G2) [93]. No detailed studies on the specific targets responsible for the anticancer effects were conducted.

As depicted in **Scheme 3.1** the click synthesis was performed by reacting the terminal alkynes (whose synthesis is described in **Chapter 2**) with the azide functionality present in the AZT using (Cu (0) nanosized, TMACl as phase transfer agent in *t*BuOH/H_2O at 40 °C. Both classical (sulfonamides) and non-classical (coumarins and sulfocumarins) CAIs have been included in the study.

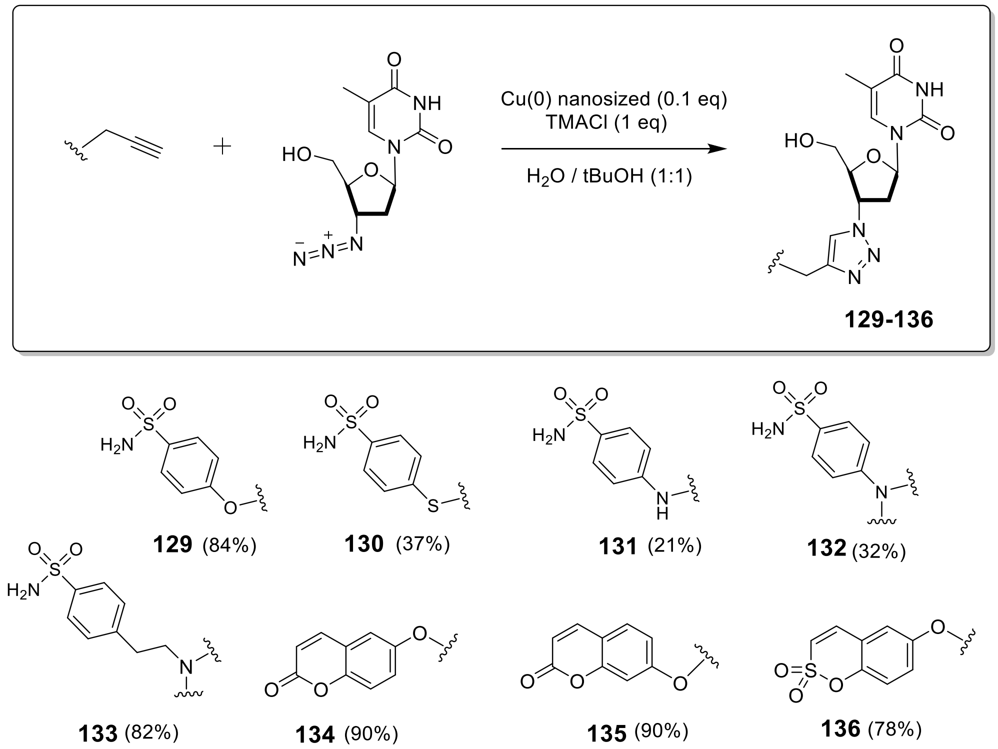

Scheme 3.1. Synthesis of compounds **129-136** by means of Copper-Catalyzed Azide–Alkyne Cycloaddition (CuAAC). Yields are reported in parenthesis.

All final compounds were obtained with high purity grade (i.e. >95 % HPLC) and good yields. Structural characterization was conducted by means of ^{1}H-NMR, ^{13}C-NMR as well as mass spectra analyses.

3.2.2 *In vitro* Biological Evaluation: hCA inhibition

The small library obtained has been evaluated against hCAs I, II, VA, VB, VII, IX and XII by means of the stopped flow CO_2 hydrase assay [94], giving interesting results against hCA XII although they do not show an exceptional selectivity profile. The inhibition data, compared to those of the standard sulfonamide inhibitor acetazolamide (**AAZ**), are reported in **Table 3.1**.

	K_I (nM)*						
	hCA I	**hCA II**	**hCA VA**	**hCAVB**	**hCA VII**	**hCA IX**	**hCA XII**
129	4666.7	9.3	59.1	141.3	51.6	6.2	78.9
130	4037.5	7.7	57.3	52.6	31.0	653.3	61.6
131	>10000	32.9	64.6	52.6	329.8	488.6	74.4
132	>10000	8.5	57.3	45.9	383.5	6557.1	74.0
133	>10000	70.7	59.4	42.9	281.1	8047.1	74.0
134	>10000	>10000	57.8	161.0	9.3	6557.1	3.6
135	>10000	>10000	179.4	151.5	9.4	4885.7	3.5
136	>10000	>10000	172.4	54.6	10.5	5852.3	2.8
AAZ	250	12.1	63.0	54.0	2.5	25.8	5.7

Table 3.1. Inhibition data of hCA I, hCA II, hCA VA, hCA VB, hCA VII, hCAIX and hCA XII with compounds **129-136** and the standard sulfonamide inhibitor acetazolamide (**AAZ**) by a Stopped flow CO_2 hydrase assay [94].* Mean from 3 different assays, by a stopped flow technique (errors were in the range of ± 5-10 % of the reported values).

These relevant hCA isoforms have been selected to assay the activity of the hybrid compounds. Besides the hCA I and II isoforms, mitochondrial hCAs VA and VB, celebral hCA VII and tumor associated hCA IX and XII have been chosen.

The structure-activity relationships (SARs) for the titled compounds **129-136** are reported below:

i) Low (for **129 and 130**) or absent (for **131-136**) inhibition activity against cytosolic hCA I can be detected for the analysed compounds. As for sulfonamide-based derivatives **129-133** this can be maybe explained by the hindrance of the **AZT** moiety inserted on the CAI scaffold. For coumarin and sulfocumarin derivatives (**134-136**), the low inhibition activity was found to be in agreement with literature data. Strong inhibition activity in the low nanomolar range can be observed for derivatives **129-133** (K_I values ranging between 7.7 nM and 70.7 nM) against hCA II. Coumarin and sulfocumarin derivatives (**134-136**), in agreement with literature, were ineffective (K_I = >10000) against the same isoform;

ii) All the synthetized compounds **129-136** turned out to be potent inhibitors of both hCA VA and B, with slight differences in K_I values detectable between the two isoforms. As for sulfonamide-based compounds, the different chemical structure did not deeply affect their inhibition profile against hCA VA, as they all showed K_I values ranging between 57.4nM and 64.6 nM. With the only exception represented by compound **129** (K_I = 141.3nM), the same trand was observed for compounds **130-133** against hCA VB, with K_I slightly different from each other. In coumarin-based compounds, the 6-substituted derivative, compound **134**, revealed to be 2.8 fold more potent against hCA VA when compared to hCA VB, whereas for the 7-substituted coumarin **135**, there is no evident selectivity for an isoform over the other. When compared to compound **134,** an opposite selectivity trand can be observed in 7-substituted sulfocoumarin **136**, which proved to be 3.2 fold more selective towards hCA VB inhibition with respect to hCA VA;

iii) A more heterogeneous inhibition profile has been showed by the titled compounds **129-136** against hCA VII. Cumarin and sulfocumarin derivatives **134-136** turned out to be very potent against this isoform (K_I values of 9.3 nM, 9.4 nM and 10.5 nM, respectively). Among the sulfonamide-based derivatives **129-133**, *O* and *S* containing compunds showed K_I values in the medium nanomolar range (51.6 nM and 31.0 nM, respectively). Noteworthy, *N* containing compounds **131-133** showed K_I values in the medium-high nanomolar range, with K_I values between 281.3 nM-383-5 nM;

iv) Inhibition potencies against hCA IX showed by the analysed compounds revealed to vary considerably within the series. Compound **129,** bearing an etheral link between the CAI and **AZT** moieties turned out to be the most potent among the series, with K_I value of 6.2 nM. *S*-etheral compound **130** and monosubstituted *N* containing compound **131** showed K_I values in the medium/high nanomolar range (653.3 nM and 488.6 nM respectively). K_I values in the high nanomolar range were observed for the other *N*-containing sulfonamides **132** and **133**.

Quite surprisingly, coumarin and sulfocoumarin based compounds showed low potency against hCA IX too, with K_I values in the high nanomolar range;

v) Strong hCA XII inhibition can be observed for all the analysed compounds, with particular meaning for coumarin and sulfocoumarin- based derivatives **134-136**, showing K_I values in the low nanomolar range (ranging between 2.8 nM and 3.6 nM). Sulfonamide-based hybrids showed similar K_I values, so that the substitution of the heteroatoms in the link between CAI and AZT and the presence of one or two AZT tails did not affect the selectivity against this hCA isoform.

3.2.3 *In vitro* Telomerase Activity Assay

Telomerase efficiency is related to the number of telomeric repeats present at the end of chromosomes [33]. First methodologies to determine telomerase activity were based on direct measurements of the telomerase products. By using the *in vitro* primer extension assay the telomerase synthetized telomeric repeats into oligonucleotide primers were evaluated [95]. Since the low abundancy of telomerase enzymes in cells, the sensitivity of this assay resulted at the threshold limit detection. A modified version of the assay was reported in 1994 with the Telomerase Repeat Amplification Protocol (TRAP) [33]. The primer-telomere repeats generated by the telomerase reaction are integrated with the polymerase chain reaction (PCR) in order to amplify the final response, thus overcoming the low sensitivity drawback discussed for the previous assay [33]. A further improvement to the TRAP methodology was reported in 2001 with the Real-Time quantitative (RTQ) PCR [96]. The usage of a fluorescent dye (SYBR Green) which is able to bind the amplicons and generate fluorescence in PCR reaction, allowed the measurements of PCR products in relation with the fluorescence produced during the extension step at each PCR cycle. This method provided a precise measurement of telomerase activity and has been used in our study (**Figure 3.8**) [96]. Determination of suppressive activity of CAI-AZT compounds on telomerase in Jurkat cell lysates has been performed by Prof. Zhdanov, from the Institute of Biomedical Chemistry in Moscow in Russia.

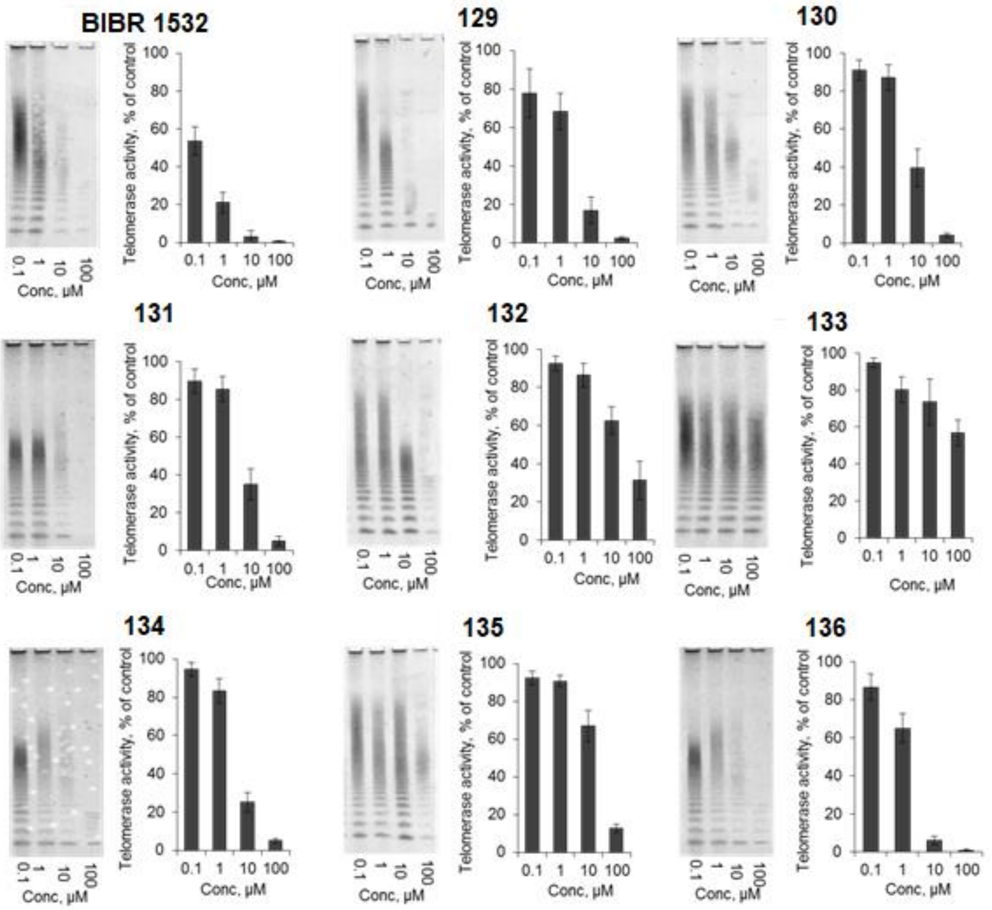

Figure 3.8. Changes of telomerase activity in cell lysates treated with different concentrations of inhibitors. Representative TRAP gel electrophoresis for treated lysates and quantification of TRAP.

IC_{50} and IC_{90} values of all the compounds are reported in **Table 3.2**, and they are calculated from the dose-depending curves reported in **Figure 3.9**, using as internal reference the highly potent and selective non-nucleosidic telomerase inhibitor **BIBR1532 (127)**.

Inhibitory Concentrations		
Compound	**IC_{50}, μM**	**IC_{90}, μM**
129	4.808	37.204
130	6.78	31.879
131	2.525	9.459
132	25.517	234.018
133	188.391	Not determined
134	5.718	72.124
135	22.795	137.262
136	48.418	174.141
BIBR 1532	0.172	5.571

Table 3.2. IC_{50} and IC_{90} values (inhibitor concentration where the response is reduced by 50% and 90% respectively).

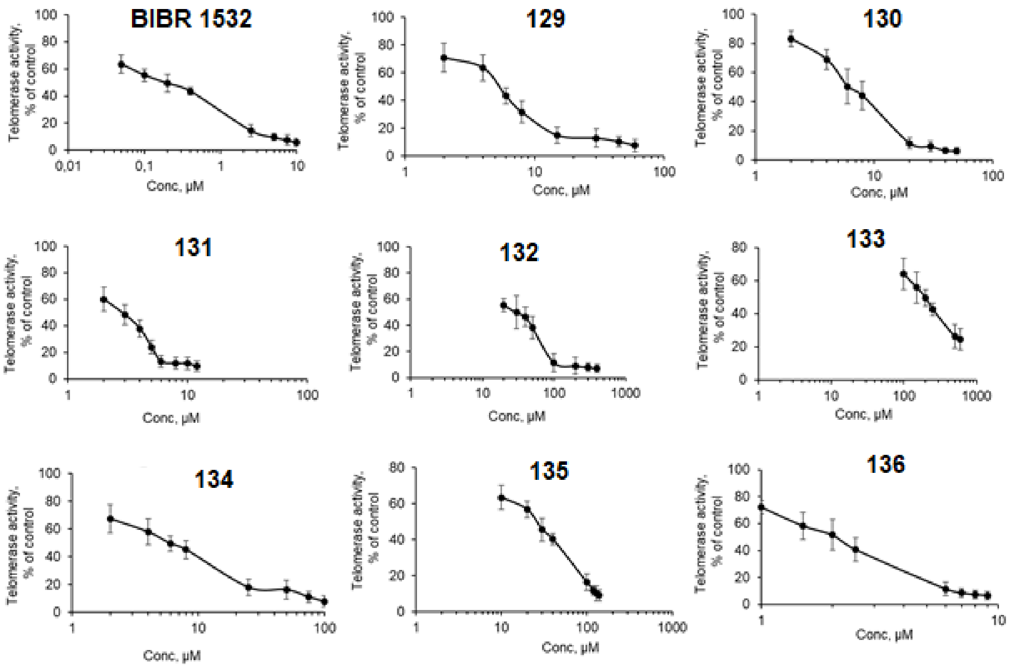

Figure 3.9. Dose-depending curves which were used for calculation of IC_{50} and IC_{90} values. N=4. These data were obtained by RTQ-TRAP.

As shown in **Table 3.2**, the hybrid compounds **129-136** revealed to be weak telomerase inhibitors, with lower activity when compared to the reference **BIBR1532**. Among the series the most active was the sulfonamide-based derivative **131** with IC_{50} and IC_{90} values of 2.5 and 9.5 micromolar respectively, followed by **129** and **130**. In particular, *S*-etheral compound **130** showed slight higher IC_{50} value when compared to the *O*-analogue **129** (6.8 vs 4.8, respectively). Interstingly, di-substituted benzensulfonamide compounds **132** and **133**, bearing two **AZT** moieties turned out to be pretty inactive towards telomerase inhibition, with particular meaning for compound **133**, which showed the lowest inhibition activity among the series (IC_{50} value of 188.4 μM). IC_{90} concentration was not calculated for this compound. Among the coumarin based compounds **134-136**, the inhibition data highlighted that the 7-substituted derivatives **135** and **136** (coumarin and sulfocoumarin-based compounds, respectively) are less potent than the 6-substituted coumarin **134.** In particular, sulfocoumarin **136** showed to be 2 fold less potent than coumarin **135** in inhibiting telomerase.

3.2.4 Crystallographic studies

In light of the promising results also as telomerase inhibitors, we determined the binding modes compounds **129** and **131** in adducts with the hCA II as a model study by X-ray experiments at atomic resolution (**Figures 3.10** and **3.11**).

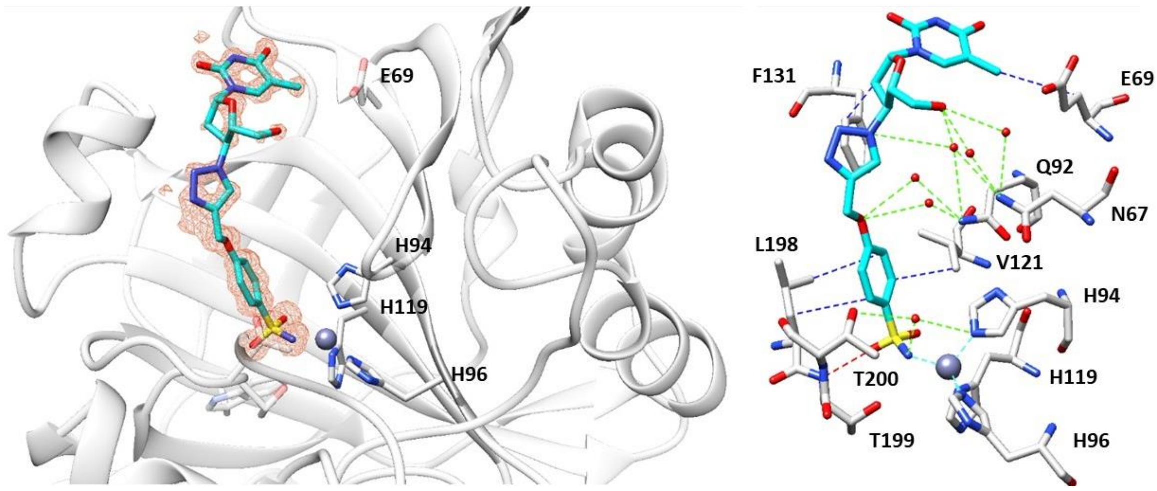

Figure 3.10. Inhibitor **129** bound in the active site of hCA II and showing the σA-weighted |Fo−Fc| map (at 2.5 σ). 1.1 Å resolution. Ligand **129** is shown in cyan. Hydrogen bonds, van der Waals interactions and Water Bridges are shown and labelled in red, blue and green respectively. Residues involved in the binding of inhibitors are also shown. PDB codes not assigned yet.

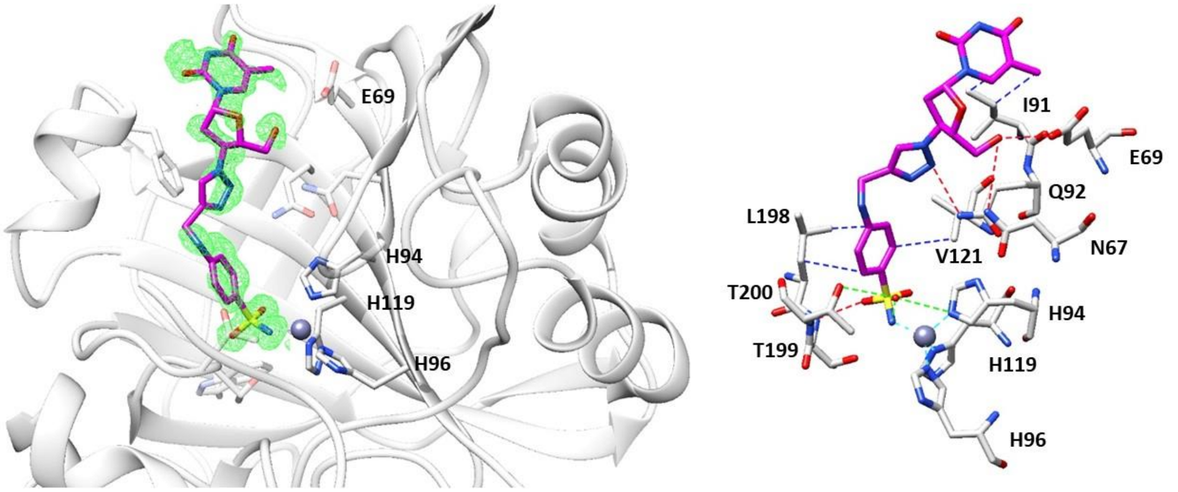

Figure 3.11. Inhibitor **131** bound in the active site of hCA II and showing the σA-weighted |Fo−Fc| map (at 2.5 σ). 1.3 Å resolution Ligand **131** is shown in cyan. Hydrogen bonds, van der Waals interactions and Water Bridges are shown and labelled in red, blue and green respectively. Residues involved in the binding of inhibitors are also shown.

The electron density maps of both hCA II-adducts accounted for the benzenesulfonamide moieties being placed at the bottom of the cavity site and coordinated to the zinc ion in the canonical tetrahedral geometry [97]. (**Figures 3.10** and **3.11**). The ligands backbones resulted stabilized within the cavity site by means of a network of hydrogen bonds as well as van der Walls interactions with substantial orientation differences of the tails as clearly showed in **Figure 3.12**.

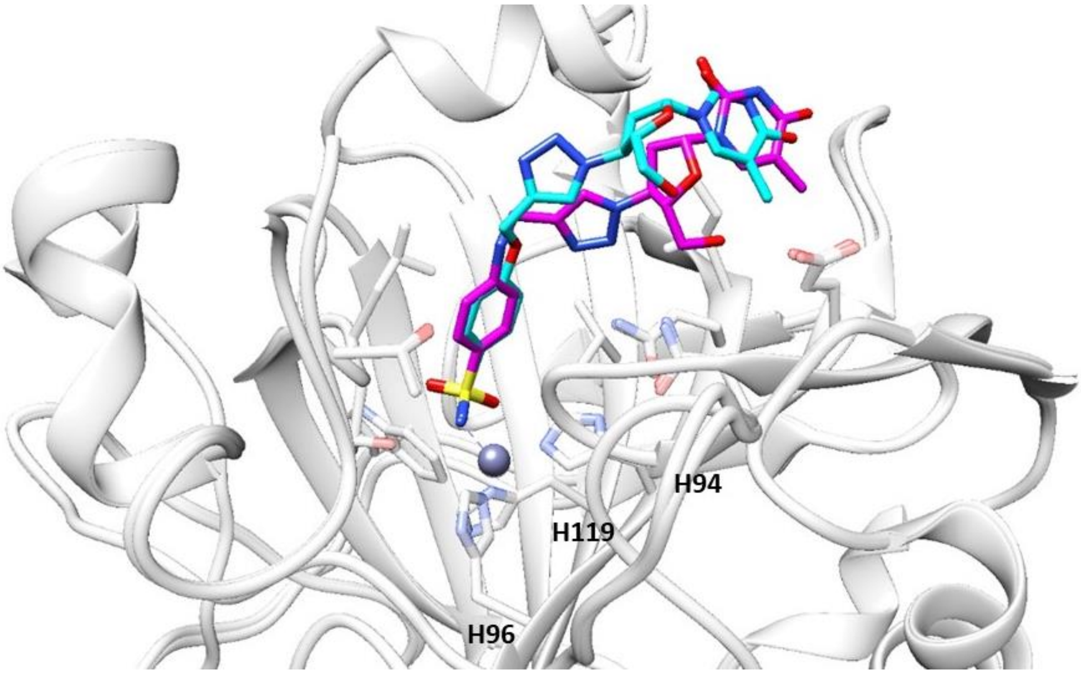

Figure 3.12. Superposition of Inhibitors **129** and **131** bound in the active site of hCA II. Ligand **131** is shown in cyan and **129** in magenta. Residues involved in the binding of inhibitors are also shown.

Noteworthy the diverse spatial orientations of the tail sections within the hCA II were ascribed to the replacement of the ethereal oxygen in **129** with the nitrogen instead as in **131**. In particular the tail section in **129** is located towards the hydrophobic half of the catalytic cleft which is further stabilized by a network of hydrogen bonds bridged with water molecules. As for the compound **131** the tail section laid to the hydrophilic section of the cavity site and directly stabilized by means of hydrogen bonds to the aminoacid residues Asn67, Glu69 and Gln92 (**Figure 3.12**). Such results were in agreement with the previously discussed CA kinetic data which showed the strongly stabilized compound **129** being 3.7-fold more potent inhibitor against the hCA II when compared to **131**.

3.3 Conclusions and Future Perspectives

In summary, to the best of our knowledge this work represents the first proof-of-concept study about the concomitant use of CAIs and AZT in the same molecular scaffold, acting as CA and Telomerase inhibitors. The aim was to create hybrid compounds able to act on two validated targets for the management of tumors. This small series of **CAI-AZT** hybrids have been synthetized and characterized. Then, inhibition potencies against the two designed targets have been evaluated. CA Inhibition data reveled that the titled compounds **129-136** strongly inhibit hCA XII, whereas few of them (**129-131**) showed medium-high inhibition potency against hCA IX. The evaluation of Telomerase activity allowed to indentify two primising derivatives, **129** and 1**31**, which showed good IC_{50} and IC_{90} values. On the same compounds, co-crystallyzation within CA II, as model, has been performed. The results highlighted a very interesting binding mode for both of them, with a crucial role played by the heteroatoms in determing the tail orientation.

Overall the results obtained for our compound series suggested a promising, although preliminary, outcome for our strategy. In this context current work is focused in extending the compounds library, developing derivatives of the sulfonamide type **131**, with the intent to enhance the inhibition potency against Telomerase. In the same time, we are performing cytotoxicity and cell viability assays on various cell lines.

3.4 References

1. Watson JD. Origin of concatemeric T7 DNA. Nature New Biol. 1972, 239, 197–01.
2. Hayflick L. & Moorhead PS. The serial cultivation of human diploid cell strains. Exp Cell Res. 1961, 25, 585–21.
3. Harley CB, Futcher AB, and Greider CW. Telomeres shorten during ageing of human fibroblasts. Nature 1990, 345, 458–60.
4. Bodnar AG. et al. Extension of life span by introduction of telomerase into normal human cells. Science. 1998, 279, 349–352.
5. Blackburn EH: Structure and function of telomeres. Nature. 1991, 350, 569-73.
6. Moyzis RK, Buckingham JM, Cram LS, et al: A highly conserved repetitive DNA sequence, (TTAGGG)n, present at the telomeres of human chromosomes. PNAS USA. 1988, 85, 6622-26.
7. O'Sullivan RJ and Karlseder J: Telomeres: protecting chromosomes against genome instability. Nat Rev Mol Cell Biol 2010, 11, 171-81.
8. De Lange T: Shelterin: the protein complex that shapes and safeguards human telomeres. Genes Dev. 2005, 19, 2100-10.
9. Palm W and de Lange T: How shelterin protects mammalian telomeres. Annu Rev Genet. 2008, 42, 301-34.
10. Smogorzewska A and de Lange T: Regulation of telomerase by telomeric proteins. Annu Rev Biochem. 2004, 73, 177-08.
11. Yaswen P, MacKenzieb KL, Keithc WN, Hentosh P, et al. Therapeutic targeting of replicative immortality. Sem. Cancer Biol. 2015, 35, S104–S128.
12. Mason M, Schuller A and Skordalakes E: Telomerase structure function. Curr Opin Struct Biol 2011, 21, 92-100.
13. Greider CW and Blackburn EH: The telomere terminal transferase of Tetrahymena is a ribonucleoprotein enzyme with two kinds of primer specificity. Cell. 1987, 51, 887-898.
14. Greider CW and Blackburn EH: Identification of a specific telomere terminal transferase activity in Tetrahymenaextracts. Cell. 1985, 43, 405-413.
15. Feng J, Funk WD, Wang SS, et al: The RNA component of human telomerase. Science 1995, 269, 1236-1241.
16. Morin GB: The human telomere terminal transferase enzyme is a ribonucleoprotein that synthesizes TTAGGG repeats. Cell. 1989, 59, 521-529.

17. Koh CM, Khattar E, Leow SC, Liu CY, Muller J, Ang WX, Li Y, Franzoso G, Li S, Guccione E, et al: Telomerase regulates MYC-driven oncogenesis independent of its reverse transcriptase activity. J Clin Invest. 2015, 125, 2109-22.
18. Park JI, Venteicher AS, Hong JY, Choi J, Jun S, Shkreli M, Chang W, Meng Z, Cheung P, Ji H, et al: Telomerase modulates Wnt signalling by association with target gene chromatin. Nature. 2009, 460, 66-72.
19. Martínez P, Blasco MA: Telomeric and extra-telomeric roles for telomerase and the telomere-binding proteins. Nat Rev Cancer. 2011, 11, 161-176.
20. Broccoli D, Young JW and de Lange T: Telomerase activity in normal and malignant hematopoietic cells. PNAS USA 1995, 92: 9082-86.
21. Masutomi, K., et al. Telomerase Maintains Telomere Structure in Normal Human Cells. Cell. 2003, 114, 241-253.
22. Kaszubowska, L. Telomere shortening and ageing of the immune system. J. Physiol. Pharmacol. 2008, 59, 169-186.
23. Flores, I., Benetti, R., and Blasco, M. A. Telomerase regulation and stem cell behaviour. Curr Opin Cell Biol. 2006, 18, 254-260.
24. Xu, D.; Erickson, S.; Szeps, M.; Gruber, A.; Sangfelt, O.; Einhorn, S.; Pisa, P.; Grandér, D. Interferon down-regulates telomerase reverse transcriptase and telomerase activity in human malignant and nonmalignant hematopoietic cells. Blood. 2000, 96, 4313–4318.
25. Passos JF, Saretzki G, Ahmed S,. Mitochondrial dysfunction accounts for the stochastic heterogeneity in telomere-dependent senescence. PLoS Biol. 2007, 5, 110.
26. Sharma, N.K.; Reyes, A.; Green, P.; Caron, M.J.; Bonini, M.G.; Gordon, D.M.; Holt, I.J.; Santos, J.H. Human telomerase acts as a hTR-independent reverse transcriptase in mitochondria. Nucleic Acids Res. 2012, 40,712–725.
27. Mitchell, J. R., Wood, E., and Collins, K. A telomerase component is defective in the human disease dyskeratosis congenital. Nature. 1999, 402, 551-555.
28. Chen G., T ai, A. K., Lin, M., Chang, FT erhorst, C., and Huber, BT. Increased proliferation of CD8+ T cells in SAP-deficient mice is associated with impaired activation-induced cell death. Eur J Immunol. 2007, 37, 663-674.
29. Hornsby PJ. Telomerase and the aging process. Exp Gerontol. 2007, 42, 575–581.
30. Babizhayev MA, Yegorov YE. Tissue formation and tissue engineering through host cell recruitment or a potential injectable cell-based biocomposite with replicative potential: Molecular mechanisms controlling cellular senescence and the involvement

of controlled transient telomerase activation therapies. J. Biomed. Mater. Res. Part A 2015, 103A, 3993–4023.

31. Shay JW, Wright WE. Use of telomerase to create bioengineered tissues. Ann. N. Y. Acad. Sci. 2005, 1057, 479–491.
32. Jaskelioff M, Muller FL, Paik JH, Thomas E, Jiang S, Adams AC, et al. Telomerase reactivation reverses tissue degeneration in aged telomerase-deficient mice. Nature. 2011, 469, 102–106.
33. Kim NW, Piatyszek MA, Prowse KR, Harley CB, et al. Specific association of human telomerase activity with immortal cells and cancer. Science. 1994, 266, 2011–2015.
34. Zhang A, Zheng C, Lindvall C, Hou M, et al. Frequent Amplification of the Telomerase Reverse Transcriptase Gene in Human Tumors. Cancer Res. 2000, 60, 6230–6235
35. Zhang A, Zheng C, Lindvall C, Wallin KL, et al. Amplification of the Telomerase Reverse Transcriptase (hTERT) Gene in Cervical Carcinomas. Genes Chromos. Cancer. 2002, 34, 269–275.
36. Takuma Y, Nouso K, Kobayashi Y, Nakamura S, Tanaka H, Matsumoto E et al. Telomerase reverse transcriptase gene amplification in hepatocellular carcinoma. J Gastroenterol Hepatol. 2004, 19, 1300–1304.
37. Teralı K, Yilmazer A. New surprises from an old favourite: The emergence of telomerase as a key player in the regulation of cancer stemness. Biochimie. 2016, 121, 170–178.
38. Rousseau P, Autexier C. Telomere biology: Rationale for diagnostics and therapeutics in cancer. RNA Biol. 2016, 12, 1078–1082.
39. Low KC, Tergaonkar V. Telomerase: central regulator of all of the hallmarks of cancer. Trends Biochem Sci. 2013, 38, 426-34.
40. Nazari-Shafti T.Z, Cooke J.P. Telomerase therapy to reserve cardiovascular senescence. Methodist Debakey Cardiovasc. J. 2015, 11, 172–175.
41. Bär C, Povedano JM, Serrano R, Benitez-Buelga C, Popkes M, et al. Telomerase gene therapy rescues telomere length, bone marrow aplasia, and survival in mice with aplastic anemia. Blood. 2016, 127, 1770–1779.
42. Weyand CM, Fujii H, Shao L, Goronzy J.J. Rejuvenating the immune system in rheumatoid arthritis. Nat Rev Rheumatol. 2009, 5, 583–588.

43. Fauce SR, Jamieson BD, Chin AC, Mitsuyasu RT.; et al. Telomerase-based pharmacologic enhancement of antiviral function of human CD8+T lymphocytes. J Immunol. 2008, 181, 7400–7406.
44. Harley CB, Liu W, Blasco M, Vera E, Andrews WH, et al. A natural product telomerase activator as part of a health maintenance program. Rejuven Res. 2011, 14, 45–56.
45. Bernardes de Jesus B, Schneeberger K, Vera E, Tejera A, Harley CB, Blasco MA. The telomerase activator TA-65 elongates short telomeres and increases health span of adult/old mice without increasing cancer incidence. Aging Cell 2011, 10, 604–621.
46. Salvador L, Singaravelu G, Harley CB, Flom P, Suram A, Raffaele JM. A Natural Product Telomerase Activator Lengthens Telomeres in Humans: A Randomized, Double Blind, and Placebo Controlled Study. Rejuven. Res. 2016, 19, 478-484.
47. Tanaka Y, Moritoh Y, Miva N. Age-dependent telomere-shortening is repressed by phosphorylated alpha-tocopherol together with cellular longevity and intracellular oxidative-stress reduction in human brain microvascular endotheliocytes. J Cell Biochem. 2007, 102, 689–703.
48. Lin J, Epel E, Cheon J, Kroenke C. et al. Analyses and comparisons of telomerase activity and telomere length in human T and B cells: insights for epidemiology of telomere maintenance. J Immunol Methods. 2010;352, 71-80.
49. Zvereva MI, Shcherbakova DM, Dontsova OA. Telomerase: structure, functions, and activity regulation. Biochemistry (Mosc). 2010, 75, 1563-83.
50. Shay JW, Wright WE. Telomeres and telomerase in normal and cancer stem cells. FEBS Lett. 2010, 584,3819–3825.
51. Schmitt CA. Cellular senescence and cancer treatment. Biochim Biophys Acta. 2007, 1775, 5-20.
52. Harley C.B. Telomerase and cancer therapeutics. Nat Rev Cancer. 2008, 8, 167–179.
53. Sprouse AA, Steding CE, Herbert B-S. Pharmaceutical regulation of telomerase and its clinical potential. J Cell Mol Med. 2012, 16, 1–7.
54. Paritala H and Firestine SM. Benzo(h)quinoline derivatives as G-quadruplex binding agents. Bioorg Med Chem Lett. 2009, 19, 1584-1587.
55. Naasani I, Seimiya H, Y amori T, and T suruo, T FJ5002: a potent telomerase inhibitor identified by exploiting the disease-oriented screening program with COMPARE analysis. Cancer Res. 1999, 59, 4004-4011.

56. Damm K, Hemmann U, Garin-Chesa P et al A highly selective telomerase inhibitor limiting human cancer cell proliferation. EMBO J. 2001, 20, 6958-68.

57. Xiaoli Wang , Cing Siang Hu , Bruce Petersen, et al. Imetelstat, a telomerase inhibitor, is capable of depleting myelofibrosis stem and progenitor cells. Blood Adv. 2018, 2, 2378-2388.

58. Hájec M, Matulová N, Votruba I, Holý A and Tloust'ová E. Inhibition of human telomerase by diphosphates of acyclic nucleoside phosphonates. Biochem Pharmacol. 2005, 15, 894–900.

59. Strahl C, and Blackburn, E. H. The effects of nucleoside analogs on telomerase and telomeres in Tetrahymena. Nucleic Acids Res. 1994, 25,893–900.

60. White EL, Parker WB, Macy LJ, et al. Comparison of the effect of Carbovir, AZT, and dideoxynucleoside triphosphates on the activity of human immunodeficiency virus reverse transcriptase and selected human polymerases. Biochem Biophys Res Comm. 1989, 161, 393–398.

61. Gomez D, Kassim A, and Olivero O. Preferential incorporation of 3-azido-2,3-dideoxythymidine (AZT) in telomeric sequences of cho cells.Int. J Oncol. 1995, 7, 1057–1060.

62. Olivero OA and Poirier MC. Preferential incorporation of 3-azido-2,3-dideoxythymidine into telomeric DNA and Z-DNA containing regions of Chinese hamster ovary cells. Mol Carcinog. 1993, 8, 81–88.

63. Armando RG, Gomez DM, Gomez DE. AZT exerts its antitumoral effect by telomeric and non-telomeric effects in a mammary adenocarcinoma model. Oncol Rep. 2016, 36, 2731-2736.

64. Datta A, Bellon M, Sinha-Datta U., et al. Persistent inhibition of telomerase reprograms adult T-cell leukemia to p53-dependent senescence. Blood. 2006, 108, 1021-9.

65. Falchetti A, Franchi A, Bordi C, Mavilia C, Masi L, Cioppi F, Recenti, R., et al. Azidothymidine induces apoptosis and inhibits cell growth and telomerase activity of human parathyroid cancer cells in culture. Bone Miner. Res. 2005, 20, 410–418.

66. Fang JL, and Beland FA. Long-term exposure to zidovudine delays cell cycle progression, induces apoptosis, and decreases telomerase activity in human hepatocytes.Toxicol Sci. 2009, 111, 120–130.

67. Murakami J, Nagai N, Shigemasa K, and Oham K. Inhibition of telomerase activity and cell proliferation by a reverse transcriptase inhibitor in gynaecological cancer cell lines. Eur J Cancer 1999, 35, 1027–1034.
68. Johnston JS, Johnson A, Gan Y, Wientjes MG and Au, J. L. Synergy between 3-azido-3-deoxythymidine and paclitaxel in human pharynx FaDu cells. Pharm Res. 2003, 20, 957–961.
69. Brown T, Sigurdson E, Rogatko A and Broccoli D. Telomerase nhibition using azidothymidine in the HT-29 colon cancer cell line. Ann Surg Oncol. 2003, 10, 910–915.
70. Hu Y, Fang KH, Shen LP, et al. The telomerase inhibitor AZT enhances differentiation and prevents overgrowth of human pluripotent stem cell-derived neural progenitors. J Biol Chem. 2018, 293, 8722-8733.
71. Olivero OA, Anderson LM, Diwan BA, Haines DC, et al. Transplacental effects of 3 -azido-2,3-dideoxythymidine (AZT): tumorigenicity in mice and genotoxicity in mice and monkeys. J Natl Cancer Inst. 1997, 5, 1602–1608.
72. Lavelle F, Riou JF, Laoui A.and Mailliet P. Telomerase: a therapeutic target for the third millennium? Crit Rev Oncol Hematol. 2000, 34, 111–126.
73. Jäger K, Walter M. Therapeutic Targeting of Telomerase. Genes (Basel). 2016, 7(7).
74. Chin L, Artandi SE, Shen Q, Tam A, Lee S-Let al. p53 deficiency rescues the adverse effects of telomere loss and cooperates with telomere dysfunction to accelerate carcinogenesis. Cell. 1999, 97, 527–538.
75. Artandi SE, Chang S, Lee SL, Alson S, et al. Telomere dysfunction promotes non-reciprocal translocations and epithelial cancers in mice. Nature. 2000, 406, 641–645.
76. Lee SH, McIntyre D, Honess D, et al. Carbonic anhydrase IX is a pH-stat that sets an acidic tumour extracellular pH in vivo. British J of Cancer. 2018, 119, 622–30
77. Tureci O, Sahin U, Vollmar E, Siemer S, Gottert E, Seitz G, et al. Human carbonic anhydrase XII: cDNA cloning, expression, and chromosomal localization of a carbonic anhydrase gene that is overexpressed in some renal cell cancers. PNAS USA 1998, 95, 7608–13.
78. Svastová E, Hulíková A, Rafajová MA, et al. Hypoxia activates the capacity of tumor-associated carbonic anhydrase IX to acidify extracellular pH. FEBS Lett. 2004, 577, 439–45.
79. Neri D, Supuran CT. Interfering with pH regulation in tumours as a therapeutic strategy. Nat Rev Drug Discov. 2011, 10, 767-77.

80. Nocentini A, Supuran CT. Carbonic anhydrase inhibitors as antitumor/antimetastatic agents: a patent review (2008-2018). Expert Opin Ther Pat. 2018;28, 729-40
81. Berrino E, Supuran CT. Novel approaches for designing drugs that interfere with pH regulation. Expert Opin Drug Discov. 2019, 14, 231–248.
82. Schwartz L, Supuran CT, Alfarouk KO. The Warburg Effect and the Hallmarks of Cancer. Anticancer Agents Med Chem. 2017, 17, 164-70.
83. Ebbesen P, Pettersen EO, Gorr TA, et al. Taking advantage of tumor cell adaptations to hypoxia for developing new tumor markers and treatment strategies. J Enzyme Inhib Med Chem. 2009, 24, 1–39.
84. Gatenby RA, Gillies RJ. Why do cancers have high aerobic glycolysis? Nat Rev Cancer. 2004, 4, 891-9.
85. Graeber TG, Osmanian C, Jacks T, et al. Hypoxia-mediated selection of cells with diminished apoptotic potential in solid tumours. Nature. 1996, 379, 88–91.
86. Pouysségur J, Dayan F, Mazure NM. Hypoxia signalling in cancer and approaches to enforce tumour regression. Nature 2006, 441, 437–43.
87. Buanne P, Renzone G, Monteleone F, et al. Characterization of carbonic anhydrase IX interactome reveals proteins assisting its nuclear localization in hypoxic cells. J Proteome Res. 201, 12, 282–92.
88. Swayampakula M, McDonald PC, Vallejo M, et al. The interactome of metabolic enzyme carbonic anhydrase IX reveals novel roles in tumor cell migration and invadopodia/MMP14-mediated invasion. Oncogene. 2017, 36, 6244–61.
89. Musumeci F, Schenone S1, Desogus A, et al. Click chemistry, a potent tool in medicinal sciences. Curr Med Chem. 2015, 22, 2022-50.
90. Kolb, H.C.; Finn, M.G.; Sharpless, K.B. Click chemistry: diverse chemical function from a few good reactions. Angew. Chem. Int. Ed Engl. 2001, 40, 2004-2021.
91. Bozorov K, Zhao J, Aisa HA. 1,2,3-Triazole-containing hybrids as leads in medicinal chemistry: A recent overview. Bioorg Med Chem. 2019, 27, 3511-3531.
92. Kosiova I, Kovackova S, Kois P. Synthesis of coumarin–nucleoside conjugates via Huisgen 1,3-dipolar cycloaddition. Tetrahedron 2007, 63, 312–320.
93. Dang Thi TA et al. Synthesis and cytotoxic evaluation of novel ester-triazole-linked triterpenoid–AZT conjugates. Bioorg Med Chem Lett. 2014, 24, 5190–94.
94. Khalifah RG. The carbon dioxide hydration activity of carbonic anhydrase I. Stop-flow kinetic studies on the native human isoenzymes B and C. J Biol Chem. 1971, 246, 2561-73.

95. Skvortsov DA, Zvereva ME, Shpanchenko OV, et al. Assays for Detection of Telomerase Activity. Acta Naturae. 2011, 3, 48–68.

96. Hou M, Xu D, Björkholm M, Gruber A. Real-time quantitative telomeric repeat amplification protocol assay for the detection of telomerase activity. Clin Chem. 2001, 47, 519-24.

97. Alterio V, Di Fiore A, D'Ambrosio K, et al. Multiple binding modes of inhibitors to carbonic anhydrases: how to design specific drugs targeting 15 different isoforms? Chem Rev. 2012, 112, 4421–4468.

<u>Chapter 4</u>: Exploration of β-fluorinated diamines as CAIs

4.1 Introduction

4.1.1 Fluorine in Medicinal Chemistry

The insertion of the fluorine moiety in organic scaffolds is a widely validated strategy in Drug Design being crucial in modulating their biological activities, drug distribution as well as enduring the stability on the molecular entities over the time when exposed to biological media [1]. To the best of our knowledge about 25% of drugs currently available on the market contain at least a fluorine atom, and such a value is expected to increase in the near future [1,2]. The importance of fluorine in Medicinal Chemistry is a quite recent achievement since this element in the 50’s still was considered abiotic and too toxic for applications having any biological purpose. The scenario slightly changed in 1970 as about 2% of the used drugs contained fluorine [2]. Despite being the most abundant halogen in our planet, fluorine possesses peculiar chemical features which make its insertion within compounds of natural source quite difficult [3,4]. The result of such a sort of inadequacy of the biosynthetic pathways to elaborate this element, the fluorocontaining metabolites are very rarely found and usually are quite toxic. Some known examples are reported in **Figure 4.1** [3].

Fluoroacetate **137** was the first fluorometabolite identified so far. It was isolated in 1943 from *Dichapetalum cymosum* in South Africa [5]. Subsequently a variety of plants across the globe were found to contain it in low concentrations too. The high toxicity of fluoroacetate **137** is mainly related to its *in vivo* conversion into the (2*R*,3*R*)-fluorocitrate **138** by the Citrate Synthetase enzyme. Fluorocitrate **138** is reported as an effective inhibitor of the enzyme Aconitase and thus results in block of cellular respiration and cell death [3,5].

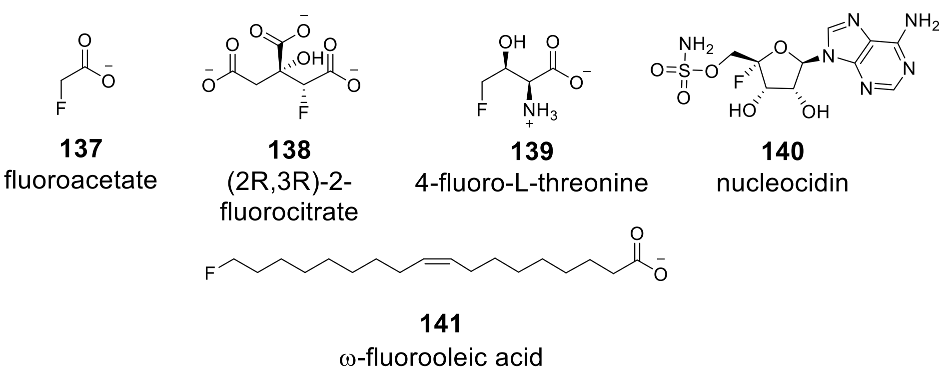

Figure 4.1. Chemical structures of some fluorinated natural products of common interest.

Other fluorometabolites (i.e. **139-141** in **Figure 4.1**) have subsequently been identified and they are all associated with high toxicity too [3,6].

The first relevant example on the beneficial use of fluorine in Medicinal Chemistry was reported by Fried and Sabo in 1953 with the fludrocortisone **142 (Figure 4.2)** [7,8]. The insertion of various halogens within the cortisol molecular scaffold was intended to explore the anti-inflammatory activity of such compounds. Among the halogenated series the fluoro derivative **142** resulted up to 10-fold more potent when compared to the unsubstituted parent compound 17α-hydroxy corticosterone acetate in determining a glucocorticoid based anti-inflammatory activity *in vivo* [8]. Afterwards in 1957 the 5-fluorouracil (5-FU) **143** was found to act as potent antimetabolite of the natural uracil [9] (**Figure 4.2**)

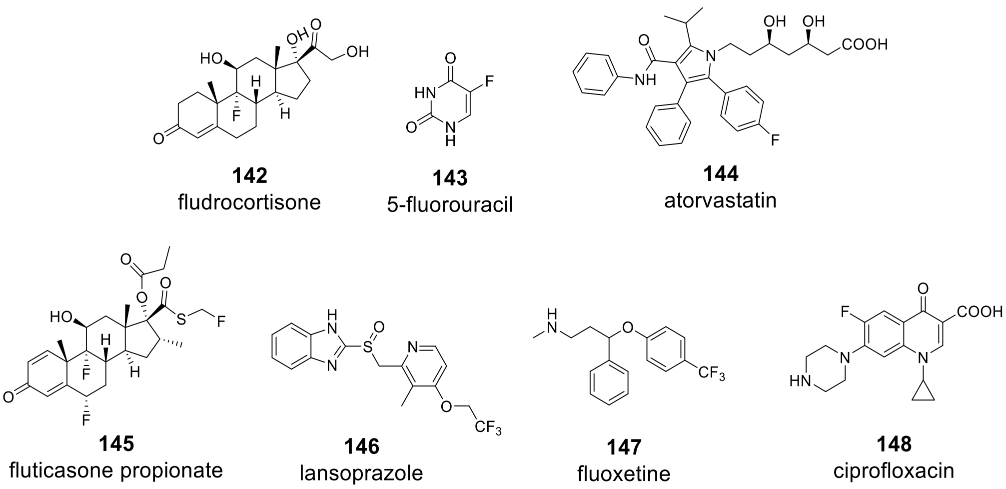

Figure 4.2. Structures of some fluorine-containing compounds available in the market.

These pioneering discoveries opened the way for a new conception of fluorine in life sciences. Nowdays the so-called "fluorine scan" has become a common practice in Drug Discovery and Development with various compounds being available in the market [1,10]. Among them, we can mention the cholesterol-lowering Atorvastatin **144**, the antidepressant Fluoxetine **147** and the anti-infective Ciprofloxacin **148** (**Figure 4.2**).

A quite interesting and used application of the fluorine is within the field of imaging for biomedical purposes by means of the positron emission tomography (PET) technique. ^{18}F containing isotopes are relatively easy and safe to handle and in addition they possess a half-life of 109.8 min [11,13]. In **Figure 4.3** are shown some of ^{18}F fluorinated drugs.

2-[^{18}F]-Fluoro-2-deoxy-D-glucose **149**, abbreviated as [^{18}F]FDG, is widely used in assessing the metabolic status of organs, including tumors [11]. [^{18}F]-6-fluoro-L-DOPA **150** and [^{18}F]-paroxetine **151** are radioligands used in deciphering the dopaminergic and serotoninergic pathways respectively in human tissues [12,13].

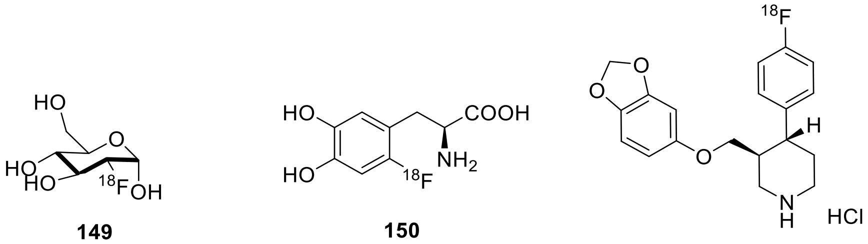

149

2-[^{18}F]-fluoro-2-deoxy-D-glucose

150

[^{18}F]-6-fluoro-L-DOPA

151

[^{18}F]-paroxetine

Figure 4.3. Structures of some [^{18}F]-drugs for imaging purposes.

Overall the biological effects from fluorine in organic scaffolds are scarcely predictable, as the insertion of this element often results in large modifications of the pharmacokinetic as well as of the pharmacodynamic properties of the compounds (**Figure 4.4**) [1,14]. As for the former, the conversion of susceptible C-Hs in molecular drugs through oxidative metabolic processes catalysed by the Cytochrome P450 monooxygenases, may be efficiently supressed with the introduction of the fluorine instead [15]. Higher oral bioavailability is usually observed for a fluorinated compound when compared to the parent molecule as consequence of an increased logD value [16] or fluorine effect on the pKa of proximal functionalities [17,18]. The latter occurs as consequence of the high electronegativity of the fluorine which is the highest among the halogen series. As reported for linear, non-conjugated aliphatic systems, such as the ethylamine, each fluorine introduced contributed to a reduction of the amine pKa by 1.6-1.7 units [19]. Not surprisingly pKa variations from the fluorine can also affect the binding efficiency and selectivity of drugs themselves onto the biological targets [1,17,20]. Fluorine induced conformational changes of the organic scaffolds can also be observed and they deeply affect their binding mode towards biological targets [1,17,20].

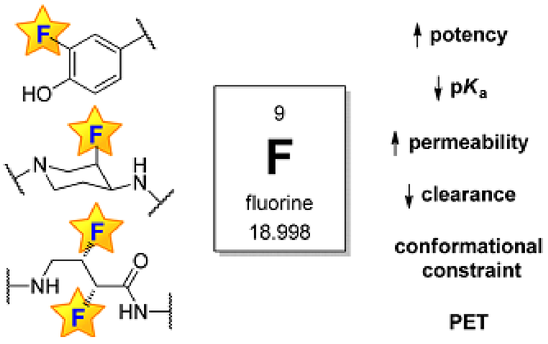

Figure 4.4. Schematic representation of the effects of fluorine insertion on molecular scaffolds [14].

Although the C-H to C-F swap into organic scaffolds of interest for theragnostic purposes appears a minimal chemical transformation, it results in profound alterations of their physico-chemical features and therefore in their druggability related parameters. In this context the fluorine element may be configured as a valuable tool for manipulating *ad hoc* specific drug properties with beneficial outcomes in the field of drug discovery and development.

4.1.2 Fluorine and C-F bond as conformational tools

The critical consequences of introducing one or more fluorine atoms in a molecule can be explained by means of the peculiar features of the C-F bond (**Table 4.1**) [21,22].

	H	**F**	O	N	C	Cl	Br
Van der Waals radius (Å)	1.20	**1.47**	1.52	1.55	1.70	1.75	1.86
Pauling electronegativity	2.1	**4.0**	3.5	3	2.5	3.2	2.8
Length of single bond to carbon (Å)	1.09	**1.40**	1.43	1.47	1.54	1.77	1.97
Strength of bond to carbon (Kcal/mol)	98	**105**	84	70	83	77	66

Table 4.1. Properties of some common elements and of their bonds to carbon [22].

Having the highest electronegativity value (χ = 4.0) fluorine has unique properties and reactivity [21-23]. Its radius lies between H and O thus allowing the replacement of H or OH groups with a sustained electronic alteration and only a slight steric impact. The high polarization of the C-F bond makes it more ionic than covalent, leading to a large dipole moment (μ C-F = 1.41 D), and the high electrostatic attraction between $F^{\delta-}$ and $C^{\delta+}$ is responsible for its strength (105 kcal/mol) and its small length (1.4 Å) (**Table 4.1)** [21,22]. However, despite the polarized nature and the three lone electron pairs on fluorine atom, organic fluorine compounds are weak hydrogen bond acceptors and π-bond donors. Indeed, the three lone pairs prefer to stay close to the high electronegative fluorine atom rather than interact in hydrogen bonding or enter in resonance. In this way, the C-F bond can be considered almost unreactive [21,22]. The main interactions of C-F bond with the chemical environment are of electrostatic type. Intermolecular interactions, such as the C-F···H-O are quite weak, whereas electrostatic intramolecular interactions are significantly stronger and thus able to deeply influence the conformation of the entire molecule. Dipole-Dipole and Charge-Dipole are the main electrostatic interactions than can be observed in a fluorinated system (**Figure 4.5 a** and **b)** [21,22].

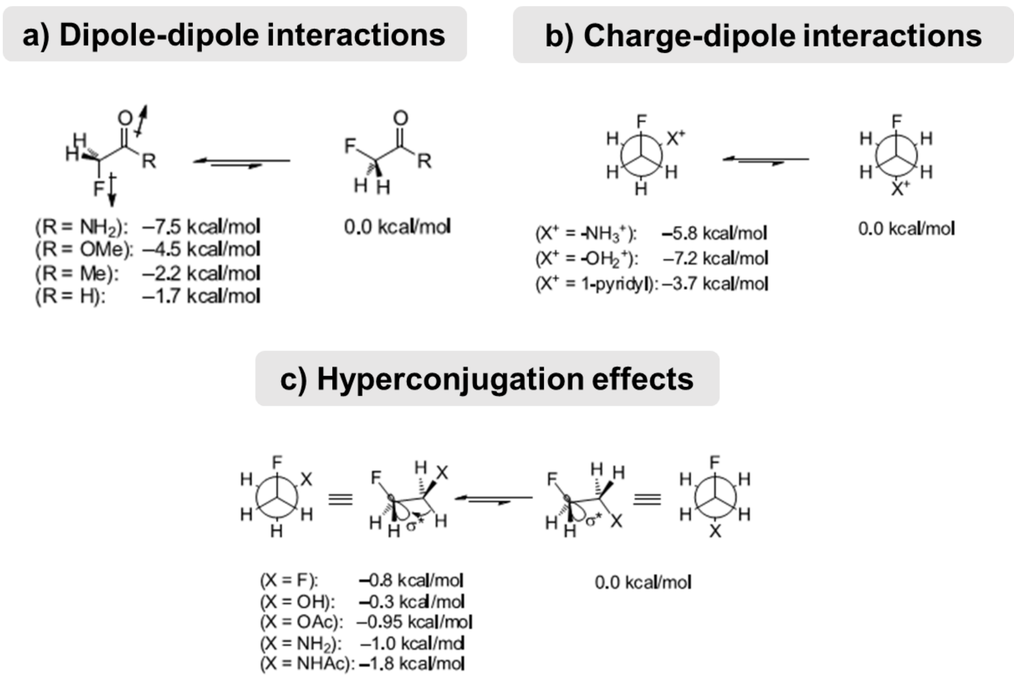

Figure 4.5. Conformational effects associated with C-F bond.

As the main example above reported are the α-fluorocarbonyl compounds, having as the most stable conformation the one with the C-F bond aligned antiparallel with respect to the dipole of the carbonyl group (**Figure 4.5 a**) [24]. The preference of this conformation is directly correlated with the intensity of the dipole on the carbonyl group [21]. An even stronger interaction may occur when the C-F neighbour group bears a formal positive charge, such as the NH_3^+ or OH_2^+ (**Figure 4.5 b**) [25,26]. In this case the intramolecular interaction between the partially negative charged fluorine and the positive charged nitrogen or oxygen forced the entire molecule to preferentially assume a *gauche* conformation over the *anti* (**Figure 4.5 b**). *gauche* conformations are also observed in non-charged molecular species such as the 1,2-difluoroethane. Hyperconjugative effects occur between the C-H σ bond electrons with to the low energy C-F σ* antibonding orbital adjacent each other (**Figure 4.5 c**) [27]. Such a phenomenon can also occur with other electron reach groups, such as lone pairs in O or N, or π-systems.

4.2 β-Fluorinated amines as CAIs

The role of polyamines acting as CAIs was previously reported and discussed in **Section 1.2.1** [28]. SARs referred to the polyamine's inhibition profiles against such enzymes revealed that the substitution grade of the amines as well as the distance occurring between them strongly affected their inhibition potency and isoform selectivity [28]. Since the polyamine's discovery as CAIs no additional works have been published on this topic and in this context is my six month experience as visiting student in the laboratories of Prof. Sébastien Thibaudeau at University of Poitiers. The project aimed to synthetize new polyamines bearing one or more fluorine atoms, to evaluate their impact on the compound's backbone as well as any variation occurring in their in vitro kinetic profiles. We began our investigations with the synthesis and *in vitro* kinetic evaluation of a small series of mono and di–β–fluorinated diamines as cases studies (**Figure 4.6**). Terminal and internal amines separated by 3 or 4 carbon atoms have being used. Once the reaction conditions have being set and the effect of fluorine on these scaffolds was assessed, we aimed to further elongate the diamine backbone up to afford the biologically valuable spermine and spermidine fluorinated analogues.

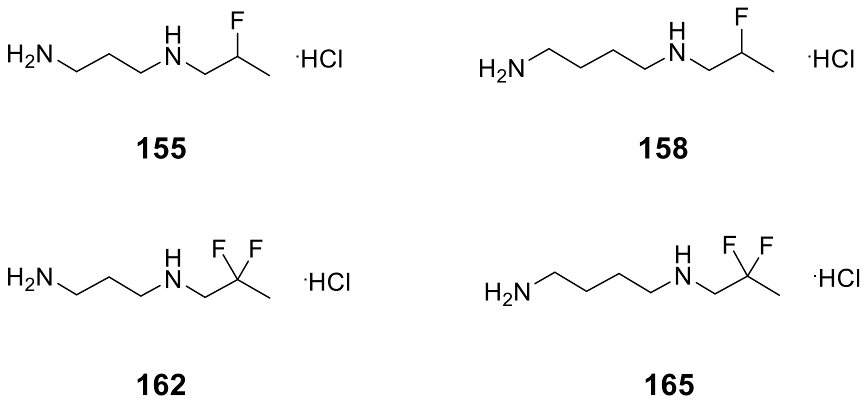

Figure 4.6. Mono- and di–β–fluorinated diamines synthetized.

4.2.1 Design and Superacid mediated synthesis

Formation of the C–F connection still represents a synthetic challenge, primarily due to the high electronegativity of fluorine and to the elevated hydration energy of the fluoride anion itself [29,30]. Methods to access fluoroamines are very limited and they mainly suffer from the formation of by-products arising from intramolecular rearrangements and dehydration reactions [31-33]. C-F driven chemistry also lacks of general substrate applicability and thus imposes that appropriated substrates have to be used even for close related synthetic ways [31-33]. Hydrogen fluoride/pyridine complex, properly known as Olah's reagent, is usually considered the first choice for the hydrofluorination of unsaturated amines [34]. We exploited superacid chemistry to introduce the fluorine in the amine scaffolds too.

The commonly accepted definition of Superacid was given by Gillespie: "any acid system that is stronger than 100% sulfuric acid", which has H_0 = -12 [35]. Fluorosulfuric acid (HSO_3F) or Hydrogen Fluoride (HF) are examples of Primary superacids, with H_0 value of about -15.1. By properly combining Lewis and/or Brønsted acids it is possible to obtain a mixture with remarkable acid properties far superior to the starting components alone (**Figure 4.7**) [36].

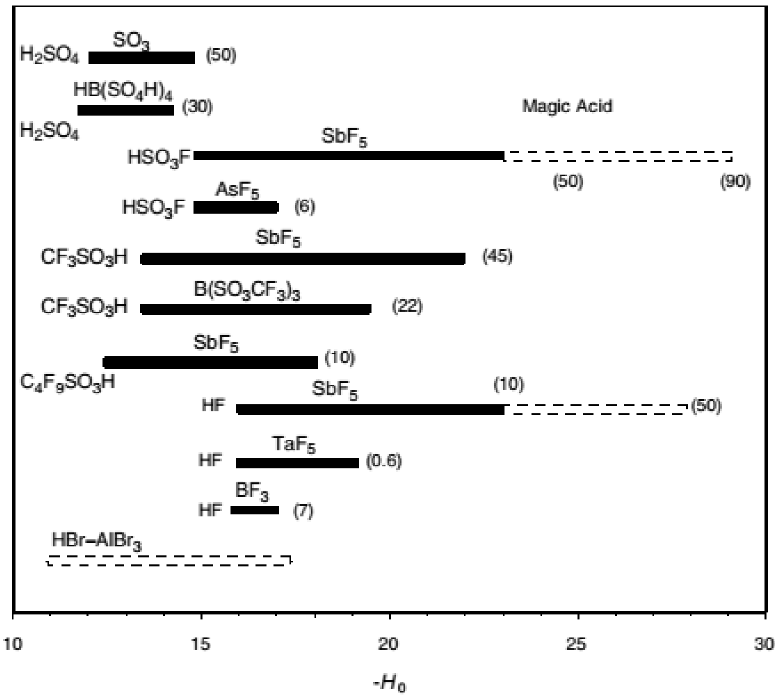

Figure 4.7. Acidity ranges for the most common superacids. The solid and open bars are measured using indicators; the broken bar is estimated by kinetic measurements; numbers in parentheses indicate mol% Lewis acid [36].

During my experience abroad, I worked on the conjugate Brønsted–Lewis superacid mixture formed by HF and SbF_5 (Fluoroantimonic Acid), the strongest liquid superacid system and with the widest acidity range (**Figure 4.7**) [36]. When added to anhydrous HF, Antimony pentafluoride ionizes the Brønsted acid and the proton is only solvated by one HF molecule.

$$2\ SbF_5 + HF \rightleftharpoons H_2F^+ + SbF_6^-\ (Sb_2F_{11}^-)$$ **Equation 4.1**

In diluted HF solutions, SbF_5 is fully ionized to the SbF_6^- anion species. Increasing the concentration of SbF_5, polymeric SbF_5 and polymeric anions (i.e. $Sb_2F_{11}^-$,$Sb_3F_{16}^-$ among others) are formed (**Equation 4.1**). Varying the concentration of SbF_5 added in the range 0–20 mol %, the acidity of neat HF can be enhanced of almost 10 units, but it's worth noting that the addition of only 1 mol% of SbF_5 is already able to increase HF H_0 value from -15 to -20 [36].

The first application of Superacids was in the 1960s, when Olah's studies focused on the use of highly acidic non-aqueous and non nucleophilic systems for studying long-lived carbocations [36]. For his contribution to carbocation chemistry Olah was awarded the Nobel Prize in Chemistry in 1994. In 1970's –1980s, Jacquesy proposed to exploit superacid based chemistry to perform oxidations, carbonylations, arylations, and isomerization protocols on synthetic or natural products with the intent to obtain efficiently bioactive compounds difficult to access by ordinary known reaction procedures. Under such highly acidic conditions, functionalized organic substrates are usually present as mono- or polyprotonated species, with generation of superelectrophilic spots endowed of enhanced reactivity towards poor nucleophiles [37]. This superelectrophilic activation method is an emerging research field with several synthetic applications reported so far [38]. Among them, the direct synthesis of fluorinated nitrogen-containing compounds in HF/SbF_5 is of peculiar interest in the Medicinal Chemistry scenario, since the great importance of F and N in Drug Design. β-Fluorination of nitrogen compounds is an example of reaction that can be easily conducted in superacidic medium $HF–SbF_5$, starting from accessible starting materials and with very good yields [39].

In order to synthesize our β-monofluorinated diamines **155** and **158**, we started by generating the main intermediate, the hydrofluorinated compound **152 (Scheme 4.1)**. After preparation of nosyl protected amine **G**, we performed the fluorination under reaction conditions reported by Thibaudeau's group (HF/SbF_5 7:1, -60°C, 10' reaction time) [39].

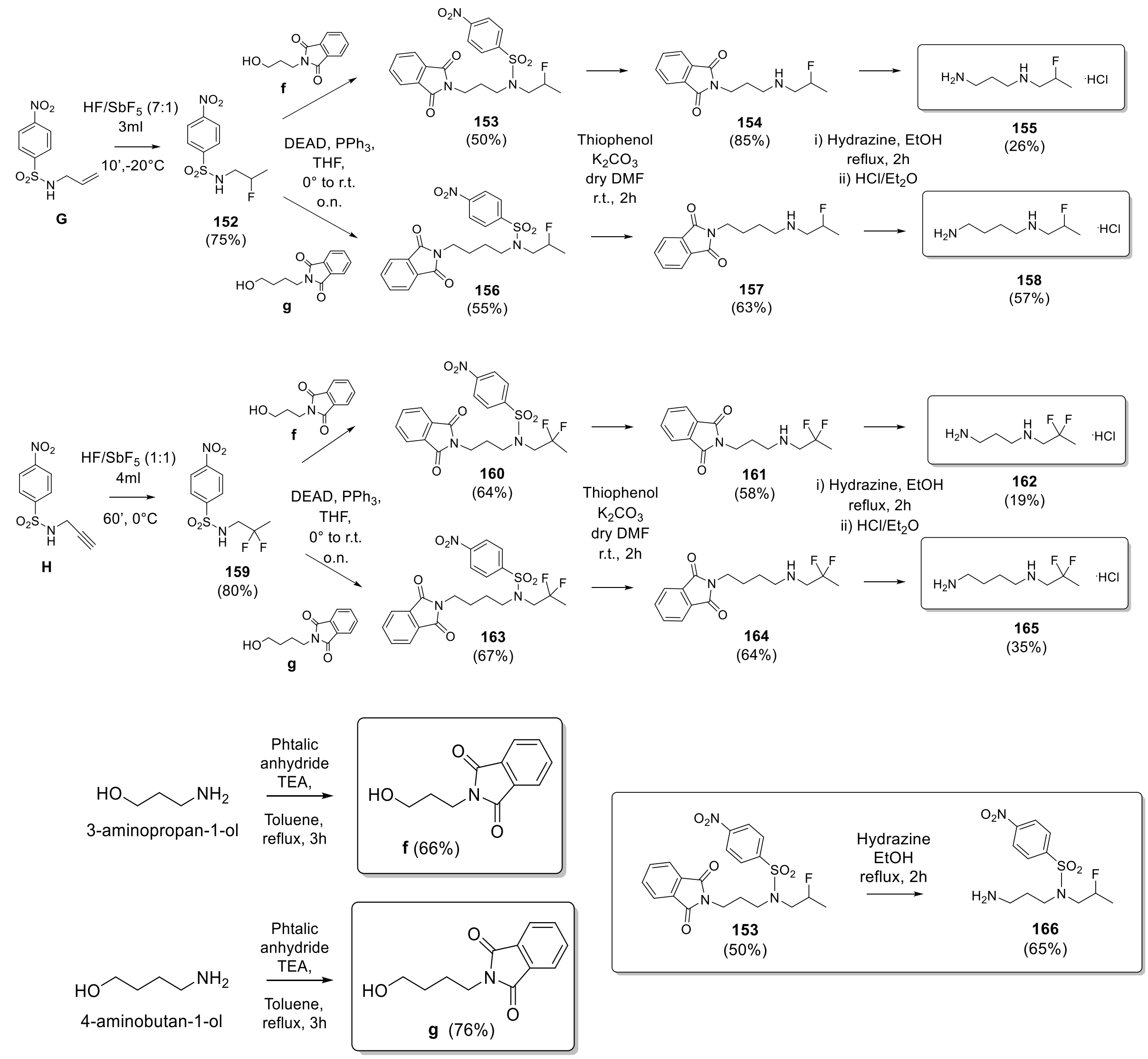

Scheme 4.1. Synthetic procedures for the preparation of β−fluorinated amine derivatives.

As shown in **Figure 4.8,** consequently to the protonation of the nitrogen atom, the strong acidity of the medium allowed the formation of a superelectrophilic dication which can be fluorinated by a poor nucleophilic species such as the solvated fluorine being in the polymeric anionic form (i.e. $Sb_nF_{5\,n+1}^{-}$). [39].

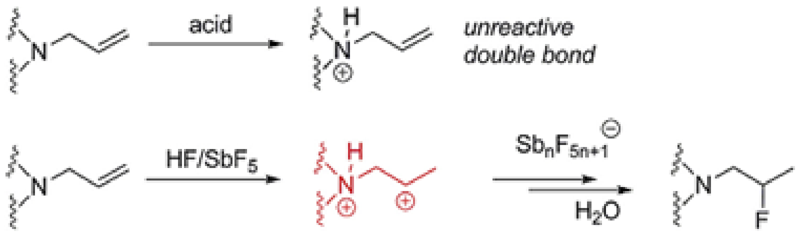

Figure 4.8. Ammonium-carbenium superelectrophilic activation in HF/SbF_5 and hydrofluorination of unsaturated amines [39,40]

Compound **152** was then treated with the previously synthetized protected alcohols **f** and **g** using a Mitsunobu coupling reaction, to afford compounds **153** and **156** [41]. The synthesis proceeded with nosyl deprotection using thiophenol [42] and removal of the phthalimide moiety with hydrazine hydrate, to obtain the free amine compounds which were converted to the corresponding hydrochloric salts **155** and **158** (**Scheme 4.1**).

The same synthetic approach was applied to the synthesis of the *gem*-difluorinated compounds **162** and **165**. Since *gem*-difluorination on Nosylated propargylamine to afford compound **159** was not earlier reported in the literature, we explored the best performing reaction conditions based on previously *gem*-difluorination reaction on aminoalkynes in superacid HF-SbF_5 [43].

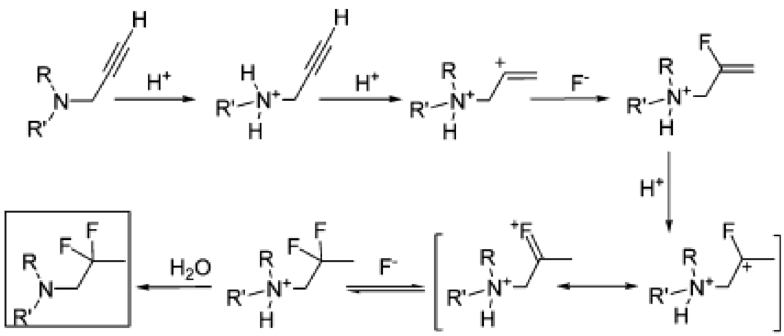

Figure 4.9. General mechanism of *gem*-difluorination involving reactive dicationic intermediates.

The mechanism proposed for this reaction involves reactive dicationic intermediates composed of vinylic ionic species adjacent to protonated N-basic sites, which are highly stabilized by mesomeric effects (**Figure 4.9**). The high electrophilic character of such species allowed their fluorination in the presence of poor nucleophiles such as the complex fluoride ion (SbF_6^- or $Sb_2F_{11}^-$) [43]. By using the conditions reported (HF/SbF_5 2:1, -20°C, 15') we observed the formation of the desired *gem*-difluorinated derivative, although with low yields recovery. We further explored alternative reaction conditions such as varying the acidic mixture (HF/SbF_5 1/1), longer reaction times (up to 60 min) and higher temperatures (up to 0°C), which allowed us to convert starting material to the corresponding product **159** in higher yield (**Scheme 4.1**).

In our work, theoretical approaches have been used to determine variations in internal and external amine pKas upon fluorination. Results obtained with Epik [44a] and DFT-based pKa predictor (Jaguar pKa [44b]) are reported in **Table 4.2**. *Ab initio* quantum mechanics calculation is a more reliable tool for pKa prediction as it takes into account the molecular conformation. As shown in **Table 4.2**, β-monofluorination on *N*-propyl-1,3-propanediamine to afford compound **155** caused a reduction of the initial pKa value of 1.3 units. As expected, the effect is more intense in the *gem*-difluorinated derivative **162**, for which the pKa difference with the non-fluorinated analogue is of 2.1 points. In agreement with the literature [19], pKas of the outer amine groups are less affected by fluorine insertion, so that the difference between the initial and the final pKa values is 0.2 for both mono and difluorinated compounds **155** and **162**.

	Inner N		**Outer N**	
	pKa FF (±0.96)	**pKa QM**	**pKa FF (±1.47)**	**pKa QM**
N-Propyl-1,3-propanediamine	10.4	10.7	10.3	10.1
155	9.1	9.4	10.3	9.9
162	8.04	8.6	10.3	9.9

Table 4.2. Amine pKas predicted using Epik and Jaguar. FF: force-field, molecular mechanics; QM: quantum-mechanics.

4.2.2 *In vitro* Biological Evaluation: hCA inhibition

Once stated the impact of fluorine insertion on molecular protonation state, the hCA inhibition evaluation have been performed on our compounds. The final compounds along with the protected precursors have been tested against five human CA isoforms using the Stopped Flow technique (**Table 4.3**) [45]. The results highlighted an interesting inhibition profile for the final compounds, with high selectivity showed against the CA IV.

	K_I (μM)*				
	hCA I	**hCA II**	**hCA IV**	**hCAIX**	**hCA XII**
152	4.5[(46)]	2.4[(46)]	0.071	2.2[(46)]	4.2[(46)]
153	>100	78.4	>100	>100	7.0
154	>100	4.26	0.13	0.14	>100
155	>100	36.9	0.034	>100	>100
156	>100	34.0	>100	>100	0.64
157	>100	69.2	89.1	>100	>100
158	>100	63.7	0.028	>100	>100
159	8.9	0.27	0.062	2.7	0.33
160	>100	88.8	>100	37.8	0.66
161	>100	62.0	83.4	>100	>100
162	>100	28.7	0.017	>100	>100
163	>100	>100	>100	3.38	0.45
164	>100	40.6	>100	9.7	4.8
165	>100	>100	0.094	>100	>100
166	>100	0.72	51.2	44.6	5.2
AAZ	0.250	0.012	0.074	0.026	0.0057

Table 4.3. CA Inhibition Data [45]. * Mean from 3 different assays, by a stopped flow technique (errors were in the range of ± 5-10 % of the reported values).

i) Several examples of fluorine containing benzensulfonamides have been reported in the literature as CAIs [46-51]. In a work from 2012 [46], β-fluorinated secondary benzensulfonamides of the type of compound **152** have been assayed against hCA I, II, IX and XII, revealing to be weak inhibitors with a flat inhibitory profile (K_I values ranging from 2.2 μM to 4.5 μM). However, activity against hCA IV has never been tested. As reported in **Table 4.3**, β-fluorinated compound **152** revealed to be a nanomolar inhibitor of this membrane associate isoform, with a K_I value of 71 nM. The *gem*-β-difluorinated compound **159**, not earlier reported in the literature, has been tested against the five hCA isoforms here considered. The obtained data (**Table 4.3)** revealed an inhibitory profile similar to the one reported for the β-monofluorinated analogue **152**. Interestingly, a stronger inhibition potency against hCA II and hCA XII can be observed for the *gem*-β-difluorinated compound **159** when compared to **152.**
In the already mentioned work from 2012, *N*-substituted β-fluorinated benzenesulfonamides and *N*-substituted aminobenzofuzed sultams were reported to be inactive against hCA I, II, IX and XII [46]. However, in subsequent papers from the same group, fluorinated tertiary benzenesulfonamides bearing fluorine have been reported to be potent and selective CA IX and XII inhibitors [49-51]. As no zinc-chelating mechanism was possible for these derivatives, a new, non-classical, mechanism of action was supposed. Starting from these data, in our work we decided to evaluate the inhibitory activity of intermediates **153, 156, 160** and **163** against the considered five human isoforms. The results showed, as expected, a weak or absent inhibition of the cytosolic hCAs I and II for these derivatives. Monoflurinated compounds **153** and **156** seemed to be ineffective against hCA IX (K_I values > 100 μM), showing instead high selectivity for hCA XII (K_I values of 7.0 μM and 0.64 μM for **153** and **156**, respectively). Both tumor associated isoforms hCA IX and XII revealed to be strongly inhibited by *gem*-β-difluorinated compounds **160** and **163**, in the low micromolar /high nanomolar range (K_I values of 0.66 μM and 0.45 μM for **160** and **163**, respectively, against hCA XII). As for hCA IV, no inhibition could be detected for any of those compounds. Moreover, the length of the carbon chain between the nitrogen atoms revealed to do not inflence their inhibition profile (**Table 4.3)**.

ii) Removal of Nosyl group from compounds **153, 156, 160** and **163** led to compounds **154**, **157**, **161** and **164,** bearing a secondary amine in the backbone. The absence of benzensulfonamide moiety was expected to be detrimental for the inhibition potency. A remarkable worsening of the inhibition potency was observed indeed for almost all the analysed compounds against hCA IX and XII. The only exception was represented by the monofluorinated compound **154**. In this compound the removal of Nosyl group led to a clear improvement of the inhibition potency against hCA II, IV and IX (K_I values of 4.26 μM, 0.13 μM and 0.14 μM, respectively). As for hCA IV, a slight reduction of the K_I values was observed in compounds **157** and **161** (89 μM and 83 μM, respectively), whereas in compound **164** such a modification didn't affect the inhibition potency against this isoform (K_I value >100 μM). An enhancement of the inhibition potency for compounds **161** and **164** was also observed against hCA II (K_I values from 89 μM to 62 μM and from >100 μM to 41 μM, respectively). In analogy to what reported for for the full protected analogues (**153, 156, 160** and **163**) in derivatives **154**, **157**, **161** and **164** hCA I was not inhibited (K_I >100 μM). Interestingly, compound **166**, synthetized from compound **153** removing phalimide moiety, showed a different inhibition profile when compared to the analogue compound **154**. Compound **166**, bearing the free primary amino group and Nosyl protected internal amine, revealed indeed to be pretty active against CA II (K_I= 0.72 μM). When compared to the parent compound **154**, a slight potency improvement against CA XII was also assessed, whereas a potency worsening against CA IV and IX was registered (**Table 4.3)**. These results highlighted a possible double inhibition mechanism due to the presence of both primary amine and tertiary benzensulfonamide in the same scaffold, but more studies are needed to support this hypothesis.

iii) As for the final compounds **155**, **158**, **162** and **165,** a very interesting inhibition profile can be observed from **Table 4.3**, with a remarkable selectivity showed for hCA IV. The K_I values spanned between 17 nM and 94 nM, with slight differences in the inhibition potency among the compounds. However, the inhibition activity seemed to do not be deeply influenced by the distance between the two *N* atoms and the presence of one or two fluorine in the backbone. Weak hCA II inhibition was also determined by compounds **155**, **158** and **162** (K_I values of 37 μM, 64 μM and 29 μM, respectively), with a selectivity index hCA II/hCA IV ranging between 1064 to 2280. The other isoforms considered (hCA I, IX and XII) are not inhibited by the final compounds **155**, **158**, **162** and **165 (**K_I values >100 μM).

4.3 Conclusions and Future Perspectives

In this work we synthetized a small series of mono and difluorinated diamines acting as inhibitors of the CA isoforms expressed in humans. The impact of fluorine in the reduction of internal amine's pKas has been determined and the results obtained were in agreement with the literature reports. The final fluorinated diamines have been assayed as hCA inhibitors against five isoforms. The fluorinated intermediates have been evaluated too, in order to explore the kinetic profiles of secondary and tertiary fluorinated benzensulfonamides, with interesting results. The most significant data have been obtained with the final compounds, for which a remarkable selectivity for hCA IV over the other isoforms considered (I, II, IX and XII) was observed. As reported in **Section 1.1.2**, hCA IV is a membrane associated isoform mostly expressed in kidney, lung, eye, brain and heart muscle, and it was found to be involved in several pathological events [52]. For example, the gene encoding hCA IV was found to be induced at 2 to 24 h after stroke in ischemic brain and peripheral white blood cells, proving its role into the inflammatory responses after stroke [53]. Moreover, the role of hCA IV, as part of a metabolon with Na^+–H^+ exchanger (NHE1) and Cl^-–HCO_3^-exchanger (AE3), has emerged as a central point in the hypertrophic cascade, leading to heart failure [54]. A deeper exploration of the exact role of this isoforms in these pathologies is needed. With a selectivity index ranging between 1064 to 2280 (hCA II/hCA IV) these small fluorinated diamines revealed to be a highly promising tools for obtain more insights into the roles of hCA IV in cardiomyocites and in the possibility to treat heart-related pathologies by means of CA IV inhibition.

Current work is focused on co-crystallization of hCA IV with some of our final fluorinated compounds in order to properly address the binding modes. Extension of the study though amine backbone elongation using amino-protected aldehyde in reductive amination conditions will be also conducted to evaluate the impact of the number of *N* atoms, the distance between them and the total length of the amine backbone on the hCA inhibition.

4.4 Related projects currently on development

4.4.1 Synthesis of fluorinated triamines

In order to further explore the behaviour of this new class of unconventional hCAIs, we planned to synthetize a series of fluorinated triamine derivatives by exploiting the superacid chemistry. Since the synthetic work still is ongoing, no inhibition data have been obtained for the final free β-fluorinated triamine derivatives yet.

4.4.1.1 Design and synthesis

In order to obtain compounds with both the primary amine terminals, we decided to use the chlorofluorinated compound **167** as the main intermediate and potassium phthalimide as amine source (**Scheme 4.2**). The chlorofluorination reaction on this substrate was already reported in literature and the products **167** and **168** were characterized in mixture [55]. Once the purification conditions were optimized, we obtained the single isomers in pure form. As expected, the desired *N*-(3-chloro-2-fluoropropyl)-4-nitrobenzenesulfonamide **167** was obtained as the major product. The next step, the substitution of the alkyl chloride with potassium phthalimide to afford compound **169** turned out to be quite challenging, with low yields and formation of unidentified byproducts. We reasonably speculated a key role in the reaction outcome was ascribed to the increased acidity of the sulfonamide proton after fluorine insertion in β position (**Scheme 4.2**). Alkylation by Mitsunobu conditions on compound **169** using the previously cited alcohol **f** and **g** was finally performed to afford the desired fluorinated triamine derivatives **170** and **171**.

In order to asses any improvements on the chlorine displacement step with potassium phthalimide, the methylated analogue of **169** (i.e. compound **173**) was prepared instead. Performing the chlorofluorination reaction on N-allyl-N-methyl-4-nitrobenzenesulfonamide **I** to afford compound **172** the alkyl substitution with potassium phtalimide was performed, to obtain **173** (**Scheme 4.2**). Unfortunately no improvements in the reaction yield were observed, mostly due to tedious purification procedures. Removal of phtalimide protecting group on compound **173** to obtain the compound **174** worked very well under standard hydrazine reaction procedures.

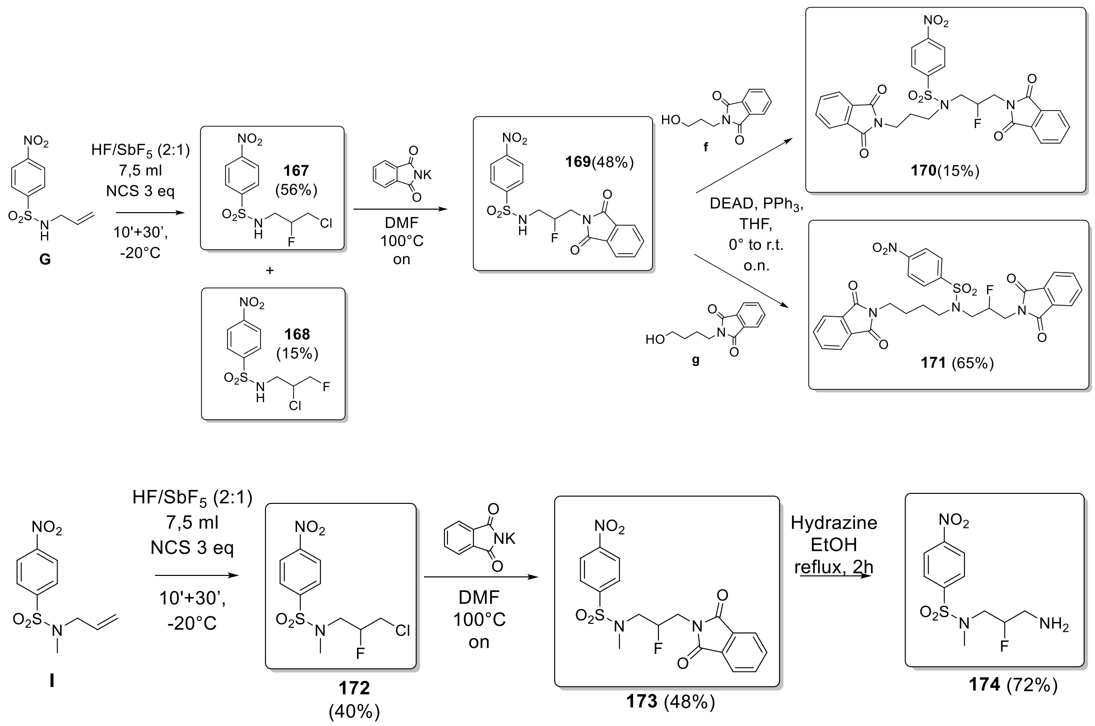

Scheme 4.2. Synthetic procedures for the preparation of protected β-fluorinated triamine derivatives **170** and **171** and their intermediates, along with compounds **172-174**.

We attempted the preparation of the difluorinated analogues of the compounds previously discussed by performing a tandem hydrofluorination/chlorofluorination reaction on Nosylated propargylamine in HF/SbF_5. To the best of our knowledge such a reaction has been reported only on *N*-acetyl propargylated piperazine [55], which unfortunately did not afford any of the desired material upon exploration of various reaction conditions. In all cases the difluoroderivative **159** was the exclusive product obtained in good yield and high purity (data not showed).

4.4.1.2 *In vitro* Biological Evaluation: hCA inhibition

All the compounds synthetized in this second series of nitrogen-containing compounds have been tested against five hCA isoforms using the Stopped Flow technique (**Table 4.4**) [45]. Interesting conclusions can be drawn from the SARs on these compounds.

	K_I (μM)*				
	hCA I	**hCA II**	**hCA IV**	**hCAIX**	**hCA XII**
167	3.02	0.026	>100	1.34	0.678
168	>100	0.28	>100	>100	0.565
169	>100	0.076	>100	>100	>100
170	>100	9.29	>100	25.13	>100
171	>100	63.1	>100	>100	>100
172	>100	>100	>100	>100	>100
173	>100	>100	>100	>100	>100
174	>100	0.79	20.1	>100	3.65
AAZ	0.250	0.012	0.074	0.026	0.0057

Table 4.4. CA Inhibition Data [45]. * Mean from 3 different assays, by a stopped flow technique (errors were in the range of ± 5-10 % of the reported values).

i) A first comparison can be done between the isomers **167** and **168**. As shown in **Table 4.4**, the insertion of fluorine in β position to the amine (**167**) resulted in a potent hCA II inhibitor, with K_I value in the low nanomolar range (0.026 μM). The isomer **168**, bearing chlorine in β position and fluorine in γ position, despite being a potent inhibitor, showed a K_I values 10 fold inferior to the one registered for the other isomer against the same isoform (0.280 μM). Low micromolar K_I values against hCA I and IX are also showed by compound **167** (3 μM and 1.3 μM) whereas the isomer **168** turned out the be inactive against the same isoforms. These data can be rationalized considering the withdrawing effect of fluorine atom, which improved the acidity of the sulfonamide function when inserted in β position. Both isomers (**167** and **168**) showed good inhibition potency against hCA XII (K_I values of 0.678 μM and 0.565 μM, respectively). Methylated analogue of **167** (compound **172**) revealed to be inactive against all the isoforms considered.

ii) Substitution of chlorine with phthalimide moiety to afford compound **169** led the K_I calculated for this compound to increase up to >100 μM against hCA I, IV, IX and XII, whereas against hCA II the inhibition potency was retained (K_I = 0.076 μM). In agreement with what observed for its chlorinated precursor (**172**), the methylated compound **173** revealed to be inactive against all the isoforms. However, after phthalamide deprotection in hydrazine to give compound **174**, the activity against hCA II, IV and XII was restored. This is an important result, which confirmed our findings about β-flurinated amines as potent hCA inhibitors.

iii) Alkylated compounds **170** and **171** obtained after Mitsunobu reaction showed K_I values of >100 μM against most of the considered isoforms, with slight inhibition only showed against hCA II and hCA IX. In particular, derivative **170** obtained after alkylation with protected alcohol **f** revealed to be slightly more potent in hCA II and IX inhibition (K_I values of 9.29 and 25.13 μM, respectively) when compared to the analogue **171**, bearing a longer spacer between benzensulfonamide and phalimido moiety (K_I values of 63.1 and >100 μM, respectively).

4.4.1.3 Conclusions and Future Perspectives

Monofluorinated benzensulfonamide derivatives have been synthetized in Superacid medium and differently derivatized. The obtained compounds as well as all their intermediates were evaluated as hCA inhibitors and the kinetic data collected led us to define interesting SARs. The influence of fluorine position in the scaffold on hCA inhibition against various isoforms has been determined. In particular, β–fluorinated/-γ–chlorinated benzensulfonamides revealed to be more potent hCA II inhibitors, when compared to the γ–fluorinated/β–chlorinated analogues (**167** vs **168**), confirming the importance of the well known withdrawing effect of fluorine in influencing the pKa of the neighbouring amine functionality. Compounds bearing phtalimide moiety have also been assayed against hCAs. The inhibition data showed high potency and selectivity against hCA II for the simplest derivative **169**, bearing a secondary benzensulfonamide and a phtalimide moiety. Methylation on benzensulfonamide revealed to be detrimental for hCA inhibition, leading to a completely inactive compound (**173**). On the other hand, benzensulfonamide alkylation with phatlimido protected alcohols restored the inhibition activity (**170, 171**). This can be maybe rationalyzed considering further interactions of the alkyl chain inserted with the enzyme cavity. In particular, the importance of the distance between the second phalimide functionality and the benzensulfonamide moiety on the inhibition potency has been highlited, supporting our hypothesis. Moreover the modest inhibition activity showed by compound **174**, bearing a primary amine functionality and methylated benzensulfonamide is worth of more explorations to assess its binding mode and the interactions within the enzyme cavity. The compounds obtained can be also used as valid tools for conformational studies, to explore the fluorine impact on their conformation.

We are currently performing the full deprotection of compounds **170** and **171**, and we planned to submit the resulted compounds to hCAs inhibition studies as well as conformational studies.

4.4.2 Synthesis of 3-fluoro-2,3,4,5-tetrahydro-[1,3]oxazepino[2,3-a]isoindol-7(11b*H*)-ones

4.4.2.1 State of the Art

A third project I was involved in during my experience abroad concerns the synthesis of enantiopure fluorinated triclcyclic compounds, using electrophilic fluorine (NFSI) instead of superacid system for the insertion of C-F into molecular scaffolds. As reported in several works *N,O*-acetal products can be used as a building blocks for the construction of a wide variety of natural and unnatural carbocyclic and azacyclic compounds including simple and complex alkaloids, thus showing great synthetic utility [56]. The possibility to insert more than one stereocentre and different heteroatoms makes these compounds versatile tools for biomedical purposes. So far, 5-, 6- and 7- membered rings fused to the isoindolin-1-one moiety by means of an oxygen atom have been reported [57,58]. However, the enantiopure fluorine containing oxazepinoisoindolinone compounds have not been described yet.

Three general methods were used to obtain such tricyclic lactames: 1) palladium catalysed cyclization between aminoalcol and 2-bromo benzaldehyde; 2) cyclodehydratation between an aminoalcohol and a chetoacid catalysed by *p*-toluensufonic or acetic acid; 3) intramolecular cyclization in acidic medium via *N*-acyliminium species [57] (**Figure 4.10**).

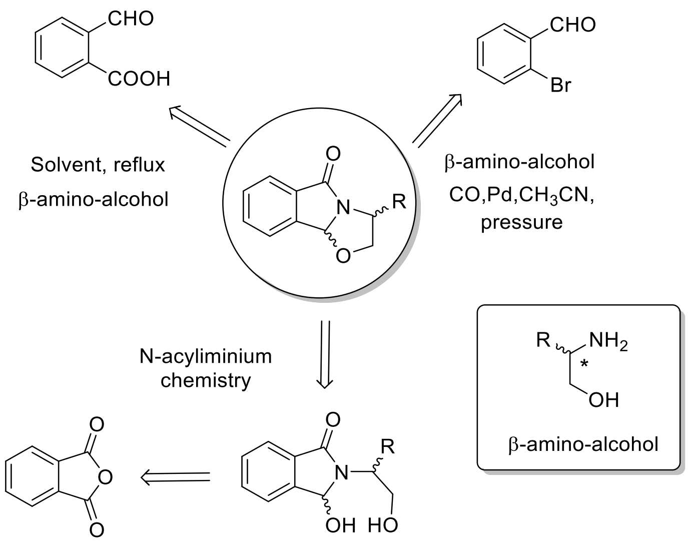

Figure 4.10. General methods used to obtain tricyclic lactames [57].

The last two strategies have been deeply investigated, and it is now well established that in some cases it is possible to control the stereochemistry of the reaction varying the position and the nature of the substituents on the aminoalcoholic chain as well as the length of the chain itself (**Figure 4.11**) [57,58].

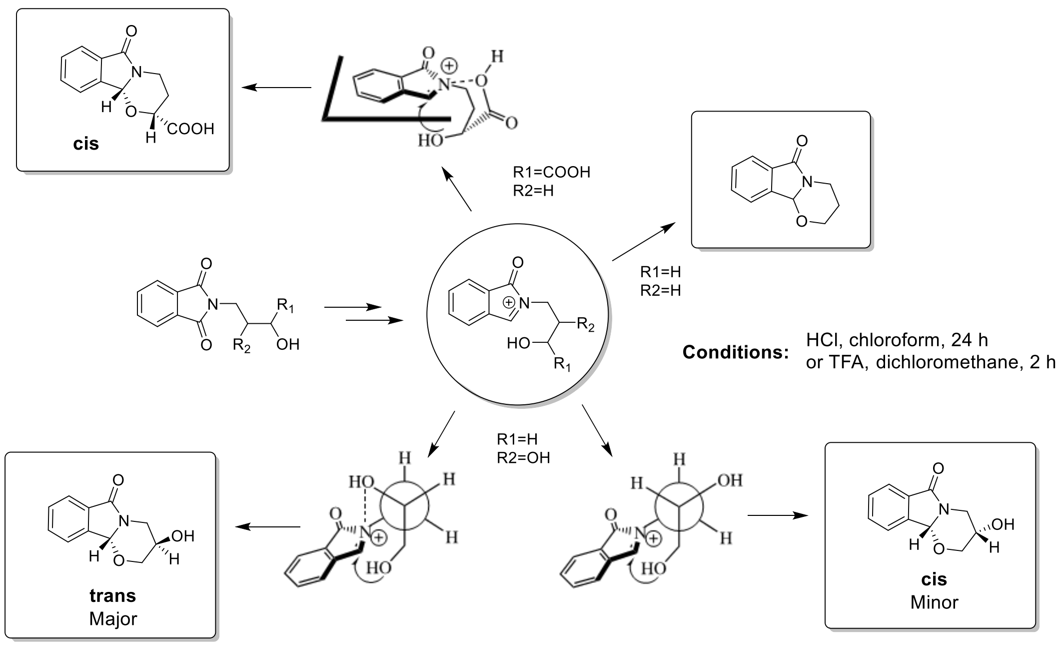

Figure 4.11. Stereoselective intramolecular oxoamidoalkylation [58].

The preferential formation of an isomer over the other one was found to be closely related to the generation of the *N*-acyliminium intermediate species upon dehydratation of the α-hydroxy-lactam with a Bronsted acid. The substituents present on the alkyl chain bearing the terminal alcohol, by means of interactions with the *N*-acyliminium ion are crucial for its spatial orientation and therefore to guide its attack towards the electrophilic *N*-acyliminium ion (**Figure 4.11**) [57,58].

4.4.2.2 Synthesis of (3*R*, 11b*R*)/(3*R*, 11b*S*)/(3*S*, 11b*R*)/(3*S*, 11b*S*)-3-fluoro-2,3,4,5-tetrahydro-[1,3]oxazepino[2,3-a]isoindol-7(11b*H*)-ones

The synthesis of the enantiopure fluorine containing oxazepinoisoindolinone started with the protection of γ-amminobutiric acid **J** using phtalic anhydride to obtain compound **175** [59]. Then, a diastereoselective approach has been used to ensure the stereoselective introduction of fluorine in our compounds (**Scheme 4.3**).

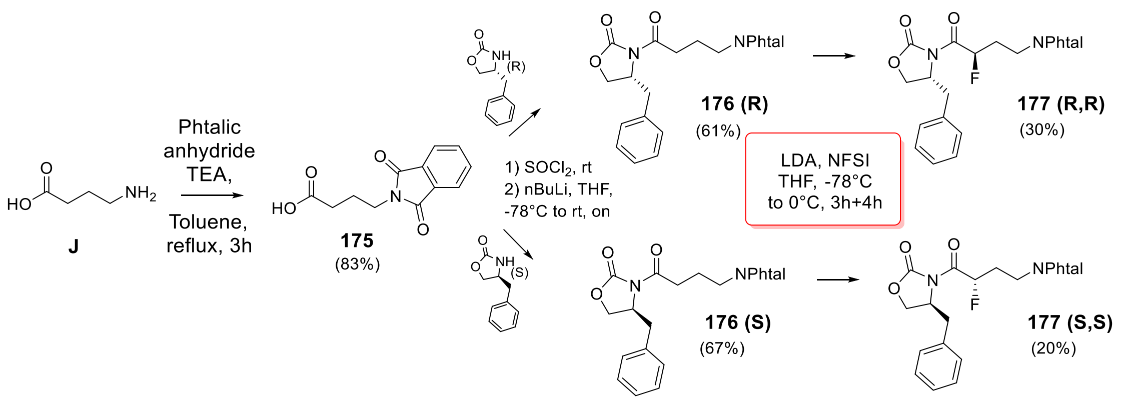

Scheme 4.3. Synthetic procedures for the preparation of derivatives **177**-(*R,R)* and **177**-(*S,S*).

(*R*)- and (*S*)-Benzyloxazolidinone have been chosen as chiral auxiliary for obtaining respectively compounds **176**-(*R)* and **176**-(*S*) with good yields [60]. The most critical reaction step was represented by the fluorination reaction to afford the derivatives **177**-(*R,R)* and **177**-(*S,S*) using LDA as base and NFSI as the electrophilic fluorine source [60]. By applying the procedures reported in literature for similar compounds we recovered low yields which were ascribed both to uncomplete consumption of starting material and cleavage of the chiral adjuvant. Different reaction conditions were investigated by means of changing the parameters reported in **Table 4.5** and thus allowing to achieve a maximum yield of 30% (entry **8** in **Table 4.5**).

Entry	eq NFSI	Base	Solvent	Deprotonation Time	Reaction Time	Extraction	Yield %
1	1.05	nBuLi/DPA	THF	60'	2h (-78°C)+2h (0°C)	DCM	14
2	1.05	nBuLi/DPA	THF	60'	2h (-78°C)+2h (0°C)	DCM	12
3	1.05	LDA	THF	60'	2h (-78°C)+2h (0°C)	DCM	22
4	1.05	titrated LDA	THF (new)	60'	2h (-78°C)	DCM	27
5	1.05	titrated LDA	THF (new)	15'	3h (-78°C)+3h (0°C)+ o.n. to r.t.	EtOAc	12
6	1.05	titrated LDA	THF (new)	60'	2h (-78°C)+2h (0°C)	EtOAc	11
7	1.5	titrated LDA	THF (new)	30'	3h (-78°C)+3h (0°C)+ o.n. 0°C	EtOAc	10
8	1.5	titrated LDA	distilled THF	60'	3h (-78°C)+4h (0°C)	EtOAc	30
9	5 (1 eq/h)	titrated LDA	distilled THF	90'	5h (-78°C)+ o.n. (0°C)	EtOAc	25

Table 4.5. Optimization of the reaction conditions.

Alternative fluorination approaches were investigated although with unsatisfying results: *i*) α-fluorination of titanium enolate (only starting material was recovered) [61] or *ii*) organocatalytic α-fluorination of aldehydes using MacMillan's catalyst [62]. With the latter no improvements in the yield were observed and several byproducts were formed.

As reported in **Scheme 4.4** $NaBH_4$ was used to remove the chiral auxiliary in order to afford in one single step both the primary and secondary alcohol [57,58,61]. The alcohols **178** as distereomeric mixture (1/1 NMR ratio) were obtained in agreement with the data reported in literature, after reduction of the imide and cleavage/reduction of the oxazolidinone [57,58].

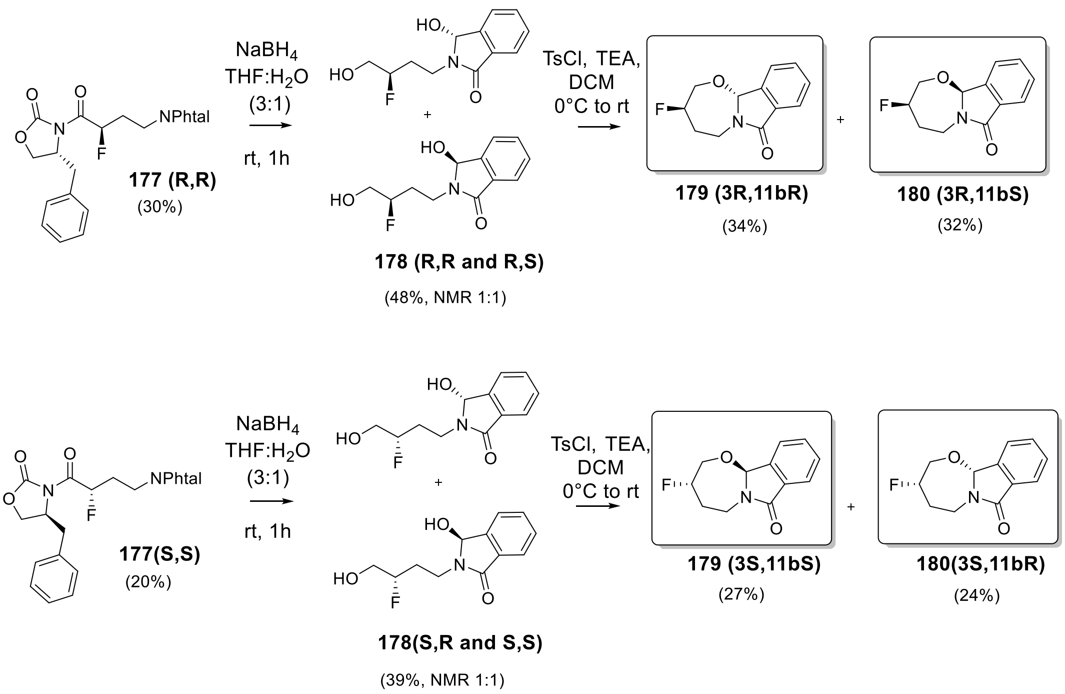

Scheme 4.4: Synthetic procedures for the preparation of derivatives **179** and **180**.

For the intramolecular oxoamidoalkylation step, we decided to perform the reaction in basic environment. By treating the distereomeric mixture of **178** with TsCl and TEA in DCM we observed the formation of the two diastereoisomers **179** and **180** in 1/1 ratio. The absolute configuration of the newly created stereocenter was determined by NOE difference experiments. Differently from what reported to occur in acidic environment, performing the cyclization step using a basic environment allows the reaction to occur through a SN_2 nucleophilic fashion of the activated primary alochols as schematically reported in **Scheme 4.5**, affording to the formation of the two diastereoisomers in equimolar amount.

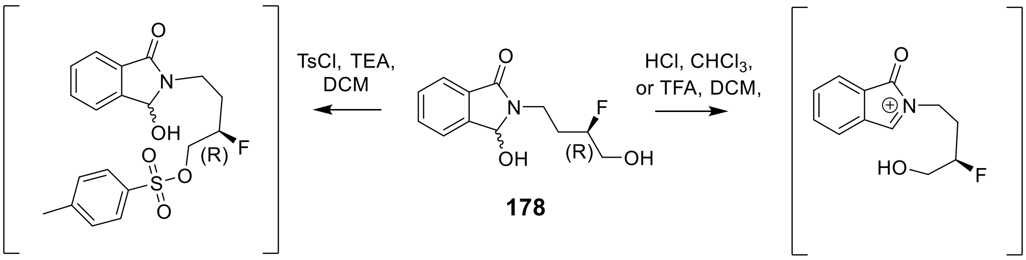

Scheme 4.5: Proposed cyclization mechanisms in basic and acidic conditions.

4.4.2.3 Conclusions and Future Perspectives

In this work, we reported the synthesis of enantiopure fluorine containing oxazepinoisoindolinone using chiral auxiliaries to ensure the stereoselective introduction of fluorine in our compounds. The cyclization step on the diastereoisomeric mixture of alcohols were performed in basic conditions, allowing to obtain diastereoisomers in equimolar amount.The possibility to easily separate the two diastereomers by flash chromatography isolating them in the same yields makes this synthetic approach advantageous, allowing to get product diversification in only one synthetic step and appreciable yields.

X-ray crystallographic studies are currently being performed on the final compounds in order to address any conformational change induced form the halogen.

4.5 References

1. Müller K, Faeh C, Diederich F. Fluorine in pharmaceuticals:looking beyond intuition. Science. 2007, 317, 1881-86.
2. Wang J, Sánchez-Roselló M, Aceña JL. et al. Fluorine in pharmaceutical industry: fluorine-containing drugs introduced to the market in the last decade (2001-2011). Chem Rev. 2014, 114, 2432-06.
3. O'Hagan D, Harper DB. Fluorine-containing natural products. J Fluor Chem. 1999, 100, 127-133.
4. Zhan CG, Dixon DA. Hydration of the Fluoride Anion: Structures and Absolute Hydration Free Energy from First-Principles Electronic Structure Calculations. J Phys Chem. 2004, 108, 2020-2029.
5. Marais JSC, Du Toit PJ. The isolation of the toxic principle "potassium cymonate" from "Gifblaar" Dichapetalum cymosum (Hook) Engl. Onderstepoort J Vet Sci Anim Ind. 1943, 18, 203.
6. Sanada M, Miyano T, Iwadare S. et al. Biosynthesis of fluorothreonine and fluoroacetic acid by the thienamycin producer, Streptomyces cattleya. Antibiot. 1986, 39, 259-265.
7. Fried J, Sabo EF. Synthesis of 17α-hydroxycorticosterone and its 9α-halo derivatives from 11-epi-17α-hydroxycorticosterone. J Am Chem Soc. 1953, 75, 2273.
8. Fried J, Sabo EF. Halogenated Corticoids. I. 9α-Halogen Derivatives of Cortisone and Hydrocortisone. J Am Chem Soc. 1957, 79, 1130-1141.
9. Heidelberger C, Chaudhuri NK, Danneberg P, et al. Fluorinated pyrimidines, a new class of tumour-inhibitory compounds. Nature. 1957, 179, 663-666.
10. Hyohdoh I, Furuichi N, Aoki T, et al. Fluorine Scanning by Nonselective Fluorination: Enhancing Raf/MEK Inhibition while Keeping Physicochemical Properties. ACS Med. Chem. Lett. 2013, 41, 1059-1063.
11. Pauwels EKJ. ^{18}F-Labeled fluorodeoxyglucose for PET imaging: the working mechanism and its clinical implication. Drugs Future 2001, 26, 659−668.
12. Stenhagen ISR, Kirjavainen AK, et al. [^{18}F] Fluorination of an arylboronic ester using [^{18}F] selectfluor bis(triflate): application to 6-[^{18}F] fluoro-L-DOPA. Chem Commun. 2013, 49, 1386−1388.
13. Lee E, Kamlet AS, Powers DC, et al. A fluoride-derived electrophilic late-stage fluorination reagent for PET imaging. Science. 2011, 334, 639−642.
14. Gillis EP, Eastman KJ, Hill MD, et al. Applications of Fluorine in Medicinal Chemistry. J Med Chem. 2015, 58, 8315-59

15. Park BK, Kitteringham NR, O'Neill PM. Metabolism of fluorine-containing drugs. Annu Rev Pharmacool. Toxicol. 2001, 41, 443−470.

16. Böhm HJ, Banner D, Bendels S, et al., Fluorine in medicinal chemistry. Chem Bio Chem., 2004, 5, 637-643.

17. van Niel MB, Collins I, Beer MS, et al. Fluorination of 3-(3-(piperidin-1-yl)propyl)indoles and 3-(3-(piperazin-1-yl)propyl)indoles gives selective human 5-HT1D receptor ligands with improved pharmacokinetic profile. J Med Chem. 1999, 42, 2087-104.

18. Rowley M, Hallett DJ, Goodacreet S, et al., 3-(4-Fluoropiperidin-3-yl)-2-phenylindoles as High Affinity, Selective, and Orally Bioavailable h5-HT2A Receptor Antagonists. J. Med. Chem. 2001, 44, 1603-1614.

19. Morgenthaler M, Schweizer E, Hoffmann-Röder A, et al. Predicting and tuning physicochemical properties in lead optimization: amine basicities. Chem Med Chem. 2007, 2, 1100−1115.

20. Cox CD, Breslin ,MJ, Whitman DB, et al. Kinesin spindle protein (KSP) inhibitors. Part V: discovery of 2-propylamino-2,4-diaryl-2,5-dihydropyrroles as potent, water-soluble KSP inhibitors, and modulation of their basicity by β-fluorination to overcome cellular efflux by P-glycoprotein. Bioorg Med Chem Lett. 2007, 17, 2697−2702

21. O'Hagan D. Understanding organofluorine chemistry. An introduction to the C-F bond. Chem Soc Rev. 2008, 37, 308-19.

22. Hunter L. The C–F bond as a conformational tool in organic and biological chemistry. Beilst J Org Chem. 2010, 6, 38

23. Pauling L. The Nature of the Chemical Bond and the Structure of Molecules and Crystals: An Introduction to Modern Structural Chemistry, Cornell University Press, Ithaca, NY, 1939.

24. Banks JW, Batsanov AS, Howard JAK, et al. The preferred conformation of α-fluoroamides. J Chem Soc, Perkin Trans. 2, 1999, 2409–2051.

25. Silla JM, Duarte CJ, Cormanich RA. Conformational analysis of 2,2-difluoroethylamine hydrochloride: double gauche effect. Beilst. J Org Chem. 2014; 10, 877–882.

26. Briggs CRS, Allen MJ, O'Hagan D, et al. The observation of a large gauche preference when 2-fluoroethylamine and 2-fluoroethanol become protonated. Org Biomol Chem., 2004, 2, 732–740.

27. Buissonneaud DY, van Mourik T, O'Hagan D. A DFT study on the origin of the fluorine gauche effect in substituted fluoroethanes. Tetrahedron. 2010, 66, 2196–2202.

28. Carta F, Temperini C, Innocenti A, et al. Polyamines inhibit carbonic anhydrases by anchoring to the zinc-coordinated water molecule. J Med Chem. 2010, 53, 5511-22.

29. Emsley J. Very strong hydrogen bonding. Chem. Soc. Rev.1980, 9, 91–124.

30. Liang T, Neumann CN, Ritter T. Introduction of Fluorine and Fluorine-Containing Functional Groups. Angew Chem Int Ed. 2013, 52, 8214–8264.

31. Fadeyi OO, Lindsley CW. Rapid, General Access to Chiral β-Fluoroamines and β, β-Difluoroamines via Organocatalysis. Org Lett. 2009, 11, 943–946.

32. Grunewald GL, Caldwell TM, Li Q, Criscione KR. Synthesis and Evaluation of 4-Fluoro-8-substituted-2,3,4,5-tetrahydro-1H-2-benzazapines as Selective Inhibitors of Phenylethanolamine N-Methyltransferase versus the α2-Adrenoceptor. J Med Chem. 2001, 44, 2849-56.

33. Fan RH, Zhou YG, Zhang WX, et al. Facile Preparation of β-Fluoro Amines by the Reaction of Aziridines with Potassium Fluoride Dihydrate in the Presence of Bu4NHSO4 J Org Chem. 2004, 69, 335-338.

34. Olah GA, Chambersand RD, Prakash GKS. Synthetic Fluorine Chemistry, ed. M. Hudlicky and A. E. Pavlath, Wiley, New York, 1992, pp. 163–204.

35. Gillespie RJ, Peel TE. Hammett acidity function for some superacid systems. J Am Chem Soc. 1973, 95, 5173-5178.

36. Olah GA, Prakash GKS, Molnar A, Sommer J. Superacids, 2nd ed.; Wiley Intersciences: New-York, 2009.

37. Jacquesy JC, Berrier C, Gesson JP, Jouannetaud MP. New Syntheses in Super Acids. Ann Chim.1984, 9, 641-648.

38. Olah GA, Klumpp DA. Superelectrophiles and Their Chemistry; Wiley Interscience: Hoboken, 2008.

39. Thibaudeau S, Martin-Mingot A, Jouannetaud MP. et al. A novel, facile route to beta-fluoroamines by hydrofluorination using superacid HF-SbF(5). Chem Commun (Camb). 2007, 14, 3198-200.

40. Thibaudeau S, Carreyre H, Martin-Mingot A. Synthesis of Fluorinated Nitrogen-Containing Compounds Through Superelectrophilic Activation in Superacid HF/SbF_5. Modern Synthesis Processes and Reactivity of Fluorinated Compounds. Progress in Fluorine Science 2017, pp 349-388.

41. Kaneda K, Taira R., Fukuzawa T.et al, Efficient synthesis of N-nosyl-protected 3-azabicyclo[4.3.0]nonen-8-one by an aniline- and nitrobenzene-mediated Pauson–Khand cyclization. Synthetic Comm. 2017, 47, 1622-1629.

42. Chung WJ, Omote M, Welch JT. The Catalytic Mannich Reaction of 1,1-Difluoro-2-trialkyl(aryl)silyl-2-trimethyl-silyloxyethenes: Preparation of β-Amino Acid Derivatives. J Org Chem. 2005, 70, 7784-87.

43. Cantet AC, Carreyre H, Gesson JP, et al. Gem-difluorination of aminoalkynes via highly reactive dicationic species in superacid HF-SbF_5: application to the efficient synthesis of difluorinated cinchona alkaloid derivatives. J Org Chem. 2008, 73, 2875-78.

44. Schrödinger Suite Release 2019-1, Schrödinger, LLC, New York, NY, 2019 (a) Epik, v.4.7; (b) Jaguar, v10.3

45. Khalifah R.G. The carbon dioxide hydration activity of carbonic anhydrase I. Stop-flow kinetic studies on the native human isoenzymes B and C. J Biol Chem. 1971, 246, 2561-73.

46. Liu F, Martin-Mingot A, Lecornué F. et al. Carbonic Anhydrases inhibitory effects of new benzenesulfonamides synthesized by using superacid chemistry. J Enzyme Inhib Med Chem. 2012, 27, 886-891.

47. Vullo D, Scozzafava A, Pastorekova S, et al. Carbonic anhydrase inhibitors: Inhibition of the tumor-associated isozyme IX with fluorine-containing sulfonamides. The first subnanomolar CA IX inhibitor discovered. Bioorg Med Chem Lett. 2004, 14, 2351–2356.

48. Blackburn GM, Türkmen H. Synthesis of alpha-fluoro- and alpha, alpha-difluoro-benzenemethanesulfonamides: New inhibitors of carbonic anhydrase. Org Biomol Chem. 2005, 3, 225–226.

49. Le Darz A, Martin-Mingot A, Bouazza F, et al. Fluorinated pyrrolidines and piperidines incorporating tertiary benzenesulfonamide moieties are selective carbonic nhydrase II inhibitors, J. Enzyme Inhib Med Chem. 2014, 30, 737-745.

50. Métayer B, Martin-Mingot A, Vullo D et al. Superacid synthesized tertiary benzenesulfonamides and benzofuzed sultams act as selective hCA IX inhibitors: toward understanding a new mode of inhibition by tertiary sulphonamides. Org Biomol Chem. 2013, 11, 7540.

51. Supuran CT, Thibaudeau S. et al. New superacid synthesized (fluorinated) tertiary benzenesulfonamides acting as selective hCA IX inhibitors: toward a new mode of carbonic anhydrase inhibition by sulphonamides, Chem Commun. 2013, 49, 6015-6017.

52. Waheed A, Sly WS. Membrane associated carbonic anhydrase IV (CA IV): a personal and historical perspective. Subcell Biochem. 2014, 75, 157-79.

53. Tang Y, Xu H, Du X. Gene expression in blood changes rapidly in neutrophils and monocytes after ischemic stroke in humans: a microarray study. J Cerebr Blood F Met. 2006, 26, 1089–1102.

54. Sterling D, Alvarez BV, Casey JR. The extracellular component of a transport metabolon. Extracellular loop 4 of the human AE1 Cl^-/HCO_3^- exchanger binds carbonic anhydrase IV. J Biol Chem. 2002, 277, 25239-46.

55. Le Darz A, Castelli U, Mokhtari N, et al. Tandem superelectrophilic activation for the regioselective chlorofluorination of recalcitrant allylic amines. Tetrahedon. 2016, 72, 674-689.

56. Groaning MD, Meyers AI. Chiral Non-Racemic Bicyclic Lactams. Auxiliary-Based Asymmetric Reactions. Tetrahedron. 2000, 56, 9843-9873.

57. Sikoraiová J, Chihab-Eddine A, et al. Diastereoselective access to chiral non-racemic [1,3]oxazolo-[2,3-a]isoindol-5-one ring systems via O-cationic cyclization. J. Heterocyclic Chem. 2002, 39, 383.

58. Sikoraiová J et al.. Acid-mediated intramolecular cationic cyclization using an oxygen atom as internal nucleophile: synthesis of substituted oxazolo-, oxazino- and oxazepinoisoindolinones. Tetrahedron Lett. 2002, 43, 4747–51.

59. Ahuja P, Husain A, Siddiqui N. Essential aminoacid incorporated GABA–phthalimide derivatives: synthesis and anticonvulsant evaluation. Med Chem Res 2014, 23, 4085.

60. Edmonds MK, Graichen FHM, Gardiner J., et al. Enantioselective Synthesis of □-Fluorinated β2-Amino Acids. Org Lett. 2008, 10, 885-887.

61. Alvarado J, Herrmann AT, Zakarian A. Stereoselective α-Fluorination of N-Acyloxazolidinones at Room Temperature within 1 h. J Org Chem. 2014, 79, 6206−20.

62. Beeson TD, MacMillan DWC. Enantioselective Organocatalytic α-Fluorination of Aldehydes. J Am Chem Soc. 2005, 127, 8826-28.

<u>Chapter 5</u>: Experimental Section

5.1 Experimental Section : Chapter 2

5.1.1 Chemistry

Anhydrous solvents and all reagents were purchased from Sigma-Aldrich (Milan, Italy), Alfa Aesar (Milan, Italy) and TCI (Milan, Italy). All reactions involving air- or moisture-sensitive compounds were performed under a nitrogen atmosphere using dried glassware and syringes techniques to transfer solutions. Nuclear magnetic resonance spectra (^{1}H-NMR: 400 MHz; ^{13}C-NMR: 100 MHz) were recorded in DMSO-d_6 using an Avance III 400 MHz spectrometer (Bruker, Milan, Italy). Chemical shifts are reported in parts per million (ppm) and the coupling constants (J) are expressed in Hertz (Hz). Splitting patterns are designated as follows: s, singlet; d, doublet; t, triplet; q, quadruplet; m, multiplet; brs, broad singlet; dd, double of doublets. The assignment of exchangeable protons (OH and NH) was confirmed by the addition of D_2O. Analytical thin-layer chromatography (TLC) was carried out on silica gel F-254 plates (Merck, Milan, Italy). Melting points (m.p.) were carried out in open capillary tubes and are uncorrected. The solvents used in MS measures were acetone, acetonitrile (Chromasolv grade), purchased from Sigma–Aldrich and mQ water 18 MΩ cm, obtained from Millipore's Simplicity system (Milan, Italy). The mass spectra were obtained using a 1200 L triple quadrupole system (Varian, Palo Alto, CA, USA) equipped by Electrospray Source (ESI) operating in both positive and negative ions. Stock solutions of analytes were prepared in acetone at 1.0 mg mL^{-1} and stored at 4 °C. Working solutions of each analyte were freshly prepared by diluting stock solutions in a mixture of mQ H_2O/CH_3CN 1:1 (v/v) up to a concentration of 1.0 μg mL^{-1}. The mass spectra of each analyte were acquired by introducing, via syringe pump at 10 μL min^{-1}, the working solution. Raw-data were collected and processed by Varian Workstation Vers. 6.8 software.

Synthethic Scheme for the preparation of the propargyl derivatives 61-74.

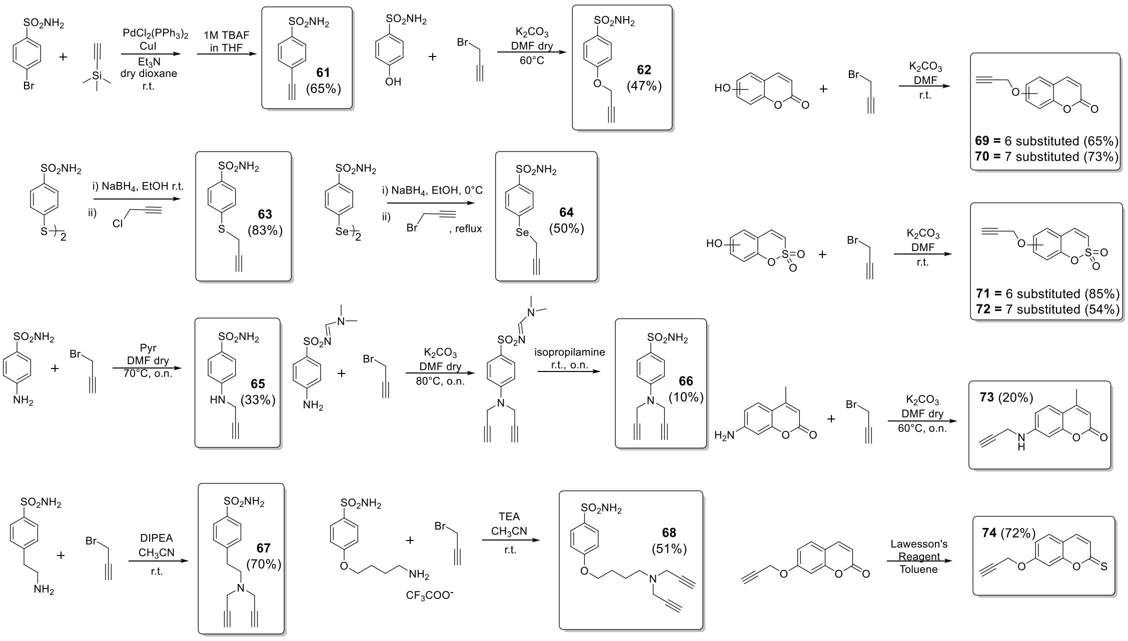

General procedure A: The proper alkyl halide (1.2 eq.) was added to a suspension of starting material (0.5 g, 1.0 eq.) and K_2CO_3 (2.0 eq.) in dry DMF (4 mL) under N_2 atmosphere. The mixture was stirred at 60° until consumption of starting material (5 h, TLC monitoring). The reaction mixture was cooled at r.t. and quenched with slush. The mixture was extracted with EtOAc (x 3) and the combined organic layers were washed with H_2O and brine solution, then dried over Na_2SO_4, filtered-off and concentrated under vacuum.

General procedure B: The proper alkyl halide (1.2 eq.) was added to a suspension of starting material (0.5 g, 1.0 eq.) and pyridine (1.2 eq.) in dry DMF (2 ml) under N_2 atmosphere and the mixture was stirred at 70°C o.n. (TLC monitoring). The reaction was quenched with H_2O (10 ml) and extracted with EtOAc (3 x 15 ml). The combined organic layers were washed with H_2O (3 x 15 ml) and brine (3 x 15 ml), dried over anhydrous Na_2SO_4, filtered-off and concentrated under vacuum to give a solid that was purified by silica gel column chromatography eluting with the appropriate mixture of EtOAc in n-Hexane to afford the desired compounds.

General procedure C: The appropriate alkynyl derivatives (0.1 g, 1.0 eq.) were dissolved in THF (5 ml) and then dicobalt octacarbonyl (1.05 eq. or 2.1 eq.) was added. The black mixture was stirred at r.t. for 40 min. (TLC monitoring). Then SiO2 was added and the solvent was removed under vacuum to give a black solid residue which was purified by silica gel column chromatography eluting with the appropriate mixture of EtOAc in n-Hexane to afford the desired compounds.

4-Ethynylbenzenesulfonamide 61. $PdCl_2(PPh_3)_2$ (0.1 eq.) and CuI (0.1 eq.) were added to a solution of 4-bromobenzenesulfonamide (0.5 g, 1.0 eq.), (trimethylsilyl)acetylene (1.2 eq.) and Et_3N (10 eq.) in dry dioxane (5.0 mL) at r.t. under N_2 atmosphere. The reaction mixture was stirred at 100°C o.n., then quenched with slush and extracted with EtOAc (2x20ml). The collected organic layers were dried over anhydrous Na_2SO_4, filtered-off and concentrated under vacuum to give a residue that was treated with a 1.0 M solution of TBAF in THF (2.0 eq.). The reaction mixture stirred at r.t. for 2h and thereafter concentrated under vacuum. The obtained residue was purified by silica gel chromatography eluting with 5% MeOH in DCM to afford the titled compound **61** as a white solid. 65% yield; δ_H (400 MHz, DMSO-d_6): 4.47 (1H, s, C*H*), 7.49 (2H, s, exchange with D_2O, SO_2NH_2), 7.71 (2H, d, *J* = 7.8, Ar-*H*), 7.85 (2H, d, *J* = 7.8, Ar-*H*). Experimental in agreement with reported data [1]

4-(Prop-2-ynyloxy)benzenesulfonamide 62. Synthetized according to the **general procedure A** using 4-hydroxybenzenesulfonamide as starting material and propargyl bromide 80% in toluene as alkyl halide. Purified by silica gel column chromatography eluting with 50% ethyl acetate in *n*-hexane to afford the titled compound **62** as a white powder. 47% yield; δ_H (400 MHz, DMSO-d_6) 3.67 (1H, br s, C*H*), 4.94 (2H, br s, CH_2), 7.17 (2H, d, *J* = 7.2, Ar-*H*), 7.28 (2H, s, exchange with D_2O, SO_2NH_2), 8.01 (2H, d, *J* = 7.2, Ar-*H*). Experimental in agreement with reported data [2]

4-(Prop-2-ynylthio)benzenesulfonamide 63. $NaBH_4$ (23 mg, 0.60 mmol, 3.0 eq.) was added portion wise to a solution of 4,4′-disulfanediyldibenzenesulfonamide (75 mg, 0.20 mmol, 1.0 eq.) in EtOH (2 mL) at r.t. under a N_2 atmosphere. After 2 h, propargyl chloride (0.42 mmol, 2.1 eq.) was slowly added and the reaction mixture was stirred at r.t. for 3 h, until complete consumption of the starting material was observed by TLC. The reaction was quenched by addition of saturated NH_4Cl aqueous solution (2 mL) and diluted with EtOAc (5 mL), The layers were separated and the aqueous layer was extracted with EtOAc (2 × 5 mL), dried over Na_2SO_4, filtered and concentrated under vacuum. The crude material was purified by silica gel flash chromatography to afford the titled compound **63** as a white solid. 83% yield; δ_H (400 MHz, DMSO-d_6): 3.22 (1H, t, *J* = 2.6, C*H*), 4.02 (2H, d, *J* = 2.6, CH_2), 7.37 (2H, s, exchange with D_2O, SO_2NH_2), 7.56 (2H, dd, *J* = 2.0, 6.7, Ar-*H*), 7.79 (2H, dd, *J* = 2.0, 6.7, Ar-*H*). Experimental in agreement with reported data [3]

4-(Prop-2-yn-1-ylselanyl)benzenesulfonamide 64. $NaBH_4$ (23 mg, 0.60 mmol, 3.0 eq.) was added portion wise to a solution of 4,4'- diselanediyldibenzenesulfonamide (94 mg, 0.20 mmol, 1.0 eq.) in EtOH (2 mL) at 0°C under N_2 atmosphere. After 30 min, propargyl bromide (0.36 mmol, 2.1 eq.) was slowly added and the reaction mixture was stirred at reflux for 3 h, until complete consumption of the starting material was observed by TLC. The reaction was quenched by addition of saturated NH_4Cl aqueous solution (2 mL) and diluted with EtOAc (5 mL). The layers were separated and the aqueous layer was extracted with EtOAc (2 x 5 mL), dried over Na_2SO_4, filtered and concentrated under vacuum. The crude material was purified by silica gel flash chromatography to afford the titled compound **64** as a white solid. 50 % yield; δ_H (400 MHz, DMSO-d_6): 5.09 (2H, d, *J* = 6.26 Hz), 6.54 (1H, t, *J* = 6.26 Hz), 7.40 (2H, br s, exchange with D_2O, SO_2NH_2,), 7.68 (2H, d, *J* = 8.61 Hz), 7.78 (2H, d, *J* = 8.59 Hz). Experimental in agreement with reported data [4].

4-(Prop-2-ynylamino)benzenesulfonamide 65. Synthetized according to the **general procedure B** using sulfanilamide as starting material and propargyl bromide 80% in toluene as alkyl halide. Purified by silica gel column chromatography eluting with 50% ethyl acetate in *n*-hexane to afford the desired product **65** as a yellow solid. 33 % yield; silica gel TLC R_f 0.30 (EtOAc/n-Hex 70 % *v/v*); δ_H (400 MHz, DMSO-d_6): 3.13 (1H, t, *J* = 2.4, C*H*), 3.97 (2H, dd, *J*= 2.4, 6.0, C*H2*), 6.73 (2H, d, *J* = 8.8, Ar-*H*), 6.76 (1H, br t, exchange with D_2O, N*H*), 6.98 (2H, br.s, exchange with D_2O, SO_2NH_2), 7.59 (2H, d, *J* = 8.8, Ar-*H*). Experimental in agreement with reported data [5].

4-(diProp-2-ynylamino)benzenesulfonamide 66. Sulfanilamide (0,5 g, 1.0 eq.) was solubilized in DMF and the solution was cooled to 0°C. Then, dimethoxy-*N*,*N*-dimethylmethanamine (1.2 eq.) was added. The solution was stirred at r.t. until consumption of starting material (2h). The reaction was quenched with DCM and precipitate formed was filtered-off, dried to afford *N*'-((4-aminophenyl)sulfonyl)-*N*,*N*-dimethylformimidamide which was used for the next step without further purification. *N*'-((4-aminophenyl)sulfonyl)-N,N-dimethylformimidamide (1.0 eq.) was solubilized in dry DMF and K_2CO_3 (3.0 eq.) was added. Then, propargyl bromide 80% in toluene (4.0 eq.) was added and the mixture was stirred at 80°C o.n. until consumption of starting material. Then the reaction was quenched with H_2O (20 ml) and extracted with EtOAc (3 x 15 ml). The combined organic layers were washed with H_2O (3 x 15 ml) and brine(3 x 15 ml), dried over Na_2SO_4, filtered-off and concentrated under vacuum to give a residue that was suspended in isopropylamine in a sealed tube and stirred at r.t. o.n. The solvent was removed in vacuo obtaining a residue that was purified by silica gel column chromatography eluting with 50% ethyl acetate in *n*-hexane to afford a sticky residue which was triturated from Et_2O to afford the titled compound **66** as a white powder: 10% yield; δ_H

(400 MHz, DMSO-d_6): 3.21 (2H, t, *J* = 2.4, 2XC*H*), 4.29 (4H, d, *J* = 2.4, 2 x CH_2), 7.03 (2H, d, *J* = 8.8, Ar-*H*), 7.08 (2H, s, exchange with D_2O, SO_2NH_2), 7.70 (2H, d, *J* = 8.8, Ar-*H*). Experimental in agreement with reported data [6].

4-(2-(diProp-2-ynylamino)ethyl)benzenesulfonamide 67. Propargyl bromide (80% in toluene) (2 eq.) and DIPEA (1.7 eq.) were added to a stirred solution of 4-(2-aminoethyl) benzensulfonamide (0.5 g, 1.0 eq.) in CH_3CN (8 ml) under N_2 atmosphere. The mixture was stirred at r.t. o.n. until consumption of starting material (TLC monitoring). The solvent was removed under reduced pressure and the obtained residue was portioned between H_2O and EtOAc followed by extraction with EtOAc (3 x 15 ml). The combined organic layers were washed with H_2O(3 x 15 ml) and brine(3 x 15 ml), then dried over Na_2SO_4 filtered-off and concentrated under vacuum to afford compound **67** as a dark oil. 70 % yield; silica gel TLC R*f* 0.40 (MeOH/DCM 10 % *v/v*); δ_H (400 MHz, DMSO-d_6): 2.75 (2H, t, *J* = 6.8, CH_2), 2.84 (2H, t, *J* = 6.8, CH_2), 3.21 (2H, br t, 2 x C*H*), 3.44 (4H, d, *J* = 2.0, 2 x CH_2), 7.37 (2H, s, exchange with D_2O, SO_2NH_2), 7.45 (2H, d, *J* = 8.4, Ar-*H*), 7.76 (2H, d, *J* = 8.4, Ar-*H*); δ_C (100 MHz, DMSO-d_6): 32.6, 41.5, 53.3, 75.8, 79.1, 125.6, 129.1, 141.9, 144.4; *m/z* (ESI positive) 277.09 $[M+H]^+$. Experimental in agreement with reported data [7].

4-(4-(diProp-2-ynylamino)butoxy)benzenesulfonamide 68. To a solution of 4-(4-aminobutoxy)benzenesulfonamide, 2,2,2-trifluoroacetate salt (synthetized as reported in literature [8]) in dry CH_3CN (8 ml) was added TEA (1.7 eq.). After 15 min, propargyl bromide (80% in toluene) (2 eq.) was added. The mixture was stirred at r.t. o.n. until consumption of starting material (TLC monitoring). The solvent was removed under reduced pressure and the residue was portioned between H_2O and EtOAc, followed by extraction with EtOAc (3 x 15 ml). The combined organic layers were washed with H_2O (3 x 15 ml) and brine (3 x 15 ml), dried over Na_2SO_4, filtered-off and concentrated under vacuum to give a dark oil, which was triturated from Et_2O to afford to the titled compound **68** as a white powder: 51% yield; m.p. 97−101°C; silica gel TLC Rf 0.62 (EtOAc/n-Hex 70 % *v/v*); δ_H (400 MHz, DMSO-d_6) 1.56 (2H, m, CH_2), 1.74 (2H, m, CH_2), 2.49 (2H, t, *J* = 6.4, CH_2), 3.07 (2H, t, *J* = 2.4, 2 x C*H*), 3.36 (4H, d, *J* = 2.4, overlapped with the water peak, 2 x CH_2), 4.06 (2H, t, *J* = 6.4, CH_2), 7.08 (2H, d, *J* = 9.0, Ar-*H*), 7.21 (2H, s, exchange with D_2O, SO_2NH_2), 7.75 (2H d, *J* = 9.0, Ar-*H*); δ_C (100 MHz, DMSO-d_6) 23.5, 26.7, 41.9, 52.2, 68.4, 76.0, 79.8, 115.2, 128.4, 133.9, 161.8; *m/z* (ESI positive) 321.12 $[M+H]^+$.

6-(Prop-2-ynyloxy)-2*H*-chromen-2-one 69. Synthetized according to the **general procedure A** using 6-hydroxy-2H-chromen-2-one as starting material and propargyl bromide 80% in toluene as alkyl halide. Reaction performed at room temperature. Compound **69** obtained as a white powder: 65% yield; m.p. 163-166°C; silica gel TLC R*f* 0.63 (EtOAc/n-Hex 50 % *v/v*); δ_H (400 MHz, DMSO-d_6) 3.64 (1H, br t, C*H*), 4.90 (2H, d, *J* = 2.1, CH_2), 6.54 (1H, d, *J* = 9.6, Ar-*H*), 7.30 (1H, dd, *J* = 2.9, 9.0, Ar-*H*), 7.38 (1H, d, *J* = 2.9, Ar-*H*), 7.41 (1H, d, *J* = 9.0, Ar-*H*), 8.06 (1H, d, *J* = 9.6, Ar-*H*); δ_C (100 MHz, DMSO-d_6) 56.0, 78.6, 78.9, 112.3, 116.8, 117.4, 119.2, 120.0, 144.0, 148.3, 153.4, 160.1; *m/z* (ESI positive) 201.19 $[M+H]^+$.

7-(Prop-2-ynyloxy)-2*H*-chromen-2-one 70. Synthetized according to the **general procedure A** using 7-hydroxy-2H-chromen-2-one as starting material and propargyl bromide 80% in toluene as alkyl halide. Reaction performed at room temperature. Compound **70** obtained as a white powder.73% yield; δ_H (400 MHz, DMSO-d_6) 3.69 (1H, t, *J*= 2.4, C*H*), 4.97 (2H, d, *J*= 2.4, CH_2), 6.36 (1H, d, *J*= 9.6, Ar-*H*), 7.03 (1H, dd, *J*= 2.4, 8.6, Ar-*H*), 7.09 (1H, d, *J*= 2.4, Ar-*H*), 7.70 (1H, d, *J*= 8.6, Ar-*H*), 8.04 (1H, d, *J*= 9.6, Ar-*H*). Experimental in agreement with reported data [9].

6-Prop-2-ynyloxy-benzo-[e][1,2]-oxathiine 2,2-dioxide 71. Synthetized according to the **general procedure A** using 6-hydroxybenzo[e][1,2]oxathiine 2,2-dioxide as starting material and propargyl bromide 80% in toluene as alkyl halide. Reaction performed at room temperature. Compound **71** obtained as a white powder, pure: 85% yield; m.p. 154-157 °C; silica gel TLC R*f* 0.50 (EtOAc/n-Hex 40 % *v/v*); δ_H (400 MHz, DMSO-d_6): 3.66 (1H, t, *J* = 2.4, C*H*), 4.90 (2H, d, *J* = 2.4, CH_2), 7.24 (1H, dd, *J* = 3.0, 9.0, Ar-*H*), 7.38 (1H, d, *J* = 3.0, Ar-*H*), 7.45 (1H, d, *J* = 9.0, Ar-*H*), 7.55 (1H, d, *J* = 10.3, Ar-*H*), 7.68 (1H, d, *J* = 10,3, Ar-*H*); δ_C (100 MHz, DMSO-d_6): 56.1, 78.8, 78.9, 115.2, 119.1, 119.6, 119.7, 123.3, 136.4, 145.0, 154.6; *m/z* (ESI positive) 237.01 $[M+H]^+$.

7-Prop-2-ynyloxy-benzo-[e][1,2]-oxathiine 2,2-dioxide 72. Synthetized according to the **general procedure A** using 7-hydroxybenzo[e][1,2]oxathiine 2,2-dioxide as starting material and propargyl bromide 80% in toluene as alkyl halide. Reaction performed at room temperature. Compound **72** obtained as a white powder. 54% yield; δ_H(400 MHz, DMSO-d_6) 3.70 (1H, t, *J* = 2.4, C*H*), 4.98 (2H, d, *J* =2.4, CH_2), 7.07 (1H, dd, *J* = 2.4, 8.4, Ar-*H*), 7.15 (1H, d, *J* = 2.4, Ar-*H*), 7.37 (1H, d, *J* = 10.4, Ar-*H*), 7.68 (2H, m, Ar-*H*); Experimental in agreement with reported data [10].

4-Methyl-7-(prop-2-ynylamino)-2*H*-chromen-2-one 73. Synthetized according to the **general procedure A** using 7-amino-4-methyl-2H-chromen-2-one as starting material and propargyl bromide 80% in toluene as alkyl halide. The yellow residue was purified by silica gel column chromatography eluting with 40% ethyl acetate in n-hexane to afford the titled compound **73** as a yellow solid. 20 % yield; δ^H (400 MHz, DMSO-d_6): 2.37 (3H, s, CH_3), 3.19 (1H, t, *J* = 2.4, C*H*), 4.02 (2H, q, *J* = 2.4, CH_2), 6.01 (1H, s, Ar-*H*), 6.54 (1H, d, *J* = 2.2, Ar-*H*), 6.70 (1H, dd, *J* = 2.2, 8.7, Ar-*H*), 7.02 (1H, t, *J* = 5.9, exchange with D_2O, N*H*), 7.52 (1H, d, *J* = 8.7, Ar-*H*); Experimental in agreement with reported data [11].

7-(Prop-2-ynyloxy)-2*H*-chromene-2-thione 74. 7-(Prop-2-ynyloxy)-2*H*-chromen-2-one **70** (0.2 g, 1.0 eq) and Lawesson's reagent (1.5 eq) were dissolved in dry toluene (10 mL), and the yellow solution was refluxed until starting material was consumed (TLC monitoring). Then the solvent was removed under vacuo, and the orange residue was partitioned between H_2O and EtOAc, followed by extraction with EtOAc (3 x 15 ml). The combined organic layers were washed with H_2O (2 x 20 mL) and brine (3 x 20 mL), dried over Na_2SO_4, filtered off, and concentrated under vacuum to give a red sticky oil that was purified by silica gel column chromatography eluting with 10% ethyl acetate in *n*-Hexane to afford the title compound as a yellow solid. 72% yield; δ_H (400 MHz, DMSO-d_6) 3.72 (1H, t, *J* = 2.4, C*H*), 5.02 (2H, d, *J* = 2.4, CH_2), 7.13 (1H, dd, *J* = 9.2, 2.4, Ar-*H*), 7.18 (1H, d, *J* = 9.2, Ar-*H*), 7.31 (1H, d, *J* = 2.4, Ar-*H*), 7.80 (1H, d, *J* = 9.2, Ar-*H*), 7.90 (1H, d, *J* = 9.2, Ar-*H*); Experimental in agreement with reported data [12].

(Prop-2-yn-1-yloxy)benzene 75. Synthetized according to the **general procedure A** using phenol as starting material and propargyl bromide 80% in toluene as alkyl halide. The residue was purified by silica gel column chromatography eluting with 10% EtOAc/n-Hexane to afford the titled compound **75** as a colourless oil. 68% yield; δ_H (400 MHz, DMSO-d_6) 3.59 (1H, t, *J* =2.4, C*H*), 4.83 (2H, d, *J* = 2.4, CH_2), 7.01 (3H, m, Ar-*H*), 7.35 (2H, m, Ar-*H*). Experimental in agreement with reported data [13].

4-Ethynylbenzenesulfonamide hexacarbonyldicobalt 76. The titled compound **76** was obtained according to the **general procedure C** previously reported using 4-ethynylbenzenesulfonamide **61** as starting material. 20 % yield; m.p. 125-127°C; silica gel TLC R*f* =0.45 (EtOAc/n-Hex 40% *v/v*). δ_H (400 MHz, DMSO-d_6) 7.21 (1H, s, C*H*), 7.44 (2H, br.s, exchange with D_2O, SO_2NH_2), 7.73 (2H, d, *J* = 8.2, Ar-*H*), 7.88 (2H, d, *J* = 8.2, Ar-*H*); δ_C(100

MHz, DMSO-d_6) 74.7, 87.5, 126.5, 130.2, 141.2, 143.3, 199.4; *m/z* (ESI negative) 466.86 $[M+H]^-$.

4-(Prop-2'-ynyloxy)benzenesulfonamide hexacarbonyldicobalt 77. The titled compound **77** was obtained according to the **general procedure C** previously reported using 4-(prop-2'-ynyloxy)benzenesulfonamide **62** as starting material. 82% yield; δ_H (400 MHz, DMSO-d_6) 5.44 (2H, s, CH_2), 6.86 (1H, s, C*H*), 7.17 (2H, d, *J* = 8.8, Ar-*H*), 7.28 (2H, br.s, exchange with D_2O, SO_2NH_2), 7.81 (2H, d, *J* = 8.8, Ar-*H*); Experimental in agreement with reported data [6]

4-(Prop-2-ynylthio)benzenesulfonamide hexacarbonyldicobalt 78. The titled compound **78** was obtained according to the **general procedure C** previously reported using 4-(prop-2-ynylthio)benzenesulfonamide 6**3** as starting material. 30% yield; m.p. 101-103°C; silica gel TLC R*f* =0.30 (EtOAc/*n*- Hex 30% v/v); δ_H (400 MHz, DMSO-d_6) 4.73 (2H, s, CH_2), 6.61 (1H, s, C*H*), 7.38 (2H, br.s, exchange with D_2O, SO_2NH_2), 7.58 (2H, d, *J* = 8.4, Ar-*H*), 7.78 (2H, d, *J* = 8.4, Ar-*H*); δ_C(100 MHz, DMSO-d_6) 74.7, 81.4, 92.3, 126.2, 127.0, 140.8, 141.0, 199.8; *m/z* (ESI positive) 513.84 $[M+H]^+$.

4-(Prop-2-ynylselanyl)benzenesulfonamidehexacarbonyldicobalt 79. The titled compound **79** was obtained according to the **general procedure C** previously reported using 4-(prop-2-ynylselanyl)benzenesulfonamide **64** as starting material. 10 % yield; m.p. 124-126°C; silica gel TLC R*f* =0.52 (EtOAc/n-Hex 40% v/v); δ_H (400 MHz, DMSO-d_6) 4.72 (2H, s, CH_2), 6.57 (1H, s, C*H*), 7.39 (2H, br.s, exchange with D_2O, SO_2NH_2), 7.75 (4H, m, Ar-*H*); δ_C(100 MHz, DMSO-d_6): 30.5, 78.0, 94.5, 127.3, 131.4, 137.0, 143.2, 200.7; *m/z* (ESI positive) 561.79 $[M+H]^+$.

4-(prop-2-ynylamino)benzenesulfonamidehexacarbonyldicobalt 80. The titled compound **80** was obtained according to the **general procedure C** previously reported using 4-(prop-2-ynylamino)benzenesulfonamide **65** as starting material. 42% yield; m.p. 110-113°C; silica gel TLC R*f* =0.54 (EtOAc/n- Hex 60% v/v).). δ_H (400 MHz, DMSO-d_6): 4.60 (2H, s, CH_2), 6.69 (1H, s, C*H*), 6.71 (2H, d, *J* = 8, Ar-*H*), 7.00 (2H, br.s, exchange with D_2O, SO_2NH_2), 7.16 (1H, m, exchange with D_2O, N*H*), 7.57 (2H, d, *J* = 8, Ar-*H*); δ_C(100 MHz, DMSO-d_6): 44.3, 74.1, 94.3, 111.1, 127.3, 130.7, 150.1, 199.9; *m/z* (ESI negative) 495.88 $[M+H]^-$.

4-(diProp-2'-ynylamino)benzenesulfonamidehexacarbonyldicobalt 81. The titled compound **81** was obtained according to the **general procedure C** previously reported using 4-(diprop-2'-ynylamino)benzenesulfonamide **66** as starting material. 79% yield; δ_H (400 MHz, DMSO-d_6) 4.75 (4H, br s, 2 x CH_2), 6.16 (2H, s, 2 x C*H*), 6.54 (2H, s, exchange with D_2O,

SO_2NH_2), 6.69 (2H, d, *J* = 8.8, Ar-*H*), 7.52 (2H, d, *J* = 8.8, Ar-*H*); Experimental in agreement with reported data [6]

4-(2-(diProp-2-ynylamino)ethyl)benzenesulfonamide hexacarbonyldicobalt 82. The titled compound **82** was obtained according to the **general procedure C** previously reported using 4-(2-(diprop-2-ynylamino)ethyl)benzenesulfonamide **67** as starting material. 22% yield; m.p. >300°C; silica gel TLC R*f* =0.86 (EtOAc/n- Hex 70% v/v); δ_H (400 MHz, DMSO-d_6) 2.89 (2H, m, CH_2), 3.04 (2H, m, CH_2), 4.27 (4H, br s, 2 x CH_2), 6.97 (2H, s, 2 x C*H*), 7.32 (2H, br.s, exchange with D_2O, SO_2NH_2), 7.47 (2H, d, *J*=8.0, Ar-*H*), 7.76 (2H, d, *J*=8.0, Ar-*H*); δ_C (100 MHz, DMSO-d_6): 33.3, 53.9, 55.6, 74.6, 90.6, 125.7, 129.0, 142.0, 143.8, 200.2; *m/z* (ESI positive) 848.77 $[M+H]^+$.

4-(4-(diProp-2-ynylamino)butoxy)benzenesulfonamide hexacarbonyldicobalt 83. The titled compound **83** was obtained according to the **general procedure C** previously reported using 4-(4-(diprop-2-ynylamino)butoxy)benzenesulfonamide **68** as starting material. 10% yield; m.p. >300°C; silica gel TLC R*f* =0.50 (EtOAc/n- Hex 40% v/v); δ_H (400 MHz, DMSO-d6): 1.67 (2H, m, CH_2), 1.82 (2H, m, CH_2), 2.85 (2H, m, CH_2), 4.09 (2H, m, CH_2), 4.21 (4H, br s, 2 x CH_2), 6.96 (2H, s, 2 x C*H*), 7.07 (2H, d, *J*=8.6, Ar-*H*), 7.22 (2H, br.s, exchange with D_2O, SO_2NH_2), 7.76 (2H, d, *J*=8.6, Ar-*H*); δ_C(100 MHz, DMSO-d_6) 23.3, 25.8, 55.4, 67.4, 74.1, 84.0, 90.2, 113.9, 127.3, 136.7, 160.1, 199.8; *m/z* (ESI positive) 892.72 $[M+H]^+$.

6-(Prop-2-ynyloxy)-2*H*-chromen-2-one hexacarbonyldicobalt 84. The titled compound **84** was obtained according to the **general procedure C** previously reported using 6-(prop-2-ynyloxy)-2*H*-chromen-2-one **69** as starting material. 60% yield; m.p. 137-140°C; silica gel TLC R*f* =0.37 (EtOAc/n-Hex 30% v/v).); δ_H (400 MHz, DMSO-d_6) 5.43 (2H, s, CH_2), 6.55 (1H, d, *J* = 9.6, Ar-*H*), 6.87 (1H, s, C*H*), 7.27 (1H, dd, *J* = 3.2, 9.2, Ar-*H*), 7.42 (2H, m, overlapped signals, Ar-*H*), 8.04 (1H, d, *J* = 9.6, Ar-*H*); δ_C(100 MHz, DMSO-d_6):68.4, 73.1, 89.8, 112.1, 116.7, 117.6, 119.3, 119.7, 144.1, 148.0, 154.0, 160.0, 199.6; *m/z* (ESI positive) 486.88 $[M+H]^+$.

7-(Prop-2-ynyloxy)-2*H*-chromen-2-one hexacarbonyldicobalt 85. The titled compound **85** was obtained according to the **general procedure C** previously reported using 7-(prop-2-ynyloxy)-2*H*-chromen-2-one **70** as starting material. 73% yield; δ_H (400 MHz, DMSO-d_6) 5.50 (2H, s, CH_2), 6.35 (1H, d, *J* = 9.4, Ar-*H*), 6.89 (1H, s, C*H*), 7.00 (1H, dd, *J* = 8.8, 2.4, Ar-*H*), 7.14 (1H, d, *J* = 2.4, Ar-*H*), 7.70 (1H, d, *J* = 8.8, Ar-*H*), 8.04 (1H, d, *J* = 9.4, Ar-*H*); Experimental in agreement with reported data [12].

6-Prop-2-ynyloxy-benzo-[e][1,2]-oxathiine 2,2-dioxide hexacarbonyldicobalt 86. The titled compound **86** was obtained according to the **general procedure C** previously reported using 6-prop-2-ynyloxy-benzo-[e][1,2]-oxathiine 2,2-dioxide **71** as starting material. 36% yield; m.p. 132-135°C; silica gel TLC R*f* =0.68 (EtOAc/n- Hex 50% v/v); δ_H (400 MHz, DMSO-d$_6$): 5.41 (2H, s, C*H*$_2$), 6.88 (1H, s, C*H*), 7.22 (1H, dd, *J*= 8.9, 2.7, Ar-*H*), 7.40 (1H, d, *J*=2.7, Ar-*H*), 7.45 (1H, d, *J*=8.9, Ar-*H*), 7.55 (1H, d, *J*=10.3, Ar-*H*), 7.67 (1H, d, *J*=10.3, Ar-*H*); δ_C(100 MHz, DMSO-d$_6$): 68.5, 73.2, 89.6, 114.6, 114.7, 118.6, 119.7, 123.4, 136.4, 144.8, 155.3, 199.7; *m/z* (ESI positive) 522.85 $[M+H]^+$.

7-Prop-2-ynyloxy-benzo-[e][1,2]-oxathiine 2,2-dioxide hexacarbonyldicobalt 87. The titled compound **87** was obtained according to the **general procedure C** previously reported using 7-prop-2-ynyloxy-benzo-[e][1,2]-oxathiine 2,2-dioxide **72** as starting material. 39% yield; m.p. 104-106 °C; silica gel TLC R*f* =0.26 (EtOAc/n- Hex 30% v/v); δ_H (400 MHz, DMSO-d$_6$): 5.51 (2H, s, C*H*$_2$), 6.88 (1H, s, C*H*) 7.03 (1H, d, *J*=8.4, Ar-*H*) 7.16 (1H, s, Ar-*H*), 7.35 (1H, d, *J*=10.4, Ar-*H*) 7.684 (2H, m, , Ar-*H*); δ_C (100 MHz, DMSO-d$_6$) 69.5, 74.4, 90.6, 104.3, 109.7, 112.4, 120.7, 133.2, 137.7, 154.2, 162.2, 200.2; *m/z* (ESI positive) 522.85 $[M+H]^+$.

4-Methyl-7-(prop-2-ynylamino)-2*H*-chromen-2-onehexacarbonyldicobalt 88. The titled compound **88** was obtained according to the **general procedure C** previously reported using 4-methyl-7-(prop-2-ynylamino)-2*H*-chromen-2-one **73** as starting material. 42% yield; m.p. >300°C; silica gel TLC R*f* =0.57 (EtOAc/n-Hex 50% v/v). δ_H (400 MHz, DMSO-d$_6$): 2.36 (3H, s, C*H*$_3$), 4.65 (2H, ,m, C*H*$_2$), 5.99 (1H, s, Ar-*H*), 6.54 (1H, s, Ar-*H*), 6.68 (1H, d, *J* = 8.8, Ar-*H*), 6.72 (1H, s, C*H*), 7.41 (1H, t, *J* = 6.4, exchange with D_2O, N*H*), 7.51 (1H, d, *J* = 8.8, Ar-*H*); δ_C(100 MHz, DMSO-d$_6$): 18.1, 44.3, 74.0, 94.0, 97.1, 107.9, 109.3, 110.6, 126.1, 151.3, 153.8, 155.5, 160.7, 199.9; *m/z* (ESI negative) 498.91 $[M+H]^-$.

7-(Prop-2-ynyloxy)-2*H*-chromene-2-thione hexacarbonyldicobalt 89. The titled compound **89** was obtained according to the **general procedure C** previously reported using 7-(prop-2-ynyloxy)-2*H*-chromene-2-thione **74** as starting material. 79% yield; δ_H(400 MHz, DMSO-d$_6$) 5.55 (2H,s, C*H*$_2$), 6.90 (1H, s, C*H*), 7.09 (1H, dd, *J* = 2.4, 8.8, Ar-*H*), 7.18 (1H, d, *J* = 9.2, Ar-*H*), 7.36 (1H, d, *J* = 2.4, Ar-*H*), 7.80 (1H, d, *J* = 8.8, Ar-*H*), 7.90 (1H, d, *J* = 9.2, Ar-*H*); Experimental in agreement with reported data.

(Prop-2-yn-1-yloxy)benzene hexacarbonyldicobalt 90. The titled compound **90** was obtained according to the **general procedure C** previously reported using (prop-2-yn-1-yloxy)benzene **75** as starting material. 80.9 % yield; δ_H (400 MHz, DMSO-d$_6$): 5.33 (2H, s, C*H*$_2$), 6.84 (1H, s, C*H*), 7.01 (3H, m, Ar-H), 7.35 (2H, t, J = 8.0, Ar-H); Experimental in agreement with reported data [13].

Synthethic Scheme for the preparation of derivatives 91-105.

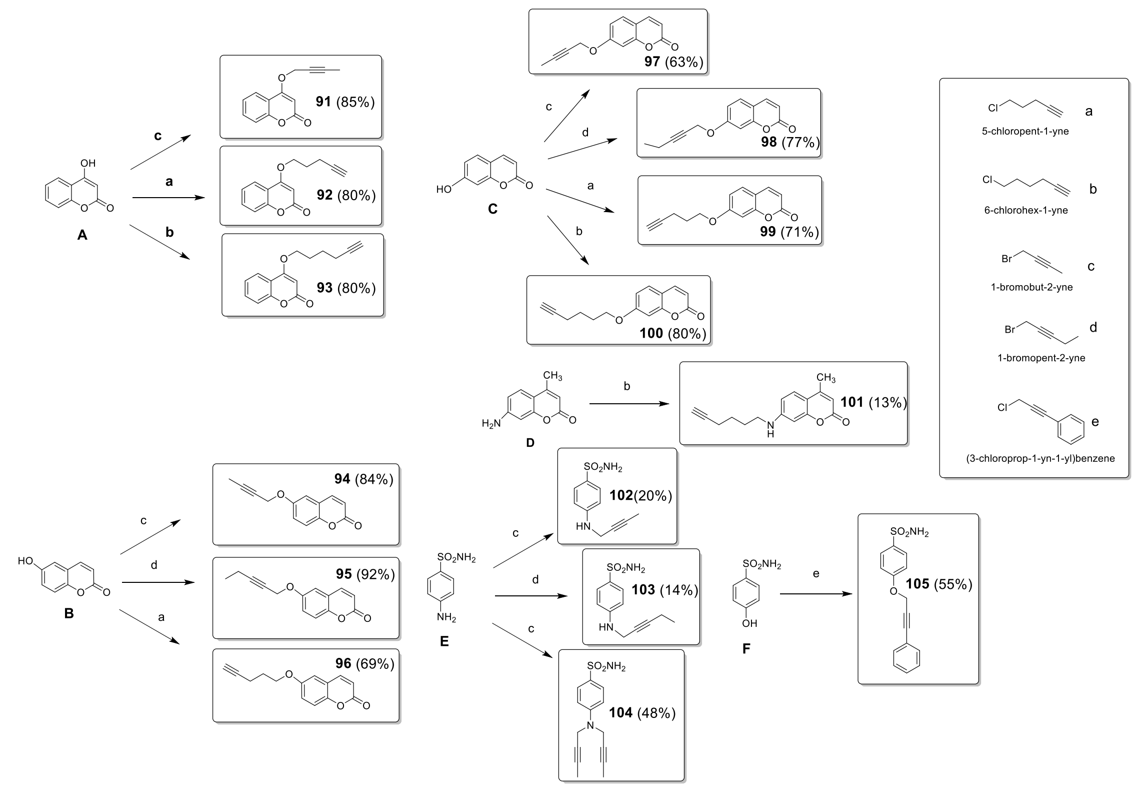

Synthethic Scheme for the preparation of derivatives 106-120.

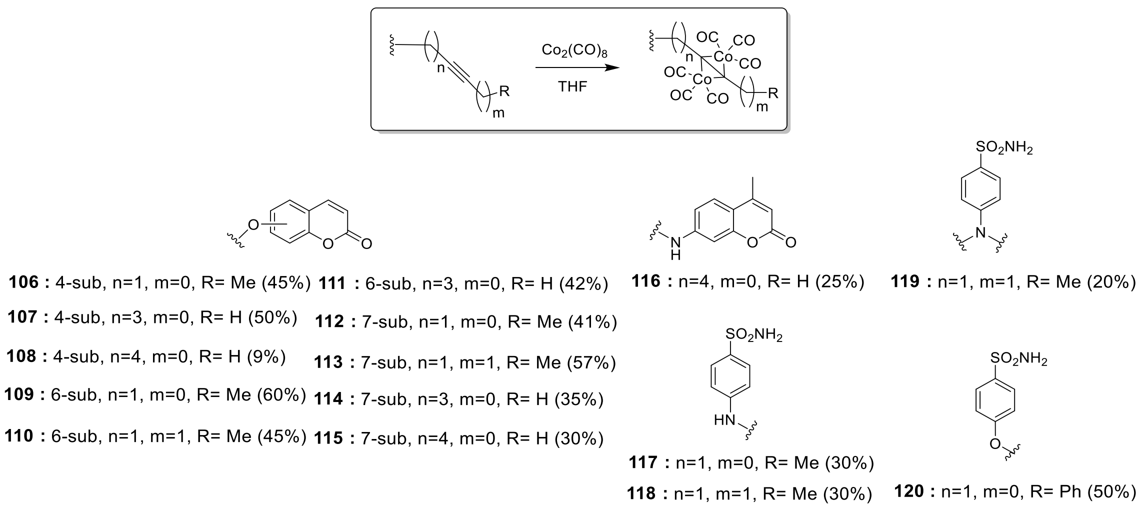

4-(but-2-yn-1-yloxy)-2H-chromen-2-one 91. Synthetized according to the **general procedure A** using 4-hydroxy-2H-chromen-2-one as starting material and 1-bromobut-2-yne as alkyl halide. Compound **91** obtained as white powder. 85% yield; m.p. 140-142 °C; silica gel TLC R*f* =0.61 (EtOAc/n- Hex 20% v/v); δH (400 MHz, DMSO-d_6) 1.94 (3H, t, *J*=2.3, CH_3), 5.09 (2H, d, *J*=2.4, CH_2), 5.97 (1H, s, Ar-*H*), 7.47 (2H, m, Ar-*H*), 7.65 (1H, m, Ar-*H*), 7.83 (1H, d, *J*=6.4, Ar-*H*); δC (100 MHz, DMSO-d_6) 3.7, 53.7, 75.3, 84.3, 87.5, 116.2, 116.4, 123.3, 125.4, 128.3, 152.5, 162.4, 169.9; *m/z* (ESI positive) 215.06 $[M+H]^+$.

4-(pent-4-yn-1-yloxy)-2H-chromen-2-one 92. Synthetized according to the **general procedure A** using 4-hydroxy-2H-chromen-2-one as starting material and 5-chloropent-1-yne as alkyl halide. Compound **92** obtained as white powder. 80% yield; m.p; 120-122 °C; silica gel TLC R*f* 0.65 (EtOAc/n-Hex 30% v/v); δH (400 MHz, DMSO-d_6) 2.05 (2H, dd, *J*=6.5, *J*=12.9, CH_2), 2.10 (1H, s, C*H*), 2.45 (2H, m, CH_2), 4.31 (2H, t, *J*=5.9, CH_2), 5.95 (1H, s, Ar-*H*), 7.41 (2H, m, *J*=7.8 2x Ar-*H*), 7.7 (1H, m, Ar-*H*), 7.89 (1H, d, *J*=7.8, Ar-*H*); δC (100 MHz, DMSO-d_6) 15.3, 29.7, 64.6, 71.3, 84.7, 86.0, 116.2, 116.4, 123.3, 125.4, 128.3, 152.5, 162.4, 168.6; *m/z* (ESI positive) 229.08 $[M+H]^+$.

4-(hex-5-yn-1-yloxy)-2H-chromen-2-one 93. Synthetized according to the **general procedure A** using 4-hydroxy-2H-chromen-2-one as starting material and 6-chlorohex-1-yne as alkyl halide. Compound **93** obtained as white powder. 80% yield; m.p; 120 -122°C; silica gel TLC R*f* 0.55 (EtOAc/n-Hex 30% v/v); δH (400 MHz, DMSO-d_6) 1.70 (2H, m, CH_2), 1.95 (2H, m, CH_2), 2.31 (2H, m, CH_2), 2.84 (1H, t, *J*=2.5, C*H*), 4.28 (2H, t, *J*=6.2, CH_2), 5.92 (1H, s, Ar-*H*), 7.39 (1H, d, *J*=7.8, Ar-*H*), 7.43 (1H, d, *J*=8.1, Ar-*H*), 7.69 (1H, t, *J*=8.1, Ar-*H*), 7.85 (1H, d, *J*=7.8, Ar-*H*); δC (100 MHz, DMSO-d_6) 18.4, 25.6, 28.1, 70.0, 72.5, 85.2, 91.5, 116.3, 117.5, 123.8, 125.2, 133.7, 153.8, 162.7, 165.9; *m/z* (ESI positive) 243.09 $[M+H]^+$.

6-(but-2-yn-1-yloxy)-2H-chromen-2-one 94. Synthetized according to the **general procedure A** using 6-hydroxy-2H-chromen-2-one as starting material and 1-bromobut-2-yne as alkyl halide. Compound **94** obtained as white powder. 84% yield; m.p; 157-159°C; silica gel TLC R*f* 0.75 (EtOAc/n-Hex 30% v/v); δH (400 MHz, DMSO-d_6) 1.87 (3H, t, *J*=1.9, CH_3), 4.83 (2H, dd, *J*=2.2, *J*=4.6, CH_2), 6.53 (1H, d, *J*=9.6, Ar-*H*), 7.27 (1H, dd, *J*=3.0, *J*=9.0, Ar-*H*), 7.34 (1H, d, *J*=2.9, Ar-*H*), 7.39 (1H, t, *J*=9.0, Ar-*H*), 8.05 (1H, d, *J*=9.6, Ar-*H*); δC (100 MHz, DMSO-d_6) 4.2, 57.6, 75.5, 84.9, 113.2, 117.7, 118.4, 120.2, 120.9, 145.0, 149.2, 154.7, 161.1; *m/z* (ESI positive) 215.06 $[M+H]^+$.

6-(pent-2-yn-1-yloxy)-2H-chromen-2-one 95. Synthetized according to the **general procedure A** using 6-hydroxy-2H-chromen-2-one as starting material and 1-bromopent-2-yne as alkyl halide. Compound **95** obtained as white powder. 92% yield; m.p; 121-123°C; silica gel TLC R*f* 0.66 (EtOAc/n-Hex 40% v/v); δH (400 MHz, DMSO-d_6) 1.08 (3H, t, *J*=7.5, CH_3) 2.25 (2H, m, CH_2), 4.84 (2H, t, *J*=2.0, CH_2), 6.53 (1H, d, *J*=9.6, Ar-*H*), 7.27 (1H, dd, *J*=3.0, *J*=9.0, Ar-*H*), 7.35 (1H, d, *J*=2.9, Ar-*H*), 7.40 (1H, d, *J*=9.0, Ar-*H*), 8.05 (1H, d, *J*= 9.6, Ar-*H*); δC (100 MHz, DMSO-d_6) 12.6, 13.9, 56.4, 79.6, 87.8, 110.9, 113.4, 113.9, 118.1, 119.2, 143.5, 145.3, 154.4, 160.8; *m/z* (ESI positive) 229.08 $[M+H]^+$.

6-(pent-4-yn-1-yloxy)-2H-chromen-2-one 96. Synthetized according to the **general procedure A** using 6-hydroxy-2H-chromen-2-one as starting material and 5-chloropent-1-yne as alkyl halide. Compound **96** obtained as white powder. 79% yield; m.p; 106-108°C; silica gel TLC R*f* 0.50 (EtOAc/n-Hex 40% v/v); δH (400 MHz, DMSO-d_6) 1.94 (2H, m, CH_2), 2.38 (2H, dd, *J*=4.9, *J*=6.8, CH_2), 2.87 (1H, s, C*H*), 4.11 (2H, t, *J*=6.1, CH_2), 6.53 (1H, d, *J*=9.6, Ar-*H*), 7.24 (1H, dd, *J*=2.6, *J*=9.0, Ar-*H*), 7.34 (1H, d, *J*=2.4, Ar-*H*), 7.37 (1H, d, *J*=9.0, Ar-*H*), 8.04 (1H, d, *J*=9.6, Ar-*H*); δ_C (100 MHz, DMSO-d_6) 15.6, 28.7, 67.7, 72.7, 84.6, 112.5, 117.6, 118.4, 120.3, 120.9, 145.1, 148.9, 155.9, 161.2; *m/z* (ESI positive) 229.08 $[M+H]^+$.

7-(but-2-yn-1-yloxy)-2H-chromen-2-one 97. Synthetized according to the **general procedure A** using 7-hydroxy-2H-chromen-2-one as starting material and 1-bromobut-2-yne as alkyl halide. Compound **97** obtained as white powder. 63% yield; m.p; 130-132°C; silica gel TLC R*f* 0.70 (EtOAc/n-Hex 30% v/v); δH (400 MHz, DMSO-d_6) 1.88 (3H, s, CH_3), 4.91 (2H, s, CH_2), 6.34 (1H, d, *J*=9.5, Ar-*H*), 7.01 (1H, d, *J*=8.6, Ar-*H*), 7.05 (1H, s, Ar-*H*), 7.68 (1H, d, *J*=8.6, Ar-*H*), 8.03 (1H, d, *J*=9.5, Ar-*H*); δC (100 MHz, DMSO-d_6) 4.2, 57.7, 75.1, 85.4, 102.7, 113.8, 113.7, 113.9, 130.5, 145.3, 156.2, 161.2, 161.6; *m/z* (ESI positive) 215.06 $[M+H]^+$.

7-(pent-2-yn-1-yloxy)-2H-chromen-2-one 98. Synthetized according to the **general procedure A** using 7-hydroxy-2H-chromen-2-one as starting material and 1-bromopent-2-yne as alkyl halide. Compound **98** obtained as white powder. 77% yield; m.p; 140-142°C; silica gel TLC R*f* 0.75 (EtOAc/n-Hex 40% v/v); δH (400 MHz, DMSO-d_6) δH (400 MHz, DMSO-d_6) 1.09 (3H, t, *J*=7.5, CH_3), 2.27 (2H, m, CH_2), 4.92 (2H, t, *J*=2.0, CH_2), 6.34 (1H, d, *J*=9.5, Ar-*H*), 7.01 (1H, dd, *J*=2.4, *J*=8.6, Ar-*H*) 7.06 (1H, d, *J*=2.4, Ar-*H*) 7.68 (1H, d, *J*=8.6, Ar-*H*) 8.03 (1H, d, *J*=9.5, Ar-*H*); δC (100 MHz, DMSO-d_6) 12.7, 14.5, 57.7, 75.3, 90.8, 102.7, 112.9, 113.7, 113.9, 130.5, 145.3, 156.2, 161.2, 161.6; *m/z* (ESI positive) 229.08 $[M+H]^+$.

7-(pent-4-yn-1-yloxy)-2H-chromen-2-one 99. Synthetized according to the **general procedure A** using 7-hydroxy-2H-chromen-2-one as starting material and 5-chloropent-1-yne as alkyl halide. Compound **99** obtained as white powder. 71% yield; m.p; 160-162°C; silica gel TLC R*f* 0.35 (EtOAc/n-Hex 40% v/v); δH (400 MHz, DMSO-d_6) 1.95 (2H, m, CH_2), 2.38 (2H, m, CH_2), 2.88 (1H, d, *J*=1.8, C*H*), 4.18 (2H, t, *J*=6.0, CH_2), 6.33 (1H, d, *J*=9.4, Ar-*H*), 6.99 (1H, d, *J*=8.6, Ar-*H*), 7.04 (1H, s, Ar-*H)*, 7.67 (1H, d, *J*=8.5, Ar-*H*), 8.03 (1H, d, *J*=9.5, Ar-*H*); δC (100 MHz, DMSO-d_6) 15.5, 28.5, 67.8, 72.7, 84.5, 102.2, 113.4, 113.5, 113.7, 130.6, 145.3, 156.4, 161.3, 162.7; *m/z* (ESI positive) 229.08 $[M+H]^+$.

7-(hex-5-yn-1-yloxy)-2H-chromen-2-one 100. Synthetized according to the **general procedure A** using 7-hydroxy-2H-chromen-2-one as starting material and 6-chlorohex-1-yne as alkyl halide. Compound **100** obtained as white powder. 80 % yield; m.p; 150-152°C; silica gel TLC R*f* 0.66 (EtOAc/n-Hex 40% v/v); δH (400 MHz, DMSO-d_6) 1.64 (2H, m, CH_2), 1.86 (2H, m, CH_2), 2.28 (2H, m, CH_2), 2.82 (1H, t, *J*=2.5, C*H*), 4.13 (2H, t, *J*=6.4, CH_2), 6.31 (1H, d, *J*=9.5, Ar-*H*), 6.97 (1H, dd, *J*=2.1, *J*=8.6, Ar-*H*), 7.01 (1H, d, *J*=2.1, Ar-*H*), 7.65 (1H, d, *J*=8.6, Ar-*H*), 8.02 (1H, d, *J*=9.5, Ar-*H*); δ_C (100 MHz, DMSO-d_6) 18.7, 25.9, 28.8, 68.8, 72.4, 85.3, 102.3, 113.3, 113.4, 113.7, 130.5, 145.3, 156.5, 161.3, 162.9; *m/z* (ESI positive) 243.09 $[M+H]^+$.

7-(hex-5-yn-1-ylamino)-4-methyl-2H-chromen-2-one 101. Synthetized according to the **general procedure A** using 7-amino-4-methyl-2H-chromen-2-one as starting material and 6-chlorohex-1-yne as alkyl halide. Compound **101** obtained as white powder. 13 % yield; m.p; 150-152°C; silica gel TLC R*f* 0.70 (EtOAc/n-Hex 20% v/v); δH (400 MHz, DMSO-d_6) 1.58 (2H, m, CH_2), 1.68 (2H, m, CH_2), 2.24 (2H, m, CH_2), 2.40 (3H, s, CH_3), 2.8 (1H, t, *J*=2.6, C*H*), 3.13 (2H, dd, *J*=6.6, *J*=12.4, CH_2), 5.93 (1H, d, *J*=1.0, Ar-*H*), 6.43 (1H, d, *J*=2.2, Ar-*H*), 6.64 (1H, dd, *J*=2.2, *J*=8.8, Ar-*H*), 6.69 (1H, dd, *J*=5.4, exchanged with D_2O, N*H*), 7.46 (1H, d, *J*=8.8, Ar-*H*); δ_C (100 MHz, DMSO-d_6) 18.5, 19.1, 26.6, 28.6, 42.9, 72.4, 85.4, 97.2, 108.4, 109.7, 111.2, 126.9, 153.6, 154.8, 156.8, 161.9; *m/z* (ESI positive) 256.12 $[M+H]^+$.

4-(but-2-yn-1-ylamino)benzenesulfonamide 102. Synthetized according to the **general procedure B** using sulfanilamide as starting material and 1-bromobut-2-yne as alkyl halide. Compound **102** obtained as white powder. 20 % yield; m.p; 120-122°C; silica gel TLC R*f* 0.50 (EtOAc/n-Hex 30% v/v); δH (400 MHz, DMSO-d_6) 1.79 (3H, t, *J*=2.2, CH_3), 3.91 (2H, dd, *J*=2.4, *J*=5.7, CH_2), 6.70 (3H, d, *J*=8.8, 2 X Ar-*H*, exchanged with D_2O, N*H*), 6.96 (2H, brs, exchanged with D_2O, SO_2NH_2), 7.57 (2H, d, *J*=8.8, Ar-*H*); δC (100 MHz, DMSO-d_6) 4.4, 33.2, 77.8, 79.5, 112.8, 128.6, 132.5, 151.9; *m/z* (ESI positive) 211.05 $[M+H]^+$.

4-(pent-2-yn-1-ylamino)benzenesulfonamide 103. Synthetized according to the **general procedure B** using sulfanilamide as starting material and 1-bromopent-2-yne as alkyl halide. Compound **103** obtained as white powder. 14 % yield; m.p; 120-122°C; silica gel TLC R*f* 0.50 (EtOAc/n-Hex 50% v/v); δH (400 MHz, DMSO-d_6) 1.06 (3H, t, *J*=7.5, CH_3), 2.18 (2H, m, CH_2), 3.92 (2H, dd, *J*=2.3, *J*=3.6, CH_2), 6.70 (3H, t, *J*=2.0, 2 X Ar-*H*, exchanged with D_2O, N*H*), 6.98 (2H, s, exchanged with D_2O, SO_2NH_2), 7.57 (2H, d, *J*=8.8, Ar-*H*); δ_C (100 MHz, DMSO-d_6) 12.3, 13.9, 28.3, 82.3, 78.6, 111.1, 127.3, 129.3, 150.8; *m/z* (ESI positive) 239.08 $[M+H]^+$.

4-(di(but-2-yn-1-yl)amino)benzenesulfonamide 104. Synthetized using the same conditions as for product **66**, using sulfanilamide as starting material and 2 eq of 1-bromobut-2-yne as alkyl halide. Compound **104** obtained as white powder. 48 % yield; m.p; 120-122°C; silica gel TLC R*f* 0.50 (EtOAc/n-Hex 30% v/v); δH (400 MHz, DMSO-d_6) 1.80 (6H, t, *J*=2.2, 2 X CH_3), 4.20 (4H, d, *J*=2.3, 2 x CH_2), 6.98 (2H, d, *J*=9.0, Ar-*H*), 7.08 (2H, brs, exchanged with D_2O, SO_2NH_2), 7.67 (2H, t, *J*=9.0, Ar-*H*); δ_C (100 MHz, DMSO-d_6) 3.4, 43.0, 79.5, 79.8, 114.6, 130.1, 130.4, 152.8; *m/z* (ESI positive) 277.09 $[M+H]^+$.

4-((3-phenylprop-2-yn-1-yl)oxy)benzenesulfonamide 105. Synthetized according to the **general procedure B** using 4-hydroxybenzenesulfonamide as starting material and (3-chloroprop-1-yn-1-yl)benzene as alkyl halide. Compound **105** obtained as white powder. 55 % yield; m.p; 138-140°C; silica gel TLC R*f* 0.36 (EtOAc/n-Hex 50% v/v); δH (400 MHz, DMSO-d_6) 5.19 (2H, s, CH_2), 7.23 (2H, d, *J*= 8.8, Ar-*H*), 7.25 (2H, s, exchanged with D_2O, SO_2NH_2), 7.45 (5H, m, Ar-*H*), 7.83 (2H, d, *J* = 8.8, Ar-*H*); δC (100 MHz, DMSO-d_6) 57.3; 85.2; 87.7; 115.9; 122.3; 128.6; 129.7, 130.1; 132.4; 137.8; 160.5. Experimental in agreement with reported data [6].

4-(but-2-yn-1-yloxy)-2H-chromen-2-one hexacarbonyldicobalt 106. The titled compound **106** was obtained according to the **general procedure C** previously reported using 4-(but-2-yn-1-yloxy)-2H-chromen-2-one **91** as starting material. Compound **106** obtained as red powder. 45 % yield; m.p; 109-111°C; silica gel TLC R*f* 0.50 (EtOAc/n-Hex 30% v/v); δH (400 MHz, DMSO-d_6) 2.75 (3H, s, CH_3), 5.66 (2H, s, CH_2), 6.12 (1H, s, Ar-*H*), 7.39 (1H, t, *J*=7.5, Ar-*H*), 7.46 (1H, d, *J*=8.3, Ar-*H*), 7.70 (1H, t, *J*=7.6, Ar-*H*), 7.86 (1H, d, *J*=7.7, Ar-*H*); δ_C (100 MHz, DMSO-d_6) 28.0, 63.0, 86.0, 116.2, 116.4, 121.6, 123.3, 125.4, 128.3, 140.3, 152.5, 162.4, 168.6, 200.1; *m/z* (ESI positive) 500.9 $[M+H]^+$.

4-(pent-4-yn-1-yloxy)-2H-chromen-2-one hexacarbonyldicobalt 107. The titled compound **106** was obtained according to the **general procedure C** previously reported using 4-(pent-4-yn-1-yloxy)-2H-chromen-2-one **92** as starting material. Compound **107** obtained as red powder. 50 % yield; m.p; 120-122°C; silica gel TLC R*f* 0.50 (EtOAc/n-Hex 30% v/v); δH (400 MHz, DMSO-d$_6$) 2.18 (2H, s, C*H*$_2$), 3.14 (2H, t, *J*=7.0, C*H*$_2$), 4.42 (2H, t, *J*=5.4, C*H*$_2$), 5.98 (1H, s, C*H*), 6.86 (1H, s, Ar-*H*), 7.39 (1H, t, *J*=7.4, Ar-*H*), 7.44 (1H, d, *J*=8.2, Ar-*H*), 7.69 (1H, t, *J*=7.4, Ar-*H*), 7.82 (1H, d, *J*=7.6, Ar-*H*);); δ_C (100 MHz, DMSO-d_6) 25.5, 33.1, 67.9, 90.8, 105.2, 109.2, 115.5, 117.4, 121.6, 123.7, 132.3, 152.8, 163.3, 165.3, 200.1; *m/z* (ESI positive) 514.9 $[M+H]^+$.

4-(hex-5-yn-1-yloxy)-2H-chromen-2-one hexacarbonyldicobalt 108. The titled compound **108** was obtained according to the **general procedure C** previously reported using 4-(hex-5-yn-1-yloxy)-2H-chromen-2-one **93** as starting material. Compound **108** obtained as red powder. 50 % yield; m.p; 120-122°C; silica gel TLC R*f* 0.50 (EtOAc/n-Hex 30% v/v); δH (400 MHz, DMSO-d$_6$) 1.85 (2H, m, C*H*$_2$), 2.04 (2H, m, C*H*$_2$), 3.03 (2H, t, *J*=7.9, C*H*$_2$), 4.34 (2H, t, *J*=6.2, C*H*$_2$), 5.96 (1H, s, Ar-*H*), 6.83 (1H, s, C*H*), 7.38 (1H, t, *J*=7.6, Ar-*H*), 7.43 (1H, d, *J*=8.3, Ar-*H*), 7.69 (1H, t, *J*=7.2, Ar-*H*) 7.82 (1H, d, *J*=7.8, Ar-*H*); δ_C (100 MHz, DMSO-d_6) 28.5, 28.9, 34.1, 70.1, 75.3, 91.7, 98.6, 116.3, 117.5, 123.6, 125.1, 133.8, 153.9, 162.7,165.9, 201.7; *m/z* (ESI positive) 528.9 $[M+H]^+$.

6-(but-2-yn-1-yloxy)-2H-chromen-2-one hexacarbonyldicobalt 109. The titled compound **109** was obtained according to the **general procedure C** previously reported using 6-(but-2-yn-1-yloxy)-2H-chromen-2-one **94** as starting material. Compound **109** obtained as red powder. 60 % yield; m.p; 107-109°C; silica gel TLC R*f* 0.50 (EtOAc/n-Hex 30% v/v); δH (400 MHz, DMSO-d$_6$) 2.66 (3H, s, C*H*$_3$), 5.43 (2H, s, C*H*$_2$), 6.54 (1H, d, *J*=9.5, Ar-*H*), 7.27 (1H, d, *J*=8.0, Ar-*H*), 7.41 (2H, s, 2 X Ar-*H*), 8.03 (1H, d, *J*=9.4, Ar-*H*); δ_C (100 MHz, DMSO-d_6) 21.2, 69.4, 92.8, 94.4, 113.1, 117.8, 118.6, 120.3, 120.7, 144.9, 149.1, 155.3, 161.1, 200.7; *m/z* (ESI positive) 500.9 $[M+H]^+$.

6-(pent-2-yn-1-yloxy)-2H-chromen-2-one hexacarbonyldicobalt 110. The titled compound **110** was obtained according to the **general procedure C** previously reported using 6-(pent-2-yn-1-yloxy)-2H-chromen-2-one **95** as starting material. Compound **110** obtained as red powder. 45 % yield; m.p; 150-152°C; silica gel TLC R*f* 0.60 (EtOAc/n-Hex 30% v/v); δH (400 MHz, DMSO-d$_6$) 1.29 (3H, t, *J*=7.3, C*H$_3$*), 2.89 (2H, dd, *J*=7.3, *J*=14.6, C*H$_2$*), 5.44 (2H, s, C*H$_2$*), 6.54 (1H, d, *J*=9.5, Ar-*H*), 7.27 (1H, dd, *J*=2.9, *J*=9.0, Ar-*H*), 7.42 (2H, m, 2 X Ar-*H*), 8.04 (1H, d, *J*=9.6, Ar-*H*); δ_C (100 MHz, DMSO-*d*$_6$) 16.6, 27.4, 69.6, 92.4, 102.1, 113.0, 117.8, 118.5, 120.3, 120.7, 144.9, 149.1, 155.4, 161.1, 200.9; *m/z* (ESI positive) 514.9 [M+H]$^+$.

6-(pent-4-yn-1-yloxy)-2H-chromen-2-one hexacarbonyldicobalt 111. The titled compound **111** was obtained according to the **general procedure C** previously reported using 6-(pent-4-yn-1-yloxy)-2H-chromen-2-one **96** as starting material. Compound **111** obtained as red powder. 42 % yield; m.p; 106-108°C; silica gel TLC R*f* 0.60 (EtOAc/n-Hex 30% v/v); δH (400 MHz, DMSO-d$_6$) 2.08 (2H, s, C*H$_2$*), 3.09 (2H, s, C*H$_2$*), 4.21 (2H, s, C*H$_2$*), 6.52 (1H, d, *J*=9.4, Ar-*H*), 6.82 (1H, s, C*H*), 7.26 (1H, d, *J*=8.1, Ar-*H*), 7.37 (2H, m, 2 X, Ar-*H*), 8.04 (1H, d, *J*=9.3, Ar-*H*); δ_C (100 MHz, DMSO-*d*$_6$) 31.1, 32.0, 68.3, 75.4, 98.2, 112.8, 117.7, 118.4, 120.3, 120.9, 145.1, 148.9, 155.9, 161.2, 201.3; *m/z* (ESI positive) 514.9 [M+H]$^+$.

7-(but-2-yn-1-yloxy)-2H-chromen-2-one hexacarbonyldicobalt 112. The titled compound **112** was obtained according to the **general procedure C** previously reported using 7-(but-2-yn-1-yloxy)-2H-chromen-2-one **97** as starting material. Compound **112** obtained as red powder. 41 % yield; m.p; 150-152°C; silica gel TLC R*f* 0.50 (EtOAc/n-Hex 30% v/v); δH (400 MHz, DMSO-d$_6$) 2.68 (3H, s, *CH$_3$*), 5.52 (2H, s, *CH$_2$*), 6.34 (1H, d, *J*=9.4, Ar-*H*), 7.01 (1H, d, *J*=8.4, Ar-*H*), 7.12 (1H, s, Ar-*H*), 7.70 (1H, d, *J*=8.5, Ar-*H*), 8.04 (1H, d, *J*=9.4, Ar-*H*); δ_C (100 MHz, DMSO-*d*$_6$) 21.3, 69.5, 92.5, 94.4, 102.7, 113.8, 113.9, 130.8, 145.3, 156.5, 161.3, 162.1, 200.7; *m/z* (ESI positive) 500.9 [M+H]$^+$.

7-(pent-2-yn-1-yloxy)-2H-chromen-2-one hexacarbonyldicobalt 113. The titled compound **113** was obtained according to the **general procedure C** previously reported using 7-(pent-2-yn-1-yloxy)-2H-chromen-2-one **98** as starting material. Compound **113** obtained as red powder. 57 % yield; m.p; 136-138°C; silica gel TLC R*f* 0.70 (EtOAc/n-Hex 30% v/v); δH (400 MHz, DMSO-d$_6$) 1.29 (3H, t, *J*=7.3, C*H$_3$*), 2.90 (2H, dd, *J*=7.3, *J*=14.6, C*H*$_2$), 5.53 (2H, s, C*H$_2$*), 6.34 (1H, d, *J*=9.5, Ar-*H*), 7.01 (1H, dd, *J*=2.3, *J*=9.8, Ar-*H*), 7.13 (1H, d, *J*=2.2, Ar-*H*), 7.70 (1H, d, *J*=8.6, Ar-*H*), 8.04 (1H, d, *J*=9.5, Ar-*H*); δ_C (100 MHz, DMSO-*d*$_6$) 16.6, 27.4, 69.7, 92.1, 102.1, 102.5, 113.7, 113.7, 113.9, 130.7, 145.3, 156.4, 161.3, 162.1, 200.8; *m/z* (ESI positive) 514.9 [M+H]$^+$.

7-(pent-4-yn-1-yloxy)-2H-chromen-2-one hexacarbonyldicobalt 114. The titled compound **114** was obtained according to the **general procedure C** previously reported using 7-(pent-4-yn-1-yloxy)-2H-chromen-2-one **99** as starting material. Compound **114** obtained as red powder.

35 % yield; m.p; 105-107°C; silica gel TLC R*f* 0.50 (EtOAc/n-Hex 30% v/v); δH (400 MHz, DMSO-d_6) 2.09 (2H, t, *J*=7.2, C*H*$_2$), 3.09 (2H, t, *J*=7.2, C*H*$_2$), 4.28 (2H, t, *J*=6.1, C*H*$_2$), 6.32 (1H, d, *J*=9.4, Ar-*H*), 6.84 (1H, s, C*H*), 7.0 (1H, d, *J*=8.5, Ar-*H*), 7.06 (1H, s, Ar-*H*), 7.66 (1H, d, *J*=8.6, Ar-*H*), 8.03 (1H, d, *J*=9.5, Ar-*H*); δ_C (100 MHz, DMSO-d_6) 31.1, 31.8, 63.4, 75.5, 98.1, 102.3, 113.5, 113.6, 113.8, 130.6, 145.4, 156.5, 161.3, 162.7, 201.2; *m/z* (ESI positive) 514.9 $[M+H]^+$.

7-(hex-5-yn-1-yloxy)-2H-chromen-2-one hexacarbonyldicobalt 115. The titled compound **115** was obtained according to the **general procedure C** previously reported using 7-(hex-5-yn-1-yloxy)-2H-chromen-2-one **100** as starting material. Compound **115** obtained as red powder. 30 % yield; m.p; 90-92°C; silica gel TLC R*f* 0.60 (EtOAc/n-Hex 30% v/v); δH (400 MHz, DMSO-d_6) 1.74 (4H, m, 2 x C*H*$_2$), 2.96 (2H, t, *J*=6.8, C*H*$_2$), 4.14 (2H, s, C*H*$_2$), 6.27 (1H, d, *J*=9.3, Ar-*H*), 6.77 (1H, s, C*H*), 6.93 (1H, d, *J*=8.4, Ar-*H*), 6.98 (1H, s, Ar-*H*), 7.61 (1H, d, *J*=8.4, Ar-*H*), 7.97 (1H, d, *J*=9.3, Ar-*H*); δ_C (100 MHz, DMSO-d_6) 21.0, 29.0, 34.1, 68.9, 75.4, 98.7, 102.2, 109.5, 113.5, 113.8, 130.5, 145.4, 156.5, 161.4, 162.9, 201.4; *m/z* (ESI positive) 528.9 $[M+H]^+$.

7-(hex-5-yn-1-ylamino)-4-methyl-2H-chromen-2-one hexacarbonyldicobalt 116. The titled compound **116** was obtained according to the **general procedure C** previously reported using 7-(hex-5-yn-1-ylamino)-4-methyl-2H-chromen-2-one **101** as starting material. Compound **116** obtained as red powder. 25 % yield; m.p; 180-182°C; silica gel TLC R*f* 0.35 (EtOAc/n-Hex 30% v/v); δH (400 MHz, DMSO-d_6) 1.75 (4H, s, 2 x C*H*$_2$), 2.34 (3H, s, C*H*$_3$), 2.96 (2H, t, *J*=7.2, C*H*$_2$), 3.17 (2H, t, *J*=5.7, C*H*$_2$), 5.93 (1H, s, Ar-*H*), 6.44 (1H, d, *J*=2.0, Ar-*H*), 6.64 (1H, dd, *J*=2.1, *J*=8.2, Ar-*H*), 6.72 (1H, t, *J*=5.0, exchanged with D_2O, N*H*), 6.8 (1H, s, C*H*), 7.45 (1H, d, *J*=8.7, Ar-*H*); δ_C (100 MHz, DMSO-d_6) 19.0, 29.1, 30.0, 34.4, 43.1, 75.4, 97.2, 98.7, 108.4, 109.7, 111.2, 126.9, 153.6, 154.7, 156.8, 161.8, 201.4; *m/z* (ESI positive) 541.9 $[M+H]^+$.

4-(but-2-yn-1-ylamino)benzenesulfonamide hexacarbonyldicobalt 117. The titled compound **116** was obtained according to the **general procedure C** previously reported using 4-(but-2-yn-1-ylamino)benzenesulfonamide **102** as starting material. Compound **117** obtained as red powder. 30 % yield; m.p; 120-122°C; silica gel TLC R*f* 0.70 (EtOAc/n-Hex 40% v/v); δH (400 MHz, DMSO-d_6) 2.56 (3H, s, C*H*$_3$), 4.62 (2H, d, *J*=3.7, C*H*$_2$), 6.75 (2H, dd, *J*=3.6, *J*=8.5, Ar-*H*), 6.99 (1H, t, *J*=6.9, N*H*), 7.16 (2H, s, exchanged with D_2O, SO_2NH_2) 7.56 (2H, m, Ar-*H*); δ_C (100 MHz, DMSO-d_6) 22.9, 36.2, 98.2, 111.1, 121.0, 127.3, 129.3, 150.8, 201.1; *m/z* (ESI positive) 510.9 $[M+H]^+$.

4-(pent-2-yn-1-ylamino)benzenesulfonamide hexacarbonyldicobalt 118. The titled compound **118** was obtained according to the **general procedure C** previously reported using 4-(pent-2-yn-1-ylamino)benzenesulfonamide **103** as starting material. Compound **118** obtained as red powder. 30 % yield; m.p; 120-122°C; silica gel TLC R*f* 0.60 (EtOAc/n-Hex 30% v/v); δH (400 MHz, DMSO-d_6) 1.14 (3H, t, *J*=7.2, CH_3), 2.72 (2H, m, CH_2), 4.61 (2H, d, *J*=6.4, CH_2), 6.70 (2H, d, *J*=8.6, Ar-*H*), 7.10 (1H, t, *J*=6.9, N*H*), 7.13 (2H, s, exchanged with D_2O, SO_2NH_2), 7.49 (2H, d, *J*=8.5, Ar-*H*); δ_C (100 MHz, DMSO-d_6) 16.5, 32.0, 45.5, 103.4, 113.8, 120.7, 129.0, 130.4, 152.3, 200.1; *m/z* (ESI positive) 524.9 $[M+H]^+$.

4-(di(but-2-yn-1-yl)amino)benzenesulfonamide hexacarbonyldicobalt 119. The titled compound **119** was obtained according to the **general procedure C** previously reported using 4-(di(but-2-yn-1-yl)amino)benzenesulfonamide **104** as starting material. Compound **119** obtained as red powder. 20 % yield; m.p; 130-132°C; silica gel TLC R*f* 0.50 (EtOAc/n-Hex 35% v/v); δH (400 MHz, DMSO-d_6) 2.65 (6H, s, 2 x CH_3), 4.97 (4H, s, 2 x CH_2), 7.03 (2H, d, *J*=7.4, Ar-*H*), 7.12 (2H, s, exchanged with D_2O, SO_2NH_2), 7.69 (2H, d, *J*=8.0, Ar-*H*); δ_C (100 MHz, DMSO-d_6) 21.6, 52.8, 93.4, 95.6, 112.6, 128.2, 131, 149.6, 200.7; *m/z* (ESI positive) 848.8 $[M+H]^+$.

4-((3-phenylprop-2-yn-1-yl)oxy)benzenesulfonamide hexacarbonyldicobalt 120. The titled compound **120** was obtained according to the **general procedure C** previously reported using 4-((3-phenylprop-2-yn-1-yl)oxy)benzenesulfonamide **105** as starting material. Compound **120** obtained as red powder. 50 % yield; m.p; 115-117°C; silica gel TLC R*f* 0.60 (EtOAc/n-Hex 40% v/v); δH (400 MHz, DMSO-d_6) 3.9 (2H, s, CH_2), 7.10 (2H, m, Ar-*H*), 7.24 (7H, m, 2H, s, exchanged with D_2O, SO_2NH_2, 5 X Ar-*H*), 7.62 (2H, m, Ar-*H*); δ_C (100 MHz, DMSO-d_6) 69.2, 104.5, 115.3, 122.5, 125.5, 127.6, 128.0, 128.6, 134.7, 160.1, 163.8, 200.1; *m/z* (ESI positive) 573.9 $[M+H]^+$.

5.1.2 CA Inibition

An Applied Photophysics stopped-flow instrument has been used for assaying the CA catalysed CO_2 hydration activity [14]. Phenol red (at a concentration of 0.2 mM) has been used as indicator, working at the absorbance maximum of 557 nm, with 20 mM Hepes (pH 7.5) as buffer, and 20 mM Na_2SO_4 (for maintaining constant the ionic strength), following the initial rates of the CA-catalyzed CO_2 hydration reaction for a period of 10-100 s. The CO_2

concentrations ranged from 1.7 to 17 mM for the determination of the kinetic parameters and inhibition constants. For each inhibitor at least six traces of the initial 5-10% of the reaction have been used for determining the initial velocity. The uncatalyzed rates were determined in the same manner and subtracted from the total observed rates. Stock solutions of inhibitor (0.1 mM) were prepared in distilled-deionized water and dilutions up to 0.01 nM were done thereafter with the assay buffer. Inhibitor and enzyme solutions were preincubated together for 15 min for sulfonamide derivatives and 6 h for coumarin and sulfocoumarin derivatives at room temperature prior to assay, in order to allow for the formation of the E-I complex. The inhibition constants were obtained by non-linear least-squares methods using PRISM 3 and the Cheng-Prusoff equation, as reported earlier [15-17] and represent the mean from at least three different determinations. All CA isofoms were recombinant ones obtained in-house as reported earlier [15-17].

5.1.3 CO release Assay

Gaseous CO was purchased from Rivoira (Milan, Italy); all the other reagents were of analytical grade and obtained from Sigma. UV-Vis absorption spectra were recorded using a Perkin Elmer Lambda EZ 201 spectrophotometer from 275 to 700 nm at the scanning rate of 200 nm/min in a disposable plastic cuvette (path length 0.44 cm). Second derivative spectra were obtained using the Lab Calc program (Galactic Industries, Salem, NH). For the differentiation process, the Savitzky-Golay method was applied using 25 data points. No changes in the wavelength or in the bandwidth were observed when the number of points was increased or decreased. A stock solution of lyophilized horse heart Mb was freshly prepared by dissolving the protein in phosphate buffered saline flushed with N2 (PBS, 0.01 M, pH 7.4) to a 20 μM final concentration. 2 mL of this solution were put in a cuvette and the UV-Vis absorption spectrum of met-Mb was recorded. Then, the solution was split in half: in the first half (reference) 10 μL of sodium dithionite (30 mg/mL) were added and the UV-Vis spectrum of deoxy-Mb was recorded. Then, the solution was flushed with CO gas and the Mb-CO spectrum was acquired. The second half (sample) was reduced with sodium dithionite and, after recording a spectrum, a CORM DMSO solution was added and gently mixed, to a final CORM concentration of 20 μM. The solution was overlaid with 300 μL of light mineral oil to prevent Mb oxygenation and CO escaping and the absorption spectrum at t=0 was recorded. Then, the sample was kept at 37° C and spectra were recorded every 30 minutes for 3 hours and then every 60 minutes until a total of 6 hours. During the assay, further additions of freshly prepared sodium dithionite solution were made when necessary. After 360 minutes the sample was flushed with CO gas to determine the total Mb concentration at the end of the assay. The assay was repeated three times for each tested compound and the mean of the three results for each time point was calculated. The curve fitting analysis was performed with Origin data analysis and graphing software (OriginLab Corporation, Northampton, Massachusetts, U.S.A.), mixing the pure deoxy-Mb and Mb-CO reference UV-Vis spectra in different proportion for each time point.

5.1.4 Animals

Sprague Dawley rats (Envigo, Varese, Italy) weighing 220-250 g at the beginning of the experimental procedure were used. Animals were housed in the Centro Stabulazione Animali da Laboratorio (University of Florence) and used at least 1 week after their arrival. Four rats were housed per cage (size 26 cm x 41 cm); animals were fed a standard laboratory diet and tap water ad libitum and kept at 23 ± 1 °C with a 12 h light/dark cycle (light at 7 A.M.). All animal manipulations were carried out according to the Directive 2010/63/EU of the European parliament and of the European Union council (22 September 2010) on the protection of animals used for scientific purposes. The ethical policy of the University of Florence complies with the Guide for the Care and Use of Laboratory Animals of the US National Institutes of Health (NIH Publication No. 85-23, revised 1996; University of Florence assurance number: A5278-01). Formal approval to conduct the experiments described was obtained from the Italian Ministry of Health (No. 54/2014-B) and from the Animal Subjects Review Board of the University of Florence. Experiments involving animals have been reported according to ARRIVE guidelines [18]. All efforts were made to minimize animal suffering and to reduce the number of animals used.

Complete Freund's adjuvant-induced rheumatoid arthritis

Articular damage was induced by injection of complete Freund's adjuvant (CFA; Sigma-Aldrich St Louis, MO, USA), containing 1 mg/ml of heat-killed and dried Mycobacterium tuberculosis in paraffin oil and mannide monooleate, into the tibiotarsal joint.17,18 Briefly, the rats were lightly anesthetized by 2% isoflurane, the left leg skin was sterilized with 75% ethyl alcohol and the lateral malleolus located by palpation. A 28-gauge needle was then inserted vertically to penetrate the skin and turned distally for insertion into the articular cavity at the gap between the tibiofibular and tarsal bone until a distinct loss of resistance was felt. A volume of 50 μl of CFA was then injected (day 1). Control rats received 50 μl of saline solution (day 1) in the tibiotarsal joint.

Administration of compounds

5b, 10b, 11b, 13b at the doses of 10, 30 and 100 mg kg-1, 15b (85.0 mg kg-1) and 5a (42.4 mg kg-1) were suspended in a 1% solution of carboxymethylcellulose sodium salt (CMC) and per os (p.o.) acutely administered on day 14 after CFA intra-articular (i.a.) injection. Ibuprofen was used as reference standard (100 mg kg-1, p.o.). Control animals were treated with vehicle (CMC).

Toxicity and Irwin test

Toxicity was evaluated after a single acute administration of compounds 100 mg kg-1. Animals were observed during 24 h. For the Irwin test, each rat was individually placed in a transparent cage (26 × 41 cm), and 26 neurobehavioural or physiological parameters were systematically assessed according to Irwin (1968). Behavioural, autonomic, and neurological manifestations produced by compound administration in rats were evaluated: motor displacement, motor reflexes, stereotypies, grooming, reaction to painful or environmental stimuli (analgesia, irritability), startle response, secretions, excretions, respiratory movements, skin colour and temperature, piloerection, exophthalmos, eyelid and corneal reflexes, muscle tone, ataxia, tremors, head twitches, jumps, convulsions, Straub tail, and other signs or symptoms. For postural reflexes (righting reflex) and other signs such as piloerection, exophthalmia (exaggerated protrusion of the eyeball), ataxia, tremors, and Straub tail, only presence or absence was recorded. Skin colour was evaluated qualitatively (pale, red, or purple); other signs were evaluated semi-quantitatively, according to the observer's personal scale (0 to + 4, − 4 to 0, or − 4 to + 4). The terms sedation and excitation express the final interpretation of a group of signs: reduced motor activity, reduced startle response, eyelid ptosis, and reduced response to manual manipulation, for the former; and increased motor activity, increased startle response, increased response to manual manipulation, and exophthalmia, for the latter. Hyperactivity includes running, jumps, and attempts to escape from the container. Trained observers not informed about the specific treatment of each animal group carried out this test.

Paw-pressure test

The nociceptive threshold of rats was determined with an analgesimeter (Ugo Basile, Varese, Italy), according to the method described by Leighton et al.[19]. Briefly, a constantly increasing pressure was applied to a small area of the dorsal surface of the hind paw using a blunt conical probe by a mechanical device. Mechanical pressure was increased until vocalization or a withdrawal reflex occurred while rats were lightly restrained. Vocalization or withdrawal reflex thresholds were expressed in grams. Rats scoring below 40 g or over 75 g during the test before drug administration were rejected (25%). For analgesia measures, mechanical pressure application was stopped at 120 g.

Incapacitance test

Weight-bearing changes were measured using an incapacitance apparatus (Linton Instrumentation, Norfolk, UK) to detect changes in postural equilibrium after a hind limb injury. [20] Rats were trained to stand on their hind paws in a box with an inclined plane (65° from horizontal). This box was placed above the incapacitance apparatus. This allowed us to independently measure the weight that the animal applied on each hind limb. The value reported for each animal is the mean of five consecutive measurements. In the absence of hind limb injury, rats applied an equal weight on both hind limbs, indicating postural equilibrium, whereas an unequal distribution of weight on the hind limbs indicated a monolateral decreased pain threshold. Data are expressed as the difference between the weight applied to the limb contralateral to the injury and the weight applied to the ipsilateral limb (Δ Weight).

Statistical analysis

Behavioural measurements were performed on ten rats for each treatment carried out in two different experimental sets. Results were expressed as mean ± (S.E.M.) with one-way analysis of variance. A Bonferroni's significant difference procedure was used as a post hoc comparison. P-values <0.05 or <0.01 were considered significant. Data were analysed using the Origin 9 software (OriginLab, Northampton, MA, USA).

References

1. Chowdhury MA, Dong Y, Chen QH, Abdellatif KR, Knaus EE. Synthesis and cyclooxygenase inhibitory activities of linear 1-(methanesulfonylphenyl or benzenesulfonamido)-2-(pyridyl)acetylene regioisomers. Bioorg Med Chem. 2008, 16, 1948-1956.
2. Nocentini A, Ferraroni M, Carta F, Ceruso M, Gratteri P, Lanzi C, Masini E, Supuran CT. Benzenesulfonamides Incorporating Flexible Triazole Moieties Are Highly Effective Carbonic Anhydrase Inhibitors: Synthesis and Kinetic, Crystallographic, Computational, and Intraocular Pressure Lowering Investigations. J Med.Chem. 2016, 59, 10692−704.
3. Angeli A, Tanini D, Capperucci A, Malevolti G, Turco F, Ferraroni M, Supuran CT. Synthesis of different thio-scaffolds bearing sulfonamide with subnanomolar carbonic anhydrase II and IX inhibitory properties and X-ray investigations for their inhibitory mechanism. Bioorg Chem. 2018, 81, 642–648.
4. Angeli A, di Cesare Mannelli L, Trallori E, Peat TS, Ghelardini C, Carta F, Supuran CT. Design, Synthesis, and X-ray of Selenides as New Class of Agents for Prevention of Diabetic Cerebrovascular Pathology. ACS Med Chem Lett. 2018, 9, 462-467.
5. Nocentini A, Vullo D, Bartolucci G, Supuran CT. N-Nitrosulfonamides: A new chemotype for carbonic anhydrase inhibition. Bioorg Med Chem. 2016, 24, 3612–3617.
6. Carta F, Di Cesare Mannelli L, Pinard M, Ghelardini C, Scozzafava A, McKenna R, Supuran CT. A class of sulfonamide carbonic anhydrase inhibitors with neuropathic pain modulating effects. Bioorg Med Chem. 2015, 23,1828-1840.
7. Babich JW, Zimmerman C, Joyal J, Lu S, Hilliger S, Maresca KP, Sheem JM. Metal complexes of poly(carboxyl)amine-containing ligands having an affinity for carbonic anhydrase IX. EP2800471A4, 2013.
8. Bozdag M, Pinard M, Carta F, Masini E, Scozzafava A, McKenna R, Supuran CT. A Class of 4-Sulfamoylphenyl-ω-aminoalkyl Ethers with Effective Carbonic Anhydrase Inhibitory Action and Antiglaucoma Effects. J Med Chem. 2014, 57, 9673−9686.
9. Nocentini A, Carta F, Ceruso M, Bartolucci G, Supuran CT. Click-tailed coumarins with potent and selective inhibitory action against the tumor-associated carbonic anhydrases IX and XII. Bioorg Med Chem. 2015, 23, 6955-6966.

10. Nocentini A, Ceruso M, Carta F, Supuran CT. 7-Aryl-triazolyl-substituted sulfocoumarins are potent, selective inhibitors of the tumor-associated carbonic anhydrase IX and XII. J Enzyme Inhib Med Chem, 2016, 31, 1226–1233.
11. Liu J, Pham PT, Skripnikova EV, Zheng S, Lovings LJ, Wang Y, Goyal N, Bellow SM, Mensah LM, Chatters AJ, Bratton MR, Wiese TE, Zhao M, Wang G, Foroozesh MA. Ligand-Based Drug Design. Discovery of 4-Trifluoromethyl-7,8-pyranocoumarin as a Selective Inhibitor of Human Cytochrome P450 1A2. J Med Chem. 2015, 58, 6481-6493.
12. Ferraroni M, Carta F, Scozzafava A, Supuran CT. Thioxocoumarins Show an Alternative Carbonic Anhydrase Inhibition Mechanism Compared to Coumarins. J Med Chem.2016, 59, 462−473.
13. Schimler SD, Hall DJ, Debbert, SL. Anticancer (hexacarbonyldicobalt)propargyl aryl ethers: Synthesis, antiproliferative activity, apoptosis induction, and effect on cellular oxidative stress. J Inorg. Biochem. 2013, 119, 28–37.
14. Khalifah RG. The carbon dioxide hydration activity of carbonic anhydrase. I. Stop-flow kinetic studies on the native human isoenzymes B and C. J Biol Chem. 1971, 246, 2561-2573
15. Bua S, Di Cesare Mannelli L, Vullo D, Ghelardini C, Bartolucci G, Scozzafava A, Supuran CT, Carta F. Design and synthesis of novel Nonsteroidal Anti-Inflammatory Drugs and Carbonic Anhydrase Inhibitors hybrids (NSAIDs-CAIs) for the treatment of rheumatoid arthritis. J Med Chem. 2017, 60, 1159−1170.
16. Akgul O, Di Cesare Mannelli L, Vullo D, Angeli A, Ghelardini C, Bartolucci G, Alfawaz Altamimi AS, Scozzafava A, Supuran CT, Carta F. Discovery of Novel Nonsteroidal Anti-Inflammatory Drugs and Carbonic Anhydrase Inhibitors Hybrids (NSAIDs−CAIs) for the Management of Rheumatoid Arthritis. J Med Chem. 2018, 61, 4961−4977.
17. Carta F, Maresca A, Scozzafava A, Supuran CT. 5- and 6-membered (thio)lactones are prodrug type carbonic anhydrase inhibitors. Bioorg Med Chem Lett. 2012, 1, 267-270.
18. McGrath JC and Lilley E. Implementing guidelines on reporting research using animals (ARRIVE etc.): new requirements for publication in BJP. Br J Pharmacol. 2015, 172, 3189–3193.
19. Leighton G, Rodriguez R, Hill R, Hughes J. Kappa-Opioid agonists produce antinociception after i.v. and i.c.v. but not intrathecal administration in the rat. Br J Pharmacol. 1988, 93, 553–560.

20. Bove SE, Calcaterra SL, Brooker RM, Huber CM, Guzman RE, Juneau PL, Schrier DJ, Kilgore KS. Weight bearing as measure of disease progression and efficacy of anti-inflammatory compounds in a model of monosodium iodoacetate-induced osteoarthritis. Osteoarthritis Cartilage. 2003, 11, 821–830.

5.2 Experimental Section : Chapter 3

5.2.1 Chemistry

Anhydrous solvents and all reagents were purchased from Sigma-Aldrich (Milan, Italy), Alfa Aesar (Milan, Italy) and TCI (Milan, Italy). All reactions involving air- or moisture-sensitive compounds were performed under a nitrogen atmosphere using dried glassware and syringes techniques to transfer solutions. Nuclear magnetic resonance spectra (^{1}H-NMR: 400 MHz; ^{13}C-NMR: 100 MHz) were recorded in DMSO-d_6 using an Avance III 400 MHz spectrometer (Bruker, Milan, Italy). Chemical shifts are reported in parts per million (ppm) and the coupling constants (J) are expressed in Hertz (Hz). Splitting patterns are designated as follows: s, singlet; d, doublet; t, triplet; q, quadruplet; m, multiplet; brs, broad singlet; dd, double of doublets. The assignment of exchangeable protons (OH and NH) was confirmed by the addition of D_2O. Analytical thin-layer chromatography (TLC) was carried out on silica gel F-254 plates (Merck, Milan, Italy). Melting points (m.p.) were carried out in open capillary tubes and are uncorrected. The solvents used in MS measures were acetone, acetonitrile (Chromasolv grade), purchased from Sigma–Aldrich and mQ water 18 MΩ cm, obtained from Millipore's Simplicity system (Milan, Italy). The mass spectra were obtained using a 1200 L triple quadrupole system (Varian, Palo Alto, CA, USA) equipped by Electrospray Source (ESI) operating in both positive and negative ions. Stock solutions of analytes were prepared in acetone at 1.0 mg mL^{-1} and stored at 4 °C. Working solutions of each analyte were freshly prepared by diluting stock solutions in a mixture of mQ H_2O/CH_3CN 1:1 (v/v) up to a concentration of 1.0 µg mL^{-1}. The mass spectra of each analyte were acquired by introducing, via syringe pump at 10 µL min^{-1}, the working solution. Raw-data were collected and processed by Varian Workstation Vers. 6.8 software.

Synthethic Scheme for the preparation of derivatives 129-136.

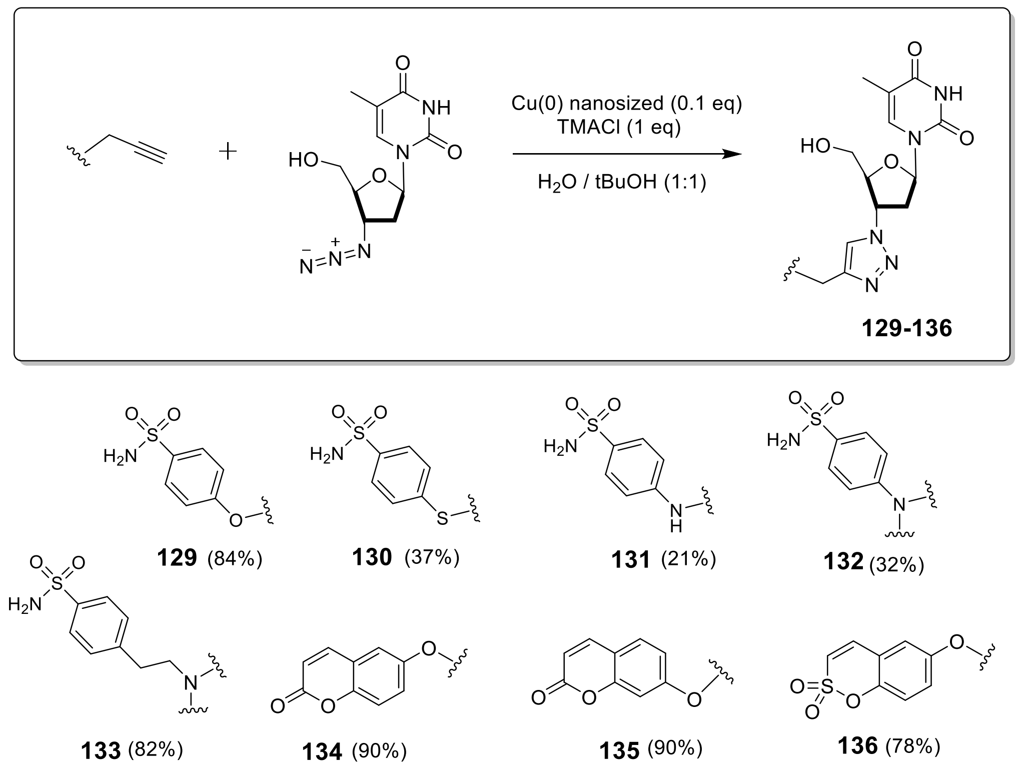

General Procedure D: To a suspension of azidonucleoside (1.1 eq. or 2.2 eq.) in H_2O/t-BuOH 1/1(4 mL) the appropriate alkyne (1.0 eq.) was added at rt, followed by copper(0) nanosized (0.1 eq.) and TMACl (1.0 eq.). The suspension was stirred at 40°C until starting materials were consumed (TLC monitoring), then diluted with MeOH (20 mL), and filtered through Celite 521®. The solvent was evaporated, affording to a residue that was triturated from EtOAc, to give a white powder.

4-((1-(2-(hydroxymethyl)-5-(5-methyl-2,4-dioxo-3,4-dihydropyrimidin-1(2H)-yl)tetrahydrofuran-3-yl)-1H-1,2,3-triazol-4-yl)methoxy)benzenesulfonamide 129. Compound **129** was obtained according to the **general procedure D** using **62** as starting material, to afford the title compound **129** as a light yellow solid: 84% yield; mp 141-143°C; silica gel TLC Rf = 0.13 (MeOH/DCM 5% v/v). δH(400 MHz, DMSO-d6): 1.85 (3H, s, CH_3), 2.73 (2H, m, CH_2), 3.70 (2H, m, CH_2), 4.27 (1H, q, *J*= 3.5, C*H*), 5.29 (2H, s, CH_2), 5.34 (1H, br t, exchange with D_2O, O*H*), 5.45 (1H, m, C*H*), 6.46 (1H, t, *J*= 6.5, C*H*), 7.24 (4H, m, overlapped signals, 2 x Ar*H*, exchange with D_2O, SO_2NH_2), 7.80 (2H, d, *J*= 8.8, Ar*H*), 7.86 (1H, s, C*H*), 8.50 (1H, s, C*H*), 11.36 (1H, br s, exchange with D_2O, N*H*); δC(100 MHz, DMSO-d6):13.1, 38.0, 55.2, 60.3, 62.0, 84.5, 85.4, 110.5, 115.6, 125.4, 128.5, 137.1, 137.4, 143.2, 151.3, 161.2, 164.6. m/z(ESIpositive) 478.2 $[M + H]^+$.

4-(((1-(2-(hydroxymethyl)-5-(5-methyl-2,4-dioxo-3,4-dihydropyrimidin-1(2H)-yl)tetrahydrofuran-3-yl)-1H-1,2,3-triazol-4-yl)methyl)thio)benzenesulfonamide 130. Compound **130** was obtained according to the **general procedure D** using **63** as starting material, to afford the title compound **130** as a white solid: 37% yield; mp 164-166°C; silica gel TLC Rf = 0.14 (MeOH/DCM 5% v/v). δH(400 MHz, DMSO-d6): 1.84 (3H, s, CH_3), 2.69 (2H, m, CH_2), 3.64 (2H, m, CH_2), 4.19 (1H, q, *J*= 3.5, C*H*), 4.45 (2H, s, CH_2), 5.38 (m, 2H, overlapped signals, 1 x C*H*, exchange with D_2O, 1 x O*H*), 6.43 (t, *J*= 6.5, 1H), 7.36 (2H, s, exchange with D_2O, SO_2NH_2), 7.57 (2H, d, *J*= 8.4, Ar*H*), 7.76 (2H, d, *J*= 8.4, Ar*H*), 7.85 (1H, s, C*H*), 8.29 (1H, s, C*H*), 11.35 (1H, br s, exchange with D_2O, N*H*)*;* δC(100 MHz, DMSO-d6): 13.1, 27.0, 37.9, 60.2, 61.6, 84.8, 85.5, 110.5, 124.2, 127.1, 127.7, 137.1, 141.9, 142.1, 144.1, 151.3, 164.6. m/z(ESIpositive) 494.1 $[M + H]^+$.

4-(((1-(2-(hydroxymethyl)-5-(5-methyl-2,4-dioxo-3,4-dihydropyrimidin-1(2H)-yl)tetrahydrofuran-3-yl)-1H-1,2,3-triazol-4-yl)methyl)amino)benzenesulfonamide 131. Compound **131** was obtained according to the **general procedure D** using **65** as starting material, to afford the title compound **130** as a white solid. 21% yield; mp 192-194°C; silica gel TLC Rf = 0.21 (MeOH/DCM 10% v/v). δH(400 MHz, DMSO-d6): 1.84 (3H, s, CH_3), 2.69 (2H, m, CH_2), 3.68 (2H, m, CH_2), 4.23 (1H, q, *J*= 3.5, C*H*), 4.40 (2H, d, *J*= 5.7, CH_2), 5.32 (1H, br t, 1H, exchange with D_2O, O*H*), 5.38 (1H, m, C*H*), 6.45 (1H, t, *J*= 6.5, C*H*), 6.74 (2H, d, *J*= 8.8, 2x Ar-*H*), 6.92 (1H, t, J=5.7, exchange with D_2O, N*H*), 6.98 (2H, s, exchange with D_2O, SO_2NH_2), 7.55 (2H, d, *J*= 8.8, 2x Ar-*H*), 7.84 (1H, s, C*H*), 8.24 (1H, s, C*H*), 11.4 (1H, br s, exchange with D_2O, N*H*). δC(100 MHz, DMSO-d6):12.2, 36.9, 37.9, 59.1, 60.7, 83.8, 84.5, 110.1, 111.2, 122.6, 127.2, 130.4, 136.3, 145.2, 150.4, 150.9, 163.7. .m/z(ESIpositive) 477.1.0 $[M + H]^+$.

4-(bis((1-(2-(hydroxymethyl)-5-(5-methyl-2,4-dioxo-3,4-dihydropyrimidin-1(2H)-yl)tetrahydrofuran-3-yl)-1H-1,2,3-triazol-4-yl)methyl)amino)benzenesulfonamide 132. Compound **132** was obtained according to the **general procedure D** using **66** as starting material, afford the title compound **132** as a light yellow solid. 32% yield; mp 206–208°C; silica gel TLC Rf = 0.17 (MeOH/DCM 10% v/v). δH(400 MHz, DMSO-d6): 1.84 (s, 6H, 2 x CH_3), 2.69 (m, 4H, 2 x CH_2), 3.68 (m, 4H, 2 x CH_2), 4.21 (q, *J*= 3.8, 2H, 2 x C*H*), 4.79 (s, 4H, 2 x CH_2), 5.35 (br t, 2H, exchange with D_2O, 2 x O*H*), 5.40 (m, 2H, 2 x C*H*), 6.45 (t, *J*= 6.4, 2H, 2 x C*H*), 7.03 (m, 4H, overlapped signals, 2 x Ar*H*, exchange with D_2O, SO_2NH_2), 7.60 (d, *J*= 8.9, 2H), 7.85 (s, 2H, 2 x C*H*), 8.28 (s, 2H, 2 x C*H*), 11.38 (br s, 2H, exchange with D_2O, 2 x N*H*). δC(100 MHz, DMSO-d6): 12.2, 36.9, 37.9, 59.1, 60.7, 83.8, 84.5, 110.1, 111.2, 122.6, 127.2, 130.4, 136.3, 145.2, 150.4, 150.9, 163.7. m/z(ESIpositive) 782.2 $[M + H]^+$.

4-(2-(bis((1-(2-(hydroxymethyl)-5-(5-methyl-2,4-dioxo-3,4-dihydropyrimidin-1(2H)-yl)tetrahydrofuran-3-yl)-1H-1,2,3-triazol-4-yl)methyl)amino)ethyl)benzenesulfonamide 133. Compound **133** was obtained according to the **general procedure D** using **67** as starting material, to afford the title compound **133** as a white solid. 82% yield; mp 117-119°C; silica gel TLC Rf = 0.13 (MeOH/DCM 10% v/v). δH(400 MHz, DMSO-d6): 1.85 (s, 6H, 2 x CH_3), 2.72 (m, 6H, overlapped signals, 3 x CH_2), 2.93 (t, *J*= 7.2, 2H, CH_2), 3.70 (m, 4H, 2 x CH_2), 3.80 (s, 4H, 2 x CH_2), 4.24 (q, *J*= 3.5, 2H, 2 x C*H*), 5.40 (m, 4H, overlapped signals, 2 x C*H*, exchange with D_2O, 2 x O*H*), 6.48 (t, *J*= 6.4, 2H, 2 x C*H*), 7.32 (br s, 2H, exchange with D_2O, SO_2NH_2), 7.41 (d, *J*= 8.3, 2H), 7.75 (d, *J*= 8.3, 2H), 7.87 (s, 2H, 2 x C*H*), 8.22 (s, 2H, 2 x C*H*), 11.40 (br s, 2H, exchange with D_2O, 2 x N*H*). δC(100 MHz, DMSO-d6): 13.1, 33.4, 37.9, 48.2, 54.7, 60.1, 61.6, 62.2, 84.8, 85.5, 110.5, 124.5, 126.5, 130.0, 137.2, 142.6, 144.6, 145.7, 151.4, 164.6. m/z(ESIpositive) 819.3 $[M + H]^+$.

1-(5-(hydroxymethyl)-4-(4-(((2-oxo-2H-chromen-6-yl)oxy)methyl)-1H-1,2,3-triazol-1-yl)tetrahydrofuran-2-yl)-5-methylpyrimidine-2,4(1H,3H)-dione 134. Compound **134** was obtained according to the **general procedure D** using **69** as starting material, to afford the title compound **134** as a white solid. 91% yield; mp 200–202°C; silica gel TLC Rf = 0.35 (MeOH/DCM 10% v/v). δH(400 MHz, DMSO-d6): 1.85 (3H, s, CH_3), 2.74 (2H, m, CH_2), 3.70 (2H, m, CH_2), 4.26 (1H, q, *J*= 3.5, C*H*), 5.25 (2H, s, CH_2), 5.45 (2H, m, overlapped signals, 1 x C*H*, exchange with D_2O, 1 x O*H*), 6.47 (1 H, t, *J*= 6.5, C*H*), 6.53 (1H, d, *J*= 9.6, Ar*H*), 7.33 (1H, dd, *J*= 2.8, 9.0, Ar*H*), 7.39 (1H, d, *J*= 9.0, Ar*H*), 7.48 (1H, d, *J*= 2.8, Ar*H*), 7.88 (1H, s, C*H*), 8.07 (1H, d, *J*= 9.6, Ar*H*), 8.54 (1H, s, C*H*), 11.37 (1H, br s, exchange with D_2O, N*H*). δC(100 MHz, DMSO-d6):13.1, 38.0, 60.3, 61.6, 62.6, 84.8, 85.4, 110.5, 112.9, 117.5, 118.3, 120.1, 120.9, 125.4, 137.1, 143.4, 144.9, 148.9, 151.3, 155.2, 161.0, 164.6.m/z(ESIpositive) 467.1.0 $[M + H]^+$ [1].

1-(5-(hydroxymethyl)-4-(4-(((2-oxo-2H-chromen-7-yl)oxy)methyl)-1H-1,2,3-triazol-1-yl)tetrahydrofuran-2-yl)-5-methylpyrimidine-2,4(1H,3H)-dione 135. Compound **135** was obtained according to the **general procedure D** using **70** as starting material, to afford the title compound **135** as a white solid. 91% yield; mp 213-215°C; silica gel TLC Rf = 0.50

(MeOH/DCM 10% v/v). δH(400 MHz, DMSO-d6): 1.85 (3H, s, CH_3), 2.73 (2H, m, CH_2), 3.69 (2H, m, CH_2), 4.27 (1H, q, *J*= 3.5, C*H*), 5.32 (2H, s, CH_2), 5.36 (1H, t, *J*= 5.0, exchange with D_2O, O*H*), 5.46 (1 H, m, C*H*), 6.34 (1H, d, *J*= 9.5, Ar*H*), 6.47 (1 H, t, *J*= 6.5, C*H*), 7.07 (1H, dd, *J*= 2.4, 8.6, Ar*H*), 7.21 (1H, d, *J*= 2.4, Ar*H*), 7.69 (1H, d, *J*= 8.6, Ar*H*), 7.86 (1H, s, C*H*), 8.04 (1H, d, *J*= 9.5, Ar*H*), 8.53 (1H, s, C*H*), 11.38 (1H, br s, exchange with D_2O, N*H*). δC(100 MHz, DMSO-d6): 13.1, 38.1, 60.4, 61.7, 62.6, 84.9, 85.5, 102.5, 110.6, 113.5, 113.6, 113.8, 125.7, 130.5, 137.2, 143.1, 145.2, 151.4, 156.2, 161.2, 162.0, 164.0. m/z(ESIpositive) 467.1 $[M + H]^+$ [2].

1-(4-(4-(((2,2-dioxidobenzo[e][1,2]oxathiin-6-yl)oxy)methyl)-1H-1,2,3-triazol-1-yl)-5-(hydroxymethyl)tetrahydrofuran-2-yl)-5-methylpyrimidine-2,4(1H,3H)-dione 136. Compound **136** was obtained according to the **general procedure D** using **72** as starting material, to afford the title compound **136** as a white solid. 78% yield; mp 200−202°C; silica gel TLC Rf = 0.47 (MeOH/DCM 10% v/v). δH(400 MHz, DMSO-d6): 1.85 (3H, s, CH_3), 2.74 (2H, m, CH_2), 3.70 (2H, m, CH_2), 4.26 (1H, q, *J*= 3.5, C*H*), 5.26 (2H, s, CH_2), 5.37 (1H, br t, exchange with D_2O, O*H*), 5.45 (1 H, m, C*H*), 6.47 (1 H, t, *J*= 6.5, C*H*), 7.29 (1H, dd, *J*= 3.0, 9.0, Ar*H*), 7.44 (1H, d, *J*= 9.0, Ar*H*), 7.47 (1H, d, *J*= 3.0, Ar*H*), 7.54 (1H, d, *J*= 10.3, Ar*H*), 7.68 (1H, d, *J*= 10.3, Ar*H*),7.87 (1H, s, C*H*), 8.51 (1H, s, C*H*), 11.38 (1H, br s, exchange with D_2O, N*H*). δC(100 MHz, DMSO-d6):13.1, 38.0, 60.3, 61.6, 62.7, 84.8, 85.4, 110.5, 115.7, 119.9, 120.4, 120.5, 124.0, 125.5, 137.1, 137.3, 143.3, 145.6, 151.4, 156.4, 164.9. m/z(ESIpositive) 503.1 $[M + H]^+$.

5.2.2 CA inhibition

An Applied Photophysics stopped-flow instrument has been used for assaying the CA catalysed CO_2 hydration activity [3]. Phenol red (at a concentration of 0.2 mM) has been used as indicator, working at the absorbance maximum of 557 nm, with 20 mM Hepes (pH 7.5) as buffer, and 20 mM Na_2SO_4 (for maintaining constant the ionic strength), following the initial rates of the CA-catalyzed CO_2 hydration reaction for a period of 10-100 s. The CO_2 concentrations ranged from 1.7 to 17 mM for the determination of the kinetic parameters and inhibition constants. For each inhibitor at least six traces of the initial 5-10% of the reaction have been used for determining the initial velocity. The uncatalyzed rates were determined in the same manner and subtracted from the total observed rates. Stock solutions of inhibitor (0.1 mM) were prepared in distilled-deionized water and dilutions up to 0.01 nM were done thereafter with the assay buffer.

Inhibitor and enzyme solutions were preincubated together for 15 min for sulfonamide derivatives and 6 h for coumarin and sulfocoumarin derivatives at room temperature prior to assay, in order to allow for the formation of the E-I complex. The inhibition constants were obtained by non-linear least-squares methods using PRISM 3 and the Cheng-Prusoff equation, as reported earlier, and represent the mean from at least three different determinations. All CA isofoms were recombinant ones obtained in-house as reported earlier.

5.2.3 Co-crystallization and X-ray Data Collection.

Crystals of native hCA II were obtained using the hanging drop vapor diffusion method. Then, 2μL of the protein solution were mixed with 2μL of a solution of 1.6 M sodium citrate and 50 mM Tris pH 8.0 and were equilibrated against the same solution at 296 K. Protein concentration was 0.4 mM in 50 mM Tris pH = 8.0. Crystals of the complex with 8a were obtained by soaking the hCAII crystals in a saturated solution of the compound dissolved in 1.2 M sodium citrate, 50 mM Tris pH 8.0, and 15% glycerol. A crystal of the complex was harvested from this solution andflashfrozen at 100 K. A data set on a crystal of the complex hCAII-inhibitor was collected to a maximum resolution of 1.10 Å, using synchrotron radiation at the ID23-1 beamline at ESRF (Grenoble, France) with a wavelength of 1.000 Å and a DECTRIS Pilatus 6 M detector. Data were integrated and scaled using the program XDS. Data processing

5.2.4 Structure Determination.

The crystal structure of hCA II (PDB code: 3P58) without solvent molecules and other heteroatoms was used to obtain initial phases of the structures using Refmac5 37 then 5% of the unique reflections were selected randomly and excluded fromthe refinement data set for the purpose of R free calculations. Inspection of the difference electron-density maps indicated the presence of an inhibitor molecule bound to the water that coordinate the catalytic zinc ion. Atomic models for the inhibitor were calculated and energy minimized using the program JLigand 1.0.39. A fractional occupancy factor of 0.5 was attributed to all the inhibitor atoms. After the introduction of the inhibitor, positive residual densities were present in the difference electron-density maps close to the inhibitor and were attributed to disordered water molecules (occupancy factors 0.5).During the refinement, anisotropic temperature factors were introduced and hydrogen atoms were added to the model. Manual building of the atomic model were carried out using COOT 38 Solvent molecules were introduced automatically using the program ARP working in the default solvent building mode. Graphical representations were generated with Chimera.

5.2.5 *In vitro* Telomerase Activity Assay

ZT and BIBR1532 (R&D Systems, Minneapolis, MN) were dissolved in dimethyl sulfoxide (DMSO) at stock concentrations of 10 mM and further diluted to appropriate concentrations in assay buffer. Telomerase activity was determined using the Telomeric Repeat Amplification Protocol (TRAP) [4] with modifications previously described by us [5,6]. Briefly, Jurkat cells (T cell leukemia cell line, ATCC, Manassas, VA) were lysed in 10 mM Tris-HCl, pH 7.5, 1 mM MgCl2, 1 mM EGTA, 0.1 mM PMSF, 5 mM 2-Mercaptoethanol, 0.5% CHAPS and 10% glycerol (all from Sigma-Aldrich, St. Louis, MO) and centrifuged for 30 min at 12000xg. Supernatants were stored at −80 °C. The protein concentration of cell extracts was determined using BCA-1 Protein Assay Kit (Sigma-Aldrich, St. Louis, MO). For elongation reaction 5 μg of total protein and appropriate concentrations of AZT and BIBR1532 were added to 30-μl of reaction mixture containing 67 mM Tris-HCl, pH 8.8, 16.6 mM (NH4)2SO4, 0.01% Tween-20, 1.5 mM MgCl2, 1 mM EGTA (all from Sigma-Aldrich, St. Louis, MO), 0.25 mM each dNTPs (Evrogen, Moscow, Russia) and Telomerase Substrate primer (TS-primer) (5′-AATCCGTCGAGCAGAGTT −3′). Elongation was performed for 30 min at 37 °C and 10 min at 96 °C to inactivate the telomerase. Copy Extended primer CX-primer, 0.1 μl) (5′-CCCTTACCCTTACCCTTACCCTAA −3′) and 2.5 Units of Taq-polymerase were added to the elongation mixture followed by the following PCR reaction: 94° C − 5 min; 30 cycles of 94° C − 30 s, 50 °C − 30 s, and 72° C − 40 s; and 72° C − 5 min. PCR product visualization was performed using 12% non-denaturing PAAG electrophoresis and TBE buffer. Ten microliters of each sample were added to each well of the gel comb. Gels were stained with SYBR Green I (Invitrogen, Grand Island, NY), photographed under UV light in a ChemiDoc™ XRS imaging system and analyzed using a GelAnalyzer 2010a. Statistical analysis involving the Student's t-test was implemented with the Statistica 6.0 software (StatSoft, Tulsa, OK). Differences described by $p \leq 0.05$ were considered significant. The results are presented as mean ± standard error of mean (SEM).

To determine IC50 and IC90 values (inhibitor concentration where the response is reduced by 50% and 90% respectively) 1 μL of were subjected to Real-Time Quantitative Telomeric Repeat

Amplification Protocol Assay (RTQ-TRAP) as described by Hou M. and co-authors [7]. The values were calculated using Prism 6 software (GraphPad, San Diego, CA) according to recommendations by Sebaugh J.L. and co-authors [8].

References

1. Supuran CT; Dedhar S; Carta F, Carbonic Anhydrase Inhibitors With Antimetastatic Activity,WO2012070024 (A1) 2012-05-31
2. Kosiova I, Kovackova S, Kois P, Synthesis of coumarin–nucleoside conjugates via Huisgen 1,3-dipolar cycloaddition, Tetrahedron 2007, 63,2, 312-320
3. Khalifah RG. The carbon dioxide hydration activity of carbonic anhydrase. I. Stop-flow kinetic studies on the native human isoenzymes B and C. J Biol Chem. 1971, 246, 2561-2573
4. Zhdanov DD, Vasina DA, Grachev VA, Orlova EV, Orlova VS, Pokrovskaya MV, Alexandrova SS, Sokolov NN. Alternative splicing of telomerase catalytic subunit hTERT generated by apoptotic endonuclease EndoG induces human CD4+ T cell death, Eur. J Cell Biol. 2017, 96, 653-664.
5. Kovalenko A, Zhdanov DD, Bibikova MV, et al., The influence of compound aITEL1296 on telomerase activity and growth of cancer cells, Biochem. Suppl. Ser. B Biomed Chem. 2012, 6, 48–54.
6. Hou M, Xu D, Björkholm M, Gruber A, Real-time quantitative telomeric repeat amplification protocol assay for the detection of telomerase activity. Clin Chem. 2001, 47, 2519-2524.
7. Sebaugh J.L., Guidelines for accurate EC50/IC50 estimation. Pharm Stat. 2011, 10, 128–134
8. Barma D.K., Elayadi A., Falck J., Corey D.R., Inhibition of telomerase by BIBR 1532 and related analogues. Bioorg Med Chem Lett. 2003, 13, 1333–1336.

5.3 Experimental Section : Chapter 4

5.3.1 Chemistry

All reactions involving air- or moisture-sensitive compounds were performed under an argon atmosphere using dried glassware and syringes techniques to transfer solutions. Reactions performed in superacid were carried out in a sealed Teflon® flask with a magnetic stirrer. No further precautions have to be taken to prevent mixture from moisture (test reaction worked out in anhydrous conditions leads to the same results as expected). Yields refer to isolated pure products.^{1}H, ^{13}C and ^{19}F NMR were recorded on a 400 MHz Bruker Advance DPX spectrometer using $CDCl_3$, or CD_3OD as solvent. COSY ^{1}H-^{1}H and ^{1}H-^{13}C experiments were used to confirm the NMR peaks assignments.Chemical shifts are reported in parts per million (ppm) and the coupling constants (J) are expressed in Hertz (Hz). Splitting patterns are designated as follows: s, singlet; d, doublet; t, triplet; q, quadruplet; p, pentet; m, multiplet; brs, broad singlet; dd, double of doublets. The mass spectra were obtained using a 1200 L triple quadrupole system (Varian, Palo Alto, CA, USA) equipped by Electrospray Source (ESI) operating in both positive and negative ions. Stock solutions of analytes were prepared in acetone at 1.0 mg mL^{-1} and stored at 4 °C. Working solutions of each analyte were freshly prepared by diluting stock solutions in a mixture of mQ H_2O/CH_3CN 1:1 (v/v) up to a concentration of 1.0 μg mL^{-1}. The mass spectra of each analyte were acquired by introducing, via syringe pump at 10 μL min^{-1}, the working solution. Raw-data were collected and processed by Varian Workstation Vers. 6.8 software. pKa predictions were performed using Schrödinger Suite Release 2019-1, Schrödinger, LLC, New York, NY, 2019 (a) Epik, v.4.7; (b) Jaguar, v10.3.

Synthesis of compounds f and g

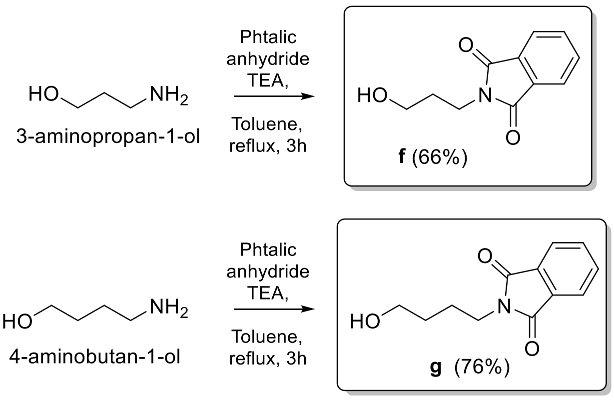

2-(3-hydroxypropyl)isoindoline-1,3-dione f. A mixture of 3-aminopropan-1-ol (2g, 1 eq), phtalic anhydride (1 eq) and TEA (0.5 eq) in toluene (40 ml) was heated at reflux in a flask fitted with Dean-Stark apparatus for 3h (TLC monitoring). When the SM was consumed, reaction was cooled at r.t. and the solvent was evaporated under reduced pressure. The residue was suspended in EtOAc and washed with HCl 2M aq solution, $NaHCO_3$ aq. s.s.and water. The organic phase was then dried over $MgSO_4$, filtered and evaporated, obtaining a white residue that was crystalized from EtOAc/Hexane, affording to compound **f** as white crystals, pure. 66% yield; silica gel TLC R*f* =0.51 (EtOAc/n- Hex 60% v/v); δ_H (400 MHz, $CDCl_3$): 1.87 (2H, p, *J*= 6.02, C*H*2), 3.61 (2H, t, *J*= 5.8, C*H*2), 3.84 (2H, t, *J*= 6.35, 5.62, C*H*2), 7.72 (2H, dd, *J*= 5.6, 2.9, Ar-*H*), 7.84 (2H, dd, *J*= 5.2, 2.9, Ar-*H*); δ_C (100 MHz, $CDCl_3$): 31.5 (CH_2), 34.4 (CH_2), 59.2 (CH_2), 123.4 (CH), 132.1 (C), 134.2 (CH), 168.9 (C). Experimental in agreement with reported data. [1]

2-(4-hydroxybutyl)isoindoline-1,3-dione g. Compound **g** were obtained following the procedure above reported, using 4-aminobutan-1-ol as starting material. 76% yield; silica gel TLC R*f* =0.46 (EtOAc/n- Hex 60% v/v); δ_H (400 MHz, $CDCl_3$): 1.60 (2H, h, *J*= 6.7, C*H*2), 1.76 (2H, p, *J*= 7.4, C*H*2), 3.67 (2H, t, *J*= 6.4, C*H*2), 3.71 (2H, t, *J*= 7.1, C*H*2), 7.69 (2H, dd, *J*= 5.47, 3.01, Ar-*H*), 7.82 (2H, dd, *J*= 5.41, 3.01, Ar-*H*); δ_C (100 MHz, $CDCl_3$): 25.2 (CH_2), 29.8 (CH_2), 37.8 (CH_2), 62.3 (CH_2), 123.3 (CH), 132.2 (C), 134.0 (CH), 168.6 (C). Experimental in agreement with reported data. [1]

Synthethic Scheme for the preparation of derivatives 152-166.

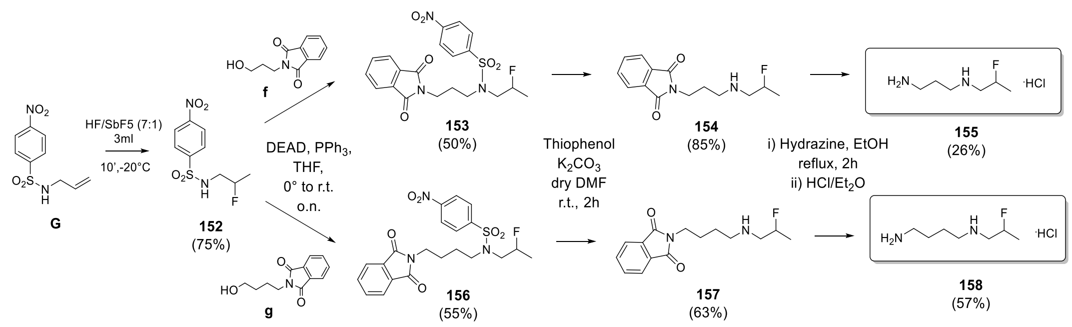

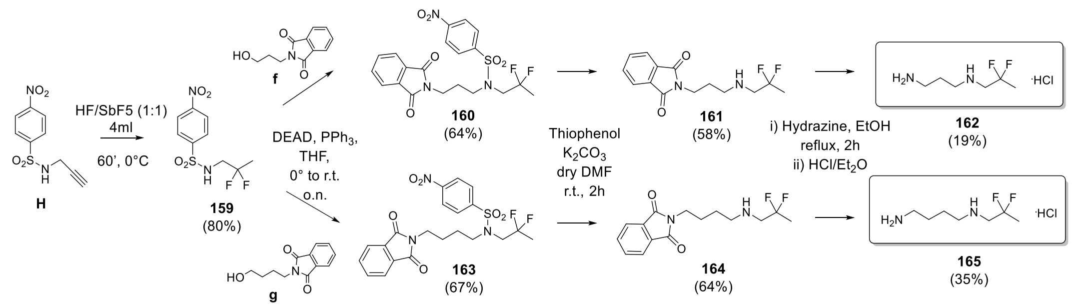

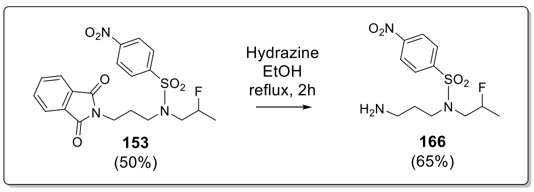

Synthethic Scheme for the preparation of derivatives 167-174.

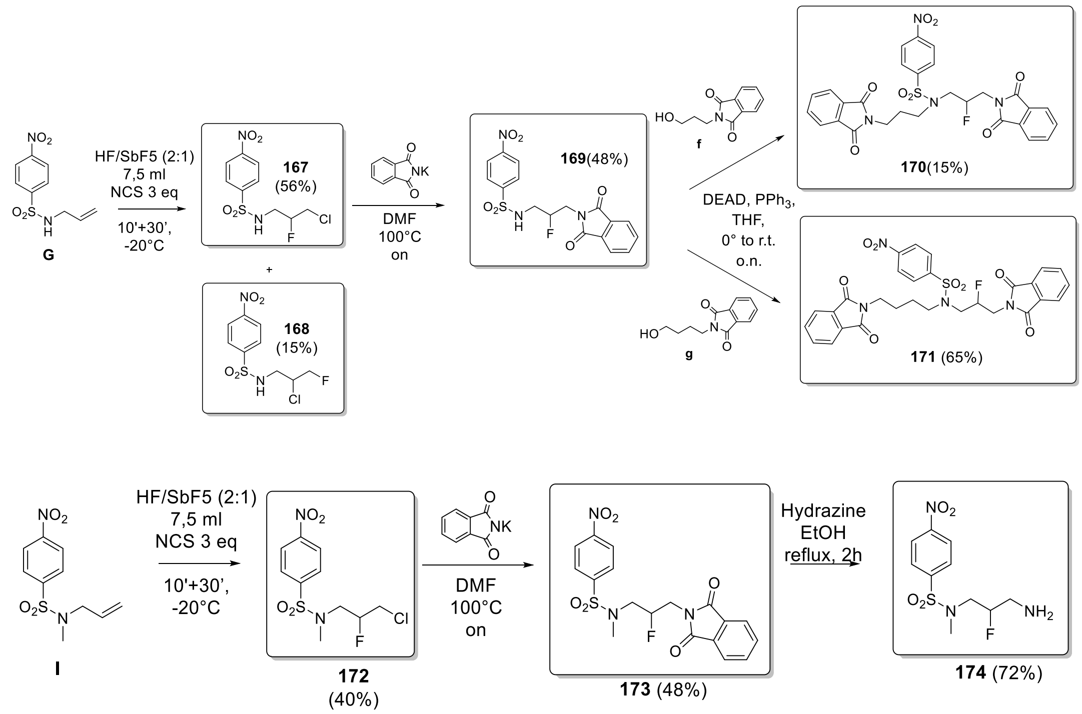

General procedure E [2,3]: To a solution of allylamine (or propargylamine, or N-methyl allylamine, 1g, 1.1 eq) and TEA (1 eq) in DCM (25 ml), p-nitrobenzen-sulfonyl chloride (1 eq) was added portionwise at 0°C. Reaction was stirred for 2h at r.t., until consumption of s.m. (TLC monitoring). Reaction was quenched with $NaHCO_3$ s.s., extracted with DCM (x2) and washed with brine, dried over $MgSO_4$, filtered and evaporated, affording to the product as yellow solid, pure.

General procedure F[4]: To an HF/SbF_5 mixture (3 mL, 2/1 molar ratio, 12.1 mol % SbF5) in a Teflon® reactor at–20°C, 3 equiv of NCS were added portionwise. After 10 min of stirring, the substrate was slowly added. The mixture was magnetically stirred at the same temperature for 30 min, then neutralized with water/ice/Na_2CO_3 up to pH 10 and extracted with DCM (x3). The combined organic phases were dried over $MgSO_4$, filtered and concentrated in vacuo. The product was purified by combiflash eluting with 20% EtOAc/PE, affording to the product as white solid.

General procedure G [5]: To a mixture of amine (2 mmol, 1 eq), alcohol (1.1 eq) and PPh_3 (1.2 eq) in THF dry (8 ml), DEAD (1.2 eq) was added at 0°C. The mixture was stirred at the same temperature for 10', then warmed gradually at r.t. over night. The solvent was evaporated and the residue portioned between water and EtOAc. Extracted with EtOAc, washed with brine, dried over $MgSO_4$, filtered and concentrated in vacuo, affording a yellow residue. Purified by combiflash, eluting with EtOAc/PE, affording to the product as white solid.

General procedure H [6]: Starting material (0.7 mmol, 1 eq) was solubilized in DMF dry (3 ml) and the solution cooled to 0°C. Then, K_2CO_3 (3 eq) and thiophenol (1.2 eq) were added. The reaction was stirred at r.t. until consumption of s.m. (2h). The reaction was diluted with EtOAc and extracted with HCl (2 N aq sol) (x3). Water phases were washed with EtOAc (x1), then neutralized with Na_2CO_3 until pH 9. The basic solution was extracted with Et_2O (x3). The organic phases were collected together and washed with Na_2CO_3 s.s., dried over Na_2SO_4, filtered and evaporated, affording to the desired product, pure.

General procedure I: Starting material (0.1 g, 1 eq) was solubilized in EtOH (10 ml) and $N_2H_4 \cdot H_2O$ (65%, 10 eq) was added. The reaction was stirred at reflux until consumption of s.m (2h). Reaction was cooled at r.t. and the insoluble residues were filtered off. The solvent was evaporated under reduced pressure and further co-evaporated with toluene and pentane. The residue was taken up with Et_2O, assisting to the formation of a precipitate that was filtered. For compounds **166 and 174** the solvent was evaporated and the residual oil solubilized in Et_2O assisting to the further formation of a precipitate. The Et_2O was removed and evaporated, affording to the product, pure. For compounds **155, 158, 162, 165** the solvent was evaporated and the residual oil solubilized in Et_2O and cooled to 0°C. Then, HCl 1M in Et_2O was added dropwise (3 eq ca.), assisting to the formation of a white precipitate. The Et_2O was removed and the white solid dried, affording to the desired product as HCl salt.

Synthesis of compound 152: hydrofluorination reaction [7]

N-(2-fluoropropyl)-4-nitrobenzenesulfonamide 152. To an HF/SbF_5 mixture (3 mL, 7/1 molar ratio, 4 mol % SbF5) in a Teflon® reactor at –20°C, N-allyl-4-nitrobenzenesulfonamide (1 mmol, 242 mg) was slowly added. The mixture was magnetically stirred for 10 min at the same temperature, then neutralized with water/ice/Na_2CO_3 up to pH 10 and extracted with DCM (x3). The combined organic phases were dried over $MgSO_4$, filtered and concentrated in vacuo, affording to a yellow solid, pure. 75% yield; silica gel TLC R*f* =0.28 (EtOAc/n- Hex 20% v/v); δ_H (400 MHz, $CDCl_3$): 1.32 (3H, dd, *J* = 23.8, 6.3, C*H*$_3$), 3.10 (1H, dddd, *J* = 18.6, 13.9, 7.6, 4.9, C*H*), 3.31 (1H, dddd, *J* = 28.3, 13.8, 7.6, 2.8, C*H*), 4.72 (1H, dm, *J* = 48.9, C*H*), 5.08 (1H, brt, N*H*), 8.06 (2H, d, *J* = 8.9, Ar-*H*), 8.38 (d, *J* = 8.8, Ar-*H*); δ_C (100 MHz, $CDCl_3$): 18.15 (d, CH_3, *J* = 21.7). 48.40 (d, CH_2, *J* = 20.9), 89.20 (d, CHF, *J* = 168.7), 124.62 (CH), 128.38 (CH), 146.05 (C), 150.32 (C); δ_F (376 MHz, $CDCl_3$): -180.0; *m/z* (ESI negative) 260.9 $[M-H]^-$. Experimental in agreement with reported data [6].

Synthesis of compound 159: *gem*-difluorination reaction

N-(2,2-difluoropropyl)-4-nitrobenzenesulfonamide 159. To an HF/SbF_5 mixture (4 mL, 1/1 molar ratio, 22 mol % SbF5) in a Teflon® reactor, 4-nitro-N-(prop-2-yn-1-yl)benzenesulfonamide (1 mmol, 240 mg) was slowly added al 0°C. The mixture was magnetically stirred at the same temperature for 60 min, then neutralized with water/ice/Na_2CO_3 up to pH 10 and extracted with DCM (x3). The combined organic phases were dried over $MgSO_4$, filtered and concentrated in vacuo, affording to a yellow solid, pure. 80% yield; silica gel TLC R*f* =0.35 (EtOAc/PE 20% v/v); δ_H (400 MHz, $CDCl_3$): 1.62 (3H, t, *J* = 19.6, C*H*$_3$), 3.44 (2H, td, *J* = 13.3, 6.6, C*H*$_2$), 5.06 (1H, t, *J* = 6.9, N*H*), 8.06 (2H, d, *J* = 8.9, Ar-*H*), 8.38 (2H, d, *J* = 8.8, Ar-*H*); δ_C (100 MHz, $CDCl_3$): 21.35 (t, CH_2, *J* = 26.1), 48.40 (t, CH_3, *J* = 29.9), 121.37 (t, CF_2, *J* = 240.1), 124.6 (CH), 128.38 (CH), 146.0 (C), 150.29 (C); δ_F (376 MHz, CDCl3): -96.9.

N-allyl-4-nitrobenzenesulfonamide G: Obtained following using the **procedure E** above reported, using allylamine as starting material. 85% yield; R*f* =0.23 (EtOAc/n- Hex 20% v/v); δ_H (400 MHz, $CDCl_3$): 3.68 (2H, dt, *J*=5.75, 1.52, C*H*$_2$), 4.85 (1H, brs, N*H*), 5.16 (2H, m, C*H*$_2$), 5.71 (1H, ddt, *J*=17.2, 10.25, 5.80, C*H*), 8.07 (2H, d, *J*=8.80, Ar-*H*), 8.37 (2H, d, *J*=8.96, Ar-*H*); Experimental in agreement with reported data. [2]

N-allyl-N-methyl-4-nitrobenzenesulfonamide I: Obtained using the **procedure E** above reported, using N-methyl allylamine as starting material. 97% yield; silica gel TLC R*f* =0.56 (EtOAc/n- Hex 20% v/v); δ_H (400 MHz, $CDCl_3$): 2.75 (3H, s, C*H*$_3$), 3.71 (2H, d, *J*=5.61, C*H*$_2$), 5.22 (2H, m, C*H*$_2$), 5.68 (1H, ddt, *J*=16.62, 10.24, 6.30), 7.98 (2H, d, *J*=8.92, Ar-*H*), 8.38 (2H, d, *J*=8.79, Ar-*H*). Experimental in agreement with reported data.

4-nitro-N-(prop-2-yn-1-yl)benzenesulfonamide H: Obtained using the **procedure E** above reported, using propargylamine as starting material. 80% yield; silica gel TLC R*f* =0.33 (EtOAc/n- Hex 20% v/v); δ_H (400 MHz, $CDCl_3$): 2.09 (1H, t, *J*=2.55, C*H*), 3.97 (2H, dd, *J*=6.14, 2.53, C*H*$_2$), 4.75 (1H, brt, N*H*), 8.10 (2H, d, *J*=8.84, Ar-*H*), 8.38 (2H, d, *J*=8.81, Ar-*H*). Experimental in agreement with reported data. [3].

N-(3-chloro-2-fluoropropyl)-4-nitrobenzenesulfonamide 167. Synthesized according to the **procedure F** using N-allyl-4-nitrobenzenesulfonamide as starting material. 56% yield; silica gel TLC R*f* =0.26 (EtOAc/PE 20% v/v); δ_H (400 MHz, $CDCl_3$): 3.43 (2H, m, C*H*$_2$), 3.66 (2H, m, C*H*$_2$), 4.77 (1H, dm, *J*= 46.84, C*H*), 4.91 (1H, brt, N*H*), 8.07 (2H, d, *J*=8.93, Ar-*H*), 8.39 (2H, d, *J*=8.89, Ar-*H* δ_C (100 MHz, $CDCl_3$): 42.0 (d, CH_2, *J* = 26.0), 44.3 (d, CH_2, *J* = 22.12), 90.2 (d, CHF, *J* = 178.0), 124.6 (CH), 128.3 (CH), 145.6 (C), 150.3 (C); δ_F (376 MHz, $CDCl_3$): -186.6; *m/z* (ESI negative) 294.9 $[M-H]^-$. Experimental in agreement with reported data. [4]

N-(2-chloro-3-fluoropropyl)-4-nitrobenzenesulfonamide 168: Synthesized according to the **procedure F** using N-allyl-4-nitrobenzenesulfonamide as starting material. 15% yield; silica gel TLC R*f* =0.29 (EtOAc/PE 20% v/v); δ_H (400 MHz, $CDCl_3$): 3.35 (1H, td, *J* = 14.0, 6.9 C*H*), 3.54 (1H, td, *J* = 11.3, 4.4, C*H*), 4.16 (1H, dtt, *J* = 15.7, 6.8, 4.5, C*H*), 4.46 (1H, ddd, *J* = 46.7, 10.0, 6.6, C*H*), 4.61 (1H, ddd, *J* = 46.4, 10.0, 4.4 Hz, C*H*), 5.07 (1H, brt, N*H*), 8.08 (2H, d, *J* = 8.9, Ar-*H*), 8.40 (d, *J* = 8.9, Ar-*H*); δ_C (100 MHz, $CDCl_3$): 45.8 (d, CH_2, *J* = 4.32), 56.6 (d, CH, *J* = 22.12), 82.5 (d, CH_2F, *J* = 177.26), 124.7 (CH), 128.5 (CH), 145.7 (C), 150.5 (C); δ_F (376 MHz, $CDCl_3$): -219.8; *m/z* (ESI negative) 294.9 $[M-H]^-$. Experimental in agreement with reported data. [4].

N-(3-chloro-2-fluoropropyl)-N-methyl-4-nitrobenzenesulfonamide 172: Synthesized according to the **procedure F** using N-allyl-N-methyl-4-nitrobenzenesulfonamide as starting material. 40% yield; silica gel TLC R*f* =0.32 (EtOAc/PE 20% v/v; δ_H (400 MHz, $CDCl_3$): 2.95 (3H, s, C*H*$_3$), 3.45 (2H, m, C*H*$_2$), 3.75 (2H, m, C*H*$_2$), 4.90 (1H, dm, *J* = 47.1, C*H*), 8.00 (2H, d, *J* = 8.7, Ar-*H*), 8.41 (2H, d, *J* = 8.8, Ar-*H*); δ_C (100 MHz, $CDCl_3$): 37.02 (CH_3), 43.11 (d, CH_2, *J*= 24.32), 51.48 (d, CH_2, *J*= 23.0), 91.07 (d, CH, *J*= 180.21, CH), 124.6 (CH), 128.6 (CH), 143.3 (C), 150.3 (C); δ_F (376 MHz, $CDCl_3$): -184.6; *m/z* (ESI negative) 355.0 $[M+HCOO]^-$.

N-(3-(1,3-dioxoisoindolin-2-yl)propyl)-N-(2-fluoropropyl)-4-nitrobenzenesulfonamide 153: Synthesized according to the **procedure G** using N-(2-fluoropropyl)-4-nitrobenzenesulfonamide **152** and 2-(3-hydroxypropyl)isoindoline-1,3-dione **f** as starting materials. 50% yield; silica gel TLC R*f* =0.33 (EtOAc/PE 30% v/v); δ_H (400 MHz, $CDCl_3$): 1.33 (3H, dd, *J* = 23.6, 6.3, C*H*$_3$), 2.00 (2H, p, *J* = 7.4, C*H*$_2$), 3.37 (4H, m, 2x C*H*$_2$), 3.68 (2H, td, *J* = 7.0, 1.5, C*H*$_2$), 4.81 (1H, dm, *J* = 49.6, C*H*), 7.73 (2H, dd, *J* = 5.4, 3.0, Ar-*H*), 7.84 (2H, dd, *J* = 5.4, 3.0, Ar-*H*), 7.97 (2H, d, *J* = 8.8, Ar-*H*), 8.35 (2H, d, *J* = 9.1, Ar-*H*); δ_C (100 MHz, $CDCl_3$): 18.54 (d, CH_3, *J* = 22.0), 27.7 (CH_2), 35.4 (CH_2), 47.3 (CH_2), 53.2, (d, CH_2, *J* = 21.77), 89.8 (d, CHF, *J* = 170.15), 123.5 (CH), 124.6 (CH), 128.4 (CH), 132.0 (C), 134.3 (CH), 145.5 (C), 150.1 (C), 168.4 (C); δ_F (376 MHz, $CDCl_3$): -176.2; *m/z* (ESI positive) 450.1 $[M+H]^+$.

N-(4-(1,3-dioxoisoindolin-2-yl)butyl)-N-(2-fluoropropyl)-4-nitrobenzenesulfonamide 156: Synthesized according to the **procedure G** using N-(2-fluoropropyl)-4-nitrobenzenesulfonamide **152** and 2-(4-hydroxybutyl)isoindoline-1,3-dione **g** as starting materials. 55% yield; silica gel TLC R*f* =0.2 (EtOAc/PE 20% v/v); δ_H (400 MHz, $CDCl_3$): 1.33 (3H, m, C*H*$_3$), 1.64 (4H, m, 2x C*H*$_2$), 3.33 (4H, m, 2x C*H*$_2$), 3.68 (2H, t, *J* = 6.5, C*H*$_2$), 4.81 (1H, dm, *J* = 49.7, C*H*), 7.72 (2H, dd, *J* = 5.5, 3.0, Ar-*H*), 7.83 (2H, dd, *J* = 5.4, 3.0, Ar-*H*), 7.99 (2H, d, *J* = 8.8, Ar-*H*), 8.33 (2H, d, *J* = 8.7, Ar-*H*); δ_C (100 MHz, $CDCl_3$): 18.57 (d, CH_3, *J* = 22.0), 25.4 (CH_2), 25.6 (CH_2), 37.2 (CH_2), 48.9 (CH_2), 53.1, (d, CH_2, *J* = 21.36), 89.6 (d, CHF, *J* = 170.82), 123.4 (CH), 124.5 (CH), 128.4 (CH), 132.0 (C), 134.2 (CH), 145.8 (C), 150.0 (C), 168.5 (C); δ_F (376 MHz, $CDCl_3$): -176.3; *m/z* (ESI positive) 464.1 $[M+H]^+$.

N-(2,2-difluoropropyl)-N-(3-(1,3-dioxoisoindolin-2-yl)propyl)-4-nitrobenzenesulfonamide 160. Synthesized according to the **procedure G** using N-(2,2-difluoropropyl)-4-nitrobenzenesulfonamide **159** and 2-(3-hydroxypropyl)isoindoline-1,3-dione **f** as starting materials. Purified by combiflash, eluting with 25% EtOAc/PE; triturated from Et_2O. 64% yield; silica gel TLC R*f* =0.56 (EtOAc/PE 30% v/v); δ_H (400 MHz, $CDCl_3$): 1.68 (3H, t, *J* = 18.8, C*H*$_3$), 2.0 (2H, p, *J* = 7.0, C*H*$_2$), 3.36 (2H, t, *J* = 7.7, C*H*$_2$), 3.63 (2H, t, *J* = 13.2, C*H*$_2$), 3.66 (2H, t, *J* = 6.9, C*H*$_2$), 7.74 (2H, dd, *J* = 5.5, 3.1, Ar-*H*), 7.85 (2H, dd, *J* = 5.4, 3.0, Ar-*H*), 7.97 (2H, d, *J* = 8.7, Ar-*H*), 8.34 (2H, d, *J* = 8.8, Ar-*H*); δ_C (100 MHz, $CDCl_3$): 21.74 (t, CH_3, *J* = 25.8), 27.4 (CH_2), 35.3 (CH_2), 47.5 (CH_2), 52.27 (t, CH_2, *J* = 30.5), 122.83 (t, CF_2, *J*= 240.7), 123.5 (CH), 124.6 (CH), 128.6 (CH), 132.0 (C), 134.3 (CH), 145.2 (C), 150.3 (C), 168.4 (C); δ_F (376 MHz, $CDCl_3$): -93.2; *m/z* (ESI positive) 468.1 $[M+H]^+$.

N-(2,2-difluoropropyl)-N-(4-(1,3-dioxoisoindolin-2-yl)butyl)-4-nitrobenzenesulfonamide 163: Synthesized according to the **procedure G** using N-(2,2-difluoropropyl)-4-nitrobenzenesulfonamide **159** and. 2-(4-hydroxybutyl)isoindoline-1,3-dione **g** as starting materials. Purified by combiflash, eluting with 25% EtOAc/PE; triturated from Et_2O. 67% yield; silica gel TLC R*f* =0.26 (EtOAc/PE 20% v/v); δ_H (400 MHz, $CDCl_3$): 1.63 (4H, m, 2x C*H*$_2$), 1.70 (3H, t, *J* = 18.8, C*H*$_3$), 3.33 (2H, t, *J* = 7.1, 6.5, C*H*$_2$), 3.62 (2H, t, *J* = 13.3, C*H*$_2$), 3.67 (2H, t, *J* = 6.5, C*H*$_2$), 7.73 (2H, dd, *J* = 5.5, 3.0, Ar-*H*), 7.84 (2H, dd, *J* = 5.4, 3.1, Ar-*H*), 8.0 (2H, d, *J* = 8.9, Ar-*H*), 8.34 (2H, d, *J* = 8.9, Ar-*H*); δ_C (100 MHz, $CDCl_3$): 21.70 (t, CH_3, *J* = 25.8), 25.0 (CH_2), 26.0 (CH_2), 37.1 (CH_2), 49.2 (CH_2), 52.03 (t, CH_2, *J* = 30.3), 122.89 (t, CF_2, *J*= 240.0), 123.3 (CH), 124.4 (CH), 128.5 (CH), 131.9 (C), 134.1 (CH), 145.5 (C), 150.0 (C), 168.4 (C); δ_F (376 MHz, $CDCl_3$): -93.2; *m/z* (ESI positive) 482.1 $[M+H]^+$.

N-(3-(1,3-dioxoisoindolin-2-yl)-2-fluoropropyl)-N-(3-(1,3-dioxoisoindolin-2-yl)propyl)-4-nitrobenzenesulfonamide 170: Synthesized according to the **procedure G** using N-(3-(1,3-dioxoisoindolin-2-yl)-2-fluoropropyl)-4-nitrobenzenesulfonamide **169** and 2-(3-hydroxypropyl)isoindoline-1,3-dione **f** as starting materials. Purified by combiflash, eluting with 40% EtOAc/PE. 14.7% yield; silica gel TLC R*f* =0.42 (EtOAc/PE 40% v/v); δ_H (400 MHz, $CDCl_3$): 2.02 (2H, td, *J* = 14.1, 6.6, C*H*$_2$), 3.28 (1H, m, C*H*), 3.43 (2H, m, 2x C*H*), 3.68 (3H, m, C*H*$_2$, C*H*), 3.85 (1H, m, C*H*), 4.02 (1H, td, *J* = 15.5, 7.2, C*H*), 4.92 (1H, dm, *J* = 49.3, C*H*), 7.72 (2H, dd, *J* = 5.5, 3.0, Ar-*H*), 7.75 (2H, dd, *J* = 5.5, 3.0, Ar-*H*), 7.82 (2H, dd, *J* = 5.5, 3.1, Ar-*H*), 7.86 (dd, *J* = 5.5, 3.1, Ar-*H*), 7.96 (2H, d, *J* = 8.8, Ar-*H*), 8.33 (2H, d, *J* = 8.8, Ar-*H*); δ_C (100 MHz, $CDCl_3$): 27.7 (CH_2), 35.4 (CH_2), 39.5 (d, CH_2, *J* = 23.82), 47.5 (CH_2), 50.3 (d, CH_2, *J* = 21.25), 90.12 (d, CHF, *J* = 179.2), 123.5 (CH), 123.7 (CH), 124.7 (CH), 128.5 (CH), 131.9 (C), 132.0 (C), 134.2 (CH), 134.5 (CH), 145.0 (C), 150.2 (C), 168.0 (C), 168.4 (C); δ_F (376 MHz, $CDCl_3$): -187.7;*m/z* (ESI positive) 595.1 $[M+H]^+$.

N-(3-(1,3-dioxoisoindolin-2-yl)-2-fluoropropyl)-N-(4-(1,3-dioxoisoindolin-2-yl)butyl)-4-nitrobenzenesulfonamide 171: Synthesized according to the **procedure G** using N-(3-(1,3-dioxoisoindolin-2-yl)-2-fluoropropyl)-4-nitrobenzenesulfonamide **169** and 2-(4-hydroxybutyl)isoindoline-1,3-dione **g** as starting materials. Purified by combiflash, eluting with 40% EtOAc/PE. 65% yield; silica gel TLC R*f* =0.34 (EtOAc/PE 40% v/v); δ_H (400 MHz, $CDCl_3$): 1.66 (4H, m, 2x C*H*$_2$), 3.22 (1H, ddd, *J* = 13.9, 8.1, 4.8, C*H*), 3.42 (2H, m, 2x C*H*), 3.67 (3H, m, C*H*$_2$, C*H*), 3.86 (1H, ddd, *J* = 23.8, 14.6, 4.2, C*H*), 4.03 (td, *J* = 15.1, 7.3, C*H*), 4.93 (1H, dm, *J* = 49.1, C*H*), 7.71 (2H, dd, *J* = 5.5, 3.0, Ar-*H*), 7.76 (2H, dd, *J* = 5.5, 3.0, Ar-*H*), 7.82 (2H, dd, *J* = 5.5, 3.0, Ar-*H*), 7.87 (2H, dd, *J* = 5.4, 3.0, Ar-*H*), 7.99 (2H, d, *J* = 8.7, Ar-*H*), 8.34 (2H, d, *J* = 8.9, Ar-*H*); δ_F (376 MHz, $CDCl_3$): -187.8; *m/z* (ESI positive) 609.1 $[M+H]^+$.

2-(3-((2-fluoropropyl)amino)propyl)isoindoline-1,3-dione 154: Synthesized according to the **procedure H** using N-(3-(1,3-dioxoisoindolin-2-yl)propyl)-N-(2-fluoropropyl)-4-nitrobenzenesulfonamide **153** as starting material. 85% yield; silica gel TLC R*f* =0.47 (MeOH/DCM 5% v/v); δ_H (400 MHz, $CDCl_3$): 1.31 (3H, dd, *J* = 23.9, 6.3, C*H*$_3$), 1.87 (2H, p, *J* = 6.9 Hz, C*H*$_2$), 2.73 (4H, m, 2x C*H*$_2$), 3.78 (2H, t, *J* = 6.9, C*H*$_2$), 4.75 (1H, dm, *J* = 49.5, C*H*), 7.71 (2H, dd, *J* = 5.5, 3.0, Ar-*H*), 7.84 (2H, dd, *J* = 5.4, 3.0, Ar-*H*); δ_C (100 MHz, $CDCl_3$): 18.95 (d, CH_3, *J* = 22.1), 29.03 (CH_2), 35.98 (CH_2), 47.01 (CH_2), 55.30 (d, CH_2, *J* = 21.03), 90.44 (d, CHF, *J* = 164.6), 123.34 (CH), 132.2 (C), 134.1 (CH), 168.6 (C); δ_F (376 MHz, $CDCl_3$): -178.9; *m/z* (ESI positive) 265.1 $[M+H]^+$.

2-(4-((2-fluoropropyl)amino)butyl)isoindoline-1,3-dione 157: Synthesized according to the **procedure H** using N-(4-(1,3-dioxoisoindolin-2-yl)butyl)-N-(2-fluoropropyl)-4-nitrobenzenesulfonamide **156** as starting material. 63% yield; silica gel TLC R*f* =0.43 (MeOH/DCM 5% v/v); δ_H (400 MHz, $CDCl_3$): 1.30 (3H, dd, *J* = 23.9, 6.3, C*H*$_3$), 1.53 (2H, m, C*H*$_2$), 1.72 (2H, tt, J = 7.9, 6.4, C*H*$_2$), 2.65 (2H, m, C*H*$_2$), 2.78 (2H, ddd, *J* = 16.9, 13.0, 8.1, C*H*$_2$), 4.76 (dm, *J* = 49.6, C*H*), 7.70 (2H, dd, *J* = 5.5, 3.0, Ar-*H*), 7.82 (2H, dd, *J* = 5.4, 3.0, Ar-*H*); δ_C (100 MHz, $CDCl_3$): 18.97 (d, CH_3, *J* = 22.1), 26.4 (CH_2), 27.4 (CH_2), 37.9 (CH_2), 49.4 (CH_2), 55.4 (d, CH_2, *J* = 21.0), 90.44 (d, CHF, *J* = 164.5), 123.3 (CH), 132.2 (C), 134.0 (CH), 168.6 (C); δ_F (376 MHz, $CDCl_3$): -179.0; *m/z* (ESI positive) 279.1 $[M+H]^+$.

2-(3-((2,2-difluoropropyl)amino)propyl)isoindoline-1,3-dione 161: Synthesized according to the **procedure H** using N-(2,2-difluoropropyl)-N-(3-(1,3-dioxoisoindolin-2-yl)propyl)-4-nitrobenzenesulfonamide **160** as starting material. 58% yield; silica gel TLC R*f* =0.71 (EtOAc/PE 60% v/v); δ_H (400 MHz, $CDCl_3$): 1.61 (3H, t, *J* = 18.7, C*H*$_3$), 1.85 (2H, p, *J* = 6.8, C*H*$_2$), 2.72 (2H, t, *J* = 6.7, C*H*$_2$), 2.90 (2H, t, *J* = 13.6, C*H*$_2$), 3.77 (2H, t, *J* = 6.9, C*H*$_2$), 7.71 (2H, dd, *J* = 5.5, 3.0, Ar-*H*), 7.84 (2H, dd, *J* = 5.4, 3.1, Ar-*H*); δ_C (100 MHz, $CDCl_3$): 21.74 (t, CH_3, *J* = 26.8), 29.0 (CH_2), 35.9 (CH_2), 47.1 (CH_2), 54.8 (t, CH_2, *J* = 28.3), 123.4 (CH), 123.8 (t, CF_2, *J* = 238.7), 132.3 (C), 134.1 (CH), 168.6 (C); δ_F (376 MHz, $CDCl_3$): -95.6; *m/z* (ESI positive) 283.1 $[M+H]^+$.

2-(4-((2,2-difluoropropyl)amino)butyl)isoindoline-1,3-dione 164: Synthesized according to the **procedure H** using N-(2,2-difluoropropyl)-N-(4-(1,3-dioxoisoindolin-2-yl)butyl)-4-nitrobenzenesulfonamide **163** as starting material. 64% yield; silica gel TLC R*f* =0.55 (EtOAc/PE 60% v/v); δ_H (400 MHz, $CDCl_3$): 1.52 (2H, tt, *J* = 7.6, 5.9, C*H*$_2$), 1.62 (3H, t, *J* = 18.7, C*H*$_3$), 1.73 (2H, tt, *J* = 7.8, 6.3, C*H*$_2$), 2.71 (2H, t, *J* = 7.1, C*H*$_2$), 2.90 (2H, t, *J* = 13.7, C*H*$_2$), 3.70 (2H, t, *J* = 7.2, C*H*$_2$), 7.71 (2H, dd, *J* = 5.5, 3.0, Ar-*H*), 7.83 (2H, dd, *J* = 5.4, 3.0, Ar-*H*); δ_C (100 MHz, $CDCl_3$): 21.81 (t, CH_3, *J* = 26.8), 26.35 (CH_2), 27.43 (CH_2), 37.88 (CH_2), 49.55 (CH_2), 54.79 (t, CH_2, *J* = 28.2), 123.3 (CH), 123.7 (t, CF_2, *J* = 237.5), 132.3 (C), 134.0 (CH), 168.5 (C); δ_F (376 MHz, $CDCl_3$): -95.8.

N-(3-amino-2-fluoropropyl)-N-methyl-4-nitrobenzenesulfonamide 174. Synthesized according to the **procedure I** using N-(3-(1,3-dioxoisoindolin-2-yl)-2-fluoropropyl)-N-methyl-4-nitrobenzenesulfonamide **173** as starting material. 72% yield; silica gel TLC R*f* =0.35 (EtOAc/PE 30% v/v); δ_H (400 MHz, CD_3OD): 2.89 (2H, m, C*H*$_2$), 2.90 (3H, s, CH_3), 3.39 (2H, m, C*H*$_2$), 4.66 (1H, dm, J = 48.7, C*H*), 8.07 (2H, d, *J* = 8.9, Ar-*H*), 8.42 (2H, d, *J* = 8.8, Ar-*H*); δ_C (100 MHz, CD_3OD): 36.98 (CH_3), 43.85 (d, CH_2, *J* = 22.0), 52.58 (d, CH_2, *J* = 22.4), 94.5

(d, CHF, *J* = 173.2), 125.54 (CH), 129.92 (CH), 144.6 (C), 151.7 (C); δ_F (376 MHz, $MeOD_4$): -191.8.

N-(3-aminopropyl)-N-(2-fluoropropyl)-4-nitrobenzenesulfonamide 166. Synthesized according to the **procedure I** using N-(3-(1,3-dioxoisoindolin-2-yl)propyl)-N-(2-fluoropropyl)-4-nitrobenzenesulfonamide **153** as starting material. 65% yield; silica gel TLC R*f* =0.28 (EtOAc/PE 30% v/v); δ_H (400 MHz, $CDCl_3$): 1.32 (3H, dd, *J* = 23.5, 6.2, CH_3), 1.73 (2H, dd, *J* = 13.9, 7.0, CH_2), 2.72 (2H, t, *J* = 6.6, CH_2), 3.34 (4H, m, 2x CH_2), 4.81 (1H, dm, *J* = 49.4, C*H*), 8.00 (2H, d, *J* = 8.7, Ar-*H*), 8.35 (2H, d, *J* = 8.9, Ar-*H*); δC (100 MHz, $CDCl_3$): 18.62 (d, CH_3, *J* = 22.0), 31.16 (CH_2), 38.7 (CH_2), 47.2 (CH_2), 53.3 (d, CH_2, *J* = 22.2), 89.5 (d, CHF, *J* = 170.7), 124.5 (CH), 128.5 (CH), 145.6 (C), 150.1 (C); δ_F (376 MHz, $CDCl_3$): -176.24; *m/z* (ESI positive) 320.1 $[M+H]^+$.

N1-(2-fluoropropyl)propane-1,3-diamine ·HCl 155. Synthesized according to the **procedure I** using 2-(3-((2-fluoropropyl)amino)propyl)isoindoline-1,3-dione **154** as starting material. 26% yield; δ_H (400 MHz, CD_3OD): 1.44 (3H, dd, *J* = 23.9, 6.3, CH_3), 2.13 (2H, m, CH_2), 3.07 (2H, t, *J* = 7.6, CH_2), 3.19 (2H, t, *J* = 7.8, CH_2), 3.27 (2H, m, overlapped with CD_3OD signal, CH_2), 5.03 (1H, dm, *J* = 54.5, C*H*); δC (100 MHz, CD_3OD): 18.2 (d, CH_3, *J* = 21.2), 24.9 (CH_2), 37.6 (CH_2), 45.8 (CH_2), 53.1 (d, CH_2, *J* = 21.0), 87.5 (d, CHF, *J* = 166.6); δ_F (376 MHz, CD_3OD): -181.3.

N1-(2-fluoropropyl)butane-1,4- diamine ·HCl 158. Synthesized according to the **procedure I** using 2-(4-((2-fluoropropyl)amino)butyl)isoindoline-1,3-dione **157** as starting material. 57% yield; δ_H (400 MHz, CD_3OD): 1.43 (3H, dd, *J* = 23.9, 6.3, CH_3), 1.79 (4H, m, 2x CH_2), 2.99 (2H, t, *J* = 7.4, CH_2), 3.12 (2H, t, *J* = 7.7, CH_2), 3.30 (2H, m, overlapped with CD_3OD signal, CH_2), 5.04 (1H, d, *J* = 53.6, C*H*); δ_C (100 MHz, CD_3OD): 17.10 (d, CH_3, *J* = 21.2), 22.7 (CH_2), 24.2 (CH_2), 38.6 (CH_2), 47.0 (CH_2, overlapped with CD_3OD signal), 51.8 (d, CH_2, *J* = 25.2), 86.4 (d, CHF, *J* = 166.6); δ_F (376 MHz, CD_3OD): -181.4.

N1-(2,2-difluoropropyl)propane-1,3- diamine ·HCl 162. Synthesized according to the **procedure I** using 2-(3-((2,2-difluoropropyl)amino)propyl)isoindoline-1,3-dione **161** as starting material. 19% yield; δ_H (400 MHz, CD_3OD): 1.80 (3H, t, *J* = 19.2, CH_3), 2.14 (2H, tt, *J* = 12.2, 6.7, CH_2), 3.07 (2H, td, *J* = 7.8, 3.4, CH_2), 3.23 (2H, m, CH_2), 3.67 (2H, t, *J* = 14.9, CH_2); δ_C (100 MHz, CD_3OD): 22.02 (t, CH_3, *J* = 24.9), 24.99 (CH_2), 37.82 (CH_2), 46.67(CH_2), 52.52 (t, CH_2, *J* = 25.7), 121.8 (t, CF_2, *J* = 239.8); δ_F (376 MHz, CD_3OD): -97.4.

N1-(2,2-difluoropropyl)butane-1,4- diamine ·HCl 165. Synthesized according to the **procedure I** using 2-(4-((2,2-difluoropropyl)amino)butyl)isoindoline-1,3-dione **164** as starting material. 35% yield; δ_H (400 MHz, CD_3OD): 1.79 (3H, t, J = 19.1, CH_3), 1.80 (4H, m, 2x CH_2), 3.00 (2H, t, J = 7.6, CH_2), 3.16 (2H, t, J = 8.4, 7.6, CH_2), 3.65 (2H, t, J = 14.9, CH_2); δ_C (100 MHz, CD_3OD): 22.06 (t, CH_3, J = 25.2), 23.89 (CH_2), 25.5 (CH_2), 40.0 (CH_2), 48.7 (CH_2, overlapped with MeOD signal), 52.37 (t, CH_2, J = 25.7), 121.8 (t, CF_2, J = 239.8); δ_F (376 MHz, CD_3OD): -97.4.

Synthethic Scheme for the preparation of compounds 175-177.

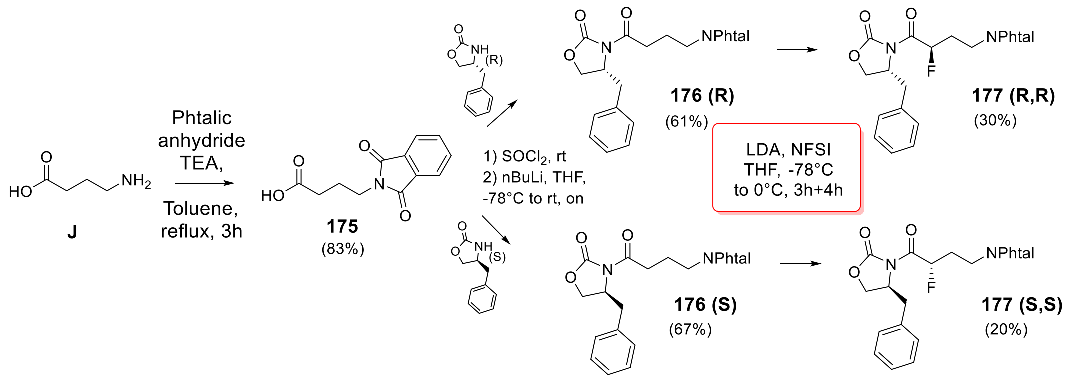

Synthethic Scheme for the preparation of the propargyl derivatives 177-180.

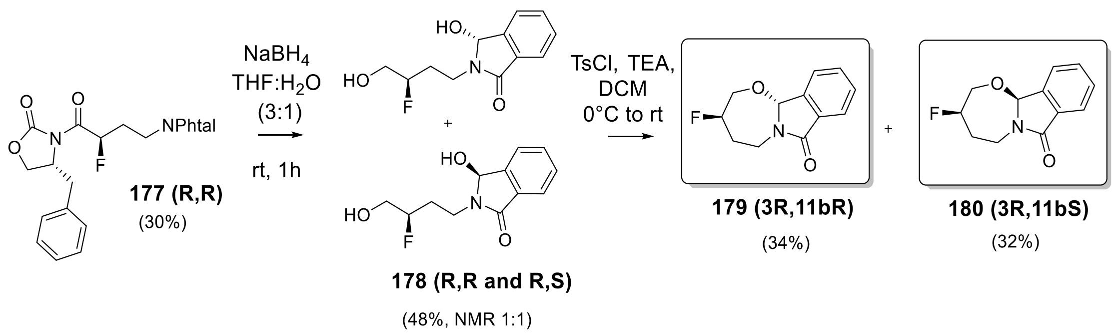

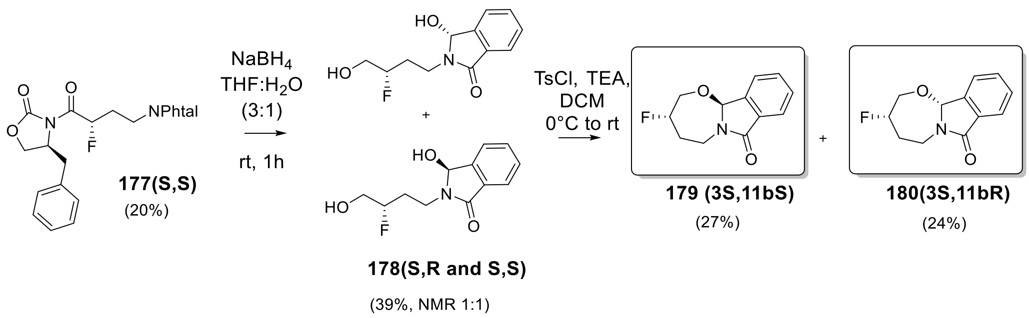

4-(1,3-dioxoisoindolin-2-yl)butanoic acid 175. A mixture of gamma-aminobutyrric acid **J** (2.0 g, 1 eq), phtalic anhydride (1 eq) and TEA (0.5 eq) in toluene (40 ml) was heated at reflux in a flask fitted with Dean-Stark apparatus for 3h (TLC monitoring). When the starting material was consumed, the reaction was cooled at r.t. and the solvent evaporated under reduced pressure. Water (100 ml) was added in the flask, followed by the addition of 3 ml of HCl 4M aq., assisting to the formation of a heavy white precipitate. The mixture was stirred for 30 min, then the precipitate was filtered and dried, affording to a white powder, pure. 83% yield; silica gel TLC R*f* =0.57 (MeOH/DCM 5% v/v); δ_H (400 MHz, $CDCl_3$): 2.01 (2H, p, *J* = 7.11, C*H₂*), 2.41 (2H, t, *J* = 7.43, CH_2), 3.73 (2H, t, *J* = 6.84, CH_2), 7.71 (2H, dd, *J*= 5.48, 3.04, Ar-*H*), 7.84 (2H, dd, *J*= 5.45, 3.04, Ar-*H*), 11.39 (1H, br s, O*H*); δ_C (100 MHz, $CDCl_3$): 23.7 (CH_2), 31.4 (CH_2), 37.2 (CH_2), 123.4 (CH), 132.1 (C), 134.1 (CH), 168.5 (C), 178.5 (C); *m/z* (ESI negative) 232.1 $[M-H]^-$. Experimental in agreement with reported data. [8]

(R)-2-(4-(4-benzyl-2-oxooxazolidin-3-yl)-4-oxobutyl)isoindoline-1,3-dione 176. 4-(1,3-dioxoisoindolin-2-yl)butanoic acid **175** (1.0 g, 1 eq) was solubilized in 10 mL of thionyl chloride and the solution stirred at r.t. under N_2 atm. After 3h, thionyl chloride was evaporated under reduced pressure until dryness and used as it is for the next step. A 1.9 M sol of n-BuLi in Hexane (1.05 eq) was added dropwise to a solution of (R)-4-benzyloxazolidin-2-one (1 eq) in dry THF (15 ml) at -78°C. After 30', 4-(1,3-dioxoisoindolin-2-yl)butanoyl chloride in dry THF (5 ml) was added dropwise to the solution at the same temperature. Reaction was allowed to stir gradually at r.t. over night (o.n.). Reaction was quenched with NaCl aq.s.s. and the mixture evaporated under reduced pressure. The residue was extracted 4 times with DCM, dried over $MgSO_4$, filtered and evaporated, affording to a yellow residue. Purified by combiflash eluting with 20% EtOAc/PE, affording to a white powder. 61% yield; silica gel TLC R*f* =0.37 (EtOAc/PE 30% v/v); δ_H (400 MHz, $CDCl_3$): 2.10 (2H, p, *J*= 6.75, CH_2), 2.77 (1H, dd, , *J*= 13.45, 9.73, C*H*), 2.99 (2H, td, *J*= 6.85, 2.71, CH_2), 3.31 (1H, dd, *J*= 13.43, 3.32, C*H*), 3.81 (2H, td, *J*= 6.75, 1.64, CH_2), 4.18 (2H, m, CH_2), 4.67 (1H, m, C*H*), 7.27 (5H, m, overlapped with $CDCl_3$ signal, Ar-*H*), 7.70 (2H, dd, *J*= 5.50, 3.0, Ar-*H*), 7.83 (2H, dd, *J*= 5.50, 3.0, Ar-*H*); δ_C (100 MHz, $CDCl_3$): 23.2 (CH_2), 32.6 (CH_2), 37.1 (CH_2), 38.0 (CH_2), 55.3 (CH), 66.4 (CH_2), 123.4 (CH), 127.4 (CH), 129.1 (CH), 129.6 (CH), 132.2 (C), 134.1 (CH), 135.5 (C), 153.6 (C), 168.6 (C), 172.3 (C); *m/z* (ESI positive) 393.1 $[M+H]^+$. [9]

(S)-2-(4-(4-benzyl-2-oxooxazolidin-3-yl)-4-oxobutyl)isoindoline-1,3-dione 176. 4-(1,3-dioxoisoindolin-2-yl)butanoyl chloride was reacted with (S)-4-benzyloxazolidin-2-one (1 eq) in dry THF (15 ml) at -78°C, following the procedure above reported, affording to the product **176** as white powder. 67% yield.

2-((R)-4-((R)-4-benzyl-2-oxooxazolidin-3-yl)-3-fluoro-4-oxobutyl)isoindoline-1,3-dione 177. To a solution of LDA (1.58 M in Tetrahydrofuran/Ethylbenzene/Heptane, 1.1 eq) in dry THF (20 ml) at -78°C, compound **176 (*R*)**(2.0 g, 1 eq) as dry THF solution (25 ml) was added dropwise. The reaction was stirred at the same temperature for 30 min. Then, NFSI (1.5 eq) was added portionwise. Reaction was stirred at -78°C for 3h and gradually warmed to 0°C in 4h. The reaction was quenched with NH_4Cl aq. s.s., extracted with EtOAc, dried over $MgSO_4$, filtered and evaporated, affording to a yellow residue, that was purified by combiflash eluting with 30% EtOAc/PE, affording to a white powder. The solid was then crystallized from EtOAc/PE, to give **177** as white needles, pure. 30% yield; silica gel TLC R*f* =0.40 (EtOAc/PE 40% v/v); δ_H (400 MHz, $CDCl_3$): 2.26 (2H, m, C*H*2), 2.78 (1H, dd, , *J*= 13.43, 9.62, C*H*), 3.34 (1H, dd, *J*= 13.51, 3.25, C*H*), 3.87 (1H, dt, *J*= 14.04, 5.79, C*H*), 4.04 (1H, ddd, *J*= 13.83, 8.17, 5.53, C*H*), 4.21 (1H, dd, *J*= 9.21, 2.71, C*H*), 4.29 (1H, dd, *J*= 9.22, 7.70, C*H*), 5.96 (1H, ddd, *J*= 49.32, 8.19, 2.79, C*H*), 7.27 (5H, m, overlapped with $CDCl_3$ signal, Ar-*H*), 7.71 (2H, dd, *J*= 5.47, 3.04, Ar-*H*), 7.84 (2H, dd, *J*= 5.48, 3.03, Ar-*H*); δ_C (100 MHz, $CDCl_3$): 31.6 (d, CH_2, *J* = 21.82), 33.8 (d, CH_2, *J* = 1.63), 37.6 (CH_2), 55.4 (CH), 67.3 (CH_2), 87.3 (d, CHF, *J* = 180.89), 123.4 (CH), 127.7 (CH), 129.2 (CH), 129.5 (CH), 132.2 (C), 134.1 (CH), 134.8 (C), 152.9 (C), 168.5 (C), 169.1 (C); δ_F (376 MHz, $CDCl_3$) -193.8; *m/z* (ESI positive) 411.1 $[M+H]^+$. [9]

2-((S)-4-((S)-4-benzyl-2-oxooxazolidin-3-yl)-3-fluoro-4-oxobutyl)isoindoline-1,3-dione 177. To a solution of LDA (1.58 M in Tetrahydrofuran/Ethylbenzene/Heptane, 1.1 eq) in dry THF (20 ml) at -78°C, compound **176 (*S*)** (2.0 g, 1 eq) was added dropwise as dry THF solution (25 ml), following the procedure above reported, affording to the product **177** as white needles. 20% yield;

2-((R)-3-fluoro-4-hydroxybutyl)-3-hydroxyisoindolin-1-one 178. Compound **177** (0.3 g, 1 eq) was solubilized in 8 ml of THF/H_2O (3:1) and the solution cooled to 0°C. Then, $NaBH_4$ (1 eq) was added portionwise. The suspension was stirred at the same temperature for 10 min, then allowed to warm at r.t. and stirred for 1h (TLC monitoring). The reaction was quenched with NH_4Cl aq. s.s., extracted with EtOAc, dried over Na_2SO_4, filtered and evaporated, affording to an oil. Purified by combiflash, eluting with 3% MeOH/DCM, to give compounds **178** as the diastereoisomeric mixture (1:1 NMR ratio), used as it is for the next step. White powder. 48% yield.

2-((S)-3-fluoro-4-hydroxybutyl)-3-hydroxyisoindolin-1-one 178. Compound **177** (0.3 g, 1 eq) was solubilized in 8 ml of THF/H_2O (3:1) and the solution cooled to 0°C. Then, $NaBH_4$ (1 eq) was added portionwise, following the procedure above reported, affording to the diastereoisomeric mixture **178** as white powder (1:1 NMR ratio), used as it is for the next step. 39% yield;

(3R,11bR)-3-fluoro-2,3,4,5-tetrahydro-[1,3]oxazepino[2,3-a]isoindol-7(11bH)-one 179 and (3R,11bS)-3-fluoro-2,3,4,5-tetrahydro-[1,3]oxazepino[2,3-a]isoindol-7(11bH)-one 180. To a solution of **178** (diastereoisomeric mixture 1:1, 100 mg, 1 eq) and TEA (2 eq) in dry DCM (3 ml), Tosyl Chloride (1.2 eq) was added portionwise at 0°C. The mixture was stirred for 2h at r.t. (TLC monitoring). Then, the reaction was quenched with $NaHCO_3$ s.s., extracted with EtOAc, washed with brine, dried over Na_2SO_4, filtered and evaporated, affording to a solid containing the mixture of the two diastereoisomers. The mixture was resolved by combiflash chromatography, eluting with 30% of EtOAc/PE. **179**, 34% yield; silica gel TLC R*f* =0.37 (EtOAc/PE 30% v/v); δ_H (400 MHz, $CDCl_3$): 2.01 (1H, dddt, *J*= 43.2, 15.7, 12.2, 3.6, C*H*), 2.17 (1H, ddtt, *J*= 15.9, 14.0, 3.7, 2.0, C*H*), 3.25 (1H, dd, *J*= 33.0, 13.8, C*H*), 3.52 (1H, ddd, *J*= 14.5, 12.2, 2.4, C*H*), 3.88 (1H, dddd, *J*= 14.0, 10.3, 3.9, 1.8, C*H*), 4.14 (1H, dt, *J*= 14.1, 3.7, C*H*), 4.69 (1H, dm *J*= 44.2, C*H*), 5.92 (1H, s, C*H*), 7.53 (1H, ddd, *J*= 7.4, 5.7, 2.8, Ar-*H*), 7.60 (2H, m, Ar-*H*), 7.79 (1H, d, *J*= 7.3); δ_C (100 MHz, $CDCl_3$): 32.4 (d, CH_2, *J*= 23.0), 35.9 (CH_2), 64.6 (d, CH_2, *J*= 20.3), 87.6 (CH), 89.4 (d, CHF, *J*= 173.0, CH), 123.1 (CH), 123.7 (CH), 130.4 (CH), 132.6 (CH), 133.2 (C), 141.3 (C), 167.9 (C); δ_F (376 MHz, $CDCl_3$): -188.7; *m/z* (ESI positive) 222.0 $[M+H]^+$. **180**, 32% yield; silica gel TLC R*f* =0.25 (EtOAc/PE 30% v/v); δ_H (400 MHz, $CDCl_3$): 2.07 (1H, m, C*H*), 2.23 (1H, m, C*H*), 3.25 (1H, dt, *J*= 12.1, 2.2, 1.5, C*H*), 3.45 (1H, ddd,, *J*= 11.4, 7.6, 4.3, C*H*), 3.75 (1H, dddd, *J*= 16.5, 12.7, 3.3, 1.4, C*H*), 4.20 (1H, ddt, *J*= 14.3, 5.7, 3.6, C*H*), 4.76 (1H, dm, *J*= 45.0, 4.8, 2.6, 1.5, C*H*), 5.8 (1H, s, C*H*), 7.56 (3H, m, Ar-*H*), 7.81 (1H, dd, *J*= 7.86, 0.84, Ar-*H*); δ_C (100 MHz, $CDCl_3$): 31.6 (d, CH_2, *J*= 21.8), 35.1 (d, CH_2, *J*= 12.8), 66.9 (d, CH_2, *J*= 29.6), 88.2 (CH), 90.1 (d, CH, *J*= 174.6), 123.2 (CH), 123.5 (CH), 130.3 (CH), 132.4 (CH), 132.8 (C), 141.2 (C), 167.6 (C); δ_F (376 MHz, $CDCl_3$): -186.1; *m/z* (ESI positive) 222.0 $[M+H]^+$.

(3S,11bS)-3-fluoro-2,3,4,5-tetrahydro-[1,3]oxazepino[2,3-a]isoindol-7(11bH)-one 179 and (3S,11bR)-3-fluoro-2,3,4,5-tetrahydro-[1,3]oxazepino[2,3-a]isoindol-7(11bH)-one 180. The titled compounds **179 and 180** were obtained following the procedure above reported, using compound **178** as starting material. The mixture of the two diastereoisomers was resolved by combiflash chromatography, eluting with 30 % of EtOAc/PE. **179**, 27% yield; **180**, 24% yield.

5.3.2 CA inhibition

An Applied Photophysics stopped-flow instrument has been used for assaying the CA catalysed CO_2 hydration activity [10]. Phenol red (at a concentration of 0.2 mM) has been used as indicator, working at the absorbance maximum of 557 nm, with 20 mM Hepes (pH 7.5) as buffer, and 20 mM Na_2SO_4 (for maintaining constant the ionic strength), following the initial rates of the CA-catalyzed CO_2 hydration reaction for a period of 10-100 s. The CO_2 concentrations ranged from 1.7 to 17 mM for the determination of the kinetic parameters and inhibition constants. For each inhibitor at least six traces of the initial 5-10% of the reaction have been used for determining the initial velocity. The uncatalyzed rates were determined in the same manner and subtracted from the total observed rates. Stock solutions of inhibitor (0.1 mM) were prepared in distilled-deionized water and dilutions up to 0.01 nM were done thereafter with the assay buffer. Inhibitor and enzyme solutions were preincubated together for 15 min for sulfonamide derivatives and 6 h for coumarin and sulfocoumarin derivatives at room temperature prior to assay, in order to allow for the formation of the E-I complex. The inhibition constants were obtained by non-linear least-squares methods using PRISM 3 and the Cheng-Prusoff equation, as reported earlier, 15 and represent the mean from at least three different determinations. All CA isofoms were recombinant ones obtained in-house as reported earlier.

References

1. Pascale R. et al, New N-(phenoxydecyl) phthalimide derivatives displaying potent inhibition activity towards alpha-glucosidase. Bioorganic Med Chem 2010, 18, 5903-5914
2. Wang KB et al, Synthesis of 3-Aza-bicyclo[3.1.0]hexan-2-one Derivatives via Gold-Catalyzed Oxidative Cyclopropanation of N-Allylynamides. Org Lett 2013, 15(10), 2374-2377
3. Ito Y. et al, Metal-free Reductive Cyclization and Isomerization of Sulfanyl-1,6-diynes Using Sodium Borohydride Chem Lett 2014, 43, 1758-1760
4. Le Darz A., Castelli U., Mokhtari N., et al. Tandem superelectrophilic activation for the regioselective chlorofluorination of recalcitrant allylic amines.Tetrahedron, 2016, 72, 674-689.
5. Kaneda K et al, Efficient synthesis of N-nosyl-protected 3-azabicyclo[4.3.0]nonen-8-one by an aniline- and nitrobenzene-mediated Pauson–Khand cyclizationSynthetic Comm 2017, 47, 1622-1629.
6. Chung WJ, Omote M, Welch JT. The Catalytic Mannich Reaction of 1,1-Difluoro-2-trialkyl(aryl)silyl-2-trimethyl-silyloxyethenes: Preparation of β-Amino Acid Derivatives. J. Org. Chem. 2005, 70, 7784-7787.
7. Liu F. et al, Superelectrophilic Activation in Superacid HF/SbF_5 and Synthesis of Benzofused Sultams. Org. Lett., 2010, 12, 868-871.
8. Ahuja P, Husain A, Siddiqui N. Essential aminoacid incorporated GABA–phthalimide derivatives: synthesis and anticonvulsant evaluation. Med Chem Res 2014, 23, 4085
9. Michael K. Edmonds, Florian H. M. Graichen, et al. Enantioselective Synthesis of α-Fluorinated β2-Amino Acids. Org Lett 2008, 10, 885
10. Khalifah RG. The carbon dioxide hydration activity of carbonic anhydrase I. Stop-flow kinetic studies on the native human isoenzymes B and C. J Biol Chem. 1971, 246, 2561-2573.